Epigenetic Regulation of NOD-Like Receptor Activity and Expression.

Claire L. Feerick

M.Sc., National University of Ireland, Galway

B.Sc., National University of Ireland, Galway

A thesis submitted to the National University of Ireland as fulfilment of the requirements for the Degree of Doctor of Philosophy

November 2018

Department of Pharmacology and Therapeutics,
College of Medicine,
National University of Ireland, Galway

Supervisor of Research: Dr. Declan McKernan

Funding Body

The research undertaken in this thesis was funded by the Hardiman Scholarship, NUIG, awarded September 2014.

Declaration

I declare that the work presented in this thesis has not been submitted for any degree or diploma at this, or any other university and that the work described herein is my own.

Signed: _____ Date: _____

Abstract

NOD-like receptors (NLRs) are a family of intracellular pathogen recognition receptors involved in the innate immune response. NOD1 and NOD2 are the best characterised members of this family, and so are the focus of this research. These receptors have been linked to a wide range of chronic inflammatory diseases, including inflammatory bowel disease. Aberrant NOD1/NOD2 expression has been associated with these states of chronic inflammation. However, the mechanism underlying NOD1/NOD2 gene expression regulation has yet to be elucidated. Therefore, this thesis aimed to investigate whether epigenetic modifications play a significant role in regulating NOD1/NOD2 activity and expression. Epigenetic modifications are heritable patterns that surround the DNA and histones, altering expression of the underlying genes. DNA methylation and histone acetylation are the best characterised of these modifications and so their effects on NOD1/NOD2 were investigated in this thesis. The cell line models used to carry out this experimentation included; HCT116 intestinal epithelial cells and THP-1 monocytic cells. Pharmacological attempts were made to induce a hypomethylated, hyperacetylated or differentiated status, after which NOD1/NOD2 pro-inflammatory responses were quantified. Cells primed with a demethylating agent (5-Aza, 5-Aza-dC or DNMT3b$^{-/-}$), or containing a DNMT3b genetic knockout (DNMT3b$^{-/-}$) were found to be consistently more responsive to NOD1/NOD2 stimulation and had increased expression. Treatment with a histone deacetylase inhibitor (SAHA) or monocyte-to-macrophage differentiation (using PMA) exhibited less conclusive effects on NOD1/NOD2 activity and expression. In conclusion, the novel experimentation carried out in this thesis suggests for the first time that NOD1/NOD2 receptor activity and expression are possibly regulated directly by DNA methylation. Future experimentation, involving DNA methylation pattern analysis, could be carried out to confirm this finding.

Acknowledgements

First and foremost, I would like to acknowledge the College of Medicine for awarding me the Hardiman scholarship. Without this financial support the work undertaken in this Ph.D. would not have been possible. I would also like to acknowledge the Pharmacology and Therapeutics department in NUIG, who provided me with additional funding, required to finance the research component of this Ph.D.

I would like to extend my sincere gratitude to my Ph.D. supervisor Dr. Declan McKernan, for his continued assistance and support over the course of this research. Thanks also to the staff members in the department of Pharmacology and Therapeutics for their guidance over the years, in particular Prof. Laurence Egan and Dr. Aideen Ryan, for their invaluable advice during our collaborative meetings.

The past four years have been a terrific experience, made all the better by the incredible people that I have encountered along the way. Thanks to my fellow Ph.D. students, past and present, in particular the "McKernan Group" members; Laura and Conor. Special thanks also to Dr. Danny Kerr and Ambrose O'Halloran, who were the two pillars of the CNS laboratory. Their commitment, technical ability and willingness to help solve issues in the laboratory meant that their contribution to the completion of this thesis was invaluable.

Last, but not least I would like to extend my deepest gratitude to my tremendously supportive family; parents (Mary and PJ) and sisters (Susan and Emer). I can say with certainty that the completion of this Ph.D. would have been impossible without their continued encouragement, advice and guidance. This unending support will never be forgotten!

Publications and Research Dissemination

Peer Reviewed Published Manuscript

1. Understanding the regulation of pattern recognition receptors in inflammatory diseases – a 'Nod' in the right direction.

   FEERICK, C. L. & MCKERNAN, D. P. 2017. *Immunology,* 150**,** 237-247.

International Conference Proceedings

1. Epigenetic Modifications Influence NOD-Like Receptor Expression and Associated Pro-Inflammatory Activity.
   Conference: *Experimental Biology 2017, Chicago, Illinois, U.S.*
   Presentation Type: *Podium and Poster Presentation*

2. DNA methylation as a potential regulator of NOD-like receptor expression and pro-inflammatory activity.
   Conference: *British Pharmacology Society, Pharmacology 2016, London, U.K.*
   Presentation Type: *Podium and Poster Presentation*

National Conference Proceedings

1. Epigenetic Patterns Influence NOD-like Receptor Expression and Associated Pro-Inflammatory Activity
   Conference: *College of Medicine, Nursing and Health Sciences Research Day 2017, NUIG, Galway*
   Presentation Type: *Podium and Poster Presentation*

2. DNA methylation – A potential regulator of NOD-like receptor expression and activity.
   Conference: Irish Society of Immunology Meeting 2016, Cork.
   Presentation Type: *Podium and Poster Presentation*

3. DNA Methylation – A Potential Regulator of NOD-like Receptor Expression and Activity
   Conference: College of Medicine, Nursing and Health Sciences Research Day 2016, NUIG, Galway
   Presentation Type: *Podium Presentation*
   (Best Presentation Award, Second Place)

4. The Role of DNA Methylation in the Regulation of NOD-Like Receptor Expression and Activity.
   Conference: College of Medicine, Nursing and Health Sciences Research Day 2015, NUIG, Galway
   Presentation Type: Poster Presentation.
   (Best Poster Award, Second Place)

5. NOD-Like Receptor Expression and Pro-Inflammatory Activity in Intestinal Epithelial and Monocytic cell lines can be altered by DNA Methylation
   Conference: Royal Academy of Medicines Ireland (RAMI) Meeting, 2015, Dublin
   Presentation Type: Podium Presentation.
   (Short-listed finalist)

Abbreviations

5-Aza	5-Azacytidine
5-Aza-dC	5-Aza-2'-deoxycytidine
A20	Tumour necrosis factor alpha-induced protein 3
ANOVA	Analysis of variance
AP-1	Activator-1
ASC	Apoptosis-associated speck-like protein containing caspase-recruitment domain
ATG16L1	Autophagy-related 16 like 1
ATP	Adenosine triphosphate
CAD	Carbamoyl phosphate synthetase/aspartate transcarbamylase/ dihydroorotase
CARD	Caspase-recruitment domain
CD	Crohn's disease
CD16	Cluster of differentiation 16
CpG	Cytosine-guanine dipeptide
DAMP	Danger-associated molecular patterns
DNA	Deoxyribonucleic acid
DNMT	DNA methyltransferase
ELISA	Enzyme-linked immunosorbent assay
Erbin	Erb-B2 receptor tyrosine kinase 2 interacting protein
ERK	Extracellular signal-regulated kinase
HDAC	Histone deacetylase
HDACi	Histone deacetylase inhibitor
Hsp	Heat shock protein
IBD	Inflammatory bowel disease
iE-DAP	γ-D-glutyamyl-mesodiaminopimelic acid
IFN-γ	Interferon-γ
IKK	Inhibitor of κB kinase
IL-6	Interleukin 6
IL-8	Interleukin 8
LPS	Lipopolysaccharide

LRR	Leucine rich repeat
MAPK	Mitogen-activated protein kinases
MDP	Muramyl dipeptide
mRNA	Messenger ribonucleic acid
NACHT	Nucleotide-binding domain
NAG	N-acetylglucosamine
NAM	N-acetylmuramic acid
NEMO	Nuclear factor-κB essential modifier
NF- κB	Nuclear factor-κB
NLR	NOD-like receptors
NOD1	NOD-like receptor 1
NOD2	NOD-like receptor 2
OMV	Outer membrane vesicle
PAMP	Pathogen-associated molecular patterns
PGN	Peptidoglycan
PMA	Phorbal 12-myristate 13-acetate
PRR	Pathogen recognition receptor
PSMA7	20S proteasome subunit alpha 7
qPCR	Quantitative polymerase chain reaction
RIP2	Receptor-interacting serine/threonine-protein kinase 2
RNA	Ribonucleic acid
RNF34	Ring finger protein 34
RPL13A	Ribosomal protein L13a
RSK1	Ribosomal S6 kinase 1
SAHA	Suberoylanilide hydroxamic acid
TAK1	Transforming growth factor beta-activated kinase 1
TLR	Toll-like receptors
TNF-α	Tumour necrosis factor alpha
TRI-DAP	L-Ala-γ-D-glutamyl-mesodiaminopimelic acid
TRIM27	Tripartite motif containing 27
TSA	Trichostatin A
TSS	Transcriptional start site
UC	Ulcerative colitis

Table of Contents

Abstract V

Acknowledgements VI

Publications and Research Dissemination VII

Abbreviations IX

Chapter 1 Introduction 1

1.1 The Innate Immune System 1

1.2 Pathogen Recognition Receptors - NOD-Like Receptors 4

1.3 Recognition of Bacteria by NOD1 and NOD2 Receptors 9

1.4 Mechanisms for Peptidoglycan Entry 11

1.5 NOD1 and NOD2 Pro-Inflammatory MAPK and NF-κB Signalling. 14

1.6 Inflammatory Cytokines 18

1.7 NLRs and TLRs Interplay 20

1.8 NOD1 and NOD2 Role in Disease 21

1.9 NOD1 and NOD2 Regulation. 27

1.10 Epigenetics 33

1.11 DNA Methylation 36

1.12 Sites of DNA Methylation – CpG Islands. 38

1.13 DNA methylation Silencing Mechanism. 39

1.14 Non-CpG Island DNA Methylation Sites 40

1.15 DNA demethylation. 41

1.16 DNA Methyltransferase Inhibitors – Azanucleosides 42

1.17 Histone Modifications – Acetylation / Deacetylation. 46

1.18 Histone Deacetylase Enzymes. 48

1.19 Histone Deacetylase Inhibitors. 50

1.20 Concluding Remarks 51

1.21 Knowledge Gaps in the Published Literature 52

1.22 Hypothesis of Current Thesis. 52

1.23 Objectives of Current Thesis. 52

Chapter 2 Materials and Methods 53

2.1 Materials 53

2.2 Cell Culture 56

2.2.1 Monolayer HCT116 intestinal epithelial cell line 56

2.2.2 Sub-culturing HCT116 cell line 58

2.2.3 Suspension THP-1 monocytic cell line....59
2.2.4 Sub-culturing THP-1 cell line....59
2.2.5 Differentiating THP-1 cell line into Macrophages....60
2.3 Determining cell density....60
2.4 Seeding cells for treatments....62
2.5 MTT Assays....63
2.6 Cell treatments....65
2.6.1 Stopping HCT116 cell treatments....66
2.6.2 Stopping THP-1 cell treatments....67
2.7 RNA Analysis....67
2.7.1 Total RNA Isolation....67
2.7.2 Total RNA Quantification and Normalisation....67
2.8 Reverse Transcription....68
2.9 Quantitative PCR....69
2.10 Protein Analysis....72
2.10.1 Protein sample preparation....72
2.10.2 Protein sample lysis....72
2.10.3 Bradford Assay....72
2.11 Western Blot Protein Analysis....74
2.11.1 Polyacrylamide gel (PAGE) preparation....74
2.11.2 Gel electrophoresis....76
2.11.3 Transfer of proteins onto nitrocellulose membrane....77
2.11.4 Blocking membrane....78
2.11.5 Primary Antibody Preparation and Incubation.....79
2.11.6 Secondary Antibody Preparation and Incubation.....80
2.11.7 Imaging western blot.....82
2.12 Enzyme-Linked Immunosorbent Assay (ELISA)....83
2.12.1 Human TNF-α and IL-6 ELISA....83
2.12.2 Human IL-8 ELISA....84
2.13 Flow cytometry....85
2.14 Bioinformatic analysis....86
2.15 Data Interpretation and Statistical Analysis....87
Chapter 3 Analysis of NOD1 activity, signalling and expression in the HCT116 intestinal cell line, following epigenetic modification....88
3.1 Introduction....88
3.2 Methods....89
3.3 Experimental Design....89
3.4 Results....92
3.4.1 DNMT1 inhibitor priming increases NOD1-induced pro-inflammatory activity.....92

3.4.2 DNMT1 inhibitor priming increases NOD1-induced pro-inflammatory RIP2 and MAPK signalling. 96
3.4.3 DNMT1 inhibitor priming increases NOD1-induced pro-inflammatory NF-κB signalling. 99
3.4.4 DNMT1 inhibitor priming increases NOD1 basal expression. 102
3.4.5 NOD1 gene contains CpG islands 104
3.4.6 DNMT3b genetic knockout was confirmed in HCT116 DNMT3b$^{-/-}$ cells 105
3.4.7 DNMT3b genetic knockout increases NOD1 pro-inflammatory activity. 107
3.4.8 DNMT3b genetic knockout increases NOD1-induced pro-inflammatory RIP2 and MAPK signalling. 109
3.4.9 DNMT3b genetic knockout increases NOD1-induced pro-inflammatory NF-κB signalling. 112
3.4.10 NOD1 expression is higher in DNMT3b-/- HCT116 cells relative to wild-type counterparts. 115
3.4.11 HDAC inhibitor priming increases NOD1-induced pro-inflammatory activity. 116
3.4.12 HDAC inhibitor priming increases NOD1-induced RIP2 and MAPK pro-inflammatory signalling in HCT116 cells. 119
3.4.13 HDAC inhibitor priming increases NOD1-induced NF-κB pro-inflammatory signalling in HCT116 cells. 122
3.4.14 HDAC inhibitor treatment has differing effects on NOD1 mRNA and protein expression. 125
3.5 Discussion of Main Findings 126
Chapter 4 Analysis of NOD2 activity, signalling and expression in the HCT116 intestinal cell line, following epigenetic modification. 130
4.1 Introduction 130
4.2 Methods 131
4.3 Experimental Design 131
4.4 Results 134
4.4.1 DNMT1 inhibitor priming increases NOD2-induced pro-inflammatory activity. 134
4.4.2 DNMT1 inhibitor priming increases NOD2-induced pro-inflammatory RIP2 and MAPK signalling. 137
4.4.3 DNMT1 inhibitor priming increases NOD2-induced pro-inflammatory NF-κB signalling. 139
4.4.4 DNMT1 inhibitor priming increases NOD2 basal expression. 141
4.4.5 NOD2 gene contains CpG islands 143
4.4.6 DNMT3b genetic knockout increases NOD2-induced pro-inflammatory activity. 144
4.4.7 DNMT3b genetic knockout increases NOD2-induced pro-inflammatory RIP2 and MAPK signalling. 146
4.4.8 DNMT3b genetic knockout increases NOD2-induced pro-inflammatory NF-κB signalling. 148
4.4.9 Basal NOD2 expression is higher in DNMT3b$^{-/-}$ HCT116 cells relative to wild-type counterparts. 150
4.4.10 HDAC inhibitor priming reduces NOD2-induced cytokine expression but increases NOD2-induced chemokine release. 151
4.4.11 HDAC inhibitor priming increases NOD2-induced RIP2 but reduces MAPK pro-inflammatory signalling in HCT116 cells 153
4.4.12 HDAC inhibitor priming reduces NOD2-induced NF-κB pro-inflammatory signalling in HCT116 cells. 155
4.4.13 HDAC inhibitor treatment reduces NOD2 receptor expression 157
4.5 Discussion of Main Findings 159
Chapter 5 Analysis of NOD1 activity, signalling and expression in the THP-1 monocytic cell line, following epigenetic modification. 162

5.1 Introduction....162
5.2 Methods....163
5.3 Experimental Design....163
5.4 Results....166
5.4.1 DNMT1 inhibitor priming increases NOD1-induced pro-inflammatory activity in THP-1 cells. 166
5.4.2 DNMT1 inhibitor priming increases NOD1-induced pro-inflammatory RIP2 and MAPK signalling in THP-1 cells. 170
5.4.3 DNMT1 inhibitor priming increases NOD1-induced pro-inflammatory NF-κB signalling in THP-1 cells. 173
5.4.4 DNMT1 inhibitor treatment increases NOD1 expression in THP-1 cells....176
5.4.5 HDAC inhibitor priming attenuates NOD1-induced pro-inflammatory cytokine expression but enhances chemokine release from THP-1 cells. 178
5.4.6 HDAC inhibitor priming increases NOD1-induced RIP2 activation but attenuates MAPK signalling in THP-1 cells. 181
5.4.7 HDAC inhibitor priming has varying effects on NF-κB signalling in THP-1 cells. 184
5.4.8 HDAC inhibitor treatment reduces NOD1 mRNA but increases NOD1 protein expression in THP-1 cells. 187
5.4.9 Treatment with 10 ng/ml PMA for 48 hours supports the most effective differentiation of THP-1 cells. 188
5.4.10 Differentiation of THP-1 cells attenuates NOD1-induced pro-inflammatory activity. 192
5.4.11 Differentiation attenuates NOD1-induced RIP2 and MAPK signalling in THP-1 cells. 194
5.4.12 Differentiation attenuates NOD1-induced NF-κB signalling in THP-1 cells. 198
5.4.13 PMA treatment reduces NOD1 expression in THP-1 cells....201
5.5 Discussion of main findings....202
Chapter 6 Analysis of NOD2 activity, signalling and expression in the THP-1 monocytic cell line, following epigenetic modification. 206
6.1 Introduction....206
6.2 Methods....207
6.3 Experimental Design....207
6.4 Results....210
6.4.1 DNMT1 inhibitor priming increases NOD2-induced pro-inflammatory activity in THP-1 cells. 210
6.4.2 DNMT1 inhibitor priming increases NOD2-induced pro-inflammatory RIP2 and MAPK signalling in THP-1 cells. 214
6.4.3 DNMT1 inhibitor priming increases NOD2-induced pro-inflammatory NF-κB signalling in THP-1 cells. 216
6.4.4 DNMT1 inhibitor treatment increases NOD2 basal expression in THP-1 cells....218
6.4.5 HDAC inhibitor priming attenuates NOD2-induced pro-inflammatory cytokine expression but enhances chemokine release from THP-1 cells. 220
6.4.6 HDAC inhibitor priming increases NOD2-induced RIP2 activation but attenuates MAPK signalling in THP-1 cells. 222
6.4.7 HDAC inhibitor priming attenuates NOD2-induced NF-κB signalling in THP-1 cells....224
6.4.8 HDAC inhibitor treatment increases NOD2 protein expression in THP-1 cells. 226
6.4.9 Differentiation of THP-1 cells attenuates NOD2-induced pro-inflammatory activity. 228
6.4.10 Differentiation attenuates NOD2-induced RIP2 and MAPK signalling in THP-1 cells. 230
6.4.11 Differentiation attenuates NOD2-induced NF-κB signalling in THP-1 cells. 232

6.4.12 Differentiation reduces NOD2 expression, but increases A20 expression, in THP-1 cells. 234
6.5 Discussion of main findings 236
Chapter 7 Discussion and Conclusions 239
7.1 Limitations and Future Directions 244
Chapter 8 Bibliography 249
Appendix 1 . Survival Data in HCT116 Cells 262
Appendix 2 . Survival Data in THP-1 Cells 267
Appendix 3 . IL-8 Time and Dose Release from HCT116 cells in response to NOD receptor activation 272
Appendix 4 . IL-8 Time and Dose Release from THP-1 cells in response to NOD receptor activation 274
Appendix 5 . MAPK / NF-κB Phosphorylation Time Response in HCT116 cells. 276
Appendix 6 . MAPK / NF-κB Phosphorylation Time Response in THP-1 cells. 280
Appendix 7 . Housekeeping Gene Validation for qPCR Analysis 284
Appendix 8 . Loading Control Validation for Western Blot Analysis 286

Chapter 1 Introduction

1.1 The Innate Immune System

The immune response is a host-defence mechanism which rests on two functional pillars; the innate and adaptive immune responses. The innate immune response is the body's first line of defence, triggering a non-specific, rapid response against challenges posed by pathogen invasion and endogenous stress. (Kawai and Akira, 2009b). In addition to providing instant relief from these challenges, the innate immune response also prepares the body for future invasion through indirect activation of the more specific, long-term adaptive immune response (Kersse et al., 2011). In this way, inflammation is considered a beneficial response to injury or invasion leading to restoration of cellular homeostasis and prevention of future infection (Janssen and Henson, 2012).

Pathogen recognition receptor (PRR) activation initiates the innate immune response. PRRs stimulated by conserved motifs of invading pathogens and endogenous signals, referred to as pathogen associated molecular patterns (PAMPs) (Kawai and Akira, 2009a) and danger associated molecular patterns (DAMPs) (Oppenheim and Yang, 2005), respectively. PAMPs are associated with most pathogenic bacteria and some viruses, including peptidoglycans (PGNs), liposaccharides (LPS), double-stranded RNA (dsRNA) and flagellin (Athman and Philpott, 2004). DAMPs include IL-1β, heat-shock proteins, uric acid, S100 proteins, ATP, saturated fatty acids and amyloid β (Bianchi, 2007). Once activated, PRRs initiate a cascade of events, leading to the activation of inflammatory mediators including; cytokines, chemokines and vasodilating agents (Fullerton and Gilroy, 2016). These mediators support host-defence by assisting the prerequisite step of the innate immune response; neutrophil transmigration from the bloodstream into surrounding tissues (Baggiolini, 1998, Filippi, 2016). Neutrophil transmigration requires neutrophil recruitment to the blood endothelial cell surface, alongside increased vascular permeability. Neutrophil recruitment is a well-defined process, involving neutrophil rolling, adhesion and crawling along the endothelial barrier. This process is supported by the inflammatory mediators produced following PRR activation. Chemokines enhance the affinity of integrins, neutrophil surface proteins, for neutrophil adhesion molecules on the

endothelium (Berczi and Szentivanyi, 2003, Filippi, 2016). Cytokines increase vascular permeability and stimulate expression of selectins, which are ligands for neutrophil adhesion molecules (Berczi and Szentivanyi, 2003, Filippi, 2016). Recruited neutrophils pass through the leaky endothelium, a process referred to as diapedesis, via the endothelial cell body (transcellular transmigration) or between endothelial cell junctions (paracellular transmigration) (Baggiolini, 1998, Filippi, 2016). Once in the tissues, immune cells initiate events which manifest physiologically as the as the "five pillars of inflammation", including; fever, erythema (redness), odema (swelling), pain and loss-of-function (Figure 1.1). These defined hallmarks of inflammation are required to assist pathogen destruction, removal of damaged cells and promote additional inflammation and repair (Janssen and Henson, 2012, Basil and Levy, 2016).

Figure 1.1: Hallmarks of Inflammation. The innate immune response manifests physiologically as the "five pillars of inflammation", including; fever, erythema (redness), odema (swelling), pain and loss-of-function. (Figure taken from (Basil and Levy, 2016).

The paradox of inflammation is that a sufficient response is required to eliminate infection and prevent tissue damage, however an excessive response can result in unwarranted inflammation that can lead to tissue damage and disease development (Janssen and Henson, 2012). Therefore, resolution of the inflammatory response is equally as important to restore homeostasis via the "five pillars of resolution; removal of microbes/cellular debris, restoration of vascular integrity, regeneration of tissue, remission of fever and relief of pain (Basil and Levy, 2016) (Figure 1.2).

Figure 1.2: Hallmarks of Resolution. Resolution of the innate immune response requires the "five pillars of resolution" to occur including; removal of microbes/cellular debris, restoration of vascular integrity, regeneration of tissue, remission of fever and relief of pain (Figure adapted from (Basil and Levy, 2016).

If inflammation is not resolved, the body will not return to its desired state of homeostasis but will instead enter a state of chronic inflammation and eventually disease (Figure 1.3). In summary, a tightly regulated inflammatory response is essential to maintain a homeostatic state and prevent disease development (Janssen and Henson, 2012).

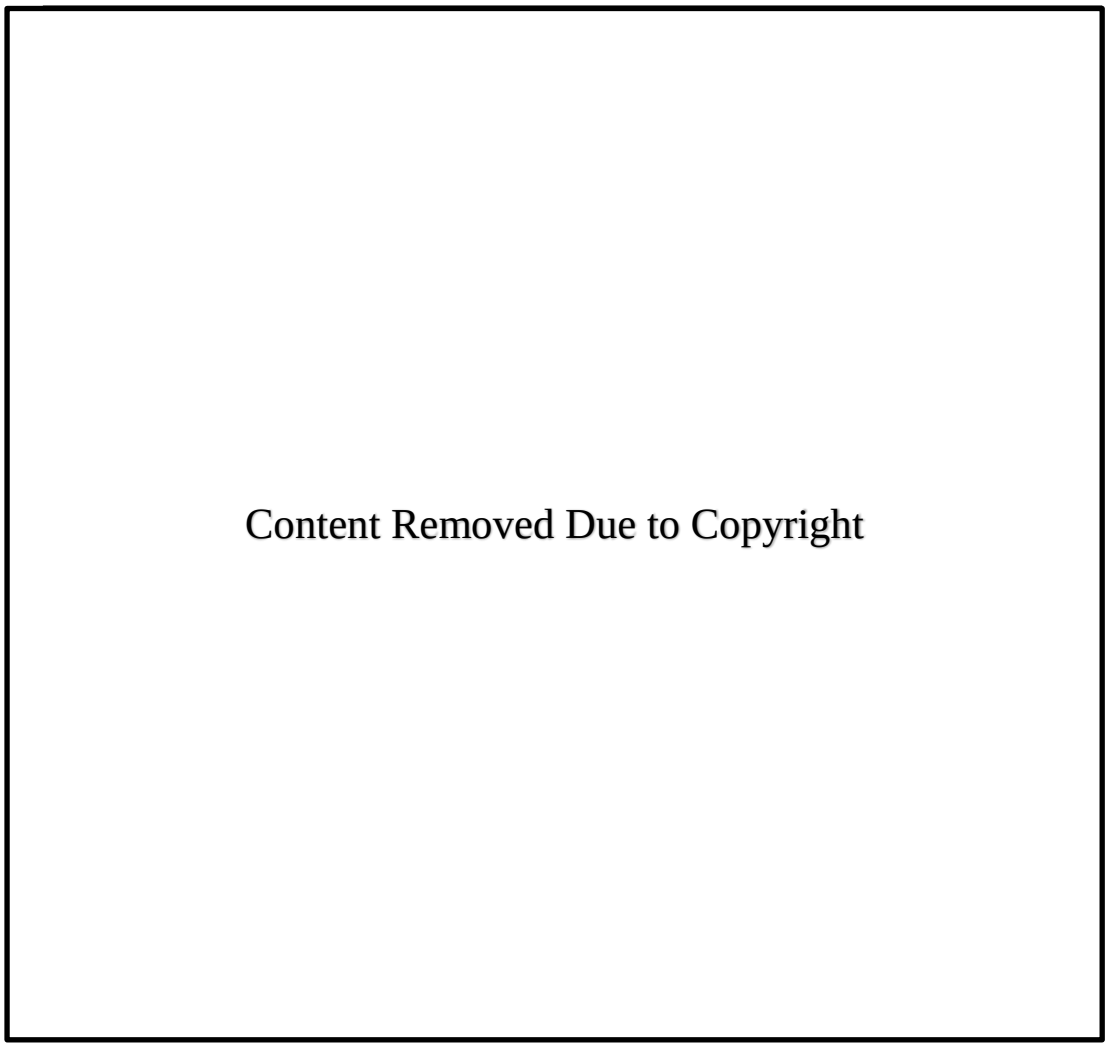

Figure 1.3: Importance of resolving the inflammatory response. Homeostasis is disrupted by insults including pathogenic infection and tissue damage. These insults are abolished by an acute inflammatory response. Once the cellular threat has been cleared, resolution of the inflammatory response is essential to return the body to a state of homeostasis. A lack of resolution results in chronic inflammation and ultimately a diseased state.

1.2 Pathogen Recognition Receptors - NOD-Like Receptors

Pattern recognition receptors (PRRs) are essential players in the initiation of the innate immune response, as highlighted above. Several PRR families have been identified including; Toll-like receptors (TLRs) (Kawasaki and Kawai, 2014), nucleotide-binding oligomerisation (NOD)-like receptors (NLRs) (Franchi et al., 2009a), retinoic acid-inducible gene-I (RIG-I)-like receptors (RLRs) (Loo and Gale, 2011), C-type

lectin receptors (CLRs) (Hoving et al., 2014) and absent in melanoma (AIM2)-like receptors (ALRs) (Thompson et al., 2011). These different PRR families are either membrane bound (TLRs and CLRs) or suspended in the cytoplasm (NLRs, RLRs, and ALRs) (Hansen et al., 2011). PRRs have the capacity to recognise tissue injury and/or different types of pathogens including, bacteria, viruses and fungi, thereby offering protection from a wide range of cellular insults (Hansen et al., 2011).

Although these PRR families differ in many ways, they do share some basic characteristics. All PRRs senses and bind PAMPs/DAMPs via a protein domain and initiate an inflammatory signal via their effector domains. Some PRRs share signalling pathways to relay their responses e.g. NOD1, NOD2 and TLR3 receptors all transduce their pro-inflammatory signal via the same pathways. Most of signalling cascades activated by PRRs result in the activation of kinases (e.g. MAPK) and transcription factors (e.g. NF-κB, AP-1 or IRF3), leading to promotion of inflammatory mediator (e.g. TNF, IL-6, IL-1β and IL-8) expression. This crossover between PRRs creates a network of immune response regulation that can assist in delivering an appropriate immune response to pathogenic invasion or tissue damage (Hansen et al., 2011).

TLRs were the first PRRs to be described (Medzhitov et al., 1997). They are a family of 10 PRRs located either on the plasma membrane or in the endosome/lysosome compartment. TLRs expressed on the cell surface can recognise bacterial and fungal PAMPs, whereas TLRs in the endosome/lysosome compartment recognise bacterial and viral PAMPs (Akira et al., 2006). Upon recognition of their respective PAMPs or DAMPs, TLRs recruit MyD88 and TRIF adaptor proteins to their effector domain, thereby initiating a signalling cascade that activates kinases (MAPK) and transcription factors (NF- κB and IRFs), which in turn promote transcription of inflammatory cytokines, chemokines and type I interferons (Kawasaki and Kawai, 2014).

RLRs are a family of three receptors that act as cytoplasmic sensors of viral RNA. Upon binding viral RNA these receptors signal to upregulate expression of IRF3 or IRF7 transcription factors that lead to increased expression of type I interferon (Kersse et al., 2011, Loo and Gale, 2011). C-type-lectins (CLRs) are a large family of trans-membrane PRRs, divided into 17 groups, which play an essential role in sensing fungi (Hoving et al., 2014). As the name suggests, these receptors are characterised by a C-type lectin domain that has the capacity to bind to the main carbohydrate structures making up the cell walls of fungi. (Hardison and Brown, 2012). CLRs transmit the

signal via adapter proteins e.g. spleen tyrosine kinase (Syk), that promote upregulation of NF-kB and MAPK signalling, which in turn trigger inflammatory mediator production (Hoving et al., 2014). Absent in melanoma (AIM2)-like receptors are cytosolic sensors of double stranded DNA that, upon activation, binds apoptosis-associated speck-like protein containing caspase recruitment domain (ASC) and accommodates ASC oligomerisation and activation (Thompson et al., 2011). Casapase-1 is subsequently recruited to, and activated by, the ASC oligomers. In this way, AIM2 guides maturation of IL-1 and IL-18 through activation of casapase-1. Following maturation these cytokines can released from the cells, thereby promoting a pro-inflammatory response (Thompson et al., 2011).

Nucleotide-binding oligomerization domain (NOD)-like receptors (NLRs) are a family of 22 intracellular PRRs that are known to recognise invading bacteria. The NLR family of PRRs is the focus of this research. These receptors play a crucial role in the innate immune response through recognition of PAMPs and DAMPs, leading to activation of adaptors and effectors required to induce an inflammatory response (Franchi et al., 2009a, Kanneganti et al., 2007). All NLRs have a similar tripartite structure consisting of a C-terminal leucine-rich repeat (LRR) domain, a central nucleotide-binding domain (NACHT domain), and a variable N-terminal domain. The LRR domain is responsible for PAMP/DAMP recognition and binding, thereby initiating the receptor activation process. The NACHT domain facilitates receptor oligomerisation in response to ligand sensing. The variable N-terminal domain possesses effector functions by recruiting and interacting with signal transduction proteins required to trigger cellular responses to pathogen invasion or tissue damage (Kim et al., 2016). The NLR family are most commonly classified according to their N-terminal domain, falling into one of four subfamilies; NLRA, NLRB, NLRC and NLRP (Figure 1.4). These subfamilies contain either an acidic transactivation domain, baculovirus inhibitor repeat (BIR), caspase recruitment domain (CARD) or pyrin domain (PYD), respectively (Ting et al., 2008, Zhong et al., 2013). The LRR domain holds the NLRs in a state of auto-inhibition by binding to the N-terminal, thereby preventing signalling transduction. Once the LRR domain encounters a receptor ligand a conformational change occurs, causing the LRR domain to release the N-terminal from its auto-inhibition. The exposed N-terminal can subsequently bind and activate different downstream signalling adaptors and effectors, depending on which NLR it

is. NLRP1, NLRP3, NLRP6, NLRP7, NLRP12, NLRC4, and NAIP, are known to form inflammasome complexes which activate caspase-1 and subsequently mature inflammatory cytokines. NOD1, NOD2, NLRP10, NLRX1, NLRC5 and CITTA have been found to activate mitogen-activated protein kinases (MAPKs), nuclear factor-κB (NF- κB) and interferon regulatory factors (IRFs) (Zhong et al., 2013). NOD1 (CARD4) and NOD2 (CARD15) receptors, which are both NLRC proteins, were the first of the NLRs to be identified and so are the most extensively studied members of the family (Inohara et al., 2001, Ogura et al., 2001b). Therefore, NOD1 and NOD2 will be the main focus of this research.

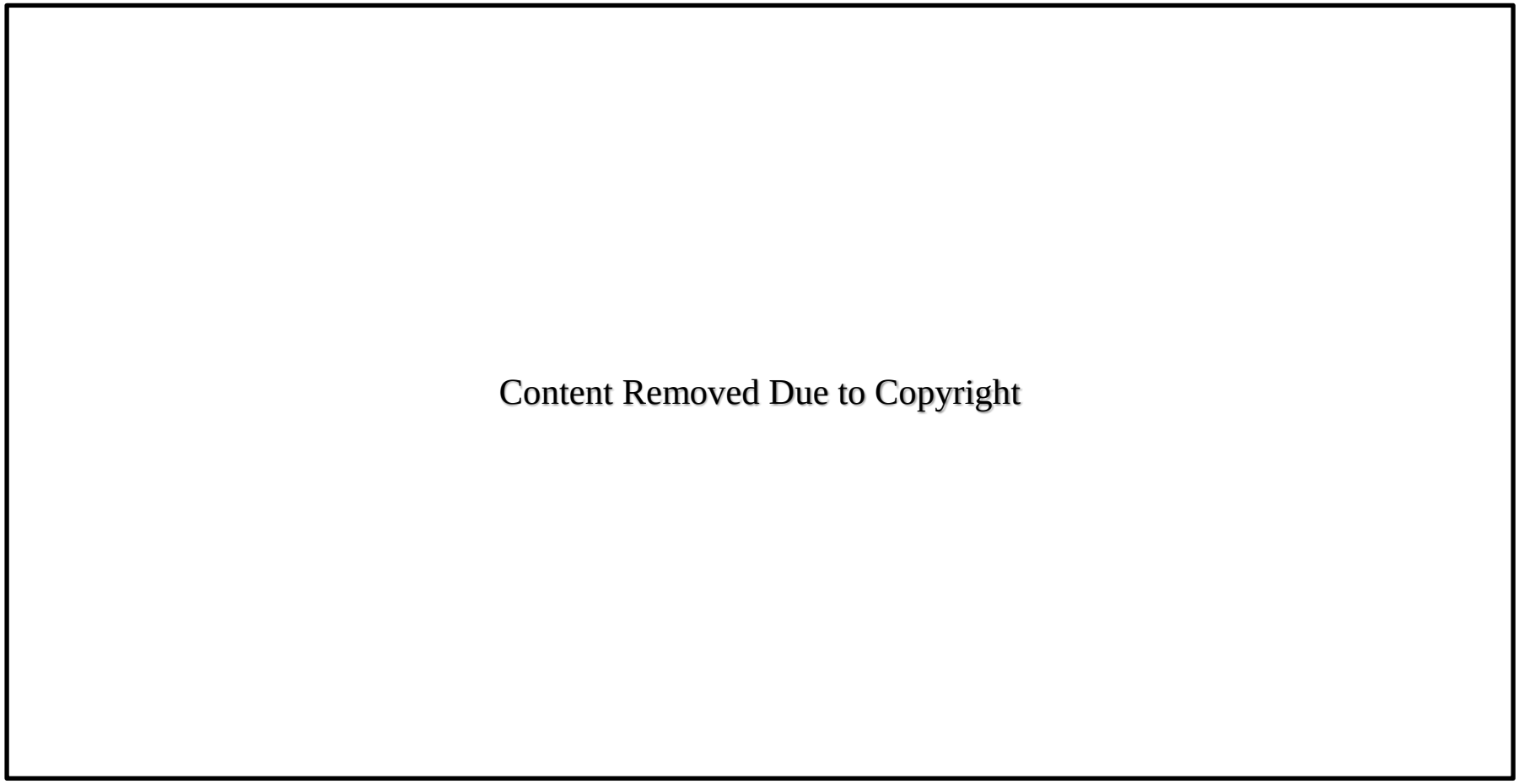

Figure 1.4: NLR classification. The 22 NOD-like receptor (NLR) family members can be classified into four main subfamilies based on their N-terminal domain. These subfamilies include; NLRA, NLRB, NLRC and NLRP whose N-terminal domain consists of and acidic transactivation domain (AD), baculovirus inhibitor repeat (BIR), caspase-recruitment and activation domain (CARD) and pyrin domain (PYD), respectively (Zhong et al., 2013).

1.3 Recognition of Bacteria by NOD1 and NOD2 Receptors

NOD1 receptors are expressed ubiquitously, whereas NOD2 receptors are found mostly in macrophages, monocytes, Paneth intestinal cells and dendritic cells (Inohara et al., 2005). It was originally thought that both NOD1 and NOD2 receptors were sensors of lipopolysaccharide (LPS), which is the main component of Gram-negative bacteria outer membranes (Chen et al., 2009). However, these studies were later refuted due to the realisation that samples used were subject to contamination. Subsequent studies revealed that NOD1 and NOD2 could recognise different components of the peptidoglycan (PGN). PGN makes up a major part of the bacterial cell wall. PGN consists of alternating N-acetylmuramic acid (NAM) and N-acetylglucosamine (NAG) residues, which are cross-linked via short peptides creating a rigid polymer around the bacterial cell (Chen et al., 2009, Kersse et al., 2011). Bacteria can be classified into two major groups based on their cell wall peptidoglycan content; Gram-negative cells have a thin peptidoglycan cell wall, whereas the wall of Gram-positive cells is much thicker due to the presence of many peptidoglycan layers (Silhavy et al., 2010). NOD1 and NOD2 can detect similar yet distinct muropeptides from the PGN (Figure 1.5). The minimal muropeptide detected by NOD1 is the dipeptide; *γ*-D-glutamyl-mesodiaminopimelic acid (iE-DAP). However, NOD1 receptor activation is approximately three-fold stronger when presented with a tripeptide from the peptidoglycan; L-Ala-*γ*-D-glutamyl-mesodiaminopimelic acid (TRI-DAP) (Girardin et al., 2003c). This tripeptide consists of the *γ*-D-glutamyl-mesodiaminopimelic acid with an additional L-Alanine attached. This would suggest that TRI-DAP is required for to provide optimal NOD1 peptidoglycan detection (Girardin et al., 2003a). Both iE-DAP and TRI-DAP are found in some Gram-positive bacteria, such as *Listeria monocytogenes* (Opitz et al., 2006), and all Gram-negative bacteria including; *Escherichia coli* (Kim et al., 2004), *Shigella flexneri* (Girardin et al., 2001), and *Helicobacter pylori* (Watanabe et al., 2011). The NOD2 receptors sense N-acetylmuramyl-L-Ala-D-isoglutamine, otherwise referred to as muramyl dipeptide (MDP), a conserved motif in the peptidoglycan of all Gram-positive, e.g. *Streptococcus pneumoniae* (Zheng et al., 2018), and Gram-negative bacteria e.g. *Shigella flexneri* (Girardin et al., 2001). Recognising all Gram-positive and –negative

bacteria, makes NOD2 a more general sensor of bacterial invasion (Girardin et al., 2003b, Inohara et al., 2003).

Early studies have suggested that cells respond to monomeric PGN components, as outlined above. However, more recent studies have begun to contest such findings, by proposing that cells initially respond to polymeric PGN instead of these monomeric moieties. Data generated using *Bacillus anthracis* found that HEK293 cells were significantly more receptive to polymeric PGN than their monomeric constituents (Iyer and Coggeshall, 2011). Polymeric PGN was also found to be a potent stimulator of immune cells, using dendritic cell activation/maturation and cytokine secretion as a marker of immune stimulation (Schaffler et al., 2014). This data supported a potential mechanism for PGN recognition, whereby polymeric PGN is recognised and internalised into host cells and subsequently trafficked to the lysosome where the polymer is degraded into monomeric motifs which are released into the cytoplasm where they can stimulate intracellular NLRs.

Figure 1.5: Bacterial Peptidoglycan. The peptidoglycan (PGN) is made up of alternating N-acetylmuramic acid (NAM) and N-acetylglucosamine (NAG) residues cross-linked via short peptides. NOD1 receptors detect γ-D-glutamyl-mesodiaminopimelic acid (iE-DAP), and to a three-fold greater extent, L-Ala-γ-D-glutamyl-mesodiaminopimelic acid (TRI-DAP). NOD2 receptors detect N-acetylmuramyl-L-Ala-D-isoglutamine, otherwise referred to as muramyl dipeptide (MDP). Figure prepared based on information from (Girardin et al., 2003a).

1.4 Mechanisms for Peptidoglycan Entry

Since NLRs are intracellular PRRs, they require bacteria to enter the cell before they can recognise and respond to their presence. Several routes of entry have been proposed for internalisation of bacteria (Franchi et al., 2009b, Caruso et al., 2014), as depicted in Figure 1.6.

Some studies suggest that the main route of uptake into immune cells e.g. macrophages is via phagocytosis, internalising the bacteria into compartments referred to as phagosomes. The pathogens can possibly move out of these internalised compartments into the surrounding cytosol, through secretion systems including type III and IV systems, where it can encounter the NLRs for activation (Chen et al., 2009). It has also been proposed that bacteria can enter cells which are incapable of phagocytosis, such as endothelial cells. The suggested mechanism of entry into these cells is through pores formed in the endothelial cell membrane by toxins secreted from bacteria, such as *Listeria*, thereby providing a direct self-sustaining route of entry into the cellular interior (Chen et al., 2009).

NOD-like receptors are generally thought to only detect invading cytosolic pathogens, however studies have now broadened the potential contribution that NLRs play in the innate immune response, by showing that peptidoglycan components can potentially traverse the cell membrane and be released into the cytosol without requiring infection. This has been shown to occur via several routes including; outer membrane vesicles (OMVs), clathrin-dependent endocytosis, bacterial secretion systems, gap junctions and oligopeptide transporters, as outlined in Figure 1.6 (Bielig et al., 2011).

Outer membrane vesicles (OMVs) are spherical vesicles released from membrane protrusions of Gram-negative bacteria e.g. *H. pylori*. These vesicles are thought to encapsulate pathogen-associated molecular patterns (PAMPs) before being released into the extracellular space. Upon encountering a host cell these OMVs will fuse with the cell membrane, releasing the PAMPs into the cells' interior where they can activate intracellular NLRs (Bielig et al., 2011). Studies have shown *H. pylori* use this method in activating NLRs in the gastric mucosa, with the vesicles thought to transfer and internalise vacuolating cytotoxin A into the intestinal epithelial cell (Fiocca et al., 1999, Kaparakis et al., 2010).

Plasma membrane transporters are embedded in the cellular membrane and assist in the transfer of different peptides across the lipid bilayer. In a study carried out on a

colonic epithelial cell line, overexpression of the hPepT1 transporter resulted in enhanced uptake of MDP, a discovery which was complimented by the reduced MDP uptake following siRNA silencing of hPepT1 expression (Vavricka et al., 2004). This role appears to be specific for MDP shuttling, since this transporter did not appear to support transport of the NOD1 ligand; iE-DAP (Ismair et al., 2006). Expression of the hPepT1 transporter is detected in the colons of IBD patients, suggesting a potential role for hPepT1 in chronic inflammatory disease. Increased expression of the hPepT1 transporter could assist extra transport of MDP across the epithelial barrier, thereby contributing to an exacerbated inflammatory response (Vavricka et al., 2004, Ingersoll et al., 2012).

Bacterial type IV secretion system, whereby the bacteria inserts a needle-like protrusion into the host cell through which peptidoglycans can enter into the host cytosol, has also been implicated in NOD1/NOD2 ligand internalisation. The role of this secretion system is highlighted with *H. pylori.* Approximately half of the world's population is thought to have this bacterium in their stomach, however the only people who suffer the associated gastric problems are those with an active *cag* pathogenicity island. It is this active gene that encodes the type IV secretion system allowing the bacterium to enter the epithelial cells, activate NOD1 receptors and promote inflammation (Viala et al., 2004).

Clathrin-dependent endocytosis, involving the encapsulation of NOD1/NOD2 ligands into endosomes has been suggested as another internalisation mechanism. Uptake was found to be dependent on dynamin and extracellular pH, requirements which are indicative of clathrin-dependent endocytosis (Lee et al., 2009). Encapsulated ligands are believed to be released from endosomes into the cytosol via transporters in the endosomal membrane. The endosomal SLC15A4 histidine transporter has been implicated in this process (Sasawatari et al., 2011). An increase in SLC15A4 expression has been documented in biopsy samples taken from the terminal ileum and colon of inflammatory bowel disease (IBD) patients. (Lee et al., 2009). This finding suggests that surplus endosomal transport of NOD1/NOD2 ligands could be a potential contributor to the excessive inflammation characteristic of IBD.

Figure 1.6: Mechanisms for Peptidoglycan Entry into Cellular Interior. Several entry mechanisms, required to deliver PGNs to the cells interior for recognition by NOD1/2 receptors, have been proposed. These include; 1) phagocytosis, 2) outer membrane vesicles (OMVs), 3) plasma membrane transporters and bacterial type III and IV secretion systems, 4) clathrin-dependent endocytosis and 5) gap junctions (Caruso et al., 2014).

1.5 NOD1 and NOD2 Pro-Inflammatory MAPK and NF-κB Signalling.

Despite differences identified in ligand recognition, NOD1 and NOD2 receptors have been found to transduce bacterial signals via similar pathways (Figure 1.7). In the absence of pathogenic stimulation, NOD1/2 receptors are suspended in the cytoplasm and kept in an inactive monomeric state by auto-inhibitory molecular interactions, whereby the LRR domain of the receptor binds back on its NACHT domain, hindering oligomerization (Ogura et al., 2001b). Inactive NOD1/2 proteins are further stabilized by chaperone proteins. By forming complexes with chaperones such as heat-shock proteins, e.g. Hsp70 or Hsp90, NOD1/2 are able to correctly assemble, avoiding premature degradation (Hahn, 2005, Lee et al., 2012, Mohanan and Grimes, 2014). These complexes are thought to contribute to bacterial tolerance, preventing an excessive inflammatory response in regions such as the intestine, where trillions of bacteria reside (Lee et al., 2012). NOD1/2 receptors recognise and bind specific components of the invading peptidoglycan (iE-DAP/TRI-DAP or MDP) via their LRR domains (Boyle et al., 2013). The monomeric receptors subsequently translocate to the plasma membrane and undergo a conformational change, allowing the NOD1/2 receptors to homo-oligomerise via their central NACHT domains (Franchi et al., 2009a, Hsu et al., 2008). These NACHT domains possess ATPase activity, which accommodates oligomerisation and activation of the receptors. Mutational analysis of NOD2 has revealed the necessity for this ATPase activity, with key residue mutations linked to severe auto-inflammatory diseases, including early-onset sarcoidosis and Blau syndrome (Zurek et al., 2012a).

Following oligomerisation and activation of NOD1 or NOD2, the activated receptors recruit and bind the serine-threonine kinase; receptor-interacting protein 2 (RIP2) kinase (Park et al., 2007, He and Wang, 2018). In the absence of NOD1/2 stimulation, it has been suggested that RIP2 activity is stifled by association with the mitogen-activated protein kinase kinase kinase 4 (MEKK4). Activation of the NOD1/2 receptor results in the dissociation of RIP2 from MEKK4, with subsequent binding of RIP2 to the NOD1 or NOD2 oligomers (Clark et al., 2008). RIP2 binds to NOD1/2 via a CARD-CARD interactions (Manon et al., 2007). Studies have been carried out to identify key residues in the CARD domains responsible for the NOD1/2-RIP2 complex formation, as well as those required to support RIP2 activation and thus pro-

inflammatory signalling (Mayle et al., 2014, Tigno-Aranjuez et al., 2010). One such study demonstrated that mutation of Tyr-474 and Lys-443 residues in RIP2 disrupted the interaction between this adapter protein and the NOD1 receptor (Mayle et al., 2014), indicating an extra level of complexity to the protein-protein interaction compared to the simple engagement once proposed. Once bound to the active NOD1/2 receptor, RIP2 is auto-phosphorylated at the Tyr-474 residue (Tigno-Aranjuez et al., 2010), thereby rendering the adapter protein active. Active RIP2 subsequently transduces the bacterial signal by instigating a series of ubiquitination events (Figure 1.7). RIP2 oligomers conjugate with K63-linked polyubiquitin chains at K209 residues positioned in their kinase domain (Hasegawa et al., 2008). RIP2 subsequently binds three E3 ubiquitin ligases; X-chromosome-linked inhibitor of apoptosis (XIAP), cellular inhibitors of apoptosis proteins (cIAP1/cIAP2) and linear ubiquitin chain assembly complex (LUBAC). These E3 ubiquitin ligases further polyubiquitinate RIP2 at K63, thereby assisting the binding and activation of the TAK1 complex which consists of; transforming growth factor *β*-activated kinase 1 (TAK1) – TAK1 binding protein 2 (TAB 2) – TAK1 binding protein 3 (TAB 3) (Hasegawa et al., 2008). The TAK1 kinase becomes highly active when associated with its complex components. Active TAK1 subsequently recruits the IKK complex for activation. This complex consists of two kinases; inhibitor of *κ*B kinase *α* (IKK*α*), and inhibitor of *κ*B kinase *β* (IKK*β*) (DiDonato et al., 1997) alongside a regulatory subunit; inhibitor of *κ*B kinase *γ* (IKK*γ*), otherwise known as nuclear factor-*κ*B (NF-*κ*B) essential modifier (NEMO) (Yamaoka et al., 1998). Phosphorylation of IKK*β* renders it active so that it can phosphorylate the NF-*κ*B inhibitor; inhibitor of *κ*B*α* (I*κ*B*α*). Due to its newly acquired phosphorylated status, I*κ*B*α* can be polyubiquitinated at K48 causing it to dissociate from the NF-*κ*B transcription factor heterodimer (p50–p65). The released inhibitor then travels to the proteasome for proteolytic degradation (Hasegawa et al., 2008). The liberated p50–p65 heterodimer, otherwise referred to simply as NF-*κ*B, translocates to the nucleus where it promotes expression of pro-inflammatory mediators; such as cytokines, anti-microbial peptides and reactive oxygen/nitrogen species (Chen et al., 2009, Shaw et al., 2008) (Figure 1.7). Phosphorylated TAK1 kinase also phosphorylates the mitogen-activating protein kinases (MAPKs); p38, extracellular signal-regulated kinase (ERK), and c-jun N-terminal kinase (JNK), which are upstream promoters of the activator protein-1 (AP1)

transcription factor. Activated activator protein-1 subsequently translocates to the nucleus in the same manner as NF-κB, where it promotes the expression of pro-inflammatory mediators (Chen et al., 2009, Vandenabeele and Bertrand, 2012) (Figure 1.7). Activation of other NLRs, such as NLRP3 by DAMPs, initiates inflammasome assembly. Active NLRP3 oligomers recruit apoptosis-associated speck-like protein containing CARD (ASC) and pro-caspase-1, with subsequent maturation of pro-caspase-1 to caspase-1. Caspase-1 has the capacity to cleave inactive pro-inflammatory cytokines to their active counterparts, such as pro-interleukin-6 (pro-IL-6) to IL-6 (Martinon and Tschopp, 2005). Therefore, although NLRs may react differently upon stimulation they have co-operative effects essential for an innate immune response.

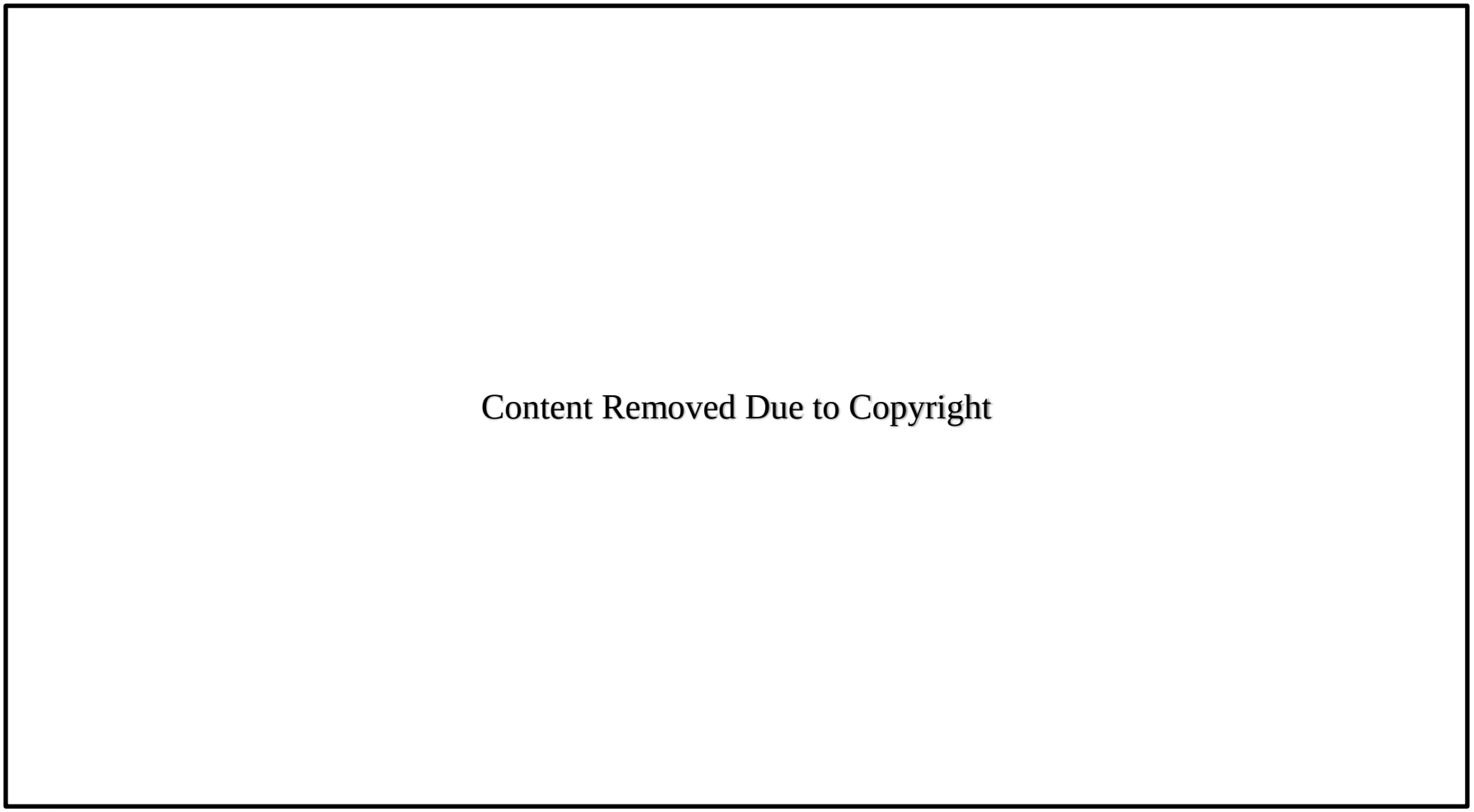

Figure 1.7: NLR pro-inflammatory signalling pathway. The biochemical pathways shown in this figure pertain to NOD1 and NOD2 receptors that have been activated by iE-DAP/TRI-DAP or MDP, respectively. (Feerick and McKernan, 2017)

1.6 Inflammatory Cytokines

NF-κB and MAPK induced pro-inflammatory mediators include; cytokines, anti-microbial peptides and reactive oxygen/nitrogen species. These mediators prompt an innate immune response by orchestrating neutrophil adhesion, vascular permeability, neutrophil transmigration, and microbial destruction (Filippi, 2016). Cytokines can be classified as either pro- or anti-inflammatory, based on whether they work to promote the inflammatory response or resolution (Baggiolini, 1998, Filippi, 2016). Inflammatory cytokines can be further categorised into interleukins (ILs), chemokines (CXCs), tumour necrosis factors (TNFs), interferons (IFNs), transforming growth factors (TGFs) and colony stimulating factors (CSFs); as summarised in Table 1.1 (Chen et al., 2017). Cytokines act to promote an appropriate immune response to bacterial insult or tissue damage, through a complex network of interactions involving the pro-inflammatory (e.g. IL-6, IL-8 and TNF-α) and anti-inflammatory (e.g. IL-4 and IL-10) members (Turner et al., 2014, Chen et al., 2017). Tight regulation of cytokine production is essential to maintain a homeostatic state. Loss of regulation can result in chronic inflammation, tissue damage and even death (Chen et al., 2017). In this thesis, cytokine expression and release will be quantified to provide insight into NOD1 and NOD2 pro-inflammatory activity under varying conditions. Tumour necrosis factor α (TNF-α), interleukin-6 (IL-6) and interleukin-8 (CXCL8/IL-8) expression and/or release were chosen to be investigated.

Content Removed Due to Copyright

Table 1.1: Summary of Cytokines. Inflammatory cytokines involved in regulating the immune response. Main sources of production and inflammatory function listed for each cytokine (Chen et al., 2017).

1.7 NLRs and TLRs Interplay

Activation of NLRs has been shown to be independent of TLR activation, with each family having different receptor ligands. However, it is becoming more apparent that there is cross-talk occurring between these two PRR families that is essential for providing our cells with a finely tuned defence mechanism against invading pathogens (Becker and O'Neill, 2007). Little is known about the exact interplay between these receptors. However, several structural and signalling characteristics shared by these PRRs are beginning to be identified.

These receptors are somewhat structurally similar, both having a leucine rich repeat (LRR) as their pathogen sensing domain (Becker and O'Neill, 2007). The NOD2 agonist, muramyl dipeptide (MDP), has been shown to increase inflammatory responses to the TLR agonist, lipopolysaccharide (LPS), in myeloid cells (Takada et al., 2002). MDP has been found to increase LPS sensitivity three fold (Traub et al., 2004). These findings are supported by the fact that both PGN and LPS are found naturally in tissues during bacterial infection and septic shock, implying that they may complement each other in inducing inflammatory responses (Fritz and Girardin, 2005). TLRs and NLRs share some components of their signalling pathways. TAK1 protein has been found to be a common protein between NLR and TLR signalling pathways and so could potentially play a significant role in the cross-talk between these two receptor families (Chen et al., 2004). The merging of signalling pathways and synergistic cytokine activation allows cells to become more sensitive to stimuli, thereby reducing the amount of bacterial exposure required to induce an inflammatory response (Fritz et al., 2005, Franchi et al., 2008). The immature pro-inflammatory cytokines, such as pro-IL-1β and pro-IL-18, produced by TLRs require cleavage by NLR inflammasome activated caspase-1. This provides another point of intersection between receptors, whereby NLRs enhance TLR pro-inflammatory response (Franchi et al., 2008).

Synergy may not be the only interaction occurring between the two pathways. A study carried out in 2004 uncovered that NOD2 stimulation reduced TLR2 activity in splenocytes (Watanabe et al., 2004). However, this negative relationship could not be identified in all cell types. Subsequent studies, by another research team investigated this relationship in macrophages and dendritic cells taken from $NOD2^{-/-}$ mice. The absence of NOD2 did not appear to have any significant effect on TLR2 activity

(Kobayashi et al., 2005). The conclusion that can be taken from these opposing studies is that the synergistic cross-talk between NLRs and TLRs may be cell type dependent.

1.8 NOD1 and NOD2 Role in Disease

The discovery of several genetic loss-of-function and gain-of-function polymorphisms fuelled extensive research to establish whether defective NOD1 and NOD2 function or regulation has a role to play in chronic inflammation. Expression studies revealed aberrant NOD1 and NOD2 expression in states of chronic inflammation, implicating the receptors in a range of inflammatory diseases (summarized in Table 1.2). Recent evidence links NOD1 and NOD2 with inflammatory bowel disease (IBD), auto-inflammatory disease, rheumatoid arthritis, allergy and cardiovascular and metabolic diseases. A substantial portion of the research currently in the literature revolves around the link between NOD1/2 and IBD.

Inflammatory bowel disease is the collective term for a group of autoimmune disorders causing chronic, transmural inflammation within varying segments of the digestive tract. The aetiology of IBD has yet to be fully elucidated; however, it is postulated that it is caused by excessive activation of the innate immune response in the mucosal cell lining (Maloy and Powrie, 2011). Crohn's disease (CD) and ulcerative colitis (UC) are the primary subtypes of IBD, whose pathologies share similarities but differ in location within the gastrointestinal tract. Ulcerative colitis is characterized by chronic inflammation localized to the colon and rectum (Maloy and Powrie, 2011). Analysis of colon mucosal biopsies from patients with UC revealed an eightfold increase in NOD1 expression relative to control biopsies. Analysis of biopsies from the same cohort of UC patients during remission revealed a reduction in NOD1 expression relative to control biopsy levels. These findings suggest heightened NOD1 expression as a contributing factor behind the UC chronic inflammatory state (Verma et al., 2013).

Crohn's Disease can manifest across any region of the gastrointestinal tract and can be further classified according to the region affected and its clinical presentation (Maglinte et al., 2003). In 2001, the first genetic links to CD were established (Ogura et al., 2001a, Hugot et al., 2001). Extensive research has demonstrated three polymorphisms within or neighbouring the LRR region of the NOD2 gene directly associated with the disease. Of the three polymorphisms, one takes the form of a

frame-shift mutation (L1007fs) whereas the other two are missense mutations (R702W and G908R) (Ogura et al., 2001a, Hugot et al., 2001, Russell et al., 2004). Interestingly, individuals who are heterozygous for NOD2 variants have a twofold to fourfold increased risk of developing CD, whereas homozygous variants have an additional risk of 20- to 40-fold (Ogura et al., 2001a, Hugot et al., 2001, Hugot et al., 2007). Regardless of this significant risk upsurge, most individuals possessing two NOD2 variants do not develop the chronic inflammatory disorder. This finding is supported by a knock-in murine study whereby the L1007fs NOD2 variant was introduced into both alleles of mice, thereby generating homozygous variants. When maintained within a specific-pathogen-free environment the variants did not spontaneously develop intestinal inflammation,(Kim et al., 2011) suggesting that other factors are involved in disease onset.

These polymorphisms have been regarded as loss-of-function, with NOD2 variants having diminished responsiveness to MDP. There have been several proposed mechanisms by which NOD2 loss-of-function results in exacerbated inflammation. NOD2 has been found to maintain the intestinal epithelial barrier by regulating antimicrobial agent release and sustaining bacterial levels and population types. NOD2 variants may lose this protective function, providing insufficient bacterial clearance and allowing excessive bacterial invasion, resulting in augmented inflammation through NOD2-independent pro-inflammatory pathways (Inohara et al., 2003, Kim et al., 2011). The NOD2 receptor is highly expressed within Paneth cells, which are specialized cells located at the base of the intestinal crypts of Lieberkühn. These cells are most numerous in the terminal ileum of the small intestine, which is interestingly the most commonly affected site in CD sufferers. These cells release antimicrobial agents, such as α-defensin, collectively referred to as cryptdins (Ogura et al., 2003, Frank et al., 2011). Disruption of Paneth cell function (and α-defensin release), potentially as a result of NOD2 deficiency, could alter the load and composition of the intestinal flora, an attribute of IBD (Frank et al., 2011). Early studies investigating the effect of NOD2 polymorphisms on release of α-defensin from Paneth cells recorded reduced release in patients with ileal CD holding the NOD2 L1007fs polymorphism (Wehkamp et al., 2004, Wehkamp et al., 2005). However, more recent data imply that the reduction recorded is in fact a secondary effect of the NOD2 knock-down, whereby defective NOD2 results in excessive inflammation,

which in turn blocks the release of α-defensin (Simms et al., 2008). Therefore, it appears that Paneth cell dysfunction may be a consequence of, as opposed to a contributor to, NOD2 loss-of-function.

Intestinal epithelial cells are exposed to trillions of bacteria on a daily basis; however, a healthy intestine appears to be able to deal with this without causing excessive inflammation (Ferreira et al., 2014). Several studies have recorded aberrant bacterial content and load in the intestines of Crohn's patients relative to healthy comparators (Seksik et al., 2003, Ott et al., 2004, Manichanh et al., 2006, Jia et al., 2012). Commensal bacteria play a crucial role in preventing pathogenic invasion and colonization by restoring the epithelial barrier and assisting mucosal immune cells in upholding a basal immune response (Rehman et al., 2011). NOD2 and commensal bacteria function in a feedback loop, whereby commensal bacteria promote NOD2 expression, which in turn negatively feeds back and prevents over-expansion of commensal communities (Biswas et al., 2012). This highlights the important role played by NOD2 in maintaining a peaceful balance between the microbiome and host immune responses. An imbalance in this relationship can result in dysbiosis, whereby pathogenic bacteria begin to outweigh symbiotic bacteria causing the intestinal epithelial barrier to become overwhelmed, thereby allowing bacterial invasion and associated inflammation to ensue (Biswas et al., 2012, Ramanan et al., 2014). Dysbiosis has been recorded in patients with CD and has also been associated with polymorphisms in NOD2 and the autophagy-related 16 like 1 (ATG16L1) genes. However, it remains unclear whether this bacterial imbalance is a consequence or cause of these genetic mutations (Frank et al., 2011, Hold et al., 2014). A defective autophagic response, as a result of the ATG16L1 polymorphism identified in CD patients, could result in an inability to clear the internalized bacteria as efficiently as is needed to counteract the increased bacterial insult (Wolfkamp et al., 2014). This combination of defective innate immune responses by NOD2 and ineffective bacterial clearance by autophagy could together be responsible for CD development and progression.

The direct association between these NLRs and IBD would suggest that NOD1 and NOD2 may be playing a role in similar disease states. Therefore, NOD1/NOD2 expression patterns have been investigated in a wide range of chronic inflammatory

diseases, as outlined below and summarized in Table 1.2. Blau syndrome is a rare dominant autoinflammatory disorder, characterized by granulomatous inflammatory arthritis, uveitis and dermatitis (Blau, 1985). Blau syndrome has been linked to three missense mutations in the NACHT domain of the NOD2 gene; R334Q, R334W and L469F (Tromp et al., 1996, Miceli-Richard et al., 2001). NOD2 has been recorded as being less responsive to MDP in Blau syndrome mutants (Dugan et al., 2015). These data propose that the effects of the R314Q mutation may manifest during translation, causing a truncated form of NOD2 to materialize that has reduced functionality (Dugan et al., 2015). Rheumatoid arthritis is a common chronic inflammatory disease affecting synovial tissue. Expression of NOD1 and NOD2 in this tissue has been found to be augmented in patients with rheumatoid arthritis, implicating these receptors in disease development and/or progression (Ospelt et al., 2009, Yokota et al., 2012, Franca et al., 2015). Allergic rhinitis is a highly prevalent disorder affecting the nasal cavity following exposure to common allergens such as pollen, dust, mould spores or animal dander. It is now believed that bacterial infection could also contribute to allergic rhinitis development through NOD1 and NOD2 activation. Studies have suggested that altered NOD1 and/or NOD2 expression may contribute to allergic rhinitis but further studies are needed to clarify their role in this disorder (Bogefors et al., 2010, Hu et al., 2013). Cardiovascular disease in the form of atherosclerosis, characterized by the accumulation and subsequent maturation of leukocytes into cholesterol-laden foam cells at vessel walls, (Ross, 1999) and Behçet's disease, a rare disorder characterized by inflammation of the blood vessel walls (Hamzaoui et al., 2012), have been associated with aberrant NOD1 and NOD2 expression (Hamzaoui et al., 2012, Nishio et al., 2011, Kanno et al., 2015, Liu et al., 2013). Finally, diet-induced adipocyte inflammation, referred to as metabolic disease, can manifest as either metabolic syndrome or gestational diabetes mellitus. Enhanced NOD1 expression has been recorded in these diet-induced conditions, supporting a role for NOD1 in ‘metainflammation’ (Zhao et al., 2011, Grundy et al., 2005, Zhou et al., 2015, Lappas, 2014). To conclude, current knowledge has identified a strong link between NOD1/NOD2 and IBD development. Support for the role of NOD1 and/or NOD2 in the other chronic inflammatory diseases, as listed in Table 1.2, is still in a relatively early stage of research and further analysis is needed to confirm their role in these diseases.

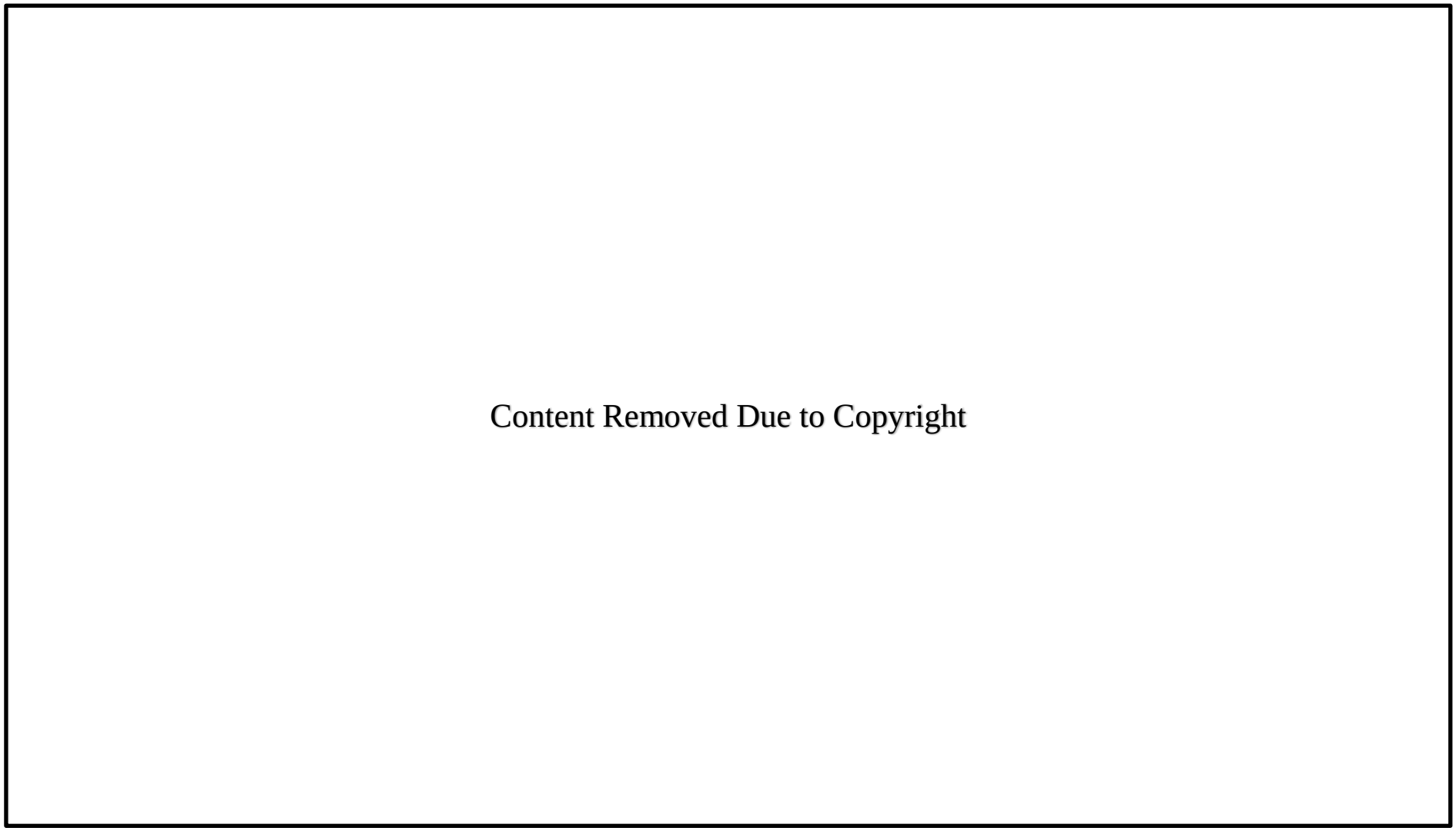
Content Removed Due to Copyright

Content Removed Due to Copyright

Table 1.2: Expression of NOD1 and NOD2 in chronic inflammatory disorders. Listed in this table are studies that have made direct links between chronic inflammatory disorders and increased NOD1/NOD2 expression and their findings. Disorders associated with NOD1/NOD2 include inflammatory bowel disease, autoimmune disease, allergic reactions, cardiovascular disease and metabolic diseases. (Feerick and McKernan, 2017)

1.9 NOD1 and NOD2 Regulation.

With many studies reporting changes in expression during disease states, it is important to understand how these receptors may be regulated. Regulation of the NOD1/NOD2 signalling pathway is necessary to maintain cellular homeostasis, thereby preventing an excessive or insufficient immune response (regulators of NOD1 and NOD2 receptors are outlined in Figure 1.7 and Table 1.3). There is growing evidence that the tumour necrosis factor-α (TNF-α) induced protein 3 (TNFAIP3) ubiquitin ligase, otherwise referred to as A20, is a negative regulator of the NOD-induced NF-κB signalling pathway. One study revealed that in cells deficient in A20, levels of polyubiquitinated RIP2 increased, which was accompanied by enhanced NF-κB signalling (Hitotsumatsu et al., 2008). In addition, cells over-expressing A20 dose-dependently inhibited NOD2 activity. It seems that NOD2 and A20 are part of a negative feedback loop as functional NOD2 has been found to be required for A20 activation (Billmann-Born et al., 2011). It has been proposed that A20 diminishes signalling through complimentary processes carried out by its different domains. The N terminus of A20 removes K63-linked polyubiquitin chains from the C terminus and adds K48-linked polyubiquitin chains to RIP2, which together switch off the NF-κB signalling (Hitotsumatsu et al., 2008, Billmann-Born et al., 2011). Interestingly, single nucleotide polymorphisms within the A20 gene have been directly associated with several chronic inflammatory diseases including rheumatoid arthritis, psoriasis and systemic lupus erythematous (Musone et al., 2011). The link between A20 and IBD has stood out with various genetic studies independently identifying this regulator as a susceptibility locus for CD (Barmada et al., 2004, Bradbury and Brown, 2007). Analysis of CD biopsy samples revealed either diminished or defective A20 protein relative to healthy control samples (Arsenescu et al., 2008). In addition, studies carried out on A20-deficient mice uncovered hypersensitivity to dextran sulphate sodium-induced colitis and increased responsiveness to TNF-α (Vereecke et al., 2010, Lee et al., 2000). Collectively, these data suggest that loss of A20-assisted regulation of NOD2 activity may result in an excessive response to commensal microbiota and unwarranted inflammatory responses.

The ring finger protein 34 (RNF34) E3 ubiquitin ligase and the 20S proteasome subunit α7 (PSMA7), have both been proposed as novel negative regulators of NOD1

signalling. *In vitro* studies have uncovered NOD1 activity to be indirectly proportional to both RNF34 (Zhang et al., 2014) and PSMA7 (Yang et al., 2013) levels. The proposed mechanism of negative regulation for RNF34 and PSMA7 is by way of the ubiquitin/proteasome pathway, whereby NOD1 is K48-ubiquitinated, thereby targeting it to the proteasome for degradation by proteolysis. This mechanism was supported by inhibition studies, whereby the inhibitory effects of RNF34 and PSMA7 on NOD1 activity were significantly impeded by treatment with a proteasome inhibitor (MG132) (Zhang et al., 2014) or small interfering RNA knockdown of PSMA7 (Yang et al., 2013), respectively. RNF34 and PSMA7 expression studies have yet to be carried out to establish whether these proteins are directly linked to chronic inflammatory disease.

Tripartite motif containing 27 (TRIM27) E3 ubiquitin ligase has been found to physically interact with NOD2 with high affinity. This mediates K48-linked ubiquitination of NOD2 leading to degradation of the receptor. In addition, MDP stimulation strengthens the NOD2–TRIM27 interaction and ubiquitination of NOD2. TRIM27 was linked directly to CD through analysis of colon sections taken from patients with CD, which showed enhanced TRIM27 expression relative to healthy patients (Zurek et al., 2012b). These data propose that up-regulated TRIM27 could dampen basal NOD2 activity, leading to disturbed intestinal homeostasis.

Erb-B2 Receptor Tyrosine Kinase 2 interacting protein (Erbin) specifically interacts with NOD2 protein and has been proposed as a negative regulator of NOD2 activity *in vitro* and *in vivo*. Erbin over-expression dose-dependently reduces MDP-induced NOD2 signalling. Conversely, Erbin knockdown resulted in increased NOD2 receptor responsiveness to MDP (McDonald et al., 2005, Kufer et al., 2006). Therefore, it appears that the molecular mechanism underlying Erbin regulation is through alteration of MDP sensitivity. The expression of this negative regulator has yet to be elucidated in disease models; however, one would expect for this protein to be down-regulated in patients suffering NOD2-associated chronic inflammation.

Carbamoyl phosphate synthetase/aspartate transcarbamylase/dihydroorotase (CAD), an essential enzyme in the *de novo* synthesis of pyrimidine nucleotides, was uncovered as another potential regulator of NOD2 by immunoprecipitation-coupled mass spectrometry to identify novel NOD2 regulators. CAD was found to directly

interact with NOD2 and over-expression of the enzyme diminished NOD2-associated NF-κB and mitogen-activating protein kinase signalling as well as bacterial management. These effects point to CAD as a potential negative regulator of NOD2 activity, an indication that was supported by CAD knockdown whereby reduced CAD expression or CAD inhibition augmented NOD2 signalling and antibacterial ability. CAD levels were quantified in the intestinal epithelium of patients with CD, with higher CAD levels being recorded in patients with CD compared with healthy controls (Richmond et al., 2012). This finding suggests that CAD up-regulation in the intestine could result in reduced NOD2 levels, subsequently leading to loss of intestinal homeostasis.

CARD8 has been investigated for its NOD2 modulating effects. CARD8 and NOD2 were found to co-localize and interact with each other through their FIIND and NACHT domains, respectively. Functional analysis revealed that CARD8 masked NOD2 bacterial management and MDP-stimulated NF-κB pro-inflammatory signalling (von Kampen et al., 2010). Analysis of colonic mucosal biopsies from patients with CD revealed significantly higher CARD8 expression relative to healthy comparators (von Kampen et al., 2010). This link to CD is reinforced by studies investigating the connection to a specific polymorphism in CARD8 (rs2043211). A recent meta-analysis identified that this CARD8 polymorphism significantly enhanced CD susceptibility (Liu et al., 2015). This CARD8 variant has also been linked to other NLR-associated diseases, including atherosclerosis, with elevated CARD8 mRNA expression recorded in atherosclerotic plaques (Paramel et al., 2013).

Research carried out so far identified fewer positive regulators of NOD1 and NOD2. Recent evidence has shown that pro-inflammatory cytokines may regulate NOD1 and NOD2 expression. Interferon-γ (IFN-γ) was found to indirectly increase NOD1 mRNA and protein expression dose and time dependently, through augmentation of nuclear IFN regulatory factor 1. NOD1 expression promotion in response to cytokines appears to be specific to IFN-γ, because other cytokines including TNF-α and IL-1β do not have an impact on NOD1 levels (Hisamatsu et al., 2003). However, TNF-α had previously been found to intensify NF-κB signalling by promoting the liberation of NF-κB from the inhibitory effects of IκBα through phosphorylation and dissociation of IκBα (Beg et al., 1993). Building on this finding, an intestinal epithelial cell line

treated with TNF-α increased NOD2 mRNA levels (Gutierrez et al., 2002). Subsequent studies using epithelial cell lines and primary intestinal epithelial cells uncovered increases in NOD2 mRNA and protein levels in response to treatment with TNF-α (Rosenstiel et al., 2003). Unlike with NOD1, IFN-γ exposure did not appear to up-regulate NOD2 expression alone; however, this cytokine did have a synergistic response alongside TNF-αwhereby IFN-γ augmented the TNF-α-induced increase in NOD2 expression (Rosenstiel et al., 2003).

Diet may also play a role in NOD regulation. Butyrate is a short-chain fatty acid that is generated as a by-product of anaerobic fermentation of dietary fibres in the intestine. A role for butyrate in the maintenance of intestinal immunity is now evident. A study found PGN-induced NF-κB transactivation to be increased sevenfold in the presence of butyrate. Additionally, butyrate appeared to significantly strengthen the interaction between the activated p65 transcription factor and pro-inflammatory cytokine/chemokine genes. Butyrate was found to increase NOD2 expression in a dose-dependent manner, without altering the receptor's half-life. Butyrate had previously been found to have histone deacetylase inhibitory properties (Candido et al., 1978). Studies showed that it also promotes NOD2 transcription by supporting acetylation of H3 and H4 at the NOD2 gene promoter (Leung et al., 2009). Interestingly, treating patients with IBD with butyrate was found to reduce intestinal inflammation, possibly by restoring a healthy NOD2 response to commensal bacteria (Scheppach et al., 1992).

The research outlined above has uncovered several NOD1/2-negative and -positive regulators. An imbalance between regulators could indirectly disrupt inflammatory homeostasis and result in an inappropriate response to bacterial insult, potentially manifesting as a NOD1/2-associated disease. Hence, reduced expression of negative regulators or enhanced expression of positive regulators could be indirectly contributing to excess inflammation in chronic inflammatory diseases. The interactions identified between each of these regulators and NOD1/2, alongside the direct link between some of these regulators and CD, suggests regulator targeting as a new therapeutic intervention point for chronic inflammatory disorders.

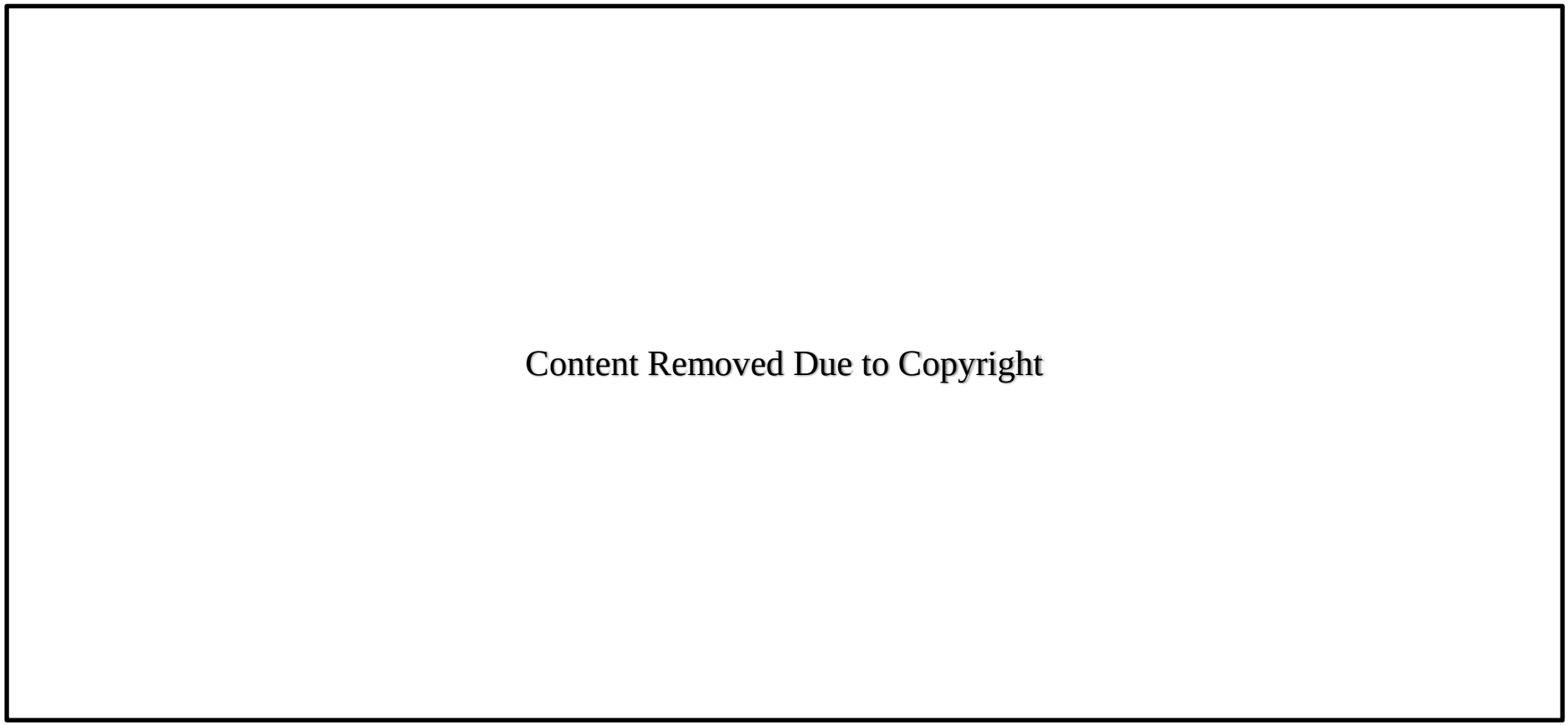
Content Removed Due to Copyright

Content Removed Due to Copyright

Table 1.3: NOD1 and NOD2 Regulators. Listed in this table are negative and positive regulators of NOD1 and NOD2 receptor activity. Regulators are classified according to regulator type, NLR regulated, target protein, mechanism of action and cell type studies have been carried out on. Negative regulators include RNF34, PSMA7, A20/TNFAIP3, TRIM27, Erbin, CAD and CARD8. Positive regulators include; IFN-γ, TNF-α and butyrate.(Feerick and McKernan, 2017)

1.10 Epigenetics

The concept of epigenetics was first introduced in the early 1940s by Conrad Waddington. The original description of epigenetics was a very general umbrella term for all molecular processes altering expression of a genotype into a phenotype (Jablonka and Lamb, 2002). As genetics advanced, so did the understanding of epigenetics, resulting in a more specific meaning for the term "epigenetics". Today, epigenetics is generally accepted as the study of modifications that result in heritable changes in gene expression independent of alterations in DNA sequence (Probst et al., 2009). Epigenetics gets its name from *"epi-"*, which is Greek for *"on top of",* since epigenetic modifications surround DNA without altering the underlying genome (Deans and Maggert, 2015).

Epigenetic mechanisms can alter gene expression by varying the availability of DNA through physical obstructions, recruitment of regulatory proteins and chromatin remodelling. Such epigenetic mechanisms include; DNA methylation, histone modifications and more recently RNA interference (Konsoula and Barile, 2012a), as outlined in Figure 1.8. DNA methylation and histone modifications are the best characterised epigenetic modifications, and so are the focus of this thesis. DNA methylation involves the addition of methyl groups (Me), with the assistance of DNA methyltransferase, to cytosine-guanine (CG) rich regions of DNA. Histone modifications involve the addition of acetyl, methyl or phosphate groups to histone protein tails. Acetylation is the chosen histone modification to be investigated in this research (Lista et al., 2013).

Global alterations in cellular methylation and histone modification patterns during early development indicate their crucial role in cell growth and differentiation. The regulatory capacity of these non-genetic processes highlights their potential role in human disease and provides a rationale for targeting the epigenome pharmacologically as a novel therapy. It is now generally accepted that alterations to the epigenome can significantly contribute to disease onset and progression through altered epigenetic protein function (Berdasco and Esteller, 2013).

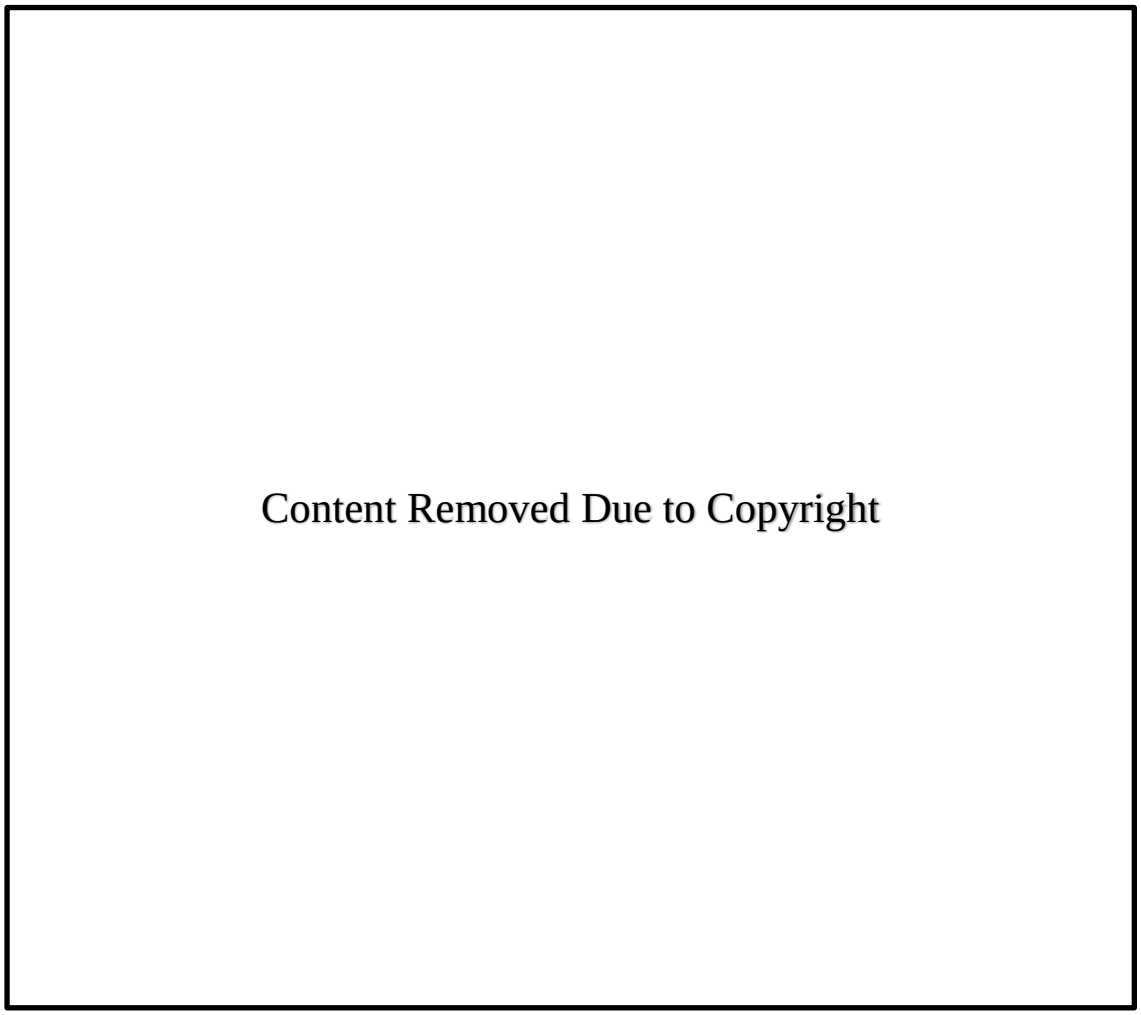

Figure 1.8. General Overview of Epigenetic Modifications. Epigenetic modifications include; DNA methylation and histone modifications. DNA methylation involves the addition of methyl groups to CpG rich regions of the DNA. Histone modifications include; acetylation, methylation and phosphorylation (Lista et al., 2013).

Epigenetic regulators can be classified according to their general mechanism of action including; epigenetic writers, which are responsible for establishing the epigenetics marks on the DNA or histone proteins; epigenetic erasers, which remove the marks put in place by the writers; epigenetic readers, which recognise epigenetic patterns thereby accommodating an appropriate response, as outlined in Figure 1.9 (Falkenberg and Johnstone, 2014). The reversible nature of epigenetic modifications renders them an appealing pharmacological target for the treatment of a vast array of diseases whereby gene expression has been exacerbated or diminished. Pharmacological intervention has the potential to promote/inhibit epigenetic writers or erasers, thereby restoring aberrant expression to healthy levels. Some epigenome targeting drugs have already been approved by the FDA for the treatment of specific cancer sub-types (Quintás-Cardama et al., 2010, Mann et al., 2007).

Figure 1.9. Epigenetic Writing, Erasing and Reading. Epigenetic patterns are established on DNA/histones by epigenetic writers (acetylases, methylases and phosphorylases), removed by epigenetic erasers (deacetylases, demethylases and phosphatases) and read by epigenetic readers (protein domains including; bromodomains and chromodomains) (Tarakhovsky, 2010).

1.11 DNA Methylation

DNA methylation is an epigenetic modification that involves the addition of a methyl group onto cytosine residues, thereby generating 5-methylcytosine. DNA methyltransferase (DNMT) enzymes catalyse the transfer of the methyl group from the methyl donor, S-adenosyl methionine, onto the C-5 position of cytosine residues that are part of cytosine-guanine dinucleotide (CpG) sequences (Lyko and Brown, 2005b).

DNA methyltransferases (DNMTs) are a family of 5 enzymes; DNMT1, DNMT2, DNMT3A, DNMT3B and DNMT3L. Three of the five members (DNMT1, DNMT3A and DNMT3B) have been identified as having methyltransferase catalytic activity. DNMT3A and DNMT3B have been shown to be responsible for establishing the original DNA methyl patterns during development; therefore they have been termed *de novo* methyltransferases. Since methyl patterns are established during early development, it is not surprising that studies have shown DNMT3A and DNMT3B to be highly expressed in embryonic stem cells and silenced in differentiated cells (Portela and Esteller, 2011). DNMT3L has not been shown to have any catalytic activity; however it appears to play an essential role in maternal genomic imprinting (Bourc'his et al., 2001). DNMT1 is highly expressed throughout the S-phase of the cell cycle and acts to maintain methylation patterns throughout subsequent rounds of semi-conservative replication. This enzyme can recognise the hemi-methylated strands and re-establishes the full methyl status (Portela and Esteller, 2011). DNMT1 has also been found to hold some *de novo* activity; however it has a 30-40 fold greater preference for hemi-methylated DNA binding. This high affinity of DNMT1 for newly replicated DNA is assisted through its conjugation with either “ubiquitin-like with PHD and RING finger domains-1” (UHRF1) or the “proliferating cell nuclear antigen” (PCNA) which are positioned at the replication fork, as outlined in Figure 1.10 (Portela and Esteller, 2011, Yu et al., 2011).

It is beginning to become more apparent that it may not be as simple as classifying these enzymes as either *de novo* or maintenance methyltransferases, as knock-out studies are highlighting crossover functions (Esteller, 2007). DNMT1 is no longer thought to be the sole enzyme maintaining methyl patterns, instead DNMT3A and DNMT3B are now believed to contribute to the maintenance also (Jones and Liang, 2009, Jones, 2012).

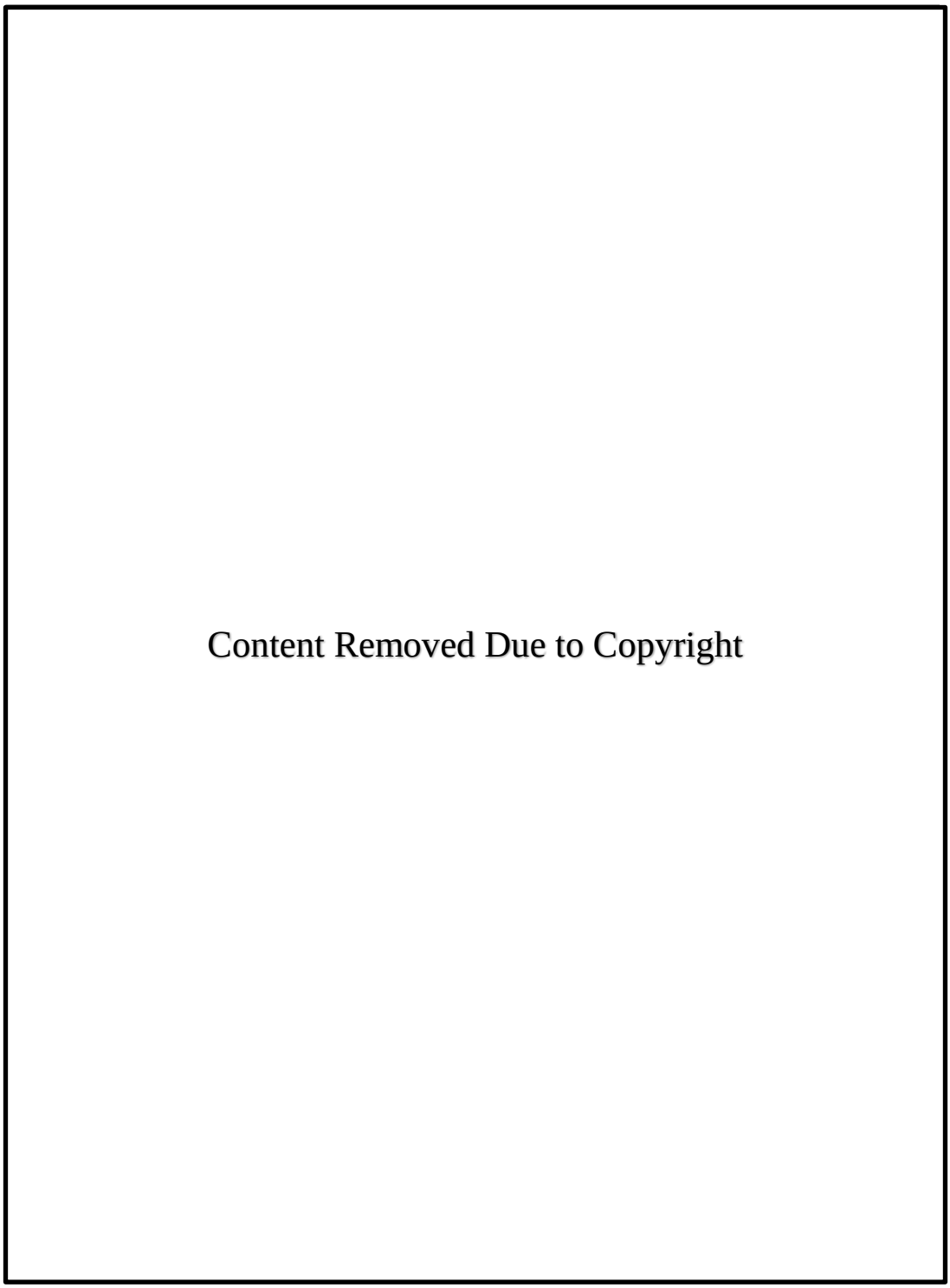

Figure 1.10. De novo and maintenance DNMT enzymes. DNMT 3A/3B establish the original *de novo* methylation patterns surrounding the DNA. DNMT1 recognises UHRF1 at the replication fork binds to hemi-methylated DNA and subsequently restores methylation patterns (Yu et al., 2011).

1.12 Sites of DNA Methylation – CpG Islands.

These CpG dinucleotides are found clustering in regions that become known as "CpG Islands" when the CpG content accounts for at least 50% of a sequence that is greater than 200 base pairs in length (Portela and Esteller, 2011). It is generally accepted that methylation at CpG islands in the transcriptional start sites (TSSs) silences the downstream gene, as depicted in Figure 1.11. More recent studies are revealing that the effects of DNA methylation on gene expression are not as clear cut. The position of the CpG islands and associated methyl groups on the gene appears to dictate the effects on the associated gene. If occurring at TSSs or repeat regions, methylation is linked to gene silencing, whereas methylation of islands in the gene bodies potentially promotes transcriptional elongation (Jones, 2012). Approximately 70% of promoter regions have CpG islands, most of which have an unmethylated status, thereby promoting transcription of the downstream gene (Saxonov et al., 2006).

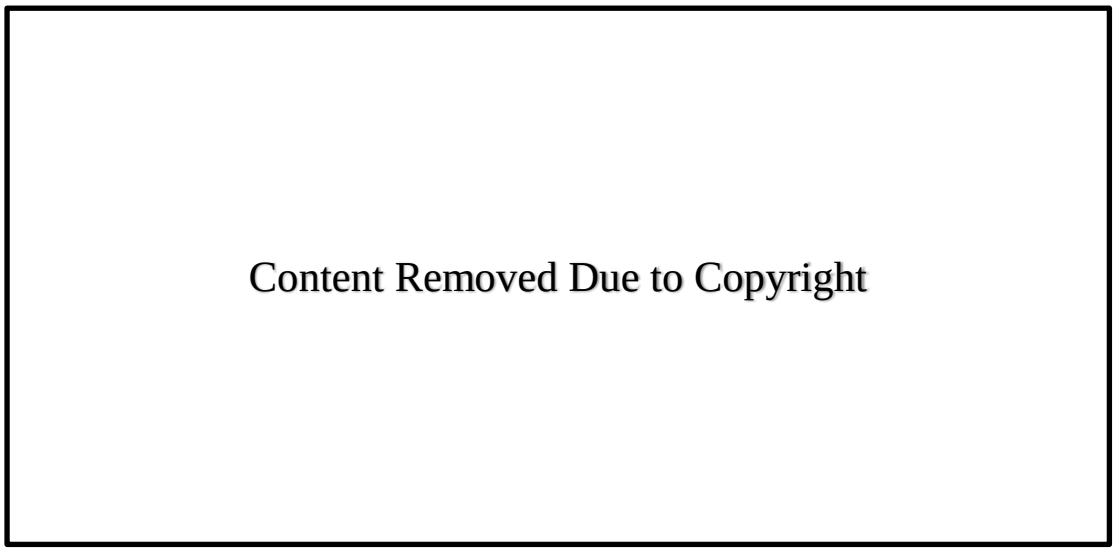

Figure 1.11. DNA Methylation at CpG islands. Unmethylated CpG islands (white circles) at promoter regions supports expression of the downstream gene. Methylated CpG islands (grey circle) at promoter regions represses expression of the downstream gene (Portela and Esteller, 2010).

1.13 DNA methylation Silencing Mechanism.

Gene silencing induced by methylation at transcriptional start sites is thought to occur through two proposed methods. Adding the methyl group onto the cytosine residue generates 5-methylcytosine, which protrudes into the major groove of the DNA helix, thereby directly blocking the association of transcriptional machinery. A more indirect method of impeding gene expression has also been studied (Figure 1.12), whereby the 5-methylcytosine attracts and binds methyl binding proteins (MDPs), such as methyl CpG binding protein 2 (MeCp2), via their methyl binding domain. These MDPs subsequently recruit chromatin remodelling proteins including histone deacetylases (HDACs) and transcriptional repressors such as Swi-independent-3a (Sin3a), which compact the chromatin thereby reinforcing transcription repression (Deaton and Bird, 2011, Choudhuri et al., 2010).

Promoter located CpG islands that are normally unmethylated can become hypermethylated, which is an underlying cause of cancer. Certain tumour suppressor gene, such as p15 or p16, expression becoming suppressed by hypermethylation of promoter region CpG Islands, thereby leaving the genome unprotected against uncontrolled proliferation leading to cancer development (Deaton and Bird, 2011).

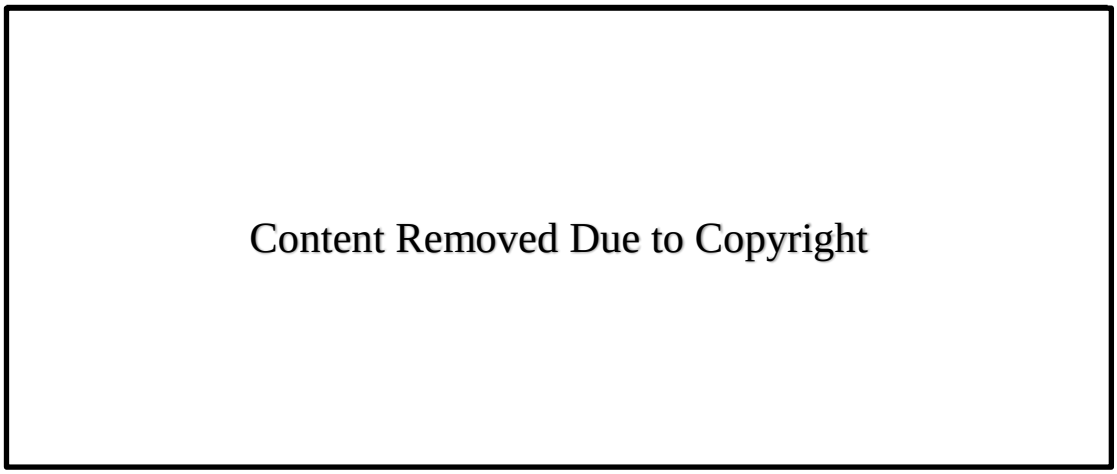

Figure 1.12. Mechanism of DNA methylation assisted gene silencing. Methyl groups physically impede binding of transcriptional machinery. Methyl binding proteins (MeCP2), chromatin remodelling proteins (HDAC) and transcriptional repressors (Sin3a) bind to the methyl groups and promote transcription of the downstream gene (Choudhuri et al., 2010).

1.14 Non-CpG Island DNA Methylation Sites

CpG islands are not the only substrate for methylation, regions referred to as "CpG island shores", which are similar to CpG islands but have a lower density of CpG dinucleotides and typically lie approximately 2kb upstream or downstream of CpG islands. With the help of CHARM (comprehensive high-throughput array-based relative methylation) analysis, it has been recently shown that tissue specific CpG methylation appears to occur at these shores instead of the originally proposed islands (Irizarry et al., 2009). In addition to CpG islands and shores, other regions of CpG methylation that contribute to transcriptional regulation are CpG shelves and open shores, which are located 2-4kb from the CpG islands and sporadically throughout the genome, respectively (Portela *et al.*, 2010).

Further studies recently carried out have now uncovered methylation at non-CpG sites, with methyl patterns being identified on CHG and CHH sites in DNA, with H representing adenine, thymine or cytosine. These unexpected methylation sites were associated with pluripotent stem cells, with these patterns being present in embryonic stem cells, deteriorating upon differentiation and being re-established in induced pluriopotent stem (iPS) cells. Therefore, it has been hypothesised that non-CpG methylation plays a role in establishing and maintaining pluripotency. However, there is still very little known about the mechanism of methylation at these sites (Lister et al., 2009, Portela and Esteller, 2011).

1.15 DNA demethylation.

Although cytosine residues are DNA methylation sites, some CpG islands resist hypermethylation. The biochemical mechanisms underlying methylation prevention at these select sites currently remains unknown, with no DNA demethylase identified to date. It was originally thought that some CpG islands resist methylation with the assistance of the tri-methylated histone; H3K4me3, which blocks *de novo* DNA methyltransferase recruitment thereby preventing the establishment of the methylation patterns at these sites (Williams et al., 2012).

There is mounting evidence that DNA demethylation is being guided by a family of proteins called ten-eleven translocation (TET) proteins. Studies have identified three member of the TET family as potential players in blocking methylation of cytosine residues; TET1, TET2 and TET3. TET1 protein was identified as an oxidising agent that could convert 5-methylcytosine (5-mC) to its aldehyde form; 5-hydroxymethylcytosine (5-hmC) (Tahiliani et al., 2009). It was originally proposed that TET proteins passively induced DNA demethylation through the production of 5-hmC, since the maintenance DNA methyltransferase DNMT1 appeared to have reduced methylating efficiency for hemi-methylated 5-hmC, thereby hindering restoration of methylation patterns during DNA replication.

However, now it is thought that DNA demethylation could actually be an active process instead of a secondary mechanism originally proposed. There is mounting evidence that the TET protein family, alongside thymine DNA glycosylase (TDG), are responsible for converting 5-methylcytosine (5-mC) to cytosine. It has been proposed that these proteins actively remove methyl groups from cytosine residues in CpG islands. The 5-hmC form of cytosine is actually an oxidation intermediary, which can undergo two further rounds of oxidation generating an aldehyde; 5-formylcytosine, and a carboxylic acid; 5-carboxycytosine. These two forms of cytosine are recognised and subsequently excised by thymine DNA glycosylase (TDG). The DNA demethylation cycle is then completed through base excision repair, which fills the excision gap with an unmethylated cytosine (He et al., 2011).

1.16 DNA Methyltransferase Inhibitors – Azanucleosides.

Due to the reversible nature of epigenetic modifications, DNA methylation patterns and associated gene expression have the potential to be reformed by hindering the restoration of hemi-methylated DNA during cell replication. A family of DNA methyltransferase inhibitors (DNMTi) have been developed that deteriorate DNA methylation patterns, thereby inducing a hypomethylated state (Quintás-Cardama et al., 2010). These drugs hinder the restoration of hemi-methylated DNA to its fully methylated form during replication by blocking the actions of the principle maintenance methyltransferase, DNMT1. DNMTi's can be classified as either nucleoside or non-nucleoside inhibitors. Further advances have been made with the nucleoside analogues, compared with non-nucleoside analogues, due to their greater activity in living cells (Yang et al., 2010). There are currently five nucleoside DNMTi's; 5-azacytidine, 5-aza-2'-deoxycytidine, zebularine, 5-fluoro-2'-deoxycytidine and dihydro-5-azacytidine, whose structural similarity to cytosine allows them to be incorporated into newly synthesised DNA (Yang et al., 2010). 5-azacytidine (Viadaza®) and 5-aza-2'-deoxycytidine (Decitabine®) are the most potent of these inhibitors, both of which have been approved in the USA for chemotherapeutic purposes by the Food and Drug Administration (FDA), as a treatment for myelodysplastic syndrome subtypes (Yang et al., 2010, Kaminskas et al., 2005).

5-azacytidine (5-aza) and 5-aza-2'-deoxycytidine (5-aza-dC), collectively termed azanucleosides, are cytidine analogues that must gain access to the cells interior to carry out their demethylating action. Human nucleotide transporters (hNTs) are known to carry naturally occurring nucleosides and nucleoside analogues across the cell membrane (Zhang et al., 2007). Therefore, it was proposed that synthetic nucleoside analogues, such as 5-aza and 5-aza-dC, utilise the same transporter proteins to enter the cell. However, the precise hNTs involved remain undefined due to the conflicting data surrounding the process (Rius et al., 2009a) (Damaraju et al., 2012) (Hummel-Eisenbeiss et al 2013) (Wu et al., 2015). Earlier studies suggested that both 5-aza and 5-aza-dC were transported by the human concentrative nucleotide transporter 1 (hCNT1), based on the link between transporter presence and sensitization to azanucleoside demethylating effects (Rius et al., 2009a). However, this belief was later challenged when rates of azanucleoside transport were quantified in *Xenopus*

oocytes transformed to express individual hNTs in order to establish which transporter contributed most significantly to the their internalisation (Damaraju et al., 2012). Based on rates of transport and associated cytotoxicity this study indicated that 5-aza and 5-aza-dC were transported by separate members of the hNT family, hCNT2 and hENT1/hENT2 respectively (Damaraju et al., 2012). When investigating transport in primary acute myelogenous leukemia cells and leukemia cell lines, 5-aza was found to strongly depend on the hENT1transporter (Hummel-Eisenbeiss et al., 2013). Another recent study investigated the transport and thus the response to 5-aza-dC in bone marrow and peripheral blood samples taken from myelodysplastic syndrome patients. It was found that lower hENT1 expression was associated with primary resistance to 5-aza-dC, thereby inferring that hENT1 is a key transporter for internalisation of this azacytosine (Wu et al., 2015). The conflicting data may be a result of azanucleoside uptake being analysed in different cell types, whereby cells with low expression of one transporter type call upon other hNTs to compensate for the deficit. Once this potential difference in transporter expression is normalised between cells being analysed, the principle transporters for each azanucleoside should become more apparent.

5-aza and 5-aza-dC have similar mechanisms of intracellular metabolism, as depicted in Figure 1.13. Once the nucleoside analogues are inside the cell they must undergo phosphorylation by a series of kinases in order to be converted into their active nucleotide form, 5-aza-2'-deoxycytidine-5'-triphosphate, for incorporation into DNA. 5-aza is firstly phosphorylated to a monophosphate form by uridine-cytidine kinase. This monophosphate then undergoes two subsequent phophorylation reactions by pyrimidine diphosphate and triphosphate to ultimately convert it to the highly active triphosphate form, which can be incorporated into nucleic acids (Kaminskas et al., 2005, Rius et al., 2009b, Issa and Kantarjian, 2009). 5-aza-dC is a deoxyribonucleoside meaning that it is incorporated exclusively into DNA once phosphorylated to 5-aza-2'-deoxycytidine-5'-triphosphate by deoxycytidine kinase and pyrimidine diphosphate/triphosphate. However, 5-aza is a ribonucleoside and so faces a cross-road when in its diphosphate form. 5-aza diphosphate has the potential to undergo another round of phosphorylation to a triphosphate or to be converted into a deoxyribonucleotide (Li et al., 1970). Typically ~80-90% will remain a ribonucleotide and so will be incorporated into RNA, resulting in ribosome

dysfunction and subsequent protein synthesis failure thereby accounting for the recorded cytotoxicity associated with exposure to this inhibitor (Glover and Leyland-Jones, 1987, Li et al., 1970). The remaining ~10-20% are reduced to a deoxyribonucleotide by ribonucleotide reductase to 5-aza-deoxycytidine diphosphate. This diphosphate is then phosphorylated to active 5-aza-2'-deoxycytidine-5'-triphosphate, which can be incorporated into DNA (Kaminskas et al., 2005, Leone et al., 2008, Li et al., 1970).

Cytidine nucleotides and activated azanucleoside analogues have an almost identical chemical structure. Due to this similar homology the analogues will be incorporated into the DNA of proliferating cells in place of cytidine. DNA methyltransferase 1 (DNMT1) will make attempts to methylate the incorporated inhibitor. The normal process of maintenance methylation by DNMT1 involves the temporary attachment of the enzyme to the cytidine nucleotide, allowing it to catalyse the methylation of the newly incorporated nucleotide. Once the full methyl pattern is restored DNMT1 detaches from the DNA strand, free to bind and catalyse other cytidines. This maintenance process is disrupted by 5-aza and 5-aza-dC. When DNMT1 binds to this nucleoside it becomes trapped on the DNA strand due to an interaction between DNMT1 and the nitrogen located at the carbon 5 position in the pyrimidine. This enzyme trapping means that it will no longer be free to restore methyl patterns on subsequent daughter strands that form during replication (Kuo et al., 2007, Yang et al., 2010). Eventually, this will result in significantly hypomethylated DNA strands following many rounds of replication (Lyko and Brown, 2005a, Jones and Taylor, 1980). Since these nucleoside analogues work by being distributed throughout the DNA, 5-aza-dC is thought to be a more potent hypomethylating agent with lesser cytotoxicity due to its sole incorporation into DNA.

Figure 1.13. Azanucleoside Mechanism of Action. Both DNA methyltransferase inhibitors, 5-Aza and 5-Aza-dC, enter the cell interior via hENT1transporters. Once inside the cell the cytosine analogues undergo several rounds of phosphorylation. 5-Aza-dC can incorporate directly into DNA since it is a deoxyribonucleoside. 5-Aza can be incorporated into both RNA (~80-90%) and DNA (~10-20%). 5-Aza requires an additional reduction step to convert it from a ribonucleoside into a deoxyribonucleoside for incorporation into DNA (Quintás-Cardama et al., 2010).

1.17 Histone Modifications – Acetylation / Deacetylation.

Histone proteins form a core histone octamer (two copies of H2A, H2B, H3 and H4), around which 146 base pairs of DNA wraps to form a nucleosome. Nucleosomes are the basic unit of compacted chromatin, and so are important in gene expression regulation (Marks et al., 2001). Each histone making up the histone octamer have a lysine-rich tail at their amino-terminal, which gives the octamer a strong positive charge. It is this positive charge that supports the strong interaction between the histones and DNA, assisting chromatin compaction (Marks et al., 2001). Post-translational modifications can also occur at the amino-terminal tails of the core histone proteins including; acetylation, methylation, ubiquitination, phosphorylation, sumoylation, ADP ribosylation, proline isomerisation, hydroxylation (Falkenberg and Johnstone, 2014). Histone acetylation and methylation are the most extensively studied of these epigenetic processes. Such histone protein modifications are associated with alterations in chromatin structure and thereby play an important role in transcription regulation. The transcriptional effects of histone acetylation/deacetylation on NLR expression will be investigated in this research.

Histone acetylation is involved in modifying chromatin structure and associated gene expression (Haberland et al., 2009). Histone acetylation and transcriptional activation are inversely related. Acetylation neutralises the positive charge of lysine residues within histone N-terminal tails, thereby reducing their affinity for surrounding DNA. Histone acetylation status is maintained by a balance in the activity of two enzymes; histone acetyl-transferases (HATs) and histone deacetylases (HDACs) (Xu et al., 2007), as outlined in Figure 1.14. HATs assist the transfer of acetyl groups from acetyl co-enzyme A onto histone tail lysine residues, promoting chromatin relaxation. Conversely, HDACs remove acetyl groups and so are associated with chromatin tightening (Konsoula and Barile, 2012b). Acetylation supports gene transcription in several ways. Firstly, the more relaxed chromatin state increases accessibility for transcriptional machinery to assemble on the unravelled target genes (Shahbazian and Grunstein, 2007, Konsoula and Barile, 2012b). In addition, the acetyl groups can be recognised by transcriptional activators via their bromodomain, thereby further assisting transcription initiation (Ruthenburg et al., 2007).

Histone deacetylation supports a transcriptional repressive state by removing the acetyl group that was acting to neutralise the positively charged lysine residue. The

now exposed positively charged lysine residues can interact with negatively charged DNA, causing the latter to wrap around histones like a spool of thread. This chromatin compaction blocks access of transcriptional machinery, thereby repressing gene expression (Shahbazian and Grunstein, 2007).

Figure 1.14. Transcriptional Regulation by Histone Acetylation. Histone acetylation by histone acetyltransferases (HATs), neutralises histone positive charge, promoting chromatin relaxation and therefore transcriptional activation. Histone deacetylation by histone deacetylases (HDACs), exposes histone positive charge, promoting chromatin compaction and therefore transcriptional repression (Chuang et al., 2009).

1.18 Histone Deacetylase Enzymes.

Histone deacetylase enzymes (HDACs) are responsible for the removal of acetyl groups from histone proteins and also a variety of non-histone proteins including transcription factors, transcription regulators, signal transduction mediators, DNA repair enzymes, nuclear import regulators, chaperone proteins, cytoskeleton proteins and inflammation mediators (Xu et al., 2007, Falkenberg and Johnstone, 2014). In humans, 18 HDAC enzymes have been identified and classified into four distinct classes (Table 1.4) based on homology to yeast HDACs (Blander and Guarente, 2004, Bhalla, 2005, Marks and Dokmanovic, 2005, Xu et al., 2007). HDAC classes include; class I HDACs (HDAC1, 2, 3 and 8), class II HDACs (HDAC4, 5, 7 and 9), class IIa (HDAC6 and 10), class III sirtuins (SIRT1-7) and class IV (HDAC11). Class III sirtuins have nicotinamide adenine dinucleotide (NAD+) cofactor dependent active sites. All other HDAC classes are independent of NAD+, but require zinc (Zn^{+2}) in their active site to carry out their enzymatic activity (Blander and Guarente, 2004). Cellular distribution of these enzymes differs between subfamilies (Table 1.4). Class I and IV subfamilies reside primarily in the nucleus, class IIB are mainly cytoplasm based, class IIA move between the nucleus and cytoplasm, and finally class III are scattered across the nucleus, cytoplasm and mitochondria (Konsoula and Barile, 2012b). Class I and II are the best characterised HDAC subfamilies. Class I HDACs are ubiquitously expressed in the nucleus of cells and exhibit strong deacetylating activity. They are structurally simple, consisting of short carboxy- and amino- terminal extensions alongside the conserved deacetylase domain (Haberland et al., 2009). Class IIa HDACs have much larger N-terminal extensions with binding sites for myocyte enhancer factor 2 (MEF2) transcription factor, rendering HDACs signal responsive. These HDACs are negatively regulated by kinases such as; protein kinase D (PKD) and calcium/calmodulin-dependent protein kinase (CaMK)(Vega et al., 2004a, Lu et al., 2000a). Upon phosphorylation, class IIa HDACs dissociate from MEF2 and move away from the nucleus and into the cytoplasm. MEF2 subsequently binds a HAT enzyme in place of the HDAC enzyme, promoting chromatin compaction and repressing transcription (Lu et al., 2000b, Miska et al., 1999, Sparrow et al., 1999, Haberland et al., 2009). Class IIa enzymes are expressed in specific tissues across the body. HDAC4 is found exclusively in the brain and growth plates of the skeleton (Vega et al., 2004b); HDAC5 and 9 are found in the heart, muscles and brain (Zhang

et al., 2002, Chang et al., 2004); HDAC7 is found occurring in endothelial cells and thymocytes (Chang et al., 2006). Class IIb, specifically HDAC6, is the primary mammalian cytoplasmic HDAC (Zhang et al., 2008). Class I HDACs appear to play a vital role in cell proliferation, in contrast with class II enzymes, which are associated with more tissue specific actions (Marks and Breslow, 2007). These differences in function are reflected in their expression distribution, with class I HDACs being ubiquitously expressed, whereas class II HDACs have more restricted expression patterns. HDAC repressor properties can be blocked by exposure to HDAC inhibitors, which are discussed in the following section.

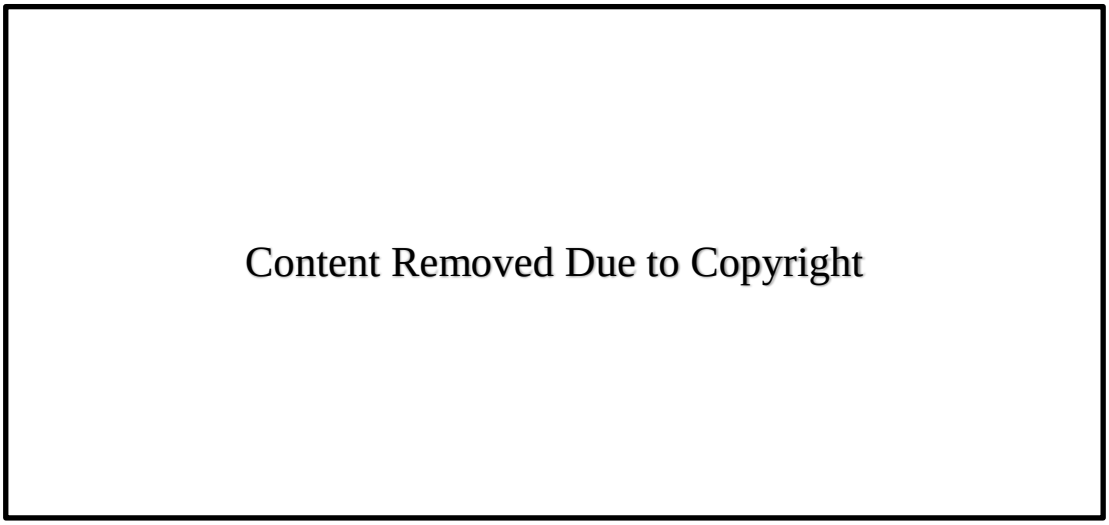

Table 1.4. HDAC Classification. HDAC enzymes are classified into four main subfamilies; class I, IIA, IIB, III and IV. These subfamilies differ in their NAD+ or Zn^{+2} requirements and cellular localisation (Konsoula and Barile, 2012b).

1.19 Histone Deacetylase Inhibitors.

Histone deacetylase inhibitors (HDACi) can alter gene expression by preventing removal of acetyl groups from histones and transcription factor complexes. By blocking class I and II HDAC activity, HDACi's promote a hyper-acetylated status, and subsequently a more relaxed chromatin, which enhances transcription machinery accessibility to DNA and transcription factor activity (Xu et al., 2005) (Glozak et al., 2005, Gryder et al., 2012). HDAC inhibitors have been isolated from both natural sources and synthetic compounds. This structurally diverse family of epigenetic repressors have different pharmacokinetic properties, target specificity and activity. HDAC inhibitors can be classified according to their structure as follows; (i) short-chain fatty acids; (ii) hydroxamic acids; (iii) cyclic peptides; (iv) benzamides; (v) ketones (Konsoula and Barile, 2012b). HDACi's also differ in their specificity, with some inhibiting all HDACs, referred to as pan-HDAC inhibitors, while others are class-specific (Bassett and Barnett, 2014).

The first HDAC inhibitor to be discovered was *n*-butyrate (Riggs et al., 1977). Butyrate is a short-chain fatty acid produced endogenously as a by-product of anaerobic bacterial fermentation of dietary fibre fermentation in the colon (Steliou et al., 2012). Butyrate was found to induce growth arrest and senescence in cancer cells (Terao et al., 2001). It was later uncovered that butyrate acted partly by inhibiting HDAC enzymes (Berni Canani et al., 2012). Efforts were made to capture the HDAC inhibiting properties of butyrate for therapeutic benefit in the treatment of cancer, where growth arrest and senesces are desirable. However these efforts were foiled by the poor pharmacokinetic profile of butyrate (first-pass hepatic clearance and short half-life) and the high doses required to reach therapeutic concentrations (Steliou et al., 2012).

Trichostatin A (TSA) was the first naturally occurring hydroxamic acid HDAC inhibitor to be discovered (Marks and Breslow, 2007). TSA was originally classified as an antifungal antibiotic but was later found to have potent HDAC inhibitory effects. TSA was shown to arrest the cell cycle at G1 and G2 phases, induce differentiation of cells and revert transformed cell morphology (Yoshida et al 1995). Suberoylanilide hydroxamic acid (SAHA) is another hydroxamic acid pan-HDAC inhibitor discovered after extensive screening and is currently the most advanced HDAC inhibitor in use (Bassett and Barnett, 2014). Both SAHA and TSA, have been FDA approved for the

treatment of cutaneous T-cell lymphoma. Treatment of transformed cells with either of these HDAC inhibitors alters the expression of a limited number (~2-10%) of genes. Among these genes are the cyclin-dependent kinase inhibitor p21 and the tumour suppressor p53, whose expression are increased following SAHA treatment. Increased p21 expression promotes cell cycle arrest in the G1 phase by blocking the assembly of cyclin-dependent kinase complexes essential for cell cycle progression (Gartel and Tyner, 1998). HDAC inhibitors have been found to induce cell death, but the mechanism has yet to be fully elucidated. It has been proposed that SAHA induces reactive oxygen species (ROS) production in transformed cells, but not normal cells. These reactive oxygen species enhance caspase activity, indirectly promoting cell death (Peart et al., 2005). Normal cell resistance to SAHA-induced ROS production is potentially a result of high thioredoxin levels. Thioredoxin is a potent ROS scavenger, thereby preventing cell death induction (Ungerstedt et al., 2005).

1.20 Concluding Remarks

NOD1 and NOD2 receptors have been linked to a wide range of chronic inflammatory diseases. Aside from the negative/positive protein regulators discussed in Section 1.9, regulation of receptor function is still in its infancy. Evidence has emerged over the past few years in the literature that could indicate a role for epigenetic modifications in NOD1 and NOD2 activity and expression, with global hypomethylated or hyperacetylated patterns being linked with states of chronic inflammation (Bayarsaihan, 2011, Karatzas et al., 2014, McDermott et al., 2016, Tsaprouni et al., 2011). These findings, alongside what is known about the influence of epigenetic modifications on gene expression, potentially provide an explanation for NOD1/NOD2 expression patterns identified in chronic inflammatory diseases. Uncovering the NOD1/NOD2 gene expression regulation mechanism is essential in order to gain a better understanding of NOD1/NOD2 dysfunction in chronic inflammatory diseases. If the epigenome is found to regulate expression/activity of NOD1/NOD2 receptors it could pave the way for novel therapeutic development.

1.21 Knowledge Gaps in the Published Literature

The following knowledge gaps existed in the published literature at the time of thesis project design;

- Mechanisms underlying aberrant NOD1 and NOD2 expression in states of chronic inflammation.
- The role played by the epigenome in regulation of NOD1 and NOD2 pro-inflammatory activity and expression.
- The effects of monocyte-to-macrophage differentiation on NOD1 and NOD2 pro-inflammatory activity and expression.

1.22 Hypothesis of Current Thesis.

Epigenetic modifications regulate NOD1 and NOD2 receptor activity and expression in intestinal epithelial cells and monocytes.

1.23 Objectives of Current Thesis.

The experimental work conducted for this thesis was designed to investigate the role of epigenetic modifications in NOD1 and NOD2 receptor pro-inflammatory activity and expression. The objectives of this experimentation were;

1. To investigate if NOD1 pro-inflammatory activity and/or expression is altered, in an intestinal epithelial cell line, under hypomethylating or hyperacetylating conditions.
2. To investigate if NOD2 pro-inflammatory activity and/or expression is altered, in an intestinal epithelial cell line, under hypomethylating or hyperacetylating conditions.
3. To investigate if NOD1 pro-inflammatory activity and/or expression is altered, in a monocytic cell line, under hypomethylating, hyperacetylating or differentiating conditions.
4. To investigate if NOD2 pro-inflammatory activity and/or expression is altered, in a monocytic cell line, under hypomethylating, hyperacetylating or differentiating conditions.

Chapter 2 Materials and Methods

2.1 Materials

Method	Product	Product Code	Supplier
Cell Culture Materials			
Cell Maintenance	RPMI-1640 Medium	G7513	Sigma Aldrich Ltd.
	McCoys 5A Medium	M8403	
	L-Glutamine	G7513	
	Penicillin/Streptomycin	P4333	
	Dulbecco's Phosphate Buffered Saline	D8537	
	Trypsin EDTA	T4174	
	Hanks Balanced Salt Solution	H9394	
	Trypan Blue	T8154	
	Fetal Bovine Serum	10270-106	Gibco (Life Technologies)
Differentiation	Phorbal 12-Myristate 13-Acetate	P8139	Sigma Aldrich Ltd.
Drug Treatments	5-Azacytidine	A2385	Sigma Aldrich Ltd.
	5-Aza-2-deoxycytidine	A3656	
	SAHA	Inh-SAHA	Invivogen
Receptor Ligands	iE-DAP	tlrl-dap	Invivogen
	TRI-DAP	tlrl-tdap	
	MDP	tlrl-mdp	
	LPS	tlrl-eklps	
Western Blotting Materials			
Cell Lysis	EGTA	E3889	Sigma Aldrich Ltd.
	Sodium Fluoride	S7920	
	Trizma Base	T1503	
	Sodium Chloride	S/3160/60	
	Sodium Deoxycholate	D6750	
	Sodium Orthovanadate	S6508	
	NP-40/Igepal CA-630	I7771	
	Protease Inhibitor Cocktail	P8340	
Bradford Assay	Bovine Serum Albumin	A9647	Sigma Aldrich Ltd.
	Bradford Reagent	B6916	
Buffer Prep	Trizma Base	T1503	Sigma Aldrich Ltd.
	Glycine	G8898	
	20% Sodium dodecyl sulphate	5030	
	Tween 20	P1379	
Sample prep	Glycerol	G5516	Sigma Aldrich Ltd.
	Bromophenol Blue	B0126	
	2-mercaptoethanol	M3148	

Method	Product	Product Code	Supplier
Gel electro-phoresis	30% Acrylamide	A3574	Sigma Aldrich Ltd.
	20% Sodium dodecyl sulphate	5030	
	Ammonium Persulfate	A3678	
	Tetramethylethylenediamine	T9281	
	Chameleon™ Duo Pre-stained Protein Ladder	P/N 928-60000	LI-COR Biosciences
Transfer	Trizma Base	T1503	Sigma Aldrich Ltd.
	Glycine	G8898	
	Nitrocellulose Membrane	10600003	GE Healthcare Life Sciences
	Filter Paper	11765345	Fisher Scientific
	Methanol	M/4062/17	
Blocking	Aptamil® Infant Milk	N/A	Supermarket
	Bovine Serum Albumin	A9647	Sigma Aldrich Ltd.
	Odyssey® Blocking Buffer (TBS)	P/N 927-50000	LI-COR Biosciences
Primary Antibodies	NOD1	3545	Cell Signalling Tech.
	NOD2	04-145	Millipore
	RSK1	9355	Cell Signalling Tech.
	p-RIP2	65746	
	p-p38	4511	
	p-ERK1/2	4370	
	p-p65	3033	
	p-IκBα	2859	
	Total RIP2	4142	
	Total p38	9926T	
	Total ERK1/2		
	Total p65	9936	
	Total IκBα		
	A20	5630	
	β-Actin	A5541	
	β-Tubulin	86298	
Secondary Antibodies	IRDye 800CW Goat anti-Rabbit IgG	926-32211	LI-COR Biosciences
	IRDye 680LT Goat anti-Mouse IgG	926-68020	
qPCR Materials			
RNA Isolation	High Pure RNA Isolation Kit	11828665001	Roche Ireland Ltd.
	Molecular Biology Grade Ethanol	BP2818-500	Fisher Scientific
	RNase AWAY ™	7002	ThermoFisher Scientific

Method	Product	Product Code	Supplier
Reverse Transcription	High Capacity cDNA Reverse Transcription Kit	4368813	Applied Biosystems
	Molecular Biology Grade Water	W4502	Sigma Aldrich Ltd.
qPCR	Lightcycler 480® Probes Master	04707494001	Roche Ireland Ltd.
	NOD1 primer	100188	
	NOD2 primer	102939	
	TNF-α primer	103295	
	IL-6 primer	144013	
	CDK2NA primer	101437	
	DNMT1 primer	102318	
	DNMT3B primer	110289	
	β-Actin primer	143636	
	β-Tubulin primer	119231	
	RPL13A primer	102119	
ELISA Materials			
Wash Buffers	Phosphate Buffered Saline Tablets	P4417	Sigma Aldrich Ltd.
Kits	Human TNF-α ELISA kit	88-7346	R & D systems
	Human IL-6 ELISA kit	88-7066	
	Human IL-8 ELISA kit	DY208	

Table 2.1. Materials utilised within the methods of the current thesis.

2.2 Cell Culture

Monolayer and suspension cell lines were used for the *in vitro* studies carried out; HCT116 intestinal cell line and THP-1 monocytic cell line, respectively.

2.2.1 Monolayer HCT116 intestinal epithelial cell line

HCT116 cells are an adherent cell line sourced from a primary culture of cells isolated from a human colonic carcinoma and supplied by American Type Culture Collection. Both wild type HCT116 (WT) and a DNMT3b knockout HCT116 ($DNMT3b^{-/-}$) variant were used to complete this work. $DNMT3b^{-/-}$ cells were generated in the Vogelstein lab by homologous recombination (Rhee et al., 2002). These cells grow as a monolayer on the hydrophilic growth surface of T25/T75/T175 culture flasks in a Hera Cell humidified incubator (Heraeus, Hanau, Germany) under standard conditions; 37 ℃, 5 % CO_2 and 95 % air. Cells were cultured in McCoys's 5A medium (Sigma Aldrich, M8403), supplemented to provide them with the appropriate growth conditions (Table 2.2). HCT116 cell density was monitored daily using the Trypan Blue Exclusion assay. To provide cells with an optimum growing environment, cell density was maintained at a concentration ranging between 2 x 10^5 cells/ml (low density) and 1 x 10^6 cells/ml (high density) (Figure 2.1).

Supplement (% v/v)	Purpose of Supplement
10% Fetal Bovine Serum	A source of essential embryonic growth factors for cell growth.
1.5% L-Glutamine	Acts as an alternative energy source to glucose and nitrogen atoms to meet high energy demands of the cells.
1% Penicillin/Streptomycin	Antibiotics that act synergistically to destroy gram-negative and gram-positive bacteria, blocking bacterial contamination.
0.1% Hygromycin	Additional antibiotic required to maintain the DNMT3b$^{-/-}$ knockout.

Table 2.2. Cell culture medium supplementation concentration (%v/v), alongside a description of purpose. Culture medium was supplemented with 10% fetal bovine serum, 1% penicillin/streptomycin and 1.5% L-glutamine to provide cells with an optimum growing environment. Culture medium for HCT116 DNMT3b-/- cells requires additional supplementation with 0.1% hygromycin to maintain the DNMT3b$^{-/-}$ genetic knockout.

Figure 2.1: HCT116 cell line. A) Low density state, with adequate space for further growth. Confluency typically observed when cells reached a density between 2 x 10^5 and 5 x 10^5 cells/ml. B) High density state, with minimal space left for further growth. Confluency typically observed when cells reached a density between 8 x 10^5 and 1 x 10^6 cells/ml (ATCC).

2.2.2 Sub-culturing HCT116 cell line

All reagents required for this process were warmed to 37 ºC using a water bath prior to retrieving flasks of cells from the incubator. Volumes of reagents required depended on flask size, see Table 2.3. Culture medium surrounding the adhered cells was removed from flask and discarded in Virkon disinfectant. Adhered cells were washed with Dulbecco's Phosphate Buffered Saline (PBS) (Sigma Aldrich, D8537), which was carefully pipetted down the side of the flask without the cells adhered to ensure not to detach the cells during washing. PBS was gently rocked over the adhered cells and subsequently discarded to remove residual medium. Trypsin-EDTA (Sigma Aldrich, T4174), diluted to a working concentration of 10 %v/v with Hanks Balanced Salt Solution (Sigma Aldrich, H9394), was pipetted onto the adhered cells and the flask was rocked back and forth to ensure even distribution. The flask was placed back in the incubator for approximately three minutes while the trypsin took effect. Following the three-minute incubation, the trypsin was neutralised with double the amount of complete McCoys medium, as highlighted in Table 2.3. The neutralised cell suspension was moved into 15 ml sterile tubes and spun in a centrifuge at 1400 rpm for five minutes. The resulting supernatant was discarded and cell pellets were re-suspended in fresh medium. Cell density was established using the haemocytometer method (see below). Cells were diluted accordingly to return cell density to the desired concentration; 2 x 10^5 cells/ml. This process was repeated every 24-48 hours, depending on the exponential growth phase of the cells.

Flask size	PBS (ml)	1X Trypsin (ml)	Neutralising Medium (ml)
T-25	3	1	2
T-75	5	4	8
T-175	10	5	10

Table 2.3: Reagent volumes for lifting adherent cells in various sized flasks. Flasks ranged in size from T-25 to T-175, smallest to largest. Different sized flasks required different volumes (ml) of PBS, trypsin and neutralising medium to lift adherent cells from flask surface.

2.2.3 Suspension THP-1 monocytic cell line

THP-1 cells are a suspension human monocytic cell line sourced from a one-year old male with acute monocytic leukaemia and were supplied by American Type Culture Collection. These cells grow as a suspension in T25/T75/T175 culture flasks in a Hera Cell humidified incubator (Heraeus, Hanau, Germany) under standard conditions; 37 ^{o}C, 5 % CO_2 and 95 % air. Cells are suspended in RPMI-1640 (Sigma Aldrich, G7513) medium supplemented to provide them with the appropriate growth conditions (Table 2.1). THP-1 cell density was monitored daily using the Trypan Blue Exclusion assay (see below). To provide cells with an optimum growing environment, cell density was maintained at a concentration ranging between 2 x 10^5 cells/ml (low density) and 1 x 10^6 cells/ml (high density) (Figure 2.2).

Figure 2.2: THP-1 cell line. A) Low density state, with adequate space for further growth. Confluency typically observed when cells reached a density between 2 x 10^5 and 5 x 10^5 cells/ml. B) High density state, with minimal space left for further growth. Confluency typically observed when cells reached a density between 8 x 10^5 and 1 x 10^6 cells/ml (ATCC).

2.2.4 Sub-culturing THP-1 cell line

All reagents required for this process were warmed to 37 ºC using a water bath prior to retrieving flasks of cells from the incubator. The cell suspension was moved into

15/50 ml sterile tubes and spun in a centrifuge at 1400 rpm for five minutes. The resulting supernatant was discarded, and cell pellets were re-suspended in fresh medium. Cell density was established using the haemocytometer method (see below). Cells were diluted accordingly to return cell density to the desired concentration; 2 x 10^5 cells/ml. This process was repeated every 24-48 hours, depending on the exponential phase of the cells.

2.2.5 Differentiating THP-1 cell line into Macrophages

THP-1 cells were treated with phorbal 12-myristate 13-acetate (PMA) (Sigma Aldrich, P8139) to differentiate the monocytic cell line into cells whose functional characteristics and phenotype closely resembled those of macrophages (Lund et al., 2016). A time and dose response for the PMA treatment was carried out to establish a standardised protocol. THP-1 cells were treated for 24/ 48/ 72 hours with 0 ng/ml, 1 ng/ml, 10 ng/ml or 100 ng/ml PMA. Cell adherence, RSK1 protein expression levels (Huber et al., 2015) and CD16+ cell surface markers (Italiani and Boraschi, 2014) were analysed to establish differentiation efficiency. Based on findings from this optimisation period, cells were chosen to be treated with 10 ng/ml of PMA for 48 hours for optimum differentiation. Following the 48-hour treatment period, the RPMI-1640 medium was replaced with fresh medium before subsequent treatments.

2.3 Determining cell density

Cell density was determined using the Trypan Blue Exclusion Assay. This assay is based on the concept that trypan blue is an impermeable dye that cannot penetrate the intact cell membrane of viable cells but can enter non-viable cells due to their compromised membrane integrity.

A 1:1 dilution of the cell suspension was made with 0.4 % Trypan Blue dye (Sigma Aldrich, T8154) and incubated at room temperature for 30 seconds. Ten µl of the homogenous cell/dye suspension was pipetted into a chamber of a Neubauer Improved Haemocytometer (Sigma Aldrich, BR717805) onto which a cover slip had been temporarily adhered. The haemocytometer was then placed under a CKX31 inverted light microscope (Olympus Corporation, Tokyo 163-0914, Japan) for investigation. The number of viable cells was counted within each of the four quadrants of the chamber, as highlighted in Figure 2.3. The general counting rule, followed to prevent

double counting cell, was to include any cells that touched the left and lower borders of each box within the four quadrants (Figure 2.3).

Worked example of a Typical Cell count:

A) Top Left Quadrant = 46 cells

B) Top Right Quadrant = 40 cells

C) Bottom Left Quadrant = 38 cells

D) Bottom Right Quadrant = 42 cells

Total Cell Count = 166 cells in the haemocytometer chamber

The total cell count then had to be mathematically manipulated to determine the cell density.

(i) *Average number of cells per Quadrant*

166 cells per chamber ÷ 4 = 41.5 cell per quadrant

(ii) *Factor in 1:1 dilution with Trypan Blue*

41.5 cells/quadrant x 2 = 83 cells per quadrant (undiluted)

(iii) *Cell Density*

The dimensions of a quadrant are 1mm x 1mm x 0.1mm i.e. (1×10^{-4} cm^3)

83 cells/quadrant x 10^4 = 445,000 cells/ml

→ Cell Density = 830,000 cells/ml

This assay was carried out during cell maintenance, to ensure cultures were maintained below 1×10^6 cells/ml. It was also utilised to establish dilutions required to reduce cell density to the optimum seeding density for subsequent treatments.

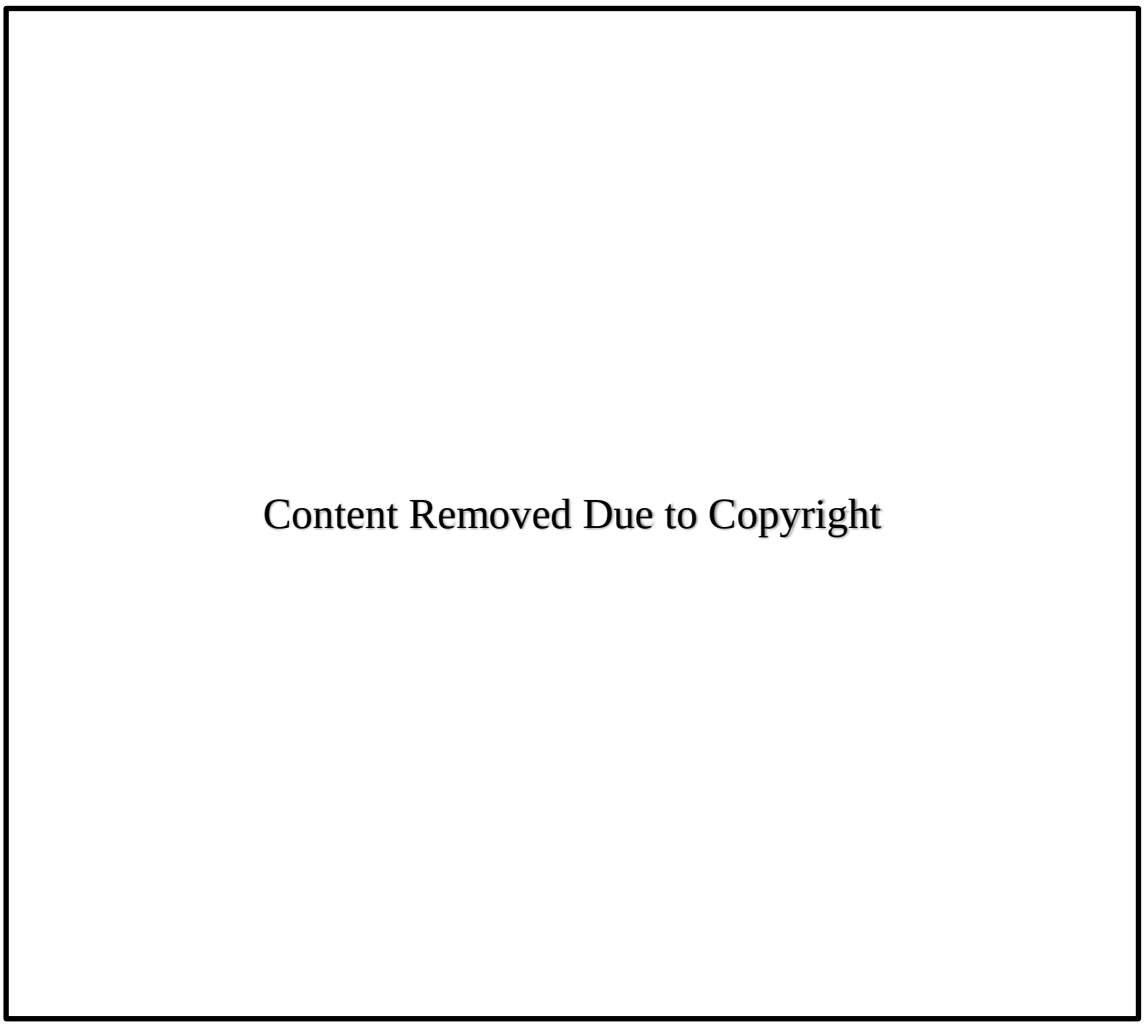

Figure 2.3: Counting chamber of a haemocytometer. Each chamber of a haemocytometer contains four counting quadrants marked A-D. The numbers of viable cells within the boundaries of these counting quadrants were recorded. The general rule followed when counting was to include cells lying on the left and lower boundaries.

2.4 Seeding cells for treatments

Cell suspension density was determined using the Trypan Blue Exclusion Assay, as described in Section 2.3. The desired density for receiving treatments varied with the assay and agent type (Table 2.4). The dilution factor required to reduce the cell density to the appropriate concentration was calculated and the cell suspension was diluted accordingly with fresh culture medium in a sterile tube. This diluted cell suspension was inverted several times to ensure homogeneity and subsequently distributed across culture plate wells. THP-1 cells were ready to be treated immediately after seeding, whereas adherent HCT116 cells required 24 hours to adhere to the plate surface before receiving treatment.

Assay Type	Agent Type	Cell density per well	Cell culture plate	Well capacity (µl)
MTT	All agents	200,000 cells/ml	96-well	200
mRNA and protein sample generation	Agents not inducing significant cell death (DNMTi, NOD1/2 ligands and cytokines)	250,000 cells/ml	6-well	2000
	Agents inducing significant cell death (SAHA and PMA)	400,000 cells/ml	6-well or 5 ml	2000 / 5000
ELISA	Agents not inducing significant cell death (DNMTi, NOD1/2 ligands)	200,000 cells/ml	24-well	500
	Agents inducing significant cell death (SAHA and PMA)	400,000 cells/ml	24-well	500

Table 2.4: Seeding cells for treatments. The cell density and culture plates chosen to be used depended on the assay and agent type.

2.5 MTT Assays

This assay was used to investigate the cell viability following exposure to potentially cytotoxic agents used over the course of this research. MTT (3-(4,5-Dimethylthiazol-2-yl)-2,5-diphenyltetrazolium bromide, a tetrazole) (Sigma Aldrich, M2128) is reduced to purple formazan in the mitochondria of living cells. MTT is only reduced when mitochondrial reductase enzymes are active, meaning formazan production can be directly related to the number of viable cells. The agent concentrations and exposure times chosen to be investigated are outlined in Table 2.5.

Agent Type	Agent	Concentrations	Time points (hrs)
Epigenome targeting drugs	5-Azacytidine	0.5, 1, 5, 10, 50 μM	24, 48, 72
	5-Aza-2-deoxycytidine	0.1, 0.5, 1, 5, 50 μM	24, 48, 72
	SAHA	1, 10, 100 μM	24, 48, 72
	TSA	1, 10, 100 μM	24, 48, 72
NOD1/2 Ligands	iE-DAP	1, 10, 100 ng/ml	1, 3, 6, 24
	TRI-DAP	1, 10, 100 ng/ml	1, 3, 6, 24
	MDP	1, 10, 100 ng/ml	1, 3, 6, 24

Table 2.5: MTT assay agent concentrations and exposure times. Cytotoxicity of epigenome targeting drugs and NOD1/2 ligands were analysed at various concentrations and time points.

The main stock of each agent was diluted accordingly to generate several stock solutions to ensure the same volume of agent (20 μl) was added to each well, bringing the cell suspension volume in each well to 220 μl. All treatments were carried out with six replicates for each concentration and time point. Each plate also included six "Untreated" wells, which contained cells that would receive no agent treatment, and six "Blank" wells, which were cell-free wells containing only culture medium. These control groups received 20 μl of culture medium instead of the agent of interest.

After the treatment, MTT solution (Table 2.6) was added to each well so that the MTT was diluted 1:10 (i.e. 22 μl of MTT was added to wells containing 220 μl of treated cell suspension.) and placed back in the incubator under standard culture conditions for three hours. Following this incubation period, the medium was carefully removed and discarded. MTT solvent was prepared as outlined in Table 2.6. Each well received 150 μl of MTT solvent, after which the plate was covered with tin foil and placed on an orbital shaker for 15 minutes to agitate cells and assist the dissolving of formazan crystals. The plate was placed in a spectrophotometer and the absorbance was read at 570 nm. Absorbance readings were used, according to the formula in Figure 2.4, to establish the percentage cell viability following exposure to the agents.

MTT Reagent	Final Volume	Component	Quantity
MTT Solution (5 mg/ml)	1 ml	Thiazolyl Blue Tetrazolium Bromide (MTT)	5 mg
		Phosphate Buffered Saline	1ml
MTT Solvent	50 ml	NP-40 (Igepal)	50 µl
		1 M HCL	200 µl
		Isopropyl Alcohol	49.75 ml

Table 2.6: MTT assay reagent components. Reagents volumes required to make up MTT solution (5 mg/ml) and MTT solvent.

$$\% \text{ Cell Viability} = \left[\frac{(\text{Absorbance} - \text{Blank})}{\text{Average (Absorbance} - \text{Blank) of Untreated Sample}} \right] \times 100$$

Figure 2.4: Percentage Cell Viability Formula. The blank absorbance was subtracted from each sample absorbance. The average (Absorbance – blank) for the untreated sample was divided into each sample. This value was multiplied by 100 to give a percentage cell viability value.

2.6 Cell treatments

Cells were seeded as outlined in section 2.4. Agent concentrations and exposure times, outlined in Table 2.7, were chosen based on their ability to induce a response without significantly diminishing cell viability (Appendix 1 and 2).

Treatment Type	Agent	Concentration	Exposure Time
DNA Methyltransferase 1 Inhibitors (DNMT1i)	5-Azacytidine	5 μM	72 hr (24hr Spiking)
	5-Aza-2-deoxycytidine	500 nM	72 hr (24hr Spiking)
Histone Deacetylase Inhibitors (HCACi)	SAHA	10 μM	48 hr
	TSA	10 μM	48hr
NOD1 Ligands	IE-DAP	10 μg/ml	3, 6, 24 hr
	TRIDAP	10 μg/ml	1, 6, 24 hr
NOD2 Ligands	MDP	10 μg/ml	2, 6, 24 hr
Differentiation	PMA	10 ng/ml	48 hr

Table 2.7: Treatment concentrations and exposure times. Working concentrations and exposure times of DNMT1 inhibitors, HDAC inhibitors, NOD1/2 ligands and differentiating agent used throughout the course of this research.

DNA methyltransferase 1 inhibitor treatments required spiking at 24-hour intervals, due to their short half-life and cytotoxic metabolites. This process involved changing the culture medium in each treatment well and adding a fresh aliquot of DNMTi.

2.6.1 Stopping HCT116 cell treatments

Culture medium was removed, leaving the cells adhered to the treatment well surface, and either discarded or stored at -80ºC for ELISA analysis. The monolayer of cells was gently washed with PBS to remove culture medium residue from each well. The monolayer of washed cells was covered with PBS and a cell scrapper was used to lift the cells off the plate surface, releasing them into the PBS. The PBS-cell suspension was removed from each well and transferred into 2 ml sterile eppendorfs and centrifuged at 1400 rpm for five minutes. The supernatants were discarded, and pellets were resuspended in either 400 μl RNA lysis buffer or 25 μl of protein lysis buffer for analysis.

2.6.2 Stopping THP-1 cell treatments

THP-1 suspension cells were pipetted directly out of each well and into sterile 2 ml eppendorfs and centrifuged at 1400 rpm for five minutes. Supernatants were either discarded or stored at -80ºC for ELISA analysis. Cell pellets were washed by re-suspending them in 1 ml of PBS and subsequently centrifuging them at 1400 rpm for five minutes. The supernatants were discarded, and pellets were resuspended in either 400 µl RNA lysis buffer or 25 µl of protein lysis buffer for analysis.

2.7 RNA Analysis

2.7.1 Total RNA Isolation

Total RNA extraction was carried out on cells using the High Pure RNA Isolation Kit (Roche, 11828665001), according to the manufacturer's instructions. Cell suspensions were spun in a centrifuge at 1400 rpm for five minutes and supernatants were discarded. Cell pellets were re-suspended in 400 µl of lysis buffer and vortexed to break open cells and release cellular contents. Lysates were subsequently run through purification spin columns, trapping nucleic acids in the glass fibre fleece. Columns were treated with DNase to degrade trapped DNA, thereby leaving only RNA in the column. This was followed by a series of washes with supplied wash buffers to remove any contaminating protein and precipitate RNA. Filter tubes were transferred into RNase/DNase free eppendorfs and collection tubes were discarded. The purified RNA was eluted from the glass fibre fleece, using the provided elution buffer, into the RNase/DNase free eppendorfs.

2.7.2 Total RNA Quantification and Normalisation

Total RNA concentration (ng/µl) was measured using a NanoDrop™ spectrophotometer (Maestrogen, Las Vegas, USA), according to the manufacturer's instructions. The purity of the RNA was established by recording the ratio of absorbancies at 260nm:280nm. Total RNA was normalised to 500-1000 ng per reaction using sterile PCR grade water.

2.8 Reverse Transcription

Reverse transcription was carried out using the High Capacity cDNA Reverse Transcription kit (Applied Biosystems, 4368813), according to the manufacturer's instructions. The MultiScribe™ Reverse Transcriptase provided in the kit was used at a concentration of 50 U/µl, as part of the reverse transcriptase (RT) mix (Table 2.8). 20 µl reactions were carried out in 0.5 ml RNase/DNase free tubes, consisting of equal volumes of normalised RNA and RT mix. A negative control, consisting of 10µl of sterile PCR grade water with 10 µl of RT mix, was included when generating a batch of cDNA to ensure the reagents were not contaminated. The tubes were placed in the thermal cycler (MJ Research, PTC200) and set to the optimized programme for the High Capacity cDNA Reverse Transcription kit, as in Table 2.9 below. Final samples were removed from the cycler and stored at -20˚C until further analysis was ready to be performed.

Component	Volume (µl)
	Per Reaction
10X RT Buffer	2.0
10X RT Random Primers	2.0
25X dNTP Mix	0.8
MultiScribe® Reverse Transcriptase	1.0
Nuclease Free Water	4.2
	10.0

Table 2.8: Reverse Transcriptase Mix Components. The required volume of each component (µl) for a reverse transcription reaction.

Step	Temperature (ºC)	Duration (hr:min:sec)
1	25	00:10:00
2	37	02:00:00
3	85	00:05:00
4	4	∞

Table 2.9: Reverse Transcription Programme. The thermal cycler was programmed to raise the sample temperature to 25˚C for 10 minutes, 37˚C for 120 minutes, 85˚C for five minutes and finally 4˚C until ready to be removed for storage at -20˚C.

2.9 Quantitative PCR

Quantitative PCR (qPCR) was carried out using the LightCycler® 480 System (Roche, 05015278001) and LightCycler® Probes Master (Roche, 04707494001). The forward and reverse primers for each gene of interest and chosen housekeeping gene were designed and supplied by the Roche Universal ProbeLibrary software (Table 2.10). The housekeeping genes chosen to act as the endogenous controls were β-Actin (Roche, 143636), β-Tubulin (Roche, 119231) or RPL13A (Roche, 102119). 10 µl qPCR reactions, carried out in triplicate in 96-well LightCycler® plates (Sarstedt, 72.1982.202), consisted of 1 µl cDNA mixed with 9 µl of Primer-Probe Master mix (Table 2.11). The "no template" (negative) control, generated for each batch of samples during reverse transcription, was also plated in triplicate for each primer, eliminating the generation of potential false positive amplification results. The plate was covered with optically clear sealing tape (Sarstedt, 95.1994) and placed in the LightCycler® 480 system and the programme was set up as outlined in Table 2.12.

Amplification curves of "Fluorescence vs Cycle Number" were generated. A Cycle Threshold (Ct) was set for each curve to eliminate background fluorescence (Figure 2.5). The LightCycler 480® software calculated the Ct value, which is the number of amplification cycles required to cross the set cycle threshold point, for each sample. If a gene is highly expressed it would take fewer amplification cycles to cross the set threshold than a gene of low expression, meaning Ct values are inversely proportional to gene expression levels. Therefore, Ct values were transformed via the $2^{-\Delta Ct}$ mathematical method (Livak and Schmittgen, 2001), to generate data that is visually representative of expression levels. These $2^{-\Delta Ct}$ values were further transformed, generating fold change values relative to the untreated samples.

Target Gene	Assay I.D.	Forward Primer	Reverse Primer
TNF	103295	TCCTCACCCACACCATCAG	GATGGCAGAGAGGAGGTTGA
IL6	144013	ACCGGGAACGAAAGAGAAG	GAAGGCAACTGGACCGAAG
β-Actin	143636	TCCTCCCTGGAGAAGAGCTA	CGTGGATGCCACAGGACT
GAPDH	101128	CTCTGCTCCTCCTGTTCGAC	ACGACCAAATCCGTTGACTC
β-Tubulin	119231	TGTACTACAACGAAGCCTACGG	GAGAGCTCCTAATTTGCTAGATCG
RPL13A	102119	CTGGACCGTCTCAAGGTGTT	GCCCCAGATAGGCAAACTT
CDK2NA	101437	GTGGACCTGGCTGAGGAG	TCTTTCAATCGGGGATGTCT
DNMT1	102318	GATGTGGCGTCTGTGAGGT	CCTTGCAGGCTTTACATTTCC
DNMT3B	110289	CCGAGAACAAATGGCTTCA	TTCCTGCCACAAGACAAACA
NOD1	100188	AGGCCTCACGCATCTTAAAC	ACAGCCAGGGCGAGATACT
NOD2	102939	CATGGCTAAGCTCCTTGCAT	CGCGGCAGTGATGTAGTTATT

Table 2.10: Roche PCR Primer Assay I.D. and Sequences. Assay I.D. and forward/reverse sequences of primers used to analyse expression of target genes.

Master Mix Components	Volume per well (µl)
Primer	0.5
Probe Master Mix (FastStart Taq DNA polymerase, reaction buffer, dNTP mix and 6.4 mM MgCl2	5.0
Nuclease Free Water	3.5
	9

Table 2.11: Primer-Probe Master Mix Components. Volumes (µl) of target gene primers, probe master mix and nuclease free water required to carry out qPCR.

Process	Cycle Number	Temperature (°C)	Time (hr:min:sec)
Denaturation	1	95	00:10:00
Amplification	45	95	00:00:15
		60	00:00:30
Cooling	1	40	00:00:10

Table 2.12: LightCycler® 480 Programme. The prepared plate was subjected to one cycle of denaturation (95˚C for 10 minutes), 45 cycles of Amplification (95˚C for 15 seconds, 60˚C for 30 seconds) and one cycle of cooling (40˚C for 10 seconds).

Figure 2.5. qPCR Amplification Plot. Amplification curves of "Fluorescence vs Cycle". A Cycle Threshold (Ct) was set to eliminate background fluorescence. Ct values generated by the LightCycler 480® system are the number of amplification cycles required to cross the set cycle threshold point (Talkington, 2013).

2.10 Protein Analysis

2.10.1 Protein sample preparation

A 990 µl aliquot of protein lysis buffer (Table 2.13) was thawed, to which 10 µl of protease inhibitor (Sigma Aldrich, P8340) was added. Cell pellets were re-suspended in 25-50 µl of the prepared lysis buffer. Samples were either lysed immediately or stored at -20ºC until ready to lyse.

Protein lysis buffer component	Concentration
Ethylene Glycol Tetra-acetic Acid	50 mM
Sodium Fluoride	50 mM
Tris-Hydrochloric Acid	1 M
Sodium Chloride	5 M
Sodium Deoxycholate	0.25 %
Sodium orthovanadate	1 mM
NP-40/Igepal CA-630	
Before use add: Protease Inhibitor	**1 %**

Table 2.13: Protein lysis buffer preparation. Protein lysis buffer components and their corresponding concentrations to make a working stock of lysis buffer.

2.10.2 Protein sample lysis

Thawed samples were placed on ice and vortexed at 10-minute intervals, over a 40-minute period, placing the samples back on ice after each vortex. For phosphorylated protein samples, after the 40-minute vortexing/icing period each sample was sonicated to ensure nuclear proteins were released.

2.10.3 Bradford Assay

The Bradford protein assay was carried out to quantify protein sample concentration (µg/ml). The principle underlying this assay is that protein molecules binding to the Coomassie Brilliant Blue G-250 of Bradford Reagent (Sigma Aldrich, B6916) under acidic conditions causes a colour change from brown to blue, which can be detected at 595 nm. A series of standards (0, 100, 250, 500, 750, 1000, 1500 and 2000 µg/ml) were generated from a 2 mg/ml stock concentration of Bovine Serum Albumin (BSA)

(Sigma Aldrich, A9647), as outlined in Table 2.14. Protein samples were diluted 1:10 to ensure they fell within the standard concentration range. Standards and unknown samples were pipetted in triplicate (5 µl/well) into a 96-well plate. Bradford reagent was subsequently added to each well (250 µl/well) using a multi-channel pipette and the plate was covered in tinfoil. The plate was placed on an orbital shaker for 30 seconds after which it was incubated at room temperature for 20 minutes. A microplate spectrophotometer was used to read the plate at a wavelength of 595 nm. The absorbance values were exported to an Excel file for analysis. The mean absorbance reading for the 0 µg/ml BSA standard, referred to as the blank, was subtracted from all the other standard and sample readings. GraphPad® Prism software (San Diego, California) was used to construct a standard curve for the BSA standards, plotting BSA concentration (µg/ml) vs Absorbance minus blank at 595 nm. Unknown protein concentrations were interpolated from the standard curve and multiplied by the dilution factor to establish the final concentration in each sample. Protein concentrations could then be normalised to 30 µg/ml, using deionised water, for subsequent Western blot analysis.

BSA Concentration (µg/ml)	2 mg/ml BSA Stock (µl)	dH_20 (µl)
0	0	200
100	10	190
250	25	175
500	50	150
750	75	125
1000	100	100
1500	150	50
2000	200	0

Table 2.14: Bradford Assay Standards. Volumes of BSA stock (µl) and deionised water (µl) required to generate the range of standards (0-2000 µg/ml) essential for carrying out a Bradford assay.

2.11 Western Blot Protein Analysis

Several buffers, outline in Table 2.15, were prepared before starting western blot analysis.

Buffer	Components	Concentration
4X Sample Buffer	Sodium dodecyl sulphate	0.06 M
	Tris-Hydrochloric Acid	1 M
	Glycerol	0.87 M
	Bromophenol Blue	0.03 M
	Before use add: 2-mercaptoethanol	**5%**
5X Running Buffer	Trizma Base	0.12 M
	Glycine	1.44 M
	Sodium dodecyl sulphate	0.5 %
10X Transfer Buffer	Trizma Base	247.65 M
	Glycine	1.92 M
10X Tris-Buffered Saline (TBS) pH = 7.6	Trizma Base	50 mM
	Sodium Chloride	150 mM
1X Tris-Buffered Saline and Tween (TBST)	10X TBS	10%
	Tween® 20	0.1%

Table 2.15: Western blot buffers prepared in-house. Reagent concentrations required to prepare western blotting buffers including; 4X sample buffer, 5X running buffer, 10X transfer buffer, 10X TBS and 1X TBST.

2.11.1 Polyacrylamide gel (PAGE) preparation

PAGE gels used to carry out the western blotting presented in the current research were hand-cast. Glass plates were cleaned with methanol to remove any residue acrylamide from previous use. A rubber gasket was positioned around the raised edges of the shorter plate, after which the spacer plate was lowered on top. The plates and gasket were held together by a set of clamps.

PAGE gels consist of a stacking gel and resolving gel. The percentage of acrylamide in the resolving gel determines the rate of protein migration and degree of protein separation. Low molecular weight proteins require high percentage gels for sufficient resolution, whereas higher molecular weight proteins are best resolved on lower

percentage gels. Therefore, the percentage of acrylamide in the resolving gel was chosen based on the protein of interests' molecular weight, as outlined in Table 2.16. The proteins investigated over the course of this research required the use of 8 % and 10 % resolving gels, whose components are outlined in Table 2.17. The polymerisation initiator, ammonium persulfate (APS), was made fresh on the day of gel preparation to ensure its best performance. APS and tetramethylethylenediamine (TEMED), the polymerisation catalyst, were added to the gel mix immediately prior to pouring the gel since polymerisation begins once they are added. Resolving gel (5.6ml) was poured between the plates. A thin layer of 2-propanol was added immediately after pouring the gel to expel any bubbles, creating a sharp divider between the resolving and the subsequent stacking gel. Once the resolving gel set, the 2-propanol was drained off before adding the stacking gel. Regardless of protein molecular weight, the stacking gel always consisted of 5 % polyacrylamide. The components of the stacking gel are outlined in Table 2.18. Stacking gel (3 ml) was pipetted onto the polymerised resolving gel. The comb, required to form sample wells, was inserted into the poured stacking gel immediately. The gel was left to set at room temperature, after which the plates were wrapped in wet tissue paper to keep the gels hydrated and stored at 4 ºC overnight.

% Acrylamide Gel	Protein Size (kDa)	Proteins Run
20	4-40	N/A
15	12-45	N/A
12.5	10-70	N/A
10	15-100	MAPK and NF-κB proteins
8	25-200	NOD1 and NOD2

Table 2.16: Choosing an appropriate resolving PAGE gel. The percentage (%) PAGE gel hand-cast (8-20%) for running samples was chosen based on the molecular weight of the protein of interest (4-200 kDa).

Components	8 % Resolving Gel (ml per gel)	10 % Resolving Gel (ml per gel)
30 % Acrylamide	2.13	3.33
1.5 M Tris-HCL (pH = 8.8)	2.00	2.50
10% Sodium dodecyl sulfate	0.08	0.00
20% Sodium dodecyl sulfate	0.00	0.05
Deionised H_20	3.70	4.05
10 % Ammonium persulfate	0.08	0.10
TEMED	0.008	0.005

Table 2.17: Components of the 8% and 10% resolving gels. Volumes of acrylamide, 1.5M Tris-HCL, 10/20% sodium dodecyl sulfate, deionised H20, ammonium persulfate and TEMED required to cast either an 8 or 10% resolving gel.

Components	5 % Stacking Gel (ml per gel)
30 % Acrylamide	0.825
1 M Tris-HCL (pH = 6.8)	1.250
20% Sodium dodecyl sulfate	0.025
Deionised H_20	2.845
10 % Ammonium persulfate	0.050
TEMED	0.005

Table 2.18: Components of the 5 % stacking gel. Volumes of acrylamide, 1M Tris-HCL, 20% sodium dodecyl sulfate, deionised H20, ammonium persulfate and TEMED required to cast the 5% stacking gel used in every hand-cast PAGE gel.

2.11.2 Gel electrophoresis

Normalised protein samples to be analysed were thawed and placed on ice. An aliquot of 4X sample buffer (Table 2.15) was thawed and prepared for use by adding 50 µl of 2-mercaptoethanol (Sigma Aldrich, M3148) in a fume hood. The prepared sample buffer was vortexed and 5 µl was pipetted into each 15 µl normalised protein sample. It was essential to vortex the sample buffer at regular intervals to ensure the glycerol was evenly distributed, thereby guaranteeing each sample would contain sufficient glycerol to support efficient loading into acrylamide gel wells. Protein samples with

sample buffer added were placed on a heating block, set at 95 ºC, for seven minutes to denature proteins. After the denaturation, samples were centrifuged at 1400 rpm for 30 seconds to return any sample that had condensed on the eppendorf lid/sides during denaturation to the base of the tube. The 20 µl of prepared samples were loaded alongside 5 µl of Chameleon Duo Pre-stained protein ladder (LI-COR Biotechnology, 928-60000). Gels were run through the stacking gel at 80 volts. Once the samples reached the top of the resolving gel, the voltage was increased to 120 volts until the dye front had run to the end of the gel.

2.11.3 Transfer of proteins onto nitrocellulose membrane

Wet transfer was carried out over the course of this research. Transfer sponges, filter paper and nitrocellulose membrane were soaked in prepared 1X transfer buffer. The transfer cassettes were opened, and a single sponge was placed on the black side of the cassette. A single layer of pre-soaked filter paper was placed on the sponge, after which the gel that had undergone electrophoresis was released from the plates and carefully slid onto the filter paper. The pre-soaked nitrocellulose membrane was placed on top of the gel and was subsequently rolled with a supplied roller to dissociate any bubbles that may have been trapped between layers and potentially impede the transfer. An additional layer of wet filter paper was placed over the membrane, followed by another round of light rolling. Finally, another sponge was place on the filter paper, after which the cassette was closed and placed in the transfer tank, ensuring to face cassette sides red-to-red and black-to-black. The transfer tank was connected to a power supply and run at 70 volts for 1 hour and 45 minutes. Once complete the membrane was lifted off the gel and transferred into a plastic box, with the side that was in direct contact with the gel facing upwards. The membrane was stained with Ponceau stain (Sigma Aldrich, P7170), as in Figure 2.6, to check that the transfer was successfully and that samples had been evenly loaded. The membrane was washed once with 1X TBS for five minutes to remove the stain, leaving the membrane ready for blocking.

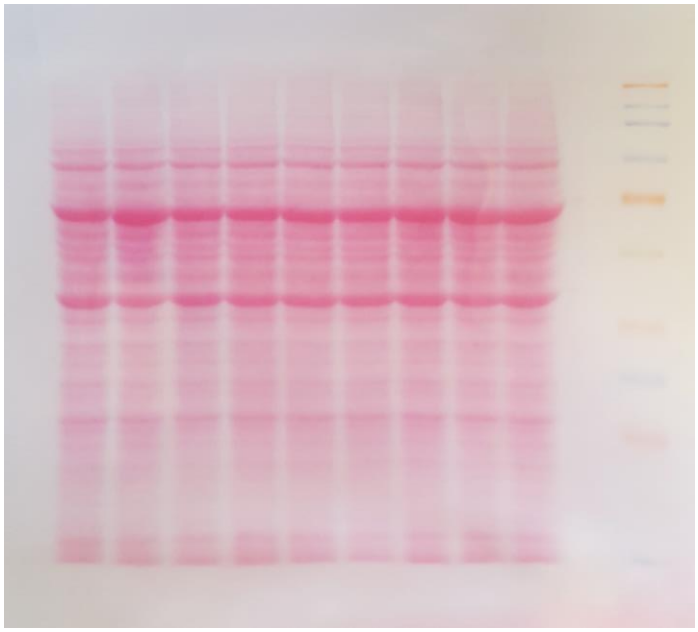

Figure 2.6: Ponceau stain of nitrocellulose membrane after transfer. The ponceau stain binds to and temporarily stains proteins transferred onto the nitrocellulose membrane, allowing for confirmation of transfer and equal loading across wells.

2.11.4 Blocking membrane

The membrane was blocked with one of three blocking buffers; 5 % milk, 5 % BSA or Odyssey® TBS Blocking Buffer (LI-COR, P/N 927-50000). This choice was dependant on the protein to be investigated, as outlined in Table 2.19. The membrane was left to block at room temperature for one hour.

Blocking Buffer	Protein of Interest
5 % Milk in 0.1 % TBST	NOD1
	NOD2
	RSK1
	A20
	β-Actin
	β-Tubulin
5 % Bovine Serum Albumin (BSA) in 0.1 % TBST	Total MAPK and NF-κB proteins
Odyssey® (TBS) Blocking Buffer (ready-to-use)	Phosphorylated MAPK and NF-κB proteins

Table 2.19: Choosing a blocking agent. The blocking agents used over the course of this research included; 5% Milk, 5% BSA or Odyssey® TBS blocking buffer. The appropriate blocking buffer was chosen based on the protein being investigated.

2.11.5 Primary Antibody Preparation and Incubation.

Primary antibodies, outlined in Table 2.20, were made up in same solution that the membrane was blocked in. Once blocking was complete, the blocking solution was discarded, and the prepared primary antibody was poured onto the membrane and incubated overnight on an orbital shaker at 4 °C. Once the incubation was complete, the primary antibody was removed, and the membrane was washed with 0.1 % TBST to remove excess antibody. The washing procedure involved pouring ~10 ml of 0.1 % TBST onto the membrane and placing it on a rocker for five-minutes, after which the TBST was discarded and the process was repeated three more times.

Primary Antibody	Dilution	Diluent
NOD1	1:1000	5% Milk in 0.1% TBST
NOD2	1:500	5% Milk in 0.1% TBST
RSK1	1:1000	5% Milk in 0.1% TBST
A20	1:1000	5% Milk in 0.1% TBST
p-RIP2	1:1000	Odyssey® (TBS) Blocking Buffer
p-p38	1:1000	Odyssey® (TBS) Blocking Buffer
p-ERK1/2	1:1000	Odyssey® (TBS) Blocking Buffer
p-p65	1:1000	Odyssey® (TBS) Blocking Buffer
p-IκBα	1:1000	Odyssey® (TBS) Blocking Buffer
Total RIP2	1:1000	5% BSA in 0.1% TBST
Total p38	1:1000	5% BSA in 0.1% TBST
Total ERK1/2	1:1000	5% BSA in 0.1% TBST
Total p65	1:1000	5% BSA in 0.1% TBST
Total IκBα	1:1000	5% BSA in 0.1% TBST
β-Actin	1:10000	5% Milk in 0.1% TBST
β-Tubulin	1:1000	5% Milk in 0.1% TBST

Table 2.20: Primary antibody preparation. Primary antibodies were made up to their suggested dilution using a diluent that matched the blocking agent for the membrane.

2.11.6 Secondary Antibody Preparation and Incubation.

Two secondary antibodies were used over the course of this research; IRDye 800CW Goat anti-Rabbit (LI-COR, 926-32211) and IRDye 680LT Goat anti-Mouse (LI-COR, 926-68020). The choice of which secondary antibody to use was made based on the primary antibody source, as outlined in Table 2.21. Monoclonal antibodies raised in rabbits (phosphorylated/total MAPK/NF-κB proteins, NOD1, RSK1 and A20) were detected using the goat anti-rabbit secondary antibody, which fluoresces green at 800 nm. Monoclonal antibodies raised in mice (Total IκBα, β-Actin, β-Tubulin and NOD2) were detected using the goat anti-mouse secondary antibody, which fluoresces red at 680 nm. The secondary antibodies were diluted 1:10000, in the same agent chosen for blocking and primary antibody incubation. The prepared secondary antibody was poured onto the membrane and allowed to incubate at room temperature, and out of direct sunlight, for one hour. Once the incubation was complete, the secondary antibody was poured away, and the membrane was washed with 0.1 % TBST to remove excess antibody. The washing procedure involved pouring ~10 ml of 0.1 % TBST onto the membrane and placing it on a rocker for five-minutes, while keeping it out of direct sunlight, after which the TBST was discarded and the process was repeated three more times.

Primary Antibody Origin	Primary Antibody	Secondary Antibody for Detection
Rabbit	p-RIP2	Goat anti-Rabbit (800 nm, Green Channel)
	p-p38	
	p-ERK	
	p-p65	
	p-IκBα	
	Total RIP2	
	Total p38	
	Total ERK	
	Total p65	
	NOD1	
	RSK1	
	A20	
Mouse	Total IκBα	Goat anti-Mouse (680 nm, Red Channel)
	β-Actin	
	β-Tubulin	
	NOD2	

Table 2.21: **Choosing the appropriate secondary antibody to detect the primary antibody.** Monoclonal antibodies raised in rabbits (phosphorylated/total MAPK/NF-Kb proteins, NOD1, RSK1 and A20) or mice (Total IκBα, β-Actin, β-Tubulin and NOD2) were detected using either goat anti-rabbit (fluoresces green at 800 nm) or goat anti-mouse (fluoresces red at 680 nm) secondary antibodies, respectively.

2.11.7 Imaging western blot.

Western blots were imaged using the Odyssey® Fc Imaging System (LI-COR Biotechnology, Cambridge, UK). Fluorescent secondary antibodies were excited at different wavelengths, with the goat anti-rabbit antibody fluorescing green at 800 nm and the goat anti-mouse fluorescing red at 680 nm. The output from this system consisted of protein bands that could be analysed in Image Studio™ Lite software by densitometry, as depicted in Figure 2.7. The protein expression was quantified relative to that of the housekeeping gene or total protein, to account for any differences in loading that could otherwise skew the data. Fold changes in protein relative expression were calculated relative to the control group. This fold change data was plotted, and statistical analysis was carried out to identify any significance between treatment groups.

Figure 2.7: Imaging western blots and quantifying protein expression. Western blots were imaged using the Odyssey® Fc Imaging System and densitometry was carried out using Image Studio™ Lite software.

2.12 Enzyme-Linked Immunosorbent Assay (ELISA)

Human pro-inflammatory cytokine release was quantified by ELISA.

2.12.1 Human TNF-α and IL-6 ELISA

Human TNF-α release was analysed using Human TNF alpha ELISA Ready-SET-Go!® kit (eBiosciences, 88-7346), according to the manufacturer's instructions. Human IL-6 release was analysed using Human IL-6 ELISA Ready-SET-Go!® kit (eBiosciences, 88-7066), according to the manufacturer's instructions. All reagents required to carry out the ELISA were provided in the kit, apart from the wash buffer (1X PBS with 0.05 % TBST) and stop solution (2N H_2SO_4) which were made-up before commencing. Nunc Maxisorp® ELISA plates (Sigma Aldrich,) were coated with 100 µl/well of capture antibody prepared in 1X coating buffer. The plate was sealed and allowed to incubate overnight at 4 °C. The following day, wells were aspirated and washed three times with 300 µl/well of wash buffer. The plate was blotted on absorbent paper to remove residual wash buffer. Wells were blocked with 1X ELISA/ELISPOT diluent (200 µl/well) at room temperature for one hour, after which the plate was aspirated and blotted to remove residue diluent. The lyophilized standard was reconstituted using deionised water and allowed to sit for 15 minutes with gentle agitation prior to further dilution. Reconstituted standard (15 ng/ml) was diluted (1/30) with 1X ELISA/ELISPOT diluent to give the top standard (200 pg/ml). A seven-point standard curve was prepared using two-fold serial dilutions with reagent diluent, as in Figure 2.8. Standards and cell culture supernatant samples were pipetted into wells (100 µl/well) in duplicate. Two wells of 1X ELISA/ELISPOT diluent were included to serve as the plate blank. The plate was covered with an adhesive strip and allowed to incubate at room temperature for two hours. Wells were aspirated/washed as before. Detection antibody, prepared in 1X ELISA/ELISPOT diluent, was added to each well (100 µl/well). The plate was covered with a new adhesive strip and allowed to incubate at room temperature for one hour. Wells were aspirated/washed as before. Avidin-HRP was diluted (1/250) with 1X ELISA/ELISPOT diluent and pipetted into each well (100 µl/well). The plate was sealed with the adhesive strip, covered with tinfoil and allowed to incubate at room temperature for 30 minutes. Wells were aspirated and washed five times with 300 µl/well of wash buffer, soaking wells for two minutes prior to aspiration. A substrate for horseradish peroxidase, 3,3',5,5'-

Tetramethylbenzidine (TMB) liquid substrate system (Sigma Aldrich, T0440), was added to each well (100 µl/well). The plate was sealed with the adhesive strip, covered with tinfoil and allowed to develop at room temperature for 20 minutes. Once a soluble blue reaction product develops, the HRP-TMB reaction was stopped with 2N H_3SO_4 (50 µl/well), forming a yellow reaction product. Optical density (OD) of each well was measured using a microplate reader set to 450 nm and 570nm, with the latter ODs acting as wavelength correction values. Subtraction of 570 nm from 450 nm OD values corrects for optical imperfections in the plate. A standard curve was constructed of TNF-α or IL-6 standards vs OD values, from which unknown cell culture supernatant TNF-α or IL-6 concentration could be interpolated using the spline fit method.

2.12.2 Human IL-8 ELISA

Human IL-8 release was analysed using Human IL-6/CXCL8 DuoSet ELISA kit (R&D systems, DY208), according to the manufacturer's instructions. All reagents required to carry out the ELISA were provided in the kit, apart from the wash buffer (1X PBS with 0.05 % TBST), block solution (1% BSA, prepared in 0.2 µm filtered PBS), reagent diluent (0.1% BSA, 0.05% Tween 20, in Tris-buffered saline [20 mM, 150 mM NaCl], pH 7.2, 0.2 µm filtered) and stop solution (2N H_3PO_4) which were made-up before commencing. Nunc Maxisorp® ELISA plates (Sigma Aldrich, USA) were coated with 100 µl/well of capture antibody (4 µg/ml) prepared in reagent diluent. The plate was sealed and allowed to incubate overnight at room temperature. The following day, wells were aspirated and washed three times with 400 µl/well of wash buffer. The plate was blotted on absorbent paper to remove residual wash buffer. Wells were blocked with blocking buffer (300 µl/well) at room temperature for one hour, after which the plate was aspirated and blotted to remove residue diluent. The recombinant human IL-8 standard was reconstituted using 0.5 ml of deionised water. Reconstituted standard (80 ng/ml) was diluted (1/40) with reagent diluent to give the top standard (2000 pg/ml). A seven-point standard curve was prepared using two-fold serial dilutions with reagent diluent, as in Figure 2.8. Standards and cell culture supernatant samples were pipetted into wells (100 µl/well) in triplicate. Two wells of reagent diluent were included to serve as the plate blank. The plate was covered with an adhesive strip and allowed to incubate at room temperature for two hours. Wells were aspirated/washed as before. Detection antibody (1.2 µg/ml), prepared in reagent diluent, was added into each well (100 µl/well). The plate was covered with a new

adhesive strip and allowed to incubate at room temperature for 2 hours. Wells were aspirated/washed as before. Streptavidin-horseradish peroxidase (HRP) stock was diluted (1/40) with reagent diluent and pipetted into each well (100 µl/well). The plate was sealed with the adhesive strip, covered with tinfoil and allowed to incubate at room temperature for 20 minutes. Wells were aspirated/washed as before. A substrate for horseradish peroxidase, 3,3',5,5'-Tetramethylbenzidine (TMB) liquid substrate system (Sigma Aldrich, T0440), was added to each well (100 µl/well). The plate was sealed with the adhesive strip, covered with tinfoil and allowed to develop at room temperature for 20 minutes. Once a soluble blue reaction product develops, the HRP-TMB reaction was stopped with 2N H_3SO_4 (50 µl/well), forming a yellow reaction product. Optical density (OD) of each well was measured using a microplate reader set to 450 nm and 570nm. OD values at 570 nm were subtracted from 450 nm OD values. A standard curve was constructed of IL-8 standards vs OD values, from which unknown cell culture supernatant IL-8 concentration could be interpolated using the spline fit method.

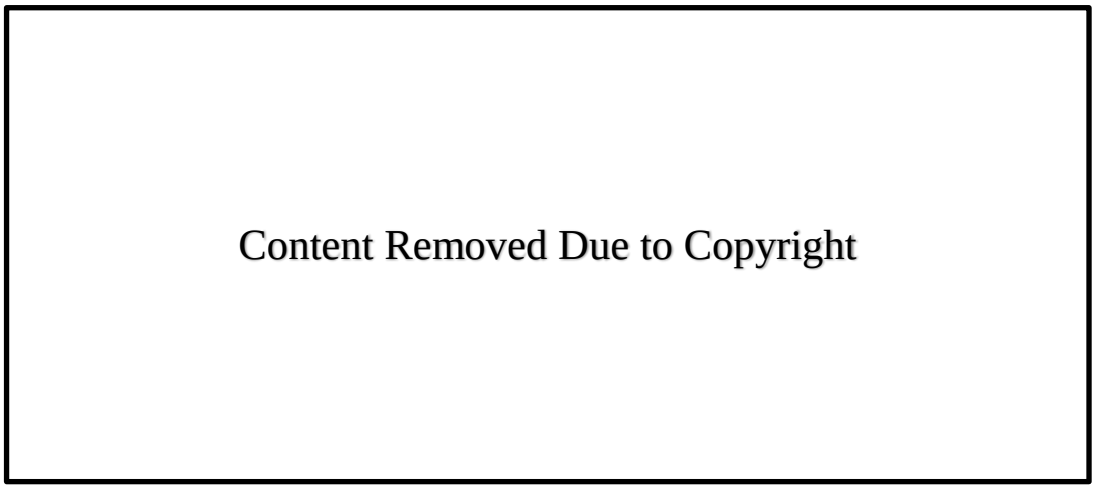

Figure 2.8: Preparation of standards for ELISAs. A seven-point standard curve was prepared for each ELISA from the reconstituted standard using 2-fold serial dilutions in reagent diluent.

2.13 Flow cytometry

Flow cytometry was only used to confirm THP-1 differentiation following PMA treatment. Cell density of each treatment group was determined using the haemocytometer method (as described in section 1.3). Cells were diluted and

transferred into a v-bottom plate at 100,000 cells/well. The plate was spun at 400 g for five minutes, to pellet the cells in the conically-shaped well bottoms. The supernatants were discarded from each well. The cells were fixed by adding paraformaldehyde (PFA) (2%) to each well (100 µl/well) and left to incubate at 4 ^{o}C for 10 minutes. Cells were washed with flow cytometry FACS staining buffer (0.5% bovine serum albumin or 5% fetal bovine serum, 0.1% sodium azide and made up in PBS) (100 µl/well). The plate was spun at 400 g for four minutes and supernatants were discarded. Cells were resuspended in the CD16/CD14 antibodies and allowed to incubate at 4 ^{o}C for 10 minutes. Cells were washed with FACS buffer (100 ul/well), spun at 400 g and the supernatants were discarded. This was repeated two additional times, after which pelleted cells were resuspended in 150 µl FACs buffer and transferred to flow cytometry tubes. Prepared samples were run on the BD FACS Canto II Multicolour flow cytometry (BD Biosciences, Wisconsin, USA). Data generated was analysed using FlowJo flow cytometry software (FlowJo LLC, Oregon, USA). Cell forward scatter area (FSC-A) versus side scatter area (SSC-A) graphs were generated by the software. Non-viable cells or doublets can skew fluorescence analysis; therefore, gating is required to ensure these are omitted. Cells were first gated to ensure only healthy cells were analysed for CD16 expression. Cells were further gated, whereby cell forward scatter height (FSC-H) was graphed versus forward scatter area (FSC-A), to ensure only a population of true single cells were considered for CD16 analysis. Fluorescence intensity from the gated cells was recorded and a representative histogram was generated.

2.14 Bioinformatic analysis

NOD1 and NOD2 sequence alignment was investigated using the Clustal Omega multiple sequence alignment computer programme (EMBL-EBI, Cambridgeshire, UK) to establish the percentage of homology between the two gene sequences. The NOD1 and NOD2 gene content was investigated using the UCSC Genome Browser (University of California Santa Cruz, Calfornia, USA) and GeneCards® software (Weizmann Institute of Science, Israel). These two computer programmes allowed us to identify the length and the exact chromosomal location of each gene and the positions of the single nucleotide polymorphisms (SNPs) associated with each gene. The CpG dinucleotide content for both NOD1 and NOD2 were investigated by the EMBOSS Newcpgreport computer software (EMBL-EBI, Cambridgeshire, UK), to

establish whether these genes have CpG dinucleotide clusters that can be classified as CpG Islands. The three criteria that each cluster must satisfy to be classed as an official CpG Island are outlined in Table 2.22.

Characteristic	Criteria
GC Content	≥ 50%
Length of Segment	> 200base pairs
Observed : Expected	> 0.6

Table 2.22: Criteria required for a CpG dinucleotide cluster to be classed as a CpG Island. For a CpG segment to be classified as a CpG Island it must meet three criteria; GC content of greater than or equal to 50%, Length of greater than 200 base pairs and a ratio of observed to expected number of CpG dinucleotides to exceed 0.6.

2.15 Data Interpretation and Statistical Analysis

Statistical analysis was carried out on data using the Statistics Package for the Social Sciences (SPSS) software (SPSS Statistics 23). Graphical representations of data were generated using GraphPad Prism 5 software. Data was tested for normality by Shapiro-Wilk's test. Parametric data were expressed as (Mean ± SEM). Statistical analysis of parametric data included independent t-tests, one-way ANOVAs and two-way ANOVAs. The number of treatment groups and independent variables determined the appropriate statistical test to carry out. Independent t-tests were used to compare data across two independent groups, with one varying factor. This analysis was carried out when investigating if epigenetic treatment altered mRNA/protein expression levels. One-way ANOVAs were used to compare data across more than two groups with one varying factor, with any significance being further investigated by Dunnett's *post hoc* test. This analysis was carried out on time response data for MAPK/NF-κB phosphorylation. Two-way ANOVAs were used to compare data sets with two independent variables, with any significance being further investigated by Bonferroni *post hoc* test. This analysis was carried out to investigate significance within data sets of cells that received epigenetic treatment and NOD1/2 receptor stimulation. Statistical significance was recognised at $p < 0.05$.

Chapter 3 Analysis of NOD1 activity, signalling and expression in the HCT116 intestinal cell line, following epigenetic modification.

3.1 Introduction

The NOD1 receptor is a ubiquitously expressed intracellular receptor that will recognise all Gram-negative bacteria (e.g. helicobacter pylori, enteroinvasive E.coli and shigella flexneri) and some Gram-positive bacteria (e.g. Listeria monocytogenes), as reviewed in (Moreira and Zamboni, 2012). Within these bacteria, NOD1 recognises the dipeptide γ-D-glutamyl-mesodiaminopimelic acid (iE-DAP), and to a greater extent the tripeptide; L-Ala-γ-D-glutamyl-mesodiaminopimelic acid (TRI-DAP) (Girardin et al., 2003). Activation of this receptor triggers pro-inflammatory signalling via RIP2, MAPK (including ERK1/2 and p38) and NF-κB (including IκBα and p65) signalling. This signalling cascade leads to the activation and translocation of transcription factors (AP-1 and NF-κB), which promote the expression of pro-inflammatory mediators including cytokines (e.g. TNF-α and IL-6) and chemokines (e.g. IL-8) (Feerick and McKernan, 2017).

Increased NOD1 expression has been linked to chronic inflammatory disorders including; ulcerative colitis (Verma et al., 2013), rheumatoid arthritis (Yokota et al., 2012), allergic rhinitis (Hu et al., 2013), atherosclerosis (Kanno et al., 2015), metabolic syndrome (Zhou et al., 2015) and gestational diabetes (Lappas, 2014), as reviewed in (Feerick and McKernan, 2017). However, the mechanism underlying regulation of NOD1 expression has yet to be elucidated.

HCT116 cells were chosen as the experimental model to investigate NOD1 regulation since intestinal epithelial cells express NOD1, are surrounded by trillions of bacteria in the gut and are involved in inflammatory bowel disease (Lee et al., 2012). NOD1 activity, signalling and expression was measured after pharmacological inhibition of DNMT1 or genetic knockout of DNMT3b. DNMT1 was pharmacologically inhibited by treatment with known demethylating agents; 5-Azacytidine (5-Aza) or 5-Aza-2-deoxycytidine (5-Aza-dC). Effects of DNMT3b genetic knockout was investigated using HCT116$^{3b-/-}$ cells, generated in the Vogelstein lab by homologous recombination (Rhee et al., 2002). To investigate if histone acetylation alters NOD1-induced responses, NOD1 activity, signalling and expression levels was measured after

treatment with a pan-histone deacetylase inhibitor; suberoylanilide hydroxamic acid (SAHA).

In this chapter it was hypothesised that NOD1 receptor activity and expression are regulated, in HCT116 intestinal epithelial cells, by epigenetic modifications.

3.2Methods

The methods used in this chapter did not differ in any way from those outlined in chapter 2.

3.3 Experimental Design

These experiments were designed to investigate if reduced DNA methylation or enhanced histone acetylation patterns altered NOD1 receptor activity, signalling and expression. HCT116 cells were primed with epigenetic modifying agents that are known to disrupt either DNA methylation (5-Aza/5-Aza-Dc/DNMT3b-/-) or histone acetylation (SAHA). NOD1 pro-inflammatory activity, signalling and basal expression was investigated in these primed cells, relative to untreated cells. NOD1 pro-inflammatory activity was analysed by stimulating the primed cells with a NOD1 ligand for 6/18hours, after which pro-inflammatory cytokine (TNF-α and IL-6) expression and chemokine (IL-8) release were quantified by qPCR and ELISA, respectively. NOD1 pro-inflammatory signalling was investigated by measuring RIP2, MAPK and NF-κB protein phosphorylation after stimulating primed HCT116 cells with NOD1 ligands for 1/3 hours, via western blotting. NOD1 basal expression was quantified in primed vs untreated cells at the mRNA and protein levels by qPCR and western blotting, respectively. All experiments were carried out with at least three independent biological replicates ($n \geq 3$). An overview of the experimental design is presented in Figure 3.1, with a more detailed breakdown outlined in the experimental design index (Table 3.1).

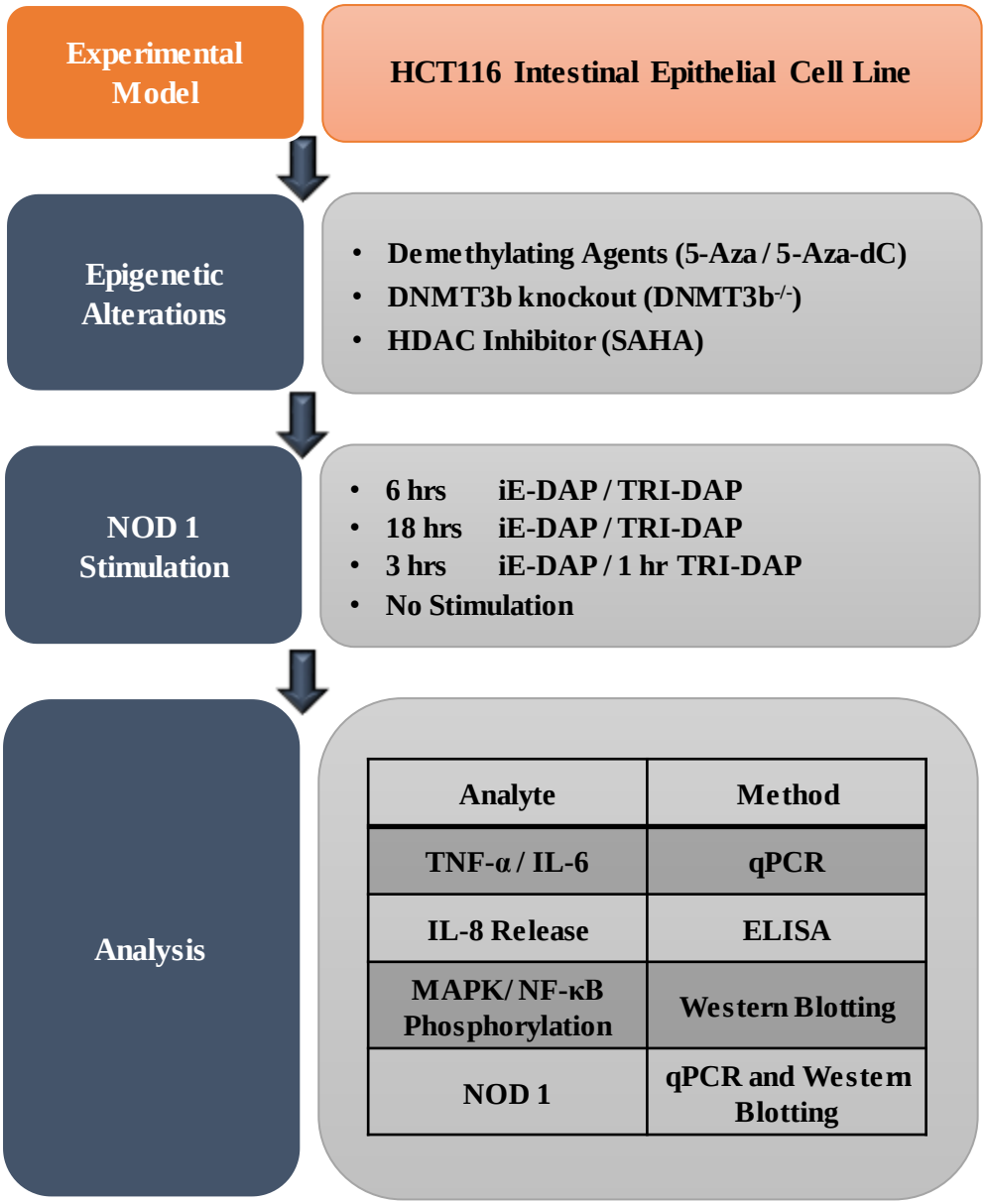

Figure 3.1. Chapter 3 Experimental Design. Outline of epigenetic treatments, NOD 1 stimulation and analysis.

Table 3.1: Chapter 3 Experimental Design Index. Breakdown of treatments, analytes and analysis methods for investigating NOD1 activity, signalling and expression in HCT116 intestinal epithelial cell line.

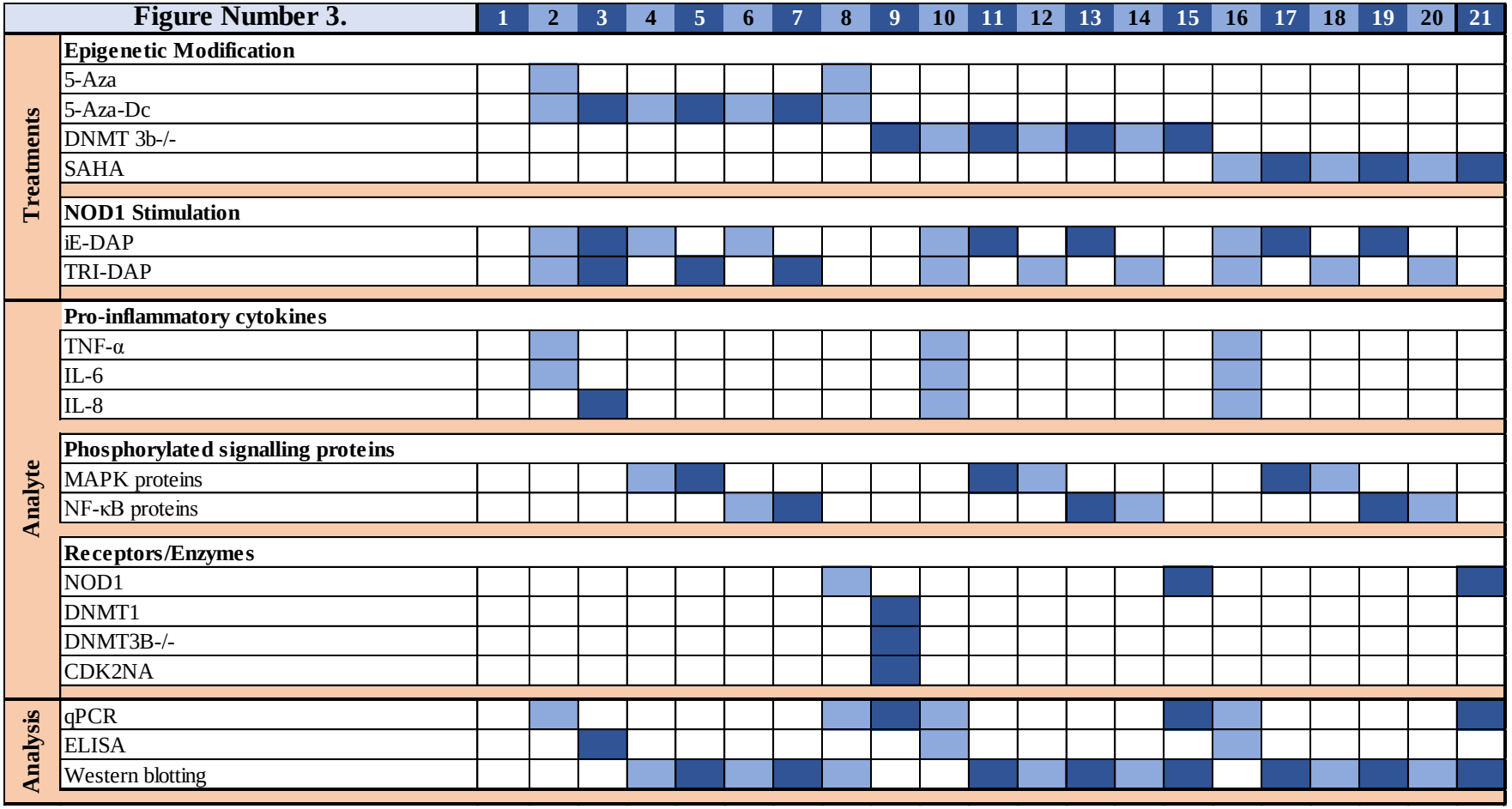

3.4 Results

3.4.1 DNMT1 inhibitor priming increases NOD1-induced pro-inflammatory activity.

To determine if disruption of DNA methylation patterns alter how HCT116 intestinal epithelial cells respond to NOD1 stimulation, cells were treated with a known demethylating agent prior to NOD1 stimulation. HCT116 cells were treated with a DNA methyltransferase 1 inhibitor, 5 μM 5-Azacytidine (5-Aza) or 500 nM 5-Aza-2'-deoxycytidine (5-Aza-dC), for 72 hours. Following exposure to one of these known demethylating agents, cells were stimulated with a NOD1 ligand, 10 μg/ml iE-DAP or TRI-DAP, for an additional 6 or 18 hours. The effects of these treatments on pro-inflammatory responses to NOD1 stimulation were investigated by quantifying pro-inflammatory cytokine/chemokine expression and release by qPCR and ELISA, respectively. The "Untreated + None" treatment group, acted as the control. Pro-inflammatory cytokine/chemokine expression or release was calculated relative to this control.

TNF-α and IL-6 mRNA expression was significantly increased in 5-Aza primed HCT116 cells (Figure 3.2 A-B). TNF-α expression increased 1.9-fold ($p < 0.05$) and 2.1-fold ($p < 0.05$) following 6 hours of NOD1 stimulation with either iE-DAP or TRI-DAP, respectively. Priming HCT116 cells with 5-Aza augmented these responses to NOD1 stimulation. Relative to the untreated control group, priming with 5-Aza exacerbated iE-DAP-induced TNF-α from 1.9-fold to 2.7-fold ($p < 0.001$, relative to untreated + iE-DAP) and TNF-α induction by TRI-DAP from 2.1-fold to 3.5-fold ($p < 0.001$, relative to untreated + TRI-DAP), as outlined in Figure 3.2 A. NOD1-induced IL-6 in untreated and 5-Aza primed cells exhibited a similar expression pattern to TNF-α. Stimulation with iE-DAP or TRI-DAP alone, increased IL-6 production by 2.3-fold ($p < 0.001$) and 2.6-fold ($p < 0.001$), respectively. Relative to the untreated control group, priming with 5-Aza increased TRI-DAP-induced IL-6 from 2.6-fold to 4.2-fold ($p < 0.001$, relative to untreated + TRI-DAP), as depicted in Figure 3.2 B. The priming effect of 5-Aza was exacerbated in 5-Aza-dC primed cells (Figure 3.2 C-D). Stimulation with TRI-DAP for 6 hours increased TNF-α mRNA expression 16.2-fold ($p < 0.001$). This response was further augmented when cells had been primed with 5-Aza-Dc. Relative to the untreated control group, priming with 5-Aza-dC increased

TRI-DAP-induced TNF-α from 16.2-fold to 50.6-fold ($p < 0.001$, relative to untreated + TRI-DAP), as exhibited in Figure 3.2 C. Basal TNF-α was directly increased 10.7-fold by 5-Aza-dC. Relative IL-6 mRNA expression was increased 9.7-fold ($p < 0.001$) and 12.3-fold ($p < 0.001$) in HCT116 cells stimulated for 6 hours with iE-DAP or TRI-DAP, respectively. Unlike TNF-α, basal IL-6 expression was not significantly altered by 5-Aza-dC. Relative to the untreated control group, priming with 5-Aza-dC exacerbated iE-DAP-induced IL-6 from 9.7-fold to 13.3-fold ($p < 0.001$, relative to untreated + iE-DAP) and TRI-DAP-induced IL-6 from 12.3-fold to 20.6-fold ($p < 0.001$, relative to untreated + TRI-DAP), as elucidated in Figure 3.2 D.
Since response patterns of HCT116 cells to 5-Aza were also observed with 5-Aza-dC, but to a higher magnitude, the remaining demethylation studies of this chapter examined only the effects of 5-Aza-dC priming.

TNF-α and IL-6 protein release from HCT116 cells was undetectable. Therefore, IL-8 release from HCT116 cells was investigated. Time and dose response was investigated to identify an appropriate ligand concentration and stimulation duration (Appendix 3). Based on this analysis, HCT116 cells were chosen to be stimulated with 10 μg/ml iE-DAP or TRI-DAP for 18 hours. Basal HCT116 IL-8 release (279.7 ± 10.2 pg/ml) increased in response to NOD1 stimulation (Figure 3.3). Stimulation with iE-DAP for 18 hours slightly increased IL-8 release (321.2 ± 3.8 pg/ml), which was not significant ($p > 0.05$). However, TRI-DAP significantly enhanced IL-8 release to 1397.35 ± 40.9 pg/ml ($p < 0.001$). In support of the qPCR TNF-α and IL-6 data, IL-8 release in response to NOD1 stimulation was exacerbated in 5-Aza-dC primed HCT116 cells. Relative to the untreated control group, priming with 5-Aza-dC increased iE-DAP-induced IL-8 release from 321.2 ± 3.8 pg/ml to 392.8 ± 5.1 pg/ml ($p < 0.001$, relative to untreated + iE-DAP) and TRI-DAP stimulated IL-8 release from 1397.35 ± 40.9 pg/ml to 2845.9 ± 37.7 pg/ml ($p < 0.001$, relative to untreated + TRI-DAP), as elucidated in Figure 3.3. These data, alongside the qPCR findings, suggest that priming with a known demethylating agent enhances responses to NOD1 ligands.

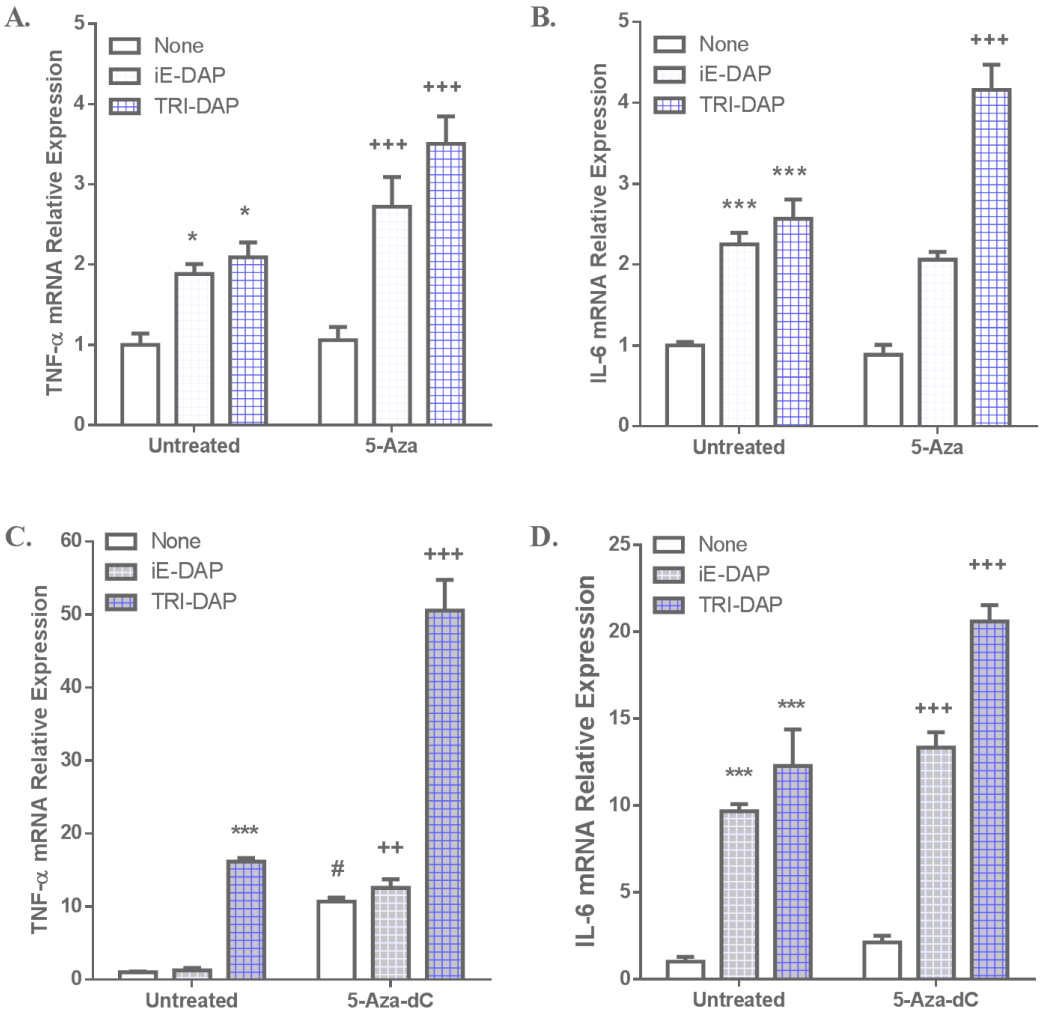

Figure 3.2: NOD1-induced pro-inflammatory cytokine expression in 5-Aza or 5-Aza-dC primed HCT116 cells. A-B) TNF-α and IL-6 mRNA relative expression in HCT116 cells primed with 5 μM 5-Aza for 72 hours and subsequently stimulated with a NOD1 ligand (10 μg/ml iE-DAP/TRI-DAP) for 6 hours. C-D) TNF-α and IL-6 mRNA relative expression in HCT116 cells primed with 500 nM 5-Aza-dC for 72 hours and subsequently stimulated with a NOD1 ligand (10 μg/ml iE-DAP/TRI-DAP) for 6 hours. β-Actin acted as the housekeeping gene. "Untreated + None" was set as the control. Data is represented as mean relative expression ± S.E.M. Statistical analysis was performed using two-way ANOVAs, followed by Bonferroni *post-hoc* test where appropriate. ***** $p < 0.05$ representing **control vs NOD1**, **#** $p < 0.05$ representing **control vs primed**, **+** $p < 0.05$ representing **NOD1 vs (primed + NOD1).**

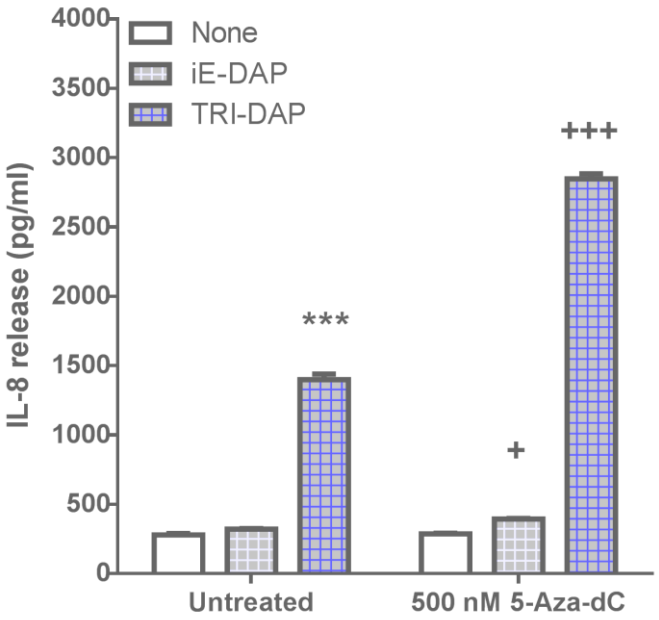

Figure 3.3: NOD1-induced pro-inflammatory IL-8 release from 5-Aza-dC primed HCT116 cells. IL-8 release (pg/ml) from HCT116 cells primed with 500 nM 5-Aza-dC for 72 hours was recorded following NOD1 stimulation with 10 μg/ml iE-DAP/TRI-DAP for 18 hours. "Untreated + None" was set as the control. Data is represented as mean absolute concentration ± S.E.M. Statistical analysis was performed using two-way ANOVAs, followed by Bonferroni *post-hoc* test where appropriate. ***** $p < 0.05$ representing **control vs NOD1**, **#** $p < 0.05$ representing **control vs primed**, **+** $p < 0.05$ representing **NOD1 vs (primed + NOD1).**

3.4.2 DNMT1 inhibitor priming increases NOD1-induced pro-inflammatory RIP2 and MAPK signalling.

Since it was found that treatment with known demethylating agent increased pro-inflammatory cytokine/chemokine expression/release, the effects of these agents on pro-inflammatory signalling, which leads to cytokine/chemokine production, was investigated next. NOD1 activation initiates a cascade of phosphorylation, involving RIP2, MAPK and NF-κB proteins. In this section, NOD1-induced phosphorylation of RIP2 and MAPK proteins was investigated in 5-Aza-dC primed HCT116 cells (Figure 3.4 and Figure 3.5). Phosphorylation time responses were carried out to select the most appropriate NOD1 stimulation duration (Appendix 5). Based on this investigation, it was decided that cells should be stimulated with iE-DAP for three hours and TRI-DAP for one hour. Phosphorylation of the NOD1 adapter protein (RIP2) and MAPK signalling proteins (ERK2 and p38) was investigated by western blot analysis. Blots were repeated for three independent experiments, with representative blots shown. Protein expression was quantified by densitometry of phosphorylated, total and housekeeping proteins. Phosphorylated protein expression was normalised relative to their total proteins, and subsequently calculated relative to the untreated control group. Analysis revealed that stimulation with iE-DAP alone increased RIP2 phosphorylation 1.6-fold ($p < 0.001$), having little effect on the MAPKs (ERK1/2 and p38). Primed cells however had enhanced responses to iE-DAP stimulation (Figure 3.4). Relative to the untreated control group, priming with 5-Aza-Dc exacerbated iE-DAP-induced p-RIP2 from 1.6-fold to 2.2-fold ($p < 0.001$, relative to untreated + iE-DAP), p-ERK2 from 1.2 to 1.7-fold ($p < 0.01$, relative to untreated + iE-DAP), and p-p38 from 1-fold to 1.3-fold ($p < 0.05$, relative to untreated + iE-DAP). Stimulation with TRI-DAP alone significantly increased phosphorylation of RIP2 (2.8 -fold, $p < 0.001$), ERK (2.3 -fold, $p < 0.05$) and p38 (1.4-fold, $p < 0.001$) (Figure 3.5). As discovered with the other NOD1 ligand, TRI-DAP responses were enhanced by 5-Aza-dC priming. Relative to the untreated control group, priming with 5-Aza-Dc augmented TRI-DAP-induced p-RIP2 from 2.8-fold to 6.1-fold ($p < 0.001$, relative to untreated + TRI-DAP), p-ERK2 from 2.3-fold to 4.4-fold ($p < 0.001$, relative to untreated + TRI-DAP), and p-p38 from 1.4-fold to 1.7-fold ($p < 0.01$, relative to untreated + TRI-DAP) (Figure 3.5). Together, these findings suggest that 5-Aza-dC priming attenuates phosphorylation of RIP2 and MAPK proteins in response to NOD1 activation, thereby

implying that treatment with a known demethylating agent supports additional pro-inflammatory responses to NOD1 ligands.

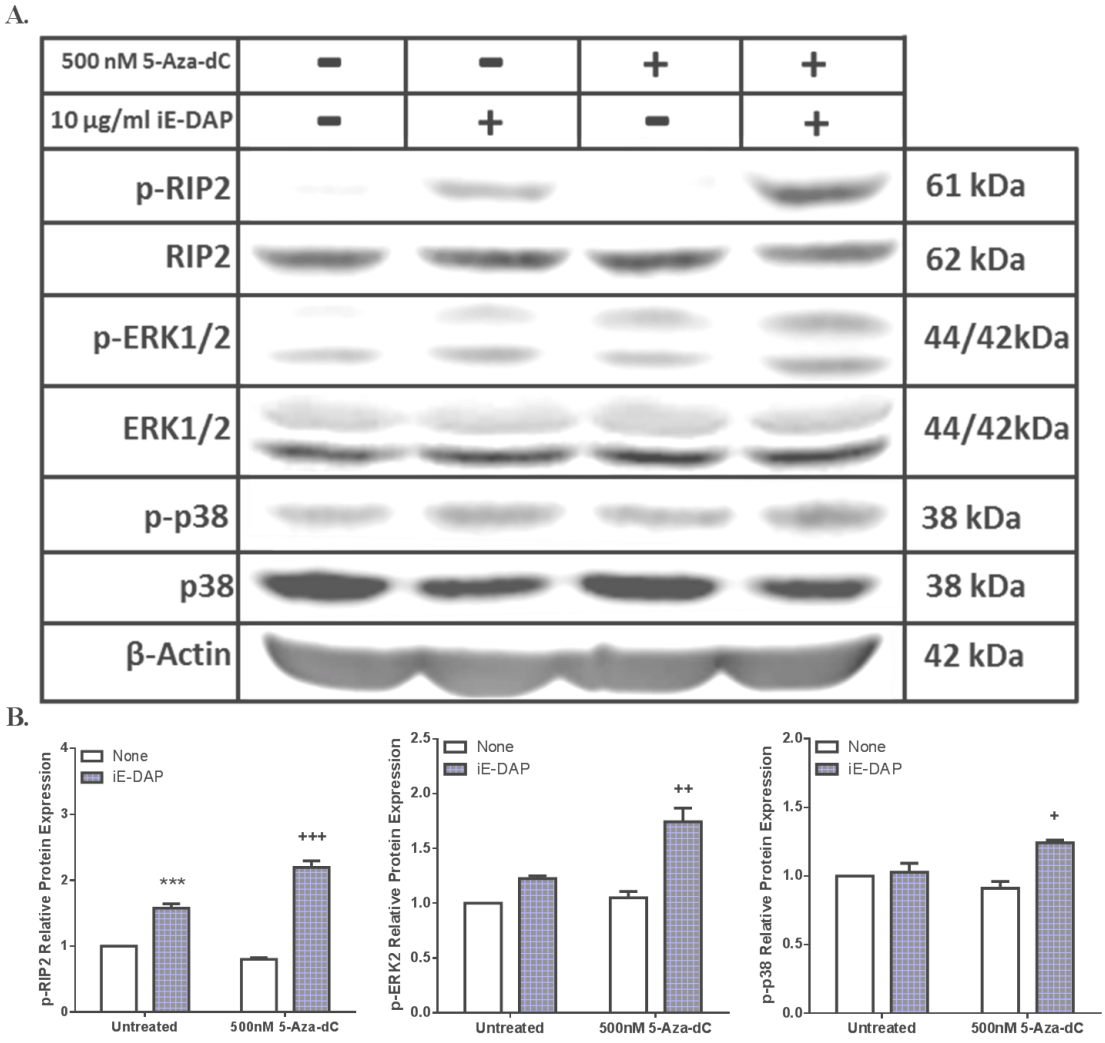

Figure 3.4: IE-DAP-induced RIP2 and MAPK signalling in 5-Aza-dC primed HCT116 cells. (A) Immunoblots of phosphorylated and total RIP2, ERK1/2 and p38 in 5-Aza-dC primed cells stimulated with iE-DAP (10 µg/ml) for three hours. β-Actin acted as the loading control. B) Densitometry of phosphorylated RIP2, ERK1/2 and p38 expression, relative to total protein expression. "Untreated + None" was set as the control. Data is represented as mean relative expression ± S.E.M. and analysed using two-way ANOVAs (followed by Bonferroni's *post-hoc* test). ***** $p < 0.05$ representing **control vs NOD1**, **#** $p < 0.05$ representing **control vs priming, +** $p < 0.05$ representing **NOD1 vs (priming + NOD1).**

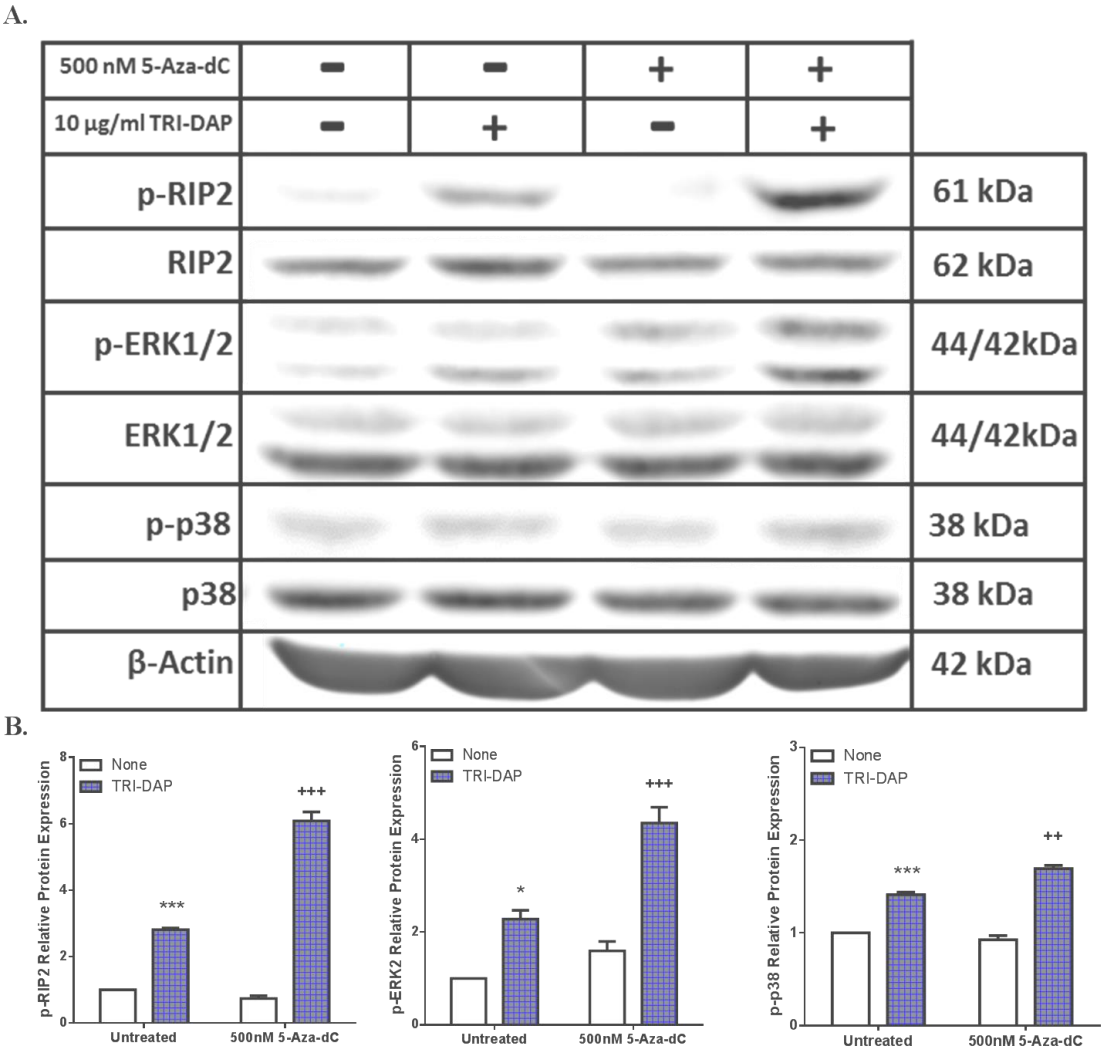

Figure 3.5: TRI-DAP-induced RIP2 and MAPK signalling in 5-Aza-dC primed HCT116 cells. (A) Immunoblots of phosphorylated and total RIP2, ERK1/2, and p38 in 5-Aza-dC primed cells stimulated with TRI-DAP (10 µg/ml) for one hour. β-Actin acted as the loading control. B) Densitometry of phosphorylated RIP2, ERK1/2, and p38 expression, relative to total protein expression. "Untreated + None" was set as the control. Data is represented as mean relative expression ± S.E.M. and analysed using two-way ANOVAs (followed by Bonferroni's *post-hoc* test). ***** $p < 0.05$ representing **control vs NOD1**, **#** $p < 0.05$ representing **control vs priming, +** $p < 0.05$ representing **NOD1 vs (priming + NOD1).**

3.4.3 DNMT1 inhibitor priming increases NOD1-induced pro-inflammatory NF-κB signalling.

In addition to MAPK activation, NOD1 pro-inflammatory signalling requires NF-κB activation. The phosphorylation cascade triggered by NOD1 stimulation phosphorylates the NF-κB inhibitor; IkBa., liberating NF-κB from its inhibitory effects. NF-Kb is subsequently exposed for phosphorylation / activation. Phosphorylation of the NF-κB subunit; p65, was investigated in this body of work. Blots were repeated in three independent experiments (n=3), with representative blots shown. Protein expression was quantified by densitometry of phosphorylated, total and housekeeping proteins (βActin). Phosphorylated protein expression was normalised relative to βActin, and subsequently calculated relative to the untreated control group.

Stimulation with iE-DAP alone for six hours was found to increase p-p65 levels by 2-fold ($p < 0.01$) and p-IκBα by 2.6-fold ($p < 0.001$). These responses to iE-DAP were not augmented by 5-Aza-dC priming (Figure 3.6). TRI-DAP alone significantly increased phosphorylation of p65 (1.5-fold $p > 0.05$) and IκBα (1.7-fold, $p < 0.01$). 5-Aza-dC priming significantly augmented TRI-DAP-induced phosphorylation. Relative to the untreated control group, priming with 5-Aza-Dc increased TRI-DAP-induced p-p65 from 1.5-fold to 5.2-fold ($p < 0.001$, relative to untreated + TRI-DAP) and p- IκBα from 1.7-fold to 2.2-fold ($p < 0.01$, relative to untreated + TRI-DAP), as depicted in Figure 3.7. The enhanced NF-κB signalling supports the RIP2 and MAPK data in the previous section. Together, these data suggest that treatment with a demethylating agent enhances NOD1 pro-inflammatory signalling in HCT116 cells.

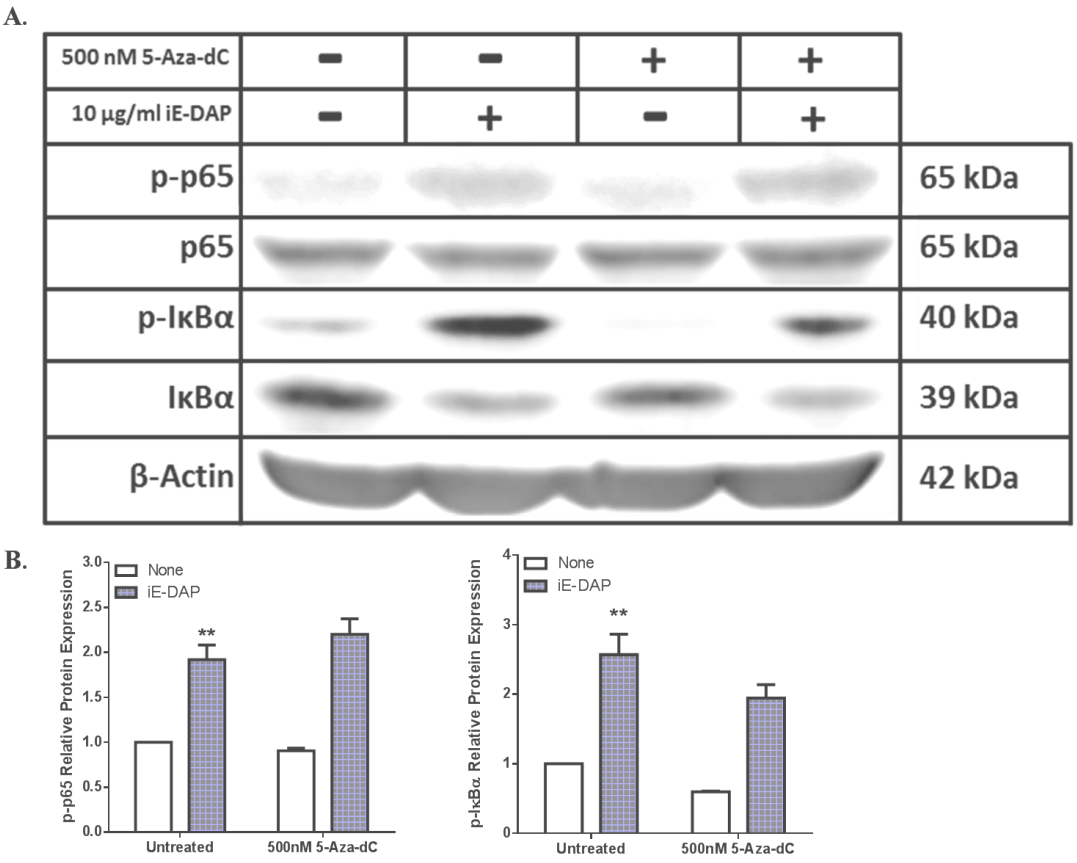

Figure 3.6: IE-DAP-induced NF-κB signalling in 5-Aza-dC primed HCT116 cells. (A) Immunoblots of phosphorylated and total p65 and IκBα in cells primed with 500 nM 5-Aza-dC for 72 hours and subsequently stimulated with IE-DAP (10 µg/ml) for three hours. β- Actin acted as the loading control. (B) Densitometry of phosphorylated p65 and IκBα expression, relative to β-Actin expression. "Untreated + None" was set as the control. Data is represented as mean relative expression ± S.E.M. and analysed using two-way ANOVAs (followed by Bonferroni's *post-hoc* test). ***** $p < 0.05$ representing **control vs NOD1**, **#** $p < 0.05$ representing **control vs primed**, **+** $p < 0.05$ representing **NOD1 vs (primed + NOD1).**

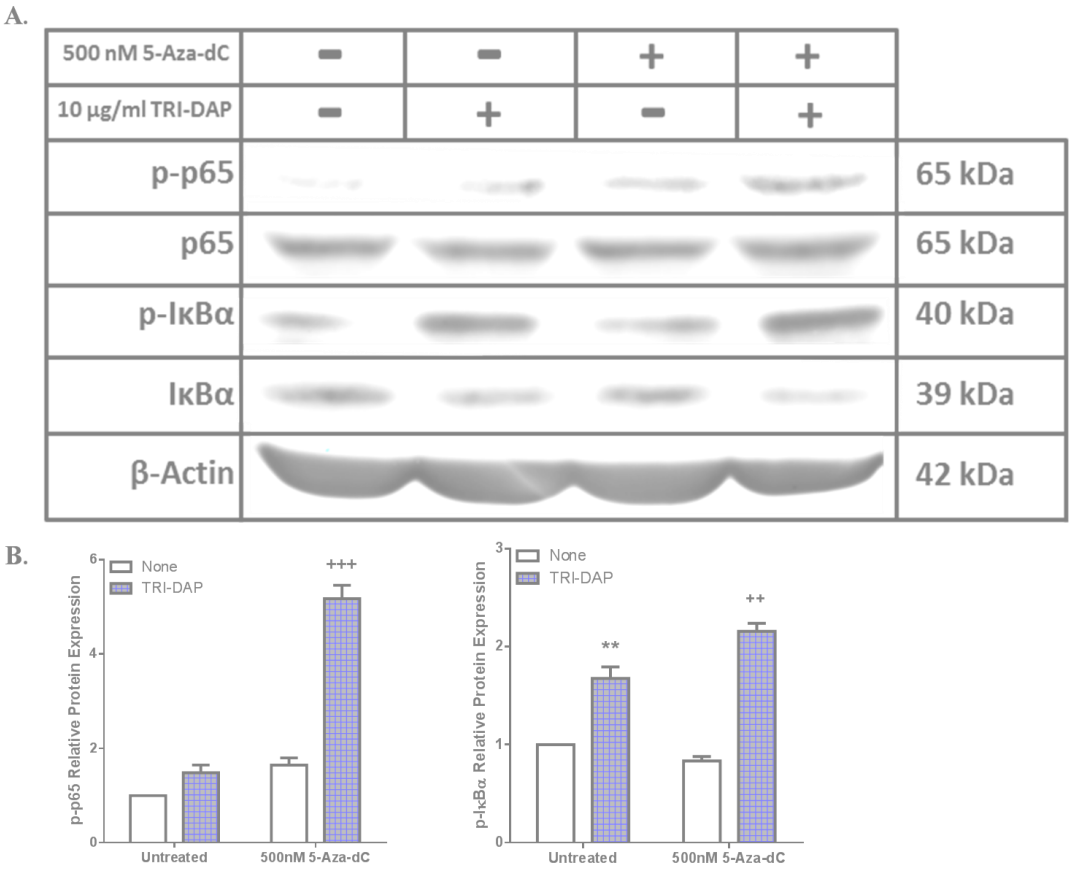

Figure 3.7: TRI-DAP-induced NF-κB signalling in 5-Aza-dC primed HCT116 cells. (A) Immunoblots of phosphorylated and total p65 and IκBα in cells primed with 500 nM 5-Aza-dC for 72 hours and subsequently stimulated with TRI-DAP (10 µg/ml) for one hour. β- Actin acted as the loading control. (B) Densitometry of phosphorylated p65 and IκBα expression, relative to β-Actin expression. "Untreated + None" was set as the control. Data is represented as mean relative expression ± S.E.M. and analysed using two-way ANOVAs (followed by Bonferroni's *post-hoc* test). ***** $p < 0.05$ representing **control vs NOD1**, **#** $p < 0.05$ representing **control vs primed**, **+** $p < 0.05$ representing **NOD1 vs (primed + NOD1).**

3.4.4 DNMT1 inhibitor priming increases NOD1 basal expression.

Since 5-Aza and 5-Aza-dC priming was found to increase responses to NOD1 ligands, the following question was posed. Are demethylating agents enhancing responses by directly altering NOD1 expression? This was investigated by quantifying NOD1 expression at the mRNA and protein levels via qPCR and western blot analysis. Independent t-test analysis revealed some significant increases in NOD1 expression (Figure 3.8). Treatment with 5-Aza was found to have no effect on NOD1 mRNA expression, however it did slightly increase NOD1 protein (1.3-fold, $p < 0.05$) (Figure 3.8 A, C, and E). As expected, 5-Aza-dC treatment mirrored the effects of 5-Aza but to a higher magnitude. Treatment with 5-Aza-dC induced a 2.2-fold increase in NOD1 mRNA ($p < 0.001$) and a 1.5-fold increase in NOD1 protein ($p < 0.01$) (Figure 3.8 B, D, and F). This suggests that the demethylating agents are increasing NOD1 expression, potentially explaining the augmented pro-inflammatory activity and signalling recorded in the earlier experimentation.

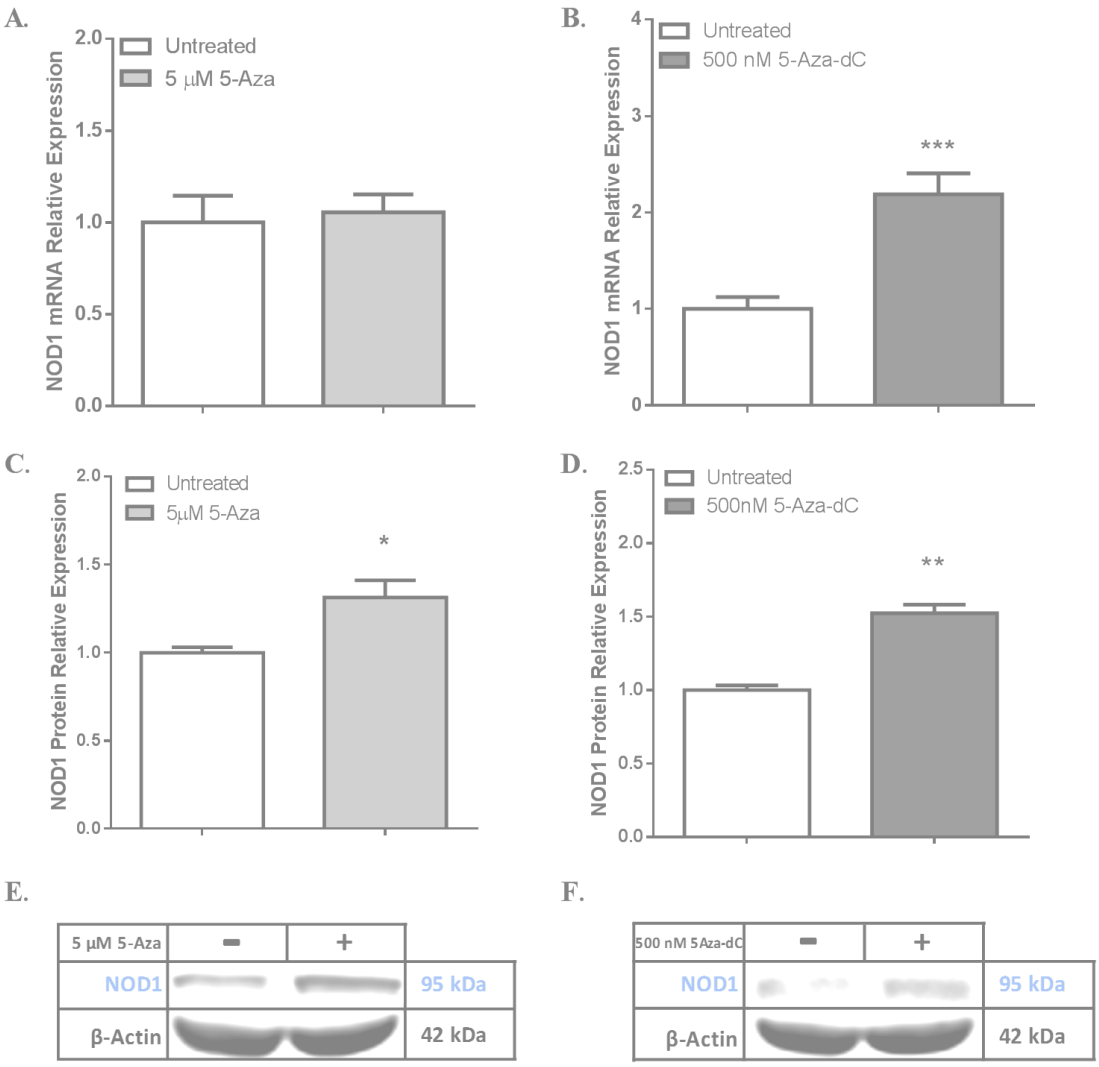

Figure 3.8. NOD1 basal expression following 5-Aza or 5-Aza-dC treatment. (A-B) NOD1 mRNA expression following 5 μM 5-Azacytidine (5-Aza) or 500 nM 5-Aza-2'-deoxycytidine (5-Aza-dC) for 72 hours, relative to β-Actin expression. (C-D) Densitometry of NOD1 protein expression following 5 μM 5-Aza or 500 nM 5-Aza-dC for 72 hours, relative to β-Actin expression. (E-F) Representative immunoblots of NOD1 protein expression following 5 μM 5-Aza or 500 nM 5-Aza-dC for 72 hours, relative to β-Actin expression. Data is represented as mean relative expression ± S.E.M. Statistical analysis was performed using independent t-tests. Significance was recognised at $p < 0.05$, with * representing $p < 0.05$, ** representing $p < 0.01$ and *** representing $p < 0.001$.

3.4.5 NOD1 gene contains CpG islands

Given that NOD1 expression was altered by known demethylating agents, it was proposed that the NOD1 gene could potentially be regulated by DNA methylation. If a gene is regulated by DNA methylation, it must have CpG islands in its sequence. Therefore, bioinformatic analysis was carried out to check for the presence of CpG islands. NOD1 was found to have two CpG islands in its sequence (Table 3.2), thereby further supporting the hypothesis that NOD1 expression is regulated by DNA methylation.

Characteristic	Requirement	CpG Island 1	CpG Island 2
GC Content	≥ 50%	69.28%	59.18%
Genomic Length	> 200 base pairs	664 base pairs	414 base pairs
Observed:Expected	> 0.6	0.87	0.88

Table 3.2. CpG Islands identified in the NOD1 gene sequence. CpG rich clusters in gene sequences must pass three main criteria to be classified as a "CpG island"; GC content must be greater than or equal to 50%, the genomic segment must exceed 200 base pair and the ratio of observed CpG dinucleotide content vs expected CpG dinucleotide content must be greater than 0.6. Details of the two CpG islands identified in the NOD1 genome sequence are outlined. Data was generated using the EMBOSS Newcpgreport computer software (EMBL-EBIM Cambridgeshire, UK).

3.4.6 DNMT3b genetic knockout was confirmed in HCT116 DNMT3b$^{-/-}$ cells.

Up to this point, the effects of pharmacological interruption of DNA methylation patterns on NOD1 activity and expression was under investigation. Focus is now switched to the effects of genetic knockout of DNMT3b, a DNA methylation enzyme, on NOD1 activity and expression. HCT116 cells with DNMT3b genetically knocked out (DNMT3b$^{-/-}$) were generated by the Vogelstein lab (Rhee et al., 2002). DNMT3b$^{-/-}$ cells were tested using qPCR to ensure the knockout had remained. DNMT3b$^{-/-}$ cells had undetectable levels of DNMT3b mRNA, whereas DNMT1 (another DNA methylation enzyme) levels matched those in wild-type cells (Figure 3.9 A-B). This confirmed a selective knockout of DNMT3b. To validate that DNMT3b$^{-/-}$ cells had diminished DNA methylation, the expression of a gene known to be regulated by DNA methylation; CDK2NA, was measured. CDK2NA mRNA was found to significantly increase 10.3-fold ($p < 0.001$) in DNMT3B-/- cells (Figure 3.9 C), thereby suggesting that DNA methylation patterns have been deteriorated in DNMT3b$^{-/-}$ cells relative to their wild-type counter-parts.

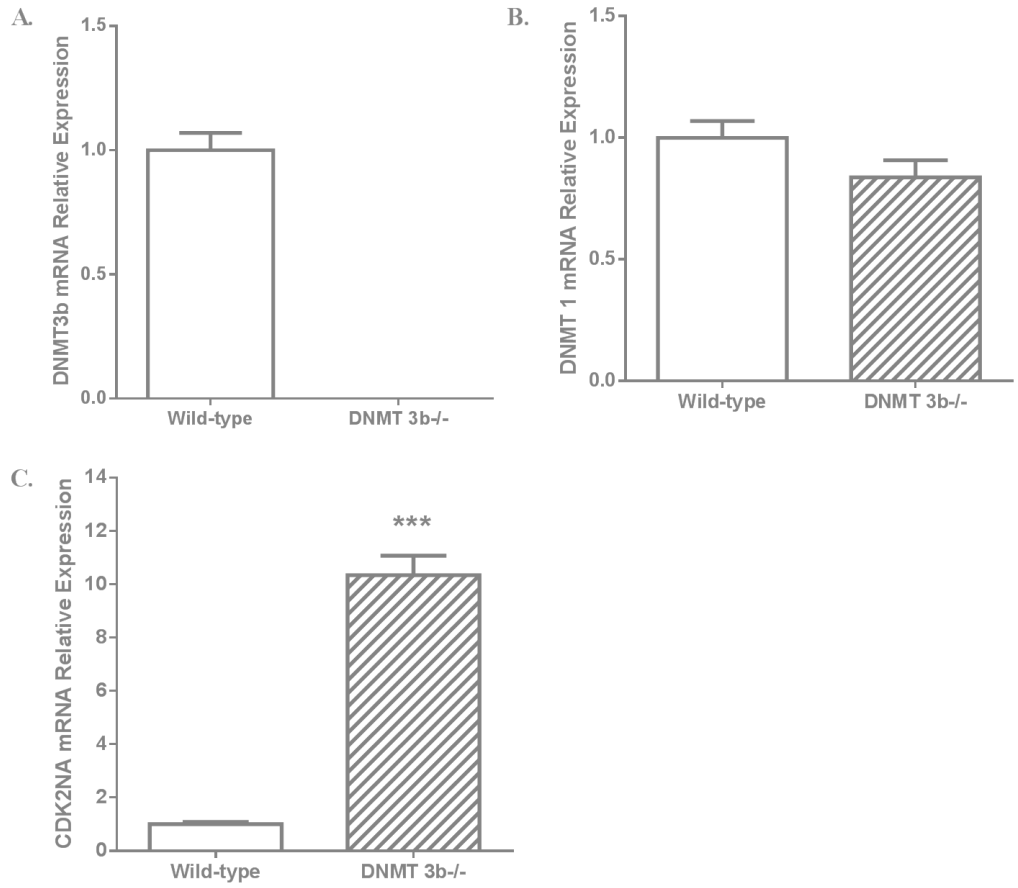

Figure 3.9. Confirmation of DNMT3b knockout and investigation of functionality. (A-C) DNMT 3b, DNMT1 and CDK2NA mRNA expression in wild-type versus DNMT 3b-/- HCT116 cells, relative to β-Actin expression. Data is represented as mean relative expression ± S.E.M. Statistical analysis was performed using independent t-tests. Significance was recognised at $p < 0.05$, with * representing $p < 0.05$, ** representing $p < 0.01$ and *** representing $p < 0.001$.

3.4.7 DNMT3b genetic knockout increases NOD1 pro-inflammatory activity.

DNMT3b knockout influence on NOD1 pro-inflammatory activity was assessed through quantification of pro-inflammatory cytokine/chemokine expression/ release, relative to wild-type HCT116 cells.

NOD1-induced TNF-α and IL-6 mRNA expression, following 6-hour stimulation with 10 μg/ml iE-DAP or TRI-DAP, was compared between wild-type HCT116 and DNMT3b$^{-/-}$ cells. Knockout of DNMT3b appeared to increase basal levels of TNF-α 4-fold ($p < 0.01$) and IL-6 19-fold ($p < 0.001$). In accordance with this basal increase, DNMT3b$^{-/-}$cells were found to be more responsive to NOD1 stimulation. Relative to the wild-type control, the DNMT3b knockout increased iE-DAP-induced of TNF-α expression from 1.7-fold to 7.7-fold ($p < 0.01$, relative to wild-type + iE-DAP) and TRI-DAP-induced TNF-α expression from 2.2-fold to 11.4-fold ($p < 0.001$, relative to wild-type + TRI-DAP) (Figure 3.10 A). The same effect was recorded for IL-6 expression, with DNMT3b$^{-/-}$cells having a superior response to NOD1 stimulation (Figure 3.10 B). Relative to the wild-type control, the DNMT3b knockout cells increased levels of iE-DAP-induced IL-6 expression from 1.7-fold to 26-fold ($p < 0.001$, relative to wild-type + iE-DAP) and TRI-DAP-induced IL-6 expression from 2.8-fold to 40.8-fold ($p < 0.001$, relative to wild-type + TRI-DAP). Since the basal levels of TNF-α and IL-6 are significantly higher in DNMT3b$^{-/-}$cells, it cannot be deciphered if the knockout is directly increasing NOD1 activity at this point.

As before, TNF-α and IL-6 release levels were not detectable from HCT116 cells. Therefore, IL-8 chemokine release was quantified after 18-hour stimulation with 10 μg/ml iE-DAP or TRI-DAP. Basal IL-8 release from wild-type cells (182.7 ± 12.1 pg/ml) was increased following stimulation with iE-DAP (407.4 ± 12.8 pg/ml, $p < 0.05$) and TRIDAP (725.9 ± 51.1 pg/ml, $p < 0.001$). Basal IL-8 levels were not increased by the genetic knockout. However, the genetic knockout enhanced the HCT116 cell response to TRI-DAP. IL-8 release increased from 725.8 ± 51.1 pg/ml to 1081 ± 69.9 pg/ml ($p < 0.01$, relative to wild-type + TRI-DAP), as depicted in Figure 3.10 C. This data provides support towards NOD1-induced pro-inflammatory activity being enhanced in cells with potentially diminished methylation patterns, once again linking NOD1 activity to DNA methylation patterns.

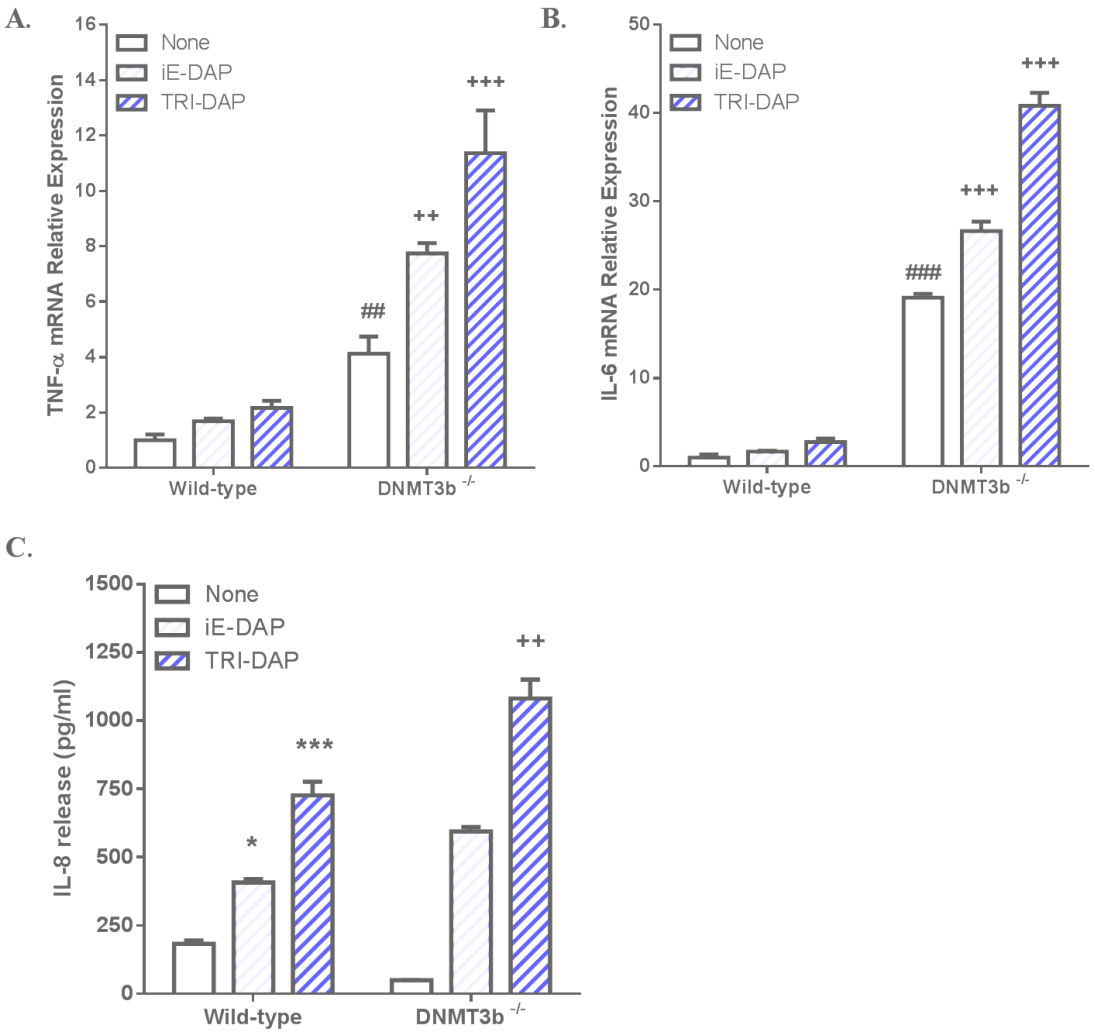

Figure 3.10: NOD1-induced pro-inflammatory cytokine expression in wild-type vs DNMT3b-/- HCT116 cells. A-B) TNF-α and IL-6 mRNA relative expression in DNMT3b-/- cells stimulated with a NOD1 ligand (10 μg/ml iE-DAP/TRI-DAP) for 6 hours. β-Actin acted as the housekeeping gene. "Wild-type + None" was set as the control. Data is represented as mean relative expression ± S.E.M. C) IL-8 release from DNMT3b-/- cells following stimulation with a NOD1 ligand (10 μg/ml iE-DAP/TRI-DAP) for 18 hours. Data is represented as mean absolute concentrations ± S.E.M. Statistical analysis was performed using two-way ANOVAs, followed by Bonferroni *post-hoc* test where appropriate. ***** $p < 0.05$ representing **control vs NOD1**, **#** $p < 0.05$ representing **control vs DNMT3b$^{-/-}$**, **+** $p < 0.05$ representing **NOD1 vs (DNMT3b$^{-/-}$ + NOD1).**

3.4.8 DNMT3b genetic knockout increases NOD1-induced pro-inflammatory RIP2 and MAPK signalling.

To build on the increased pro-inflammatory activity recorded in DNMT3b-/- cells, NOD1-associated pro-inflammatory signalling was examined next in these cells. RIP2 and MAPK (ERK1/2 and p38) phosphorylation, induced by NOD1 ligands, was measured in these knockout cells relative to their wild-type counterparts. The stimulation duration required to detect phosphorylation was chosen as before, based on the wild-type HCT116 preliminary phosphorylation time response analysis (Appendix 5). Cells were chosen to be stimulated with iE-DAP for three hours and TRI-DAP for one hour. Phosphorylation of the NOD1 adapter protein (RIP2) and MAPK signalling proteins (ERK1/2 and p38) was investigated by western blot analysis. Blots were repeated in three independent experiments (n = 3), with representative blots shown. Protein expression was quantified by densitometry of phosphorylated, total and housekeeping proteins. Phosphorylated protein expression was normalised relative to their total proteins, and subsequently calculated relative to the untreated wild-type ("control") group.

Significant increases in p-RIP2 (2.2-fold, $p < 0.05$) and p-ERK1/2 (3-fold, $p < 0.01$) were recorded when wild-type cells were stimulated with iE-DAP. The DNMT3b knockout appears to directly increase basal p-RIP2 levels (2.6-fold, $p < 0.01$). Relative to the wild-type control, the DNMT3b-/- cells appeared to increase iE-DAP-induced levels of p-ERK2 from 3-fold to 4.7-fold ($p < 0.01$, relative to wild-type + iE-DAP) and p-p38 from 1.1-fold to 2.9-fold ($p < 0.001$, relative to wild-type + iE-DAP), as outlined in Figure 3.11. Similar responses were recorded in cells stimulated with TRI-DAP, but at a higher magnitude. TRI-DAP increased p- RIP2 (2.9-fold, $p < 0.001$), p-ERK2 (3.7-fold, $p < 0.01$) and p-p38 (1.9-fold, $p < 0.01$) in wild-type HCT116 cells. Basal levels of phosphorylated RIP2 and MAPKs were increased in DNMT3b-/- cells ($p < 0.001$). Relative to the wild-type control, the DNMT3b-/- cells had exacerbated responses to TRI-DAP (Figure 3.12), represented by increased p-RIP2 from 2.9-fold to 3.8-fold ($p < 0.01$, relative to wild-type + TRI-DAP), p-ERK2 from 3.7-fold to 19.6-fold ($p < 0.001$, relative to wild-type + TRI-DAP) and p-p38 from 1.9-fold to 4.7-fold ($p < 0.001$, relative to wild-type + TRI-DAP). Together, these data suggest DNMT3b-/- cells have a pronounced pro-inflammatory signalling response to NOD1 ligands.

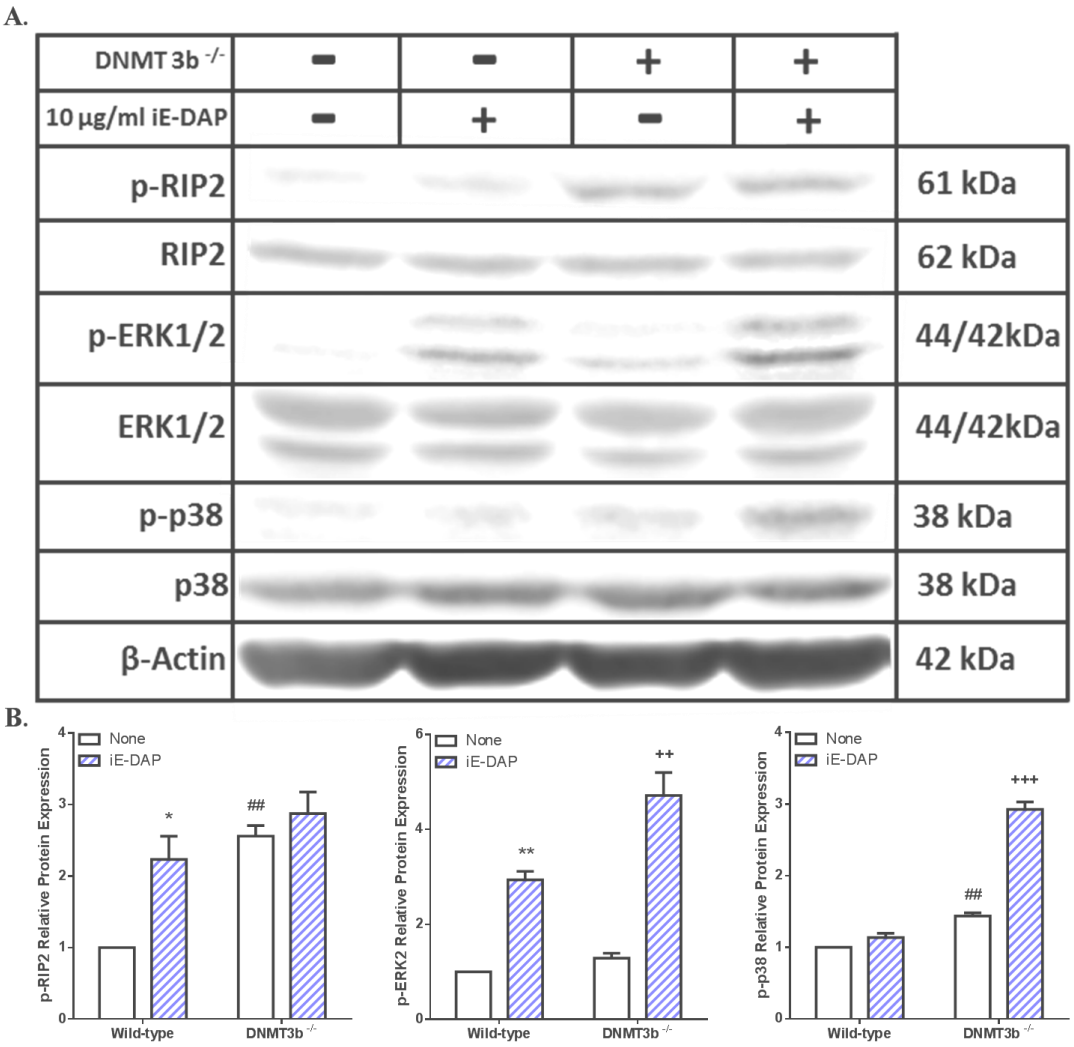

Figure 3.11: IE-DAP-induced RIP2 and MAPK signalling in wild-type vs DNMT3b-/- HCT116 cells. A) Immunoblots of phosphorylated and total RIP2, p38 and ERK1/2 in wild-type and DNMT3b-/- cells stimulated with iE-DAP (10 µg/ml) for three hours. β-Actin acted as the loading control. B) Densitometry of phosphorylated RIP2, p38 and ERK2 expression, relative to total expression. Untreated wild-type cells were set as the "control" group. Data are presented as mean ± S.E.M and analysed using two-way ANOVAs (followed by Bonferroni's *post-hoc* test). ***** $p < 0.05$ representing **control vs NOD1**, **#** $p < 0.05$ representing **control vs DNMT3b$^{-/-}$**, **+** $p < 0.05$ representing **NOD1 vs (DNMT3b$^{-/-}$ + NOD1).**

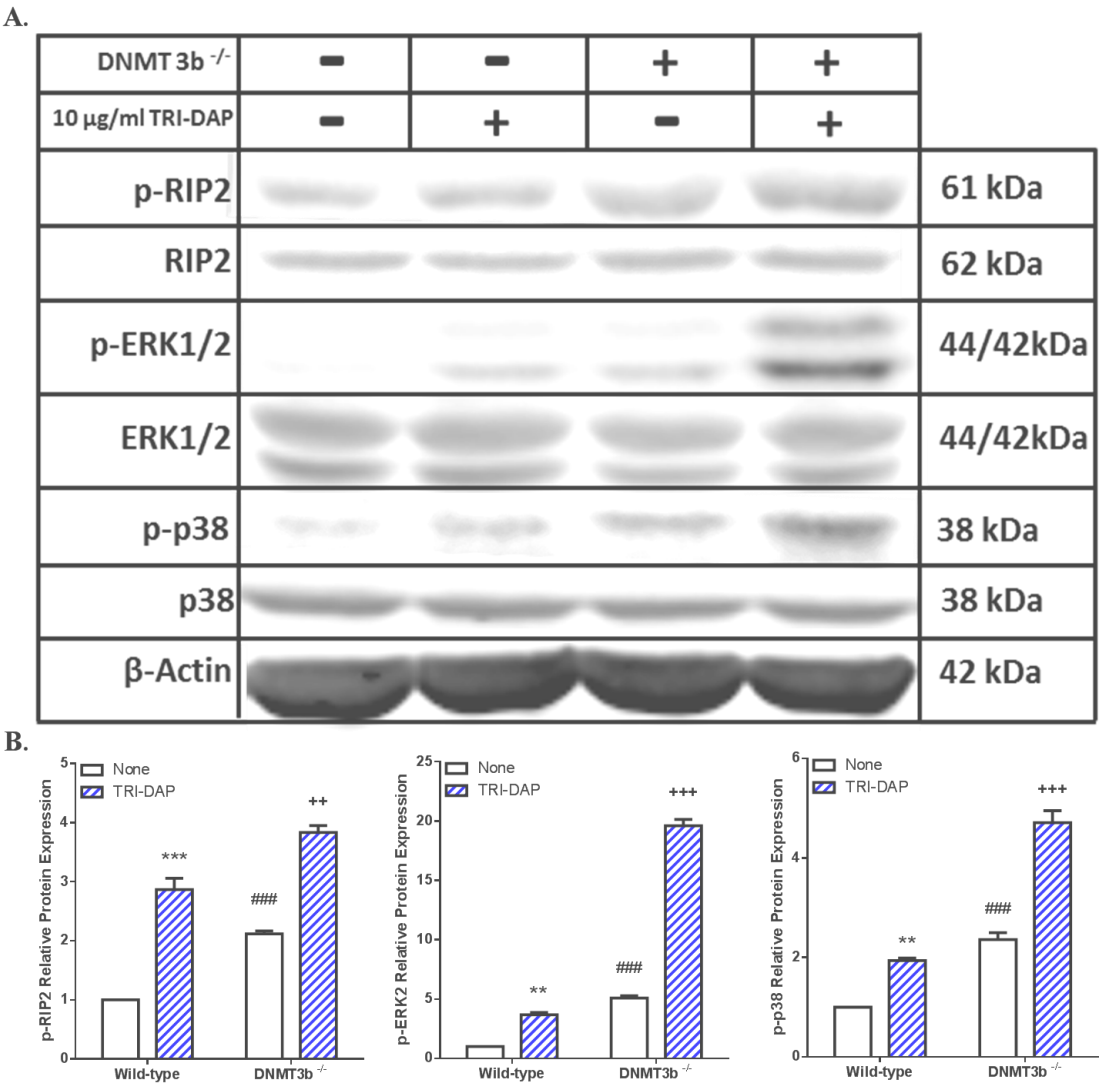

Figure 3.12: TRI-DAP-induced RIP2 and MAPK signalling in wild-type vs DNMT3b-/- HCT116 cells. A) Immunoblots of phosphorylated and total RIP2, p38 and ERK1/2 in wild-type and DNMT3b-/- cells stimulated with TRI-DAP (10 µg/ml) for one hour. β-Actin acted as the loading control. B) Densitometry of phosphorylated RIP2, p38 and ERK2 expression, relative to total expression. Untreated wild-type cells were set as the "control" group. Data are presented as mean ± S.E.M and analysed using two-way ANOVAs (followed by Bonferroni's *post-hoc* test). ***** $p < 0.05$ representing **control vs NOD1**, **#** $p < 0.05$ representing **control vs DNMT3b$^{-/-}$**, **+** $p < 0.05$ representing **NOD1 vs (DNMT3b$^{-/-}$ + NOD1).**

3.4.9 DNMT3b genetic knockout increases NOD1-induced pro-inflammatory NF-κB signalling.

To complete the analysis of NOD1 pro-inflammatory signalling in DNMT3b-/- cells, relative to wild-type HCT116 cells, NF-κB signalling was investigated. To do this, NOD1-induced phosphorylation of p65 and IκBα was analysed. The same NOD1 stimulation duration was chosen to detect NF-κB proteins, as was used for RIP2 and MAPK detection. Blots were repeated in three independent experiments (n = 3), with representative blots shown. Protein expression was quantified by densitometry of phosphorylated, total and housekeeping proteins. Phosphorylated protein expression was normalised relative to the β-Actin housekeeping gene, and subsequently calculated relative to the untreated wild-type ("control") group.

Stimulation of wild-type cells with 10 μg/ml IE-DAP for three hours didn't significantly increase NF-κB protein phosphorylation. Basal p-p65 was significantly higher in DNMT3b-/- cells (2.2-fold, $p < 0.05$). Relative to the wild-type control, DNMT3b knockout increased iE-DAP-induced expression of p-p65 from 1.3-fold to 2.7-fold ($p < 0.01$, relative to wild-type + iE-DAP) and p-IκBα from 1.8-fold to 2.3-fold ($p < 0.001$, relative to wild-type + iE-DAP), as shown in Figure 3.13. HCT116 wild-type cells were more responsive to TRI-DAP than iE-DAP, increasing p-p65 (2.7-fold, $p < 0.001$) and p-IκBα (1.8-fold, $p < 0.05$). Again, DNMT3b-/- cells were found to have greater basal p-p65 expression (4.2-fold, $p < 0.001$). Relative to the wild-type control, DNMT3b knockout significantly increased TRI-DAP-induced expression of p-p65 from 2.7-fold to 6.2-fold, ($p < 0.001$, relative to wild-type + TRI-DAP) and p-IκBα from 1.8-fold to 3.2-fold ($p < 0.01$, relative to wild-type + TRI-DAP), as shown in Figure 3.14. The enhanced NF-B signalling, alongside the increased RIP2 and MAPK activation, together suggest DNMT3b-/- cells are more responsive than wild-type cells to NOD1 stimulation.

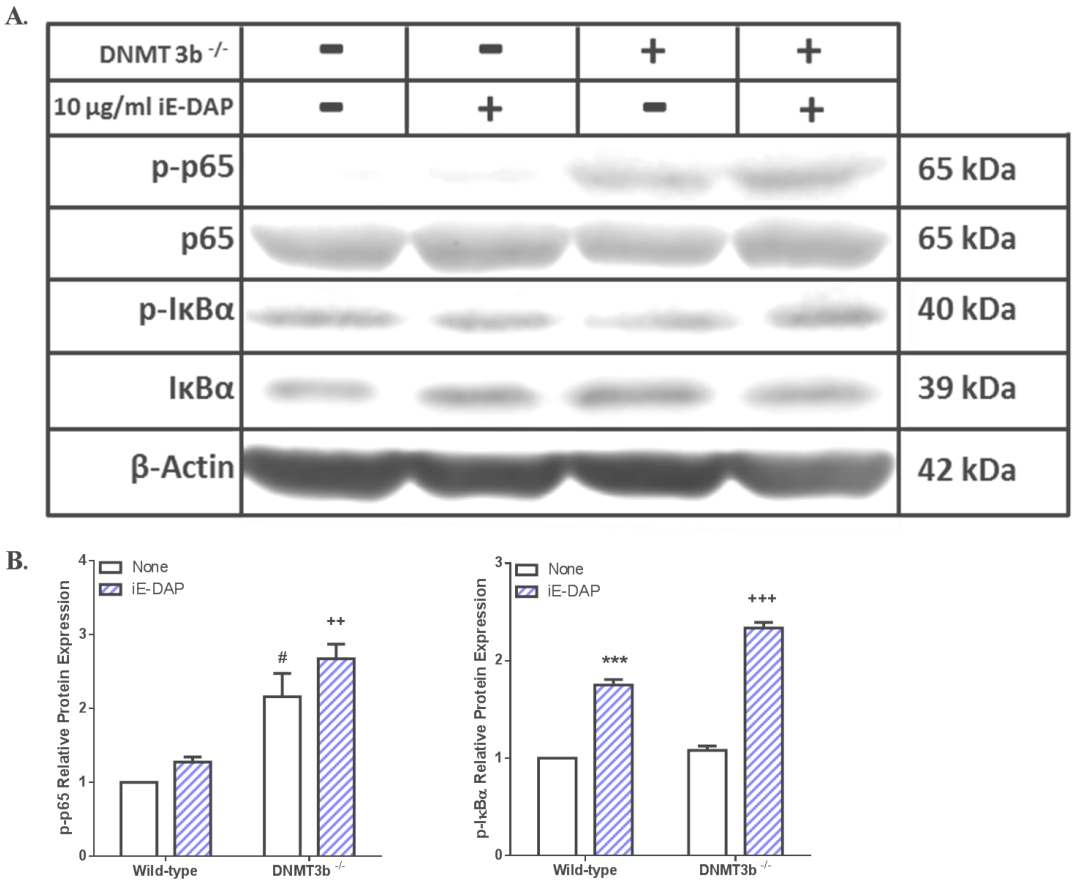

Figure 3.13: IE-DAP-induced NF-κB signalling in wild-type vs DNMT3b-/- HCT116 cells. A) Immunoblots of phosphorylated and total p65 and IκBα in wild-type and DNMT3b-/- cells stimulated with iE-DAP (10 µg/ml) for three hours. β-Actin acted as the loading control. B) Densitometry of phosphorylated p65 and IκBα expression, relative to β-Actin expression. Untreated wild-type cells were set as the "control" group. Data are presented as mean ± S.E.M and analysed using two-way ANOVAs (followed by Bonferroni's *post-hoc* test). ***** $p < 0.05$ representing **control vs NOD1**, **#** $p < 0.05$ representing **control vs DNMT3b$^{-/-}$**, **+** $p < 0.05$ representing **NOD1 vs (DNMT3b$^{-/-}$ + NOD1).**

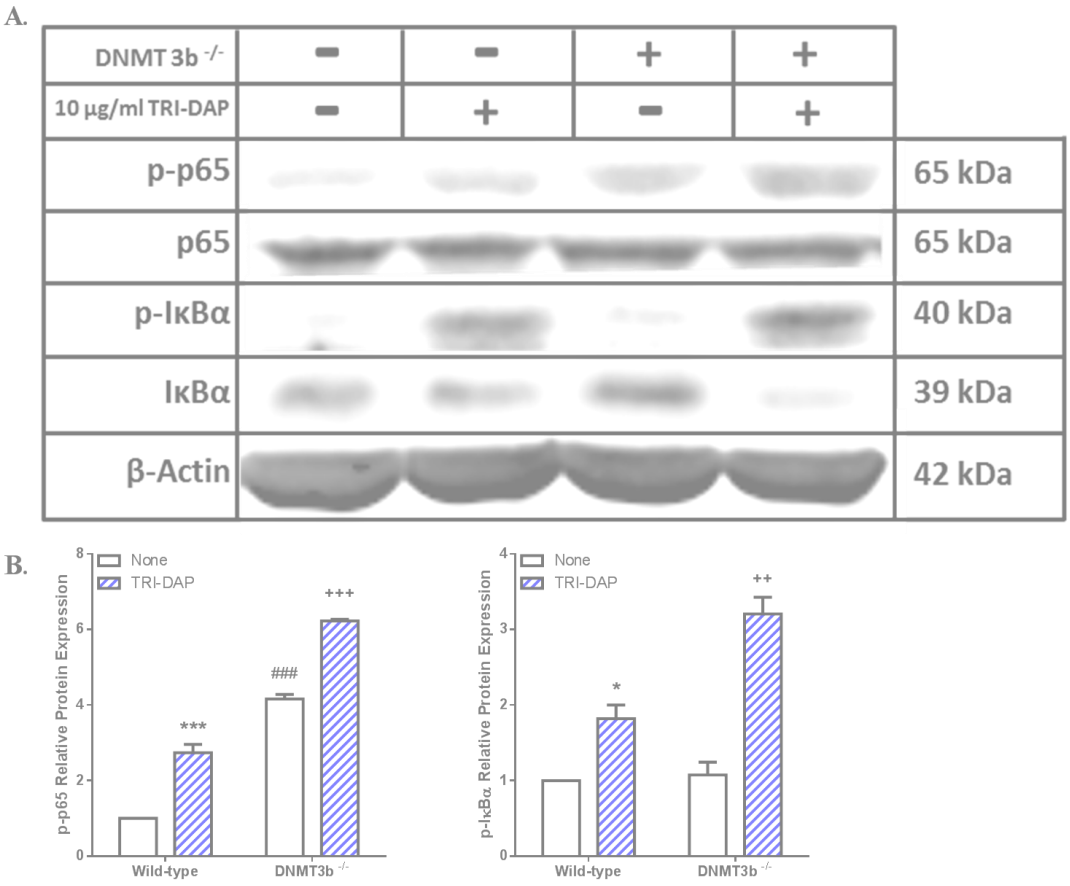

Figure 3.14: TRI-DAP-induced NF-κB signalling in wild-type vs DNMT3b-/- HCT116 cells. A) Immunoblots of phosphorylated and total p65 and IκBα in wild-type and DNMT3b-/- cells stimulated with TRI-DAP (10 µg/ml) for one hour. β-Actin acted as the loading control. B) Densitometry of phosphorylated p65 and IκBα expression, relative to β-Actin expression. Untreated wild-type cells were set as the "control" group. Data are presented as mean ± S.E.M and analysed using two-way ANOVAs (followed by Bonferroni's *post-hoc* test). ***** $p < 0.05$ representing **control vs NOD1**, **#** $p < 0.05$ representing **control vs DNMT3b$^{-/-}$**, **+** $p < 0.05$ representing **NOD1 vs (DNMT3b$^{-/-}$ + NOD1).**

3.4.10 NOD1 expression is higher in DNMT3b-/- HCT116 cells relative to wild-type counterparts.

The experimentation carried out thus far on the DNMT3b-/- cells found NOD1-induced pro-inflammatory activity and signalling to surpass levels triggered in wild-type cells under the same conditions. To investigate the potential explanation for these recorded increases, NOD1 basal expression was quantified in DNMT3b-/- cells at the mRNA and protein levels, via qPCR and western blot analysis, respectively. NOD1 mRNA expression was 1.9-fold higher in DNMT3b-/- cells ($p < 0.001$). These knockout cells were also found to express 1.7-fold more NOD1 protein ($p < 0.001$), relative to wild-type HCT116 cells (Figure 3.15). These data suggest that the greater pro-inflammatory activity and signalling recorded in DNMT3b-/-, cells could be a direct result of more abundant NOD1 expression within these cells

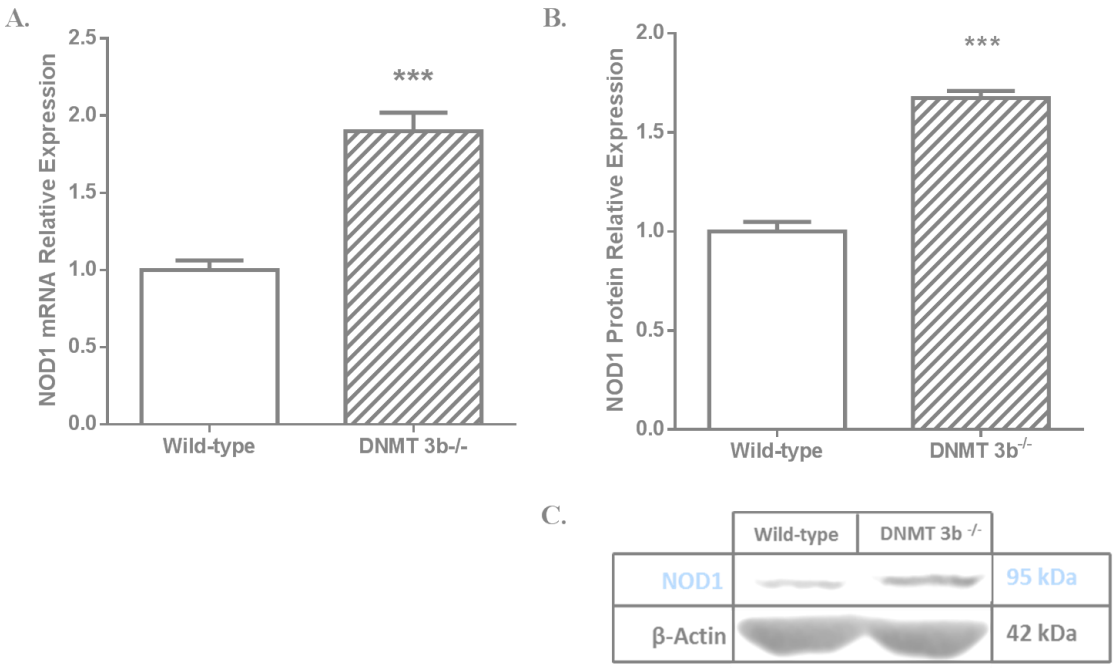

Figure 3.15. NOD1 basal expression in DNMT3b-/- cells. (A) NOD1 mRNA expression in DNMT3b-/- cells, relative to β-Actin expression. (B) Densitometry of NOD1 protein expression in DNMT3b-/- cells, relative to β-Actin expression. (C) Representative immunoblot of NOD1 protein expression in DNMT3b-/- cells. Data is represented as mean relative expression ± S.E.M. Statistical analysis was performed using independent t-tests. Significance was recognised at $p < 0.05$, with * representing $p < 0.05$, ** representing $p < 0.01$ and *** representing $p < 0.001$.

3.4.11 HDAC inhibitor priming increases NOD1-induced pro-inflammatory activity.

The research focus shifts to the effects of another epigenetic modification; histone acetylation, on NOD1-associated activity. HCT116 cells were treated with a well-established histone deacetylase inhibitor (HDACi); suberoylanilide hydroxamic acid (SAHA). HCT116 cells were treated with 10 μM SAHA for 48 hours and subsequently stimulated with 10 μg/ml NOD1 ligands for either six or 18 hours.

The effects of SAHA priming on pro-inflammatory responses to NOD1 stimulation were investigated by quantifying pro-inflammatory cytokine/chemokine expression and release by qPCR and ELISA, respectively. Expression values were normalised relative to the chosen housekeeping gene. RPL13A was the housekeeping gene of choice since β-Actin was found to be directly altered by SAHA, unlike RPL13A, which remained unchanged by SAHA treatments (see Appendix 7). The "Untreated + None" treatment group, was set as the control. Pro-inflammatory cytokine/chemokine expression or release was calculated relative to this control.

Stimulation of HCT116 cells with TRI-DAP alone for six hours increased TNF-α expression 4.4-fold ($p < 0.001$). Basal TNF-α expression was significantly increased in SAHA primed cells (3.9-fold, $p < 0.001$). Stimulation of SAHA primed cells didn't increase TNF-α expression beyond the heightened basal levels ($p > 0.05$). IL6 expression following SAHA priming followed a similar pattern, with basal IL-6 levels significantly increasing 8.1-fold ($p < 0.01$) after exposure to SAHA. Unlike TNF-α, however, IL-6 expression from NOD1 stimulated SAHA-primed cells was significantly augmented. Relative to the untreated control, priming with SAHA enhanced iE-DAP-induced IL-6 from 1.8-fold to 13.5-fold ($p < 0.001$, relative to untreated + iE-DAP) and TRI-DAP-induced IL-6 from 2.7-fold to 15.3-fold ($p < 0.001$, relative to untreated + TRI-DAP), as outlined in Figure 3.16 A- B.

Once again, TNF-α and IL-6 release was below the limits of detection, therefore IL-8 release was investigated. Basal IL-8 release from HCT116 cells (484.6 ± 10.7 pg/ml) was significantly increased following 18 hours of stimulation with 10 μg/ml TRI-DAP alone (1100.7 ± 41.7 pg/ml, $p < 0.001$). Basal IL-8 release was enhanced by SAHA priming (1112.7 ± 35.7 pg/ml, $p < 0.01$). SAHA priming exacerbated the IL-8 release in response to IE-DAP (1168.2 ± 29.4 pg/ml, $p < 0.001$) and TRI-DAP (1931.4 ± 186.3 pg/ml, $p < 0.001$) (Figure 3.16 C). These findings highlight a SAHA-associated

increase in pro-inflammatory cytokine/chemokine production, independent of NOD1 stimulation. This basal increase could account for the enhanced NOD1 activity uncovered in SAHA-primed cells.

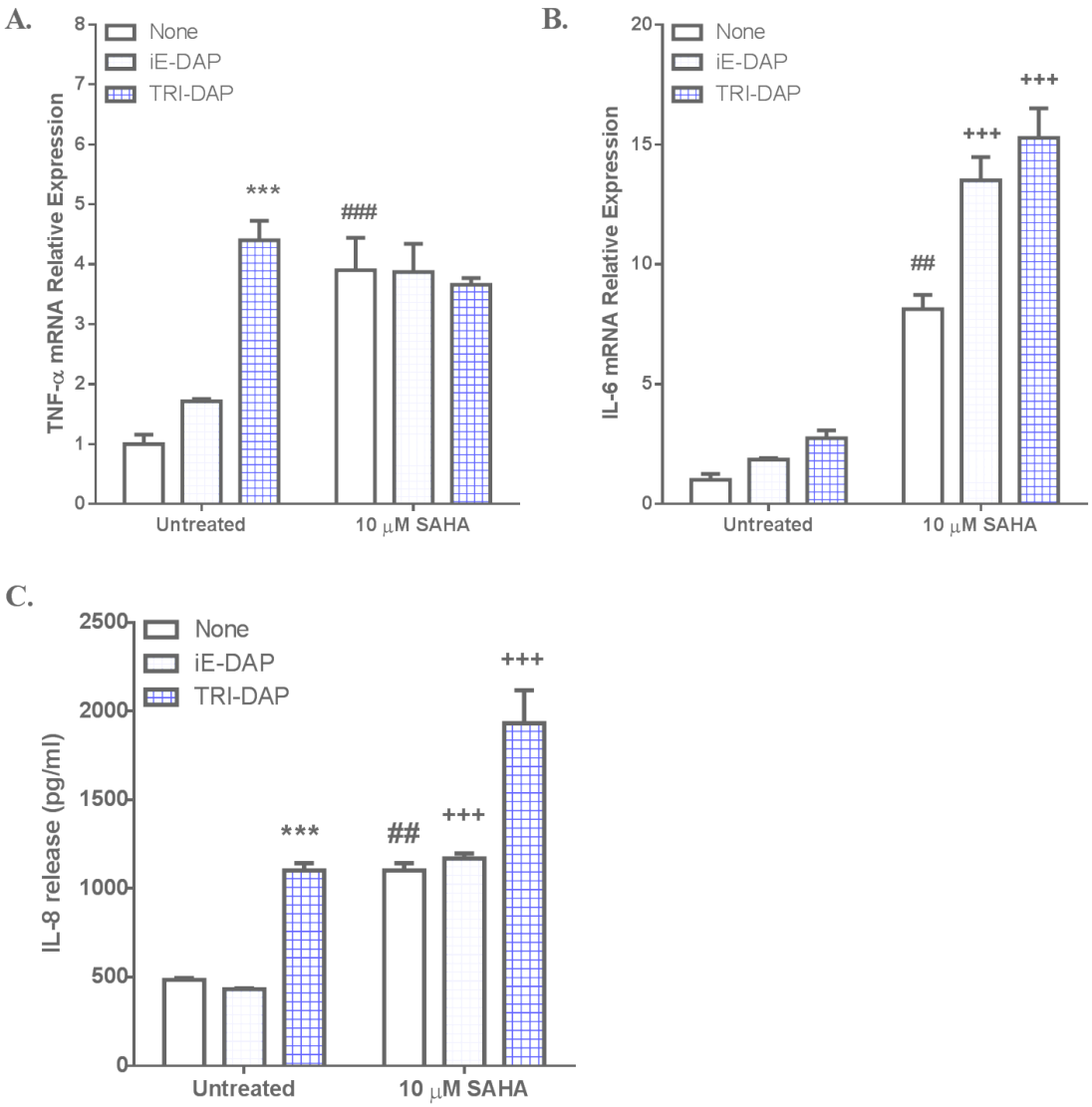

Figure 3.16: NOD1-induced pro-inflammatory activity in SAHA primed HCT116 cells. (A-B) TNF-α and IL-6 mRNA relative expression in HCT116 cells primed with 10 μM SAHA for 48 hours and subsequently simulated with a NOD1 ligand (10 μg/ml iE-DAP/TRI-DAP) for 6 hours. RPL13A acted as the housekeeping gene. "Untreated + None" was set as the control group. Data is represented as mean relative expression ± S.E.M. C) IL-8 release from HCT116 cells primed with 10 μM SAHA for 48 hours and stimulated with a NOD1 ligand (10 μg/ml iE-DAP/TRI-DAP) for 18 hours. Data is represented as absolute values ± S.E.M. Statistical analysis was performed using two-way ANOVAs, followed by Bonferroni *post-hoc* test where appropriate. ***** $p < 0.05$ representing **control vs NOD1**, **#** $p < 0.05$ representing **control vs primed**, **+** representing $p < 0.05$ **NOD1 vs (primed + NOD1).**

3.4.12 HDAC inhibitor priming increases NOD1-induced RIP2 and MAPK pro-inflammatory signalling in HCT116 cells.

As a follow-up to the increased pro-inflammatory activity recorded in SAHA-primed cells, NOD1-induced RIP2 activation and MAPK signalling were quantified in the absence or presence of SAHA priming.

Blots were repeated in three independent experiments (n = 3), with representative blots shown. Protein expression was quantified by densitometry of phosphorylated, total and housekeeping proteins. Phosphorylated protein expression was normalised relative to the chosen housekeeping gene (β-Tubulin) since SAHA was found at times to have a direct effect on total expression. β-Tubulin was chosen to be the housekeeping gene for SAHA-related protein analysis, since β-Actin was found to be directly altered by SAHA, unlike β-Tubulin (see Appendix 8). Normalised expression values were subsequently calculated relative to the "untreated and unstimulated" ("control") group.

Stimulation with IE-DAP alone for six hours significantly increased p-RIP2 (1.6-fold, $p < 0.001$) and p-ERK2 (2.6-fold, $p < 0.001$) levels. These responses were attenuated by SAHA priming. Basal p-ERK2 was reduced to 0.3-fold following SAHA treatment ($p < 0.001$), which would explain the reduced responses to IE-DAP stimulation (Figure 3.17). TRIDAP alone was found to significantly increase phosphorylation of ERK (2.9-fold, $p < 0.001$) and p38 (1.4-fold, $p < 0.05$). SAHA priming increased basal levels of p-RIP2 expression 3.3-fold ($p < 0.001$), which most likely accounts for the enhanced p-RIP2 produced by SAHA-primed cells in response to TRI-DAP from 1.6-fold 4.8-fold ($p < 0.001$, relative to untreated + TRI-DAP), as illustrated in Figure 3.18. The patterns identified here, suggest that SAHA effects on NOD1 are not direct.

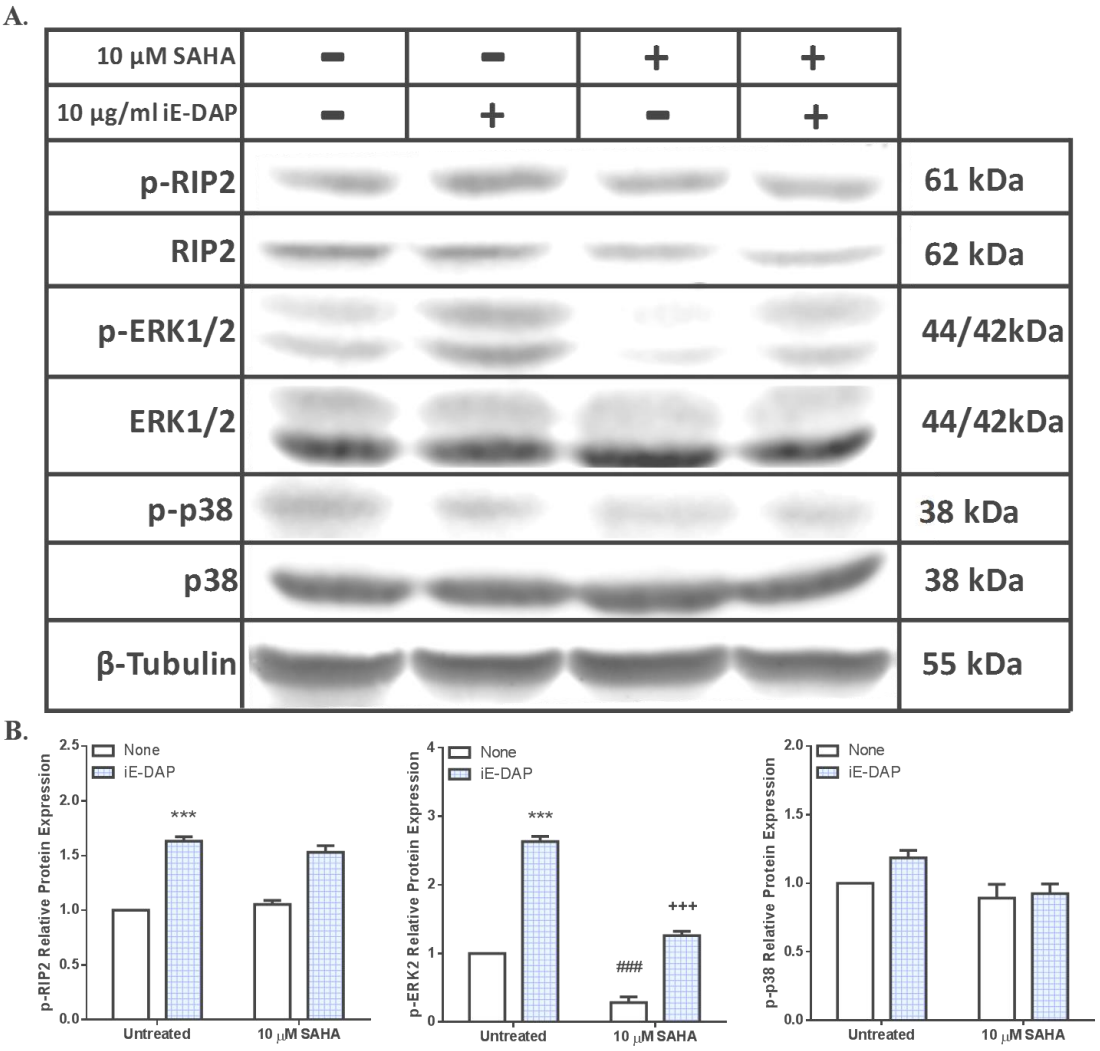

Figure 3.17: IE-DAP-induced RIP2 and MAPK signalling in SAHA-primed HCT116 cells. A) Immunoblots of phosphorylated and total RIP2, p38 and ERK1/2 in cells primed with 10 µM SAHA for 48 hours and subsequently stimulated with iE-DAP (10 µg/ml) for three hours. β-Tubulin acted as the loading control. B) Densitometry of phosphorylated RIP2, p38 and ERK2 expression, relative to β-Tubulin expression. "Untreated + None" was set as the control group. Data is represented as mean relative expression ± S.E.M. and analysed using two-way ANOVAs (followed by Bonferroni's *post-hoc* test). ***** $p < 0.05$ representing **control vs NOD1**, **#** $p < 0.05$ representing **control vs primed**, **+** $p < 0.05$ representing **NOD1 vs (primed + NOD1).**

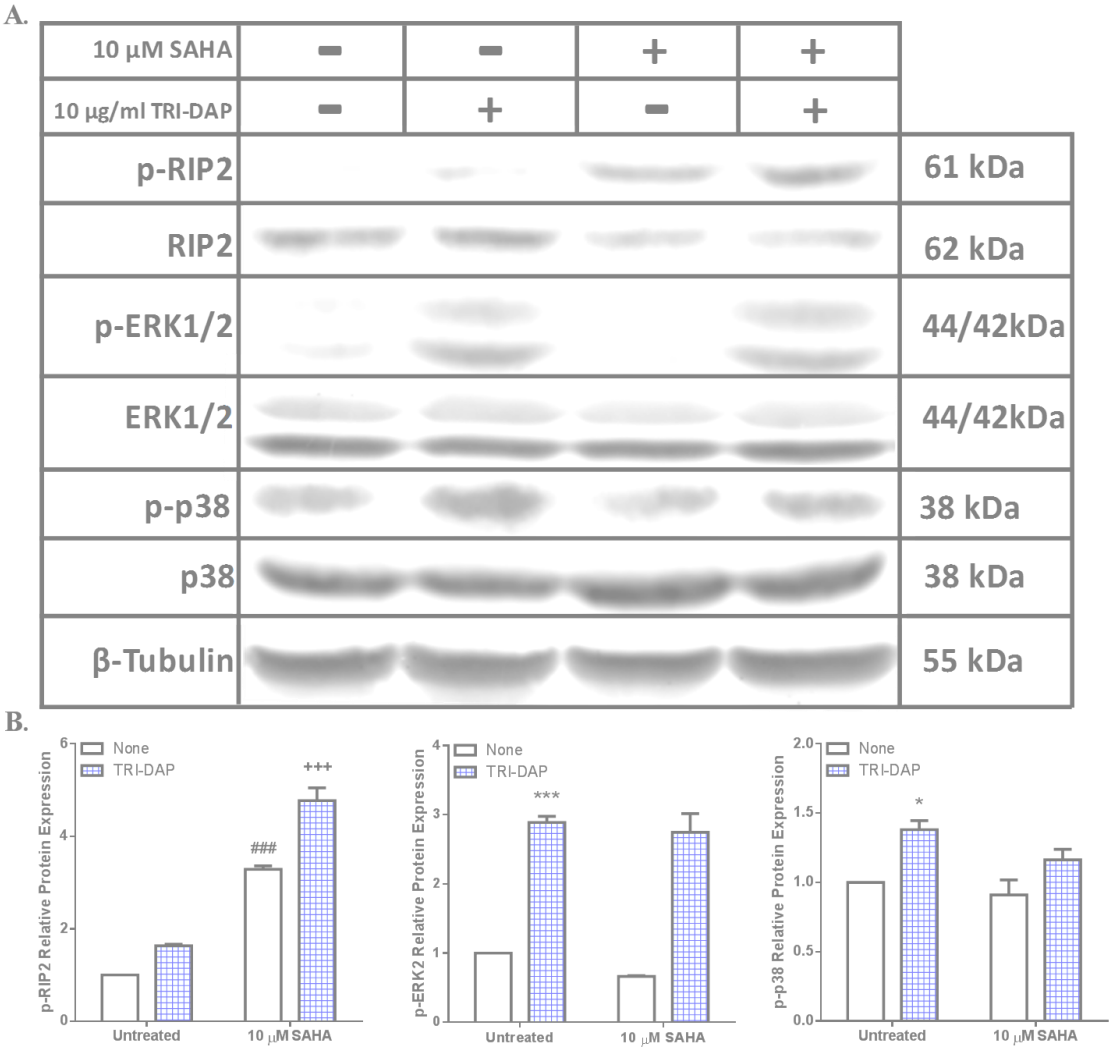

Figure 3.18: TRI-DAP-induced RIP2 and MAPK signalling in SAHA-primed HCT116 cells. A) Immunoblots of phosphorylated and total RIP2, p38 and ERK1/2 in cells primed with 10 µM SAHA for 48 hours and subsequently stimulated with TRI-DAP (10 µg/ml) for one hour. β-Tubulin acted as the loading control. B) Densitometry of phosphorylated RIP2, p38 and ERK2 expression, relative to β-Tubulin expression. "Untreated + None" was set as the control group. Data is represented as mean relative expression ± S.E.M. and analysed using two-way ANOVAs (followed by Bonferroni's *post-hoc* test). ***** $p < 0.05$ representing **control vs NOD1**, **#** $p < 0.05$ representing **control vs primed**, **+** $p < 0.05$ representing **NOD1 vs (primed + NOD1).**

3.4.13 HDAC inhibitor priming increases NOD1-induced NF-κB pro-inflammatory signalling in HCT116 cells.

To build on the findings in the previous section, phosphorylation of p65 and IκBα was investigated in SAHA primed HCT116 cells. Phosphorylated p65 and IκBα expression levels were quantified relative to β-Tubulin. Normalised expression values were calculated relative to the "untreated and unstimulated" ("control") group.

Stimulation of cells with iE-DAP significantly increased IκBα phosphorylation (1.3-fold, $p < 0.01$). Basal IκBα levels were reduced by SAHA priming (0.5-fold, $p < 0.001$), which potentially accounts for the reduced iE-DAP induced p-IκBα production from 1.3-fold to 0.4-fold ($p < 0.001$, relative to untreated + iE-DAP) in SAHA-primed cells (Figure 3.19). As previously recorded, cells were more responsive to TRI-DAP stimulation than iE-DAP. TRI-DAP alone increased phosphorylation of p65 (2.3-fold, $p < 0.001$) and IκBα (4.7-fold, $p < 0.001$). Basal levels of p-p65 were increased 1.7-fold by SAHA treatment ($p < 0.01$), however, this priming did not enhance p-p65 production in response to TRI-DAP stimulation ($p > 0.05$). Activation of IκBα showed a similar pattern to what was recorded following iE-DAP stimulation, but to a greater magnitude. Stimulation of untreated cells with TRI-DAP increased IκBα phosphorylation 4.7-fold ($p < 0.001$). This response was strongly attenuated by SAHA-priming. Relative to the untreated control, priming with SAHA reduced TRI-DAP-induced p-IκBα from 4.7-fold to 1.2-fold ($p < 0.001$, relative to untreated + TRI-DAP), as depicted in Figure 3.20.

Therefore, the effect of SAHA priming on NF-κB signalling was conflicting. SAHA-priming increased basal levels of p65 but didn't enhance responses to NOD1 stimulation. Conversely, SAHA-priming was found to reduce basal p-IκBα which appeared to contribute to reduced p-IκBα responses to NOD1 stimulation. This suggests that SAHA is altering basal NF-κB signalling via a NOD1-independent pathway.

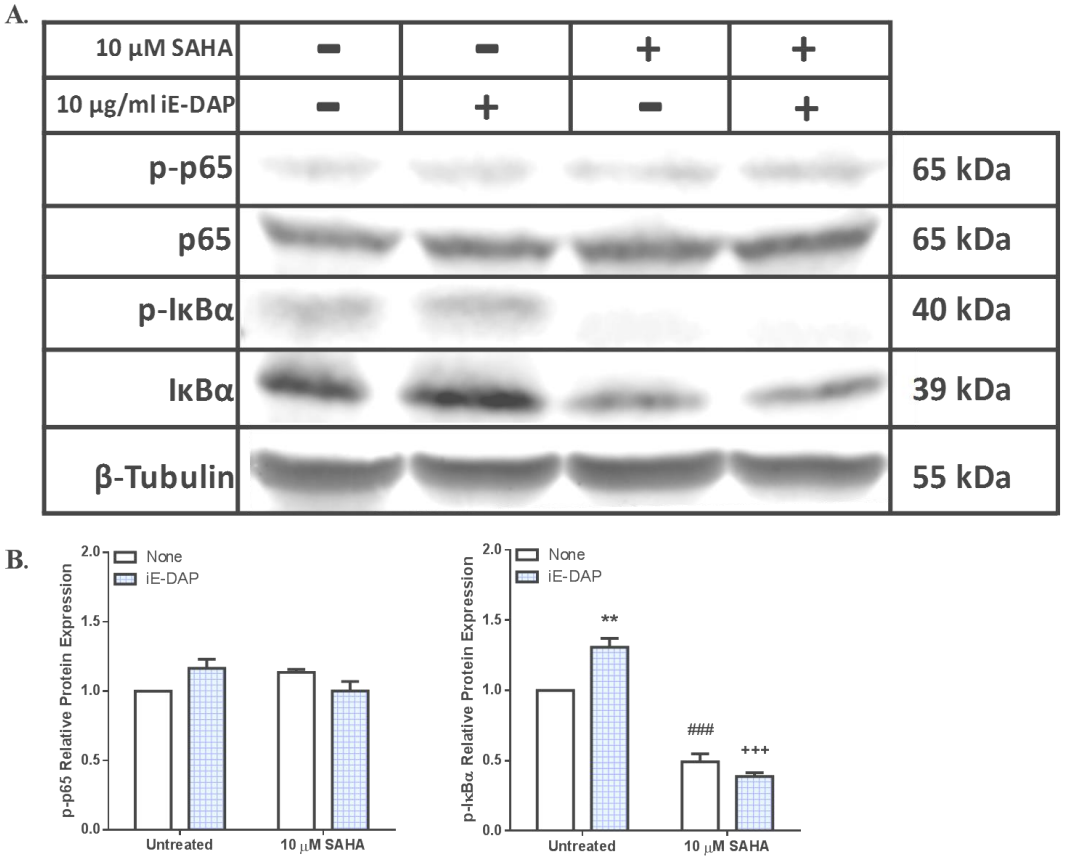

Figure 3.19: IE-DAP-induced NF-κB signalling in SAHA-primed HCT116 cells. (A) Immunoblots of phosphorylated and total p65 and IκBα in cells primed with 10 µM SAHA for 48 hours and subsequently stimulated with iE-DAP (10 µg/ml) for three hours. β- Tubulin acted as the loading control. (B) Densitometry of phosphorylated p65 and IκBα expression, relative to β-Tubulin expression. "Untreated + None" was set as the control group. Data is represented as mean relative expression ± S.E.M. and analysed using two-way ANOVAs (followed by Bonferroni's *post-hoc* test). ***** $p < 0.05$ representing **control vs NOD1**, **#** $p < 0.05$ representing **control vs primed**, **+** $p < 0.05$ representing **NOD1 vs (primed + NOD1).**

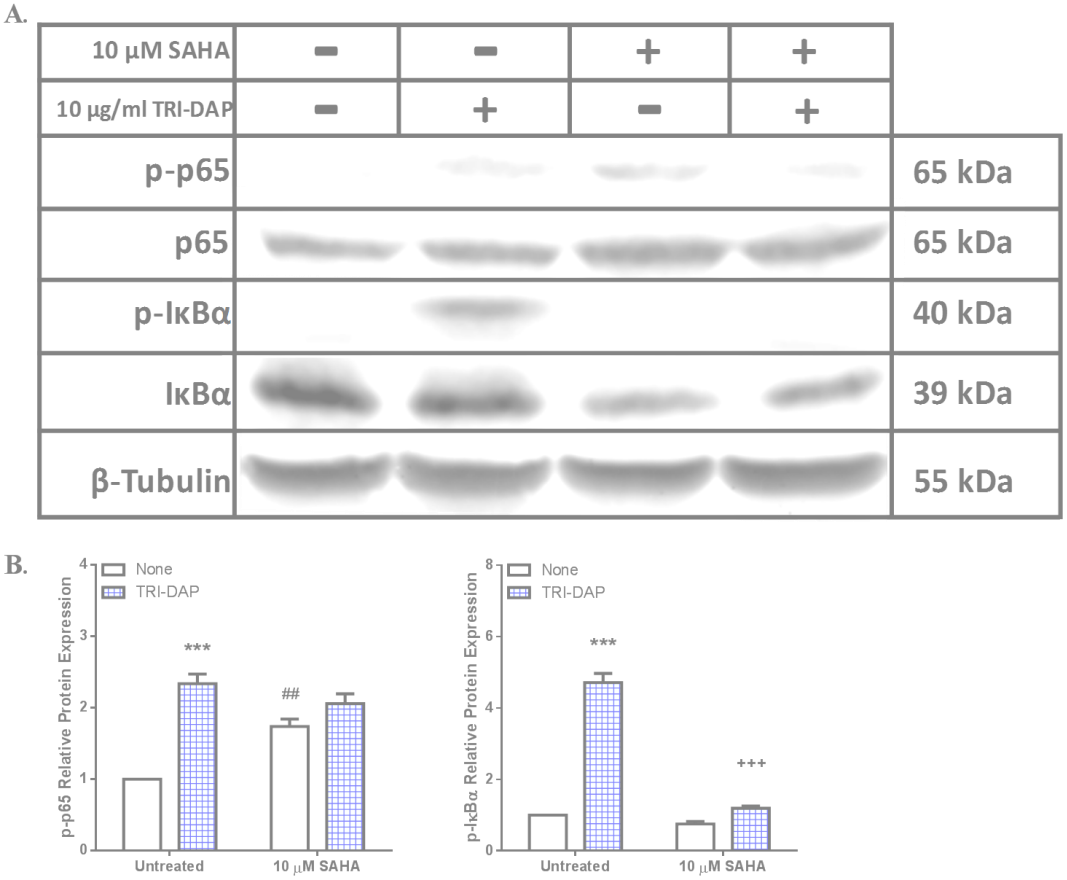

Figure 3.20: TRI-DAP-induced NF-κB signalling in SAHA-primed HCT116 cells. (A) Immunoblots of phosphorylated and total p65 and IκBα in cells primed with 10 µM SAHA for 48 hours and subsequently stimulated with TRI-DAP (10 µg/ml) for one hour. β- Tubulin acted as the loading control. (B) Densitometry of phosphorylated p65 and IκBα expression, relative to β-Tubulin expression. "Untreated + None" was set as the control group. Data is represented as mean relative expression ± S.E.M. and analysed using two-way ANOVAs (followed by Bonferroni's *post-hoc* test). ***** $p < 0.05$ representing **control vs NOD1**, **#** $p < 0.05$ representing **control vs primed**, **+** $p < 0.05$ representing **NOD1 vs (primed + NOD1).**

3.4.14 HDAC inhibitor treatment has differing effects on NOD1 mRNA and protein expression.

The recorded effects of SAHA-priming on NOD1 activity and signalling were varied, preventing a clear pattern of effect to be established. Therefore, NOD1 mRNA and protein basal expression following SAHA treatment were measured to establish if SAHA had a direct effect on receptor expression. NOD1 mRNA was halved following treatment with 10 μM SAHA for 48 hours (0.5-fold, $p < 0.05$) (Figure 3.21 A). However, NOD1 protein nearly doubled post SAHA treatment (1.8-fold, $p < 0.01$) (Figure 3.21 B-C). Therefore, effects of SAHA on NOD1 expression differed at the mRNA and protein levels.

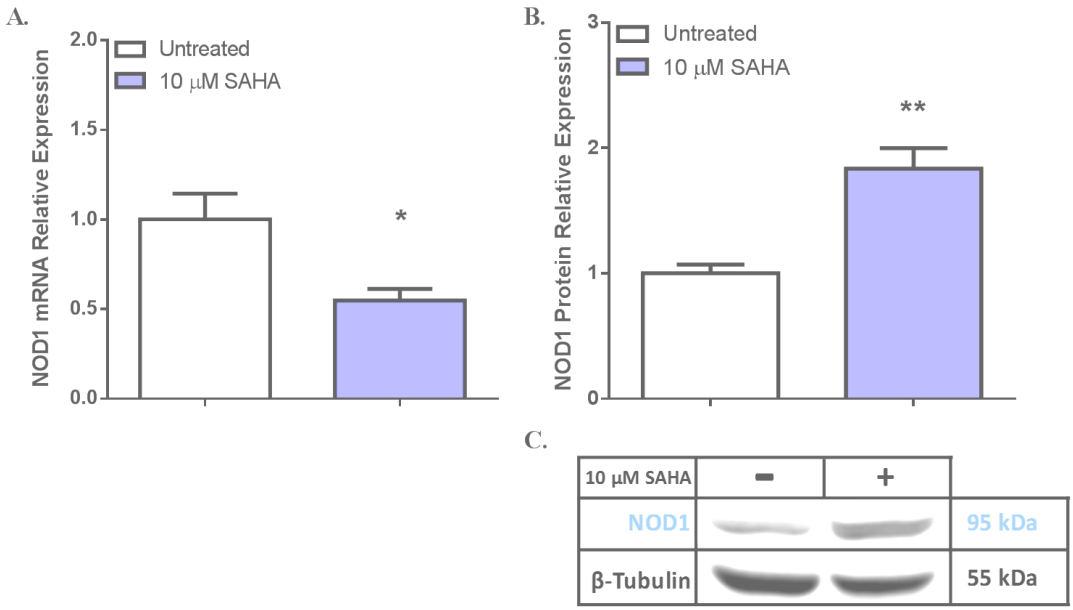

Figure 3.21. NOD1 basal expression in SAHA treated HCT116 cells. (A) NOD1 mRNA expression in HCT116 cells treated with 10 μM SAHA for 48 hours, relative to β-Tubulin expression. (B) Densitometry of NOD1 protein expression in SAHA treated cells, relative to β-Tubulin expression. (C) Representative immunoblot of NOD1 protein expression in SAHA treated cells. Data is represented as mean relative expression ± S.E.M. Statistical analysis was performed using independent t-tests. Significance was recognised at $p < 0.05$, with * representing $p < 0.05$, ** representing $p < 0.01$ and *** representing $p < 0.001$.

3.5 Discussion of Main Findings

The effects of DNA methylation and histone acetylation on NOD1 activity in HCT116 intestinal epithelial cells were investigated here. DNA methylation patterns were disrupted pharmacologically using 5-Azacytidine or 5-Aza-2'-deoxycytidine, which block methylation maintenance functions of the DNMT1 enzyme (Yang et al., 2010). Priming with these agents appeared to significantly increase expression of NOD1 pro-inflammatory cytokines; TNF-α and IL-6 mRNA. Attempts were made to quantify release of these pro-inflammatory cytokines; however, TNF and IL-6 release was found to be below levels of detection. For this reason, focus was switched to IL-8 release quantification. Priming with 5-Aza-dC increased IL-8 release, which echoed the patterns of mRNA data. This reinforces the theory that demethylation potentially increases NOD1 pro-inflammatory activity. This enhanced NOD1 activity was further supported by findings in DNMT3b$^{-/-}$ HCT116 cells relative to their wild-type counterparts. Genetic knockout of the DNA methylation enzyme; DNMT3b, increased NOD1 activity in the same way as 5-Aza-dC priming, represented by exacerbated TNF-α and IL-6 expression and IL-8 release. Therefore, it appears that pharmacological inhibition or genetic knockout of DNA methyltransferases enhances HCT116 cell responses to NOD1 pro-inflammatory activity.

Building on these findings, pro-inflammatory signalling analysis revealed a supportive pattern, whereby both 5-Aza-dC priming and DNMT3b-/- significantly enhanced RIP2/MAPK/NF-κB activation in HCT116 cells. These patterns led to the examination of NOD1 expression, which was found to increase following DNA methylation disruption. Together, these findings suggest that DNA methylation is potentially playing a direct role in NOD1 expression regulation in intestinal epithelial cells. This is a feasible regulation mechanism since bioinformatic analysis revealed the presence of two CpG islands (EMBOSS Newcpgreport, EMBL-EBIM Cambridgeshire, UK), the sites required to support regulatory DNA methylation, in the NOD1 gene (Portela and Esteller, 2010).

Histone acetylation studies carried out in this chapter revealed much more conflicting patterns to those identified with DNA methylation. Treatment with SAHA; a HDAC inhibitor, increased basal levels of TNF-α / IL-6 expression and IL-8 release. This NOD1-independent increase potentially accounts for the augmented NOD1 pro-

inflammatory activity recorded in SAHA-primed HCT116 cells. Mixed effects of SAHA on NOD1 associated RIP2/MAPK/NF-κB signalling, also indicated a NOD1-independent mechanism at play. SAHA treatment lowered NOD1 mRNA expression, potentially via the upregulation of a negative regulator. However, this decrease didn't remain at the protein level, instead NOD1 was increased. These conflicting findings could be a result of differences in mRNA and protein stability. It has been reported previously that treatment with HDAC inhibitors promote a hyperacetylated state of histone H3 at the promoter and transcribing regions of the *hsp70* gene, and subsequently increases expression of the gene (Zhao et al., 2006). Hsp70 is a chaperone protein that stabilises NOD1 and NOD2 receptor stability, therefore upregulation of this stabilising protein could account for the increased NOD1 protein. In conclusion, the current findings suggest for the first time that NOD1 receptor responses in intestinal epithelial cells are potentially regulated directly by DNA methylation and indirectly altered by histone acetylation.

Limitations and Future Work.

Some limitations of the work presented in this chapter surround the measurement of cytokine/chemokine expression and release, as well as the differences observed in NOD1 mRNA and protein data following SAHA treatment. As already mentioned, TNF-α and IL-6 cytokine release from HCT116 cells was not detectable and so IL-8 release was quantified instead. Therefore, the qPCR data didn't match the ELISA data in terms of the analyte chosen to be investigated. In order to acquire a more complete picture of the effects of hypomethylated or hyperacetylated states on IL-8 production, IL-8 mRNA expression could also be analysed by qPCR. It would be interesting to determine if the strong increases recorded in IL-8 cytokine release are matched at the mRNA level. This data could also provide insight into the unexpected increase in IL-8 release from cells primed with SAHA. If IL-8 mRNA patterns matched that of the release data, it would support the theory that SAHA is increasing basal IL-8 expression, regardless of NOD1 stimulation. There is also scope to investigate the mechanistic reasons underlying why significant increases were detected in TNF-α/IL-6 mRNA expression but not in TNF-α/IL-6 release. This could be a result of mRNA not being translated to protein, or perhaps the proteins are being generated within the HCT116 cells, but are unable to be released from the interior, thereby potentially

accounting for the lack of detectable TNF-α/IL-6 in the cell medium being analysed by ELISA. The HCT116 intestinal epithelial cell line could potentially have defective secretion systems as a result of the cancer phenotype. This could be investigated by lysing the HCT116 cells and subsequently quantifying TNF-α/IL-6 protein levels by ELISA. If TNF-α/IL-6 protein is detectable under these conditions, it would imply that HCT116 cells could have faulty modes of cytokine secretion possibly as a result of defective Golgi apparatus and/or molecular transporters. Further analysis could be carried out by quantifying TNF-α/IL-6 release from primary cells under the same experimental conditions to establish if the defective TNF-α/IL-6 release was due to the cancer phenotype.

Additional experimentation could be carried out to explore the differences in NOD1 mRNA and protein expression uncovered in this chapter following SAHA treatment. As mentioned earlier, SAHA treatment has previously been found to increase expression of the Hsp70 chaperone protein. Therefore, expression of the Hsp70 could be quantified after SAHA treatment, by qPCR and western blotting methods, to establish if the greater NOD1 protein expression is possibly a result of enhanced stabilisation by Hsp70. This additional experimentation could potentially answer several questions that remain at the end of this chapter.

Chapter 4 Analysis of NOD2 activity, signalling and expression in the HCT116 intestinal cell line, following epigenetic modification.

4.1 Introduction

NOD2 is an intracellular NOD-like receptor that is more selectively distributed across the body, with expression only recorded in macrophages, monocytes, Paneth intestinal cells and dendritic cells (Inohara et al., 2003). Although NOD2 is more selective in its distribution, it acts as a more general sensor of bacteria, responding to all Gram negative (e.g. *Salmonella typhimurium* and *Shigella flexneri*) and positive bacteria (e.g. *S. pneumoniae* and *S. aureus*), as reviewed in (Moreira and Zamboni, 2012). NOD2 recognises a conserved motif in the peptidoglycan of these bacteria; muramyl dipeptide (MDP). NOD2 receptors share the same signalling pathway with NOD1. Activation of this receptor triggers pro-inflammatory signalling via RIP2, MAPK (including ERK1/2 and p38) and NF-κB (including IκBα and p65) signalling. This signalling cascade leads to the activation and translocation of transcription factors (AP-1 and NF-κB), which promote the expression of pro-inflammatory mediators including cytokines (e.g. TNF-α and IL-6) and chemokines (e.g. IL-8) (Hasegawa et al., 2008). Aberrant NOD2 expression has been linked to many chronic inflammatory disorders, as reviewed in (Feerick and McKernan, 2017), of which Crohn's disease has been best characterised (Ogura et al., 2001, Hugot et al., 2001). However, the mechanism underlying regulation of NOD2 expression has yet to be elucidated.

The aim of this chapter was to uncover whether NOD2 responses in intestinal epithelial cells are altered by an epigenetic modification, namely DNA methylation or histone acetylation. The HCT116 intestinal epithelial cell line was chosen as the experimental model since it is one of the few cell types that is known to express NOD2, these cells would encounter trillions of bacteria in the gut (Lee et al., 2012) and have been directly associated with Crohn's disease (Ogura et al 2003). The effects of DNA methylation on NOD2 regulation were investigated via pharmacological inhibition of DNMT1 (5-Aza and 5-Aza-dC) or genetic knockout of DNMT3b ($DNMT3B^{-/-}$ cells, generated by the Vogelstein lab (Rhee et al., 2002). The impact of histone acetylation

on NOD2 regulation was examined using a pan-histone deacetylase inhibitor; suberoylanilide hydroxamic acid (SAHA).

In this chapter it was hypothesised that NOD2 receptor activity and expression are regulated, in HCT116 intestinal epithelial cells, by epigenetic modifications.

4.2 Methods

The methods used in this chapter did not differ in any way from those outlined in chapter 2.

4.3 Experimental Design

These experiments were designed to investigate if DNA hypomethylation or histone hyperacetylation altered NOD2 receptor activity, signalling and expression. HCT116 cells were primed with epigenetic modifying agents that are known to disrupt either DNA methylation or histone acetylation. DNA methylation was disrupted by 5-Aza/5-Aza-dC/DNMT3b$^{-/-}$. Histone acetylation patterns were targeted by SAHA priming. NOD2 pro-inflammatory activity, signalling and basal expression was investigated in these primed cells, relative to untreated cells.

NOD2 pro-inflammatory activity was analysed by stimulating the primed cells with MDP for 6/18hours, after which pro-inflammatory cytokine (TNF-α and IL-6) expression and chemokine (IL-8) release were quantified by qPCR and ELISA, respectively. NOD2 pro-inflammatory signalling was investigated by measuring RIP2, MAPK and NF-κB protein phosphorylation after stimulating primed HCT116 cells with a MDP for two hours, via western blotting. Finally, NOD2 basal expression was quantified in primed vs untreated cells at the mRNA and protein levels by qPCR and western blotting, respectively. All experiments were carried out with at least three independent biological replicates ($n \geq 3$). An overview of the experimental design is presented in Figure 4.1, with a more detailed breakdown outlined in the experimental design index (Table 4.1).

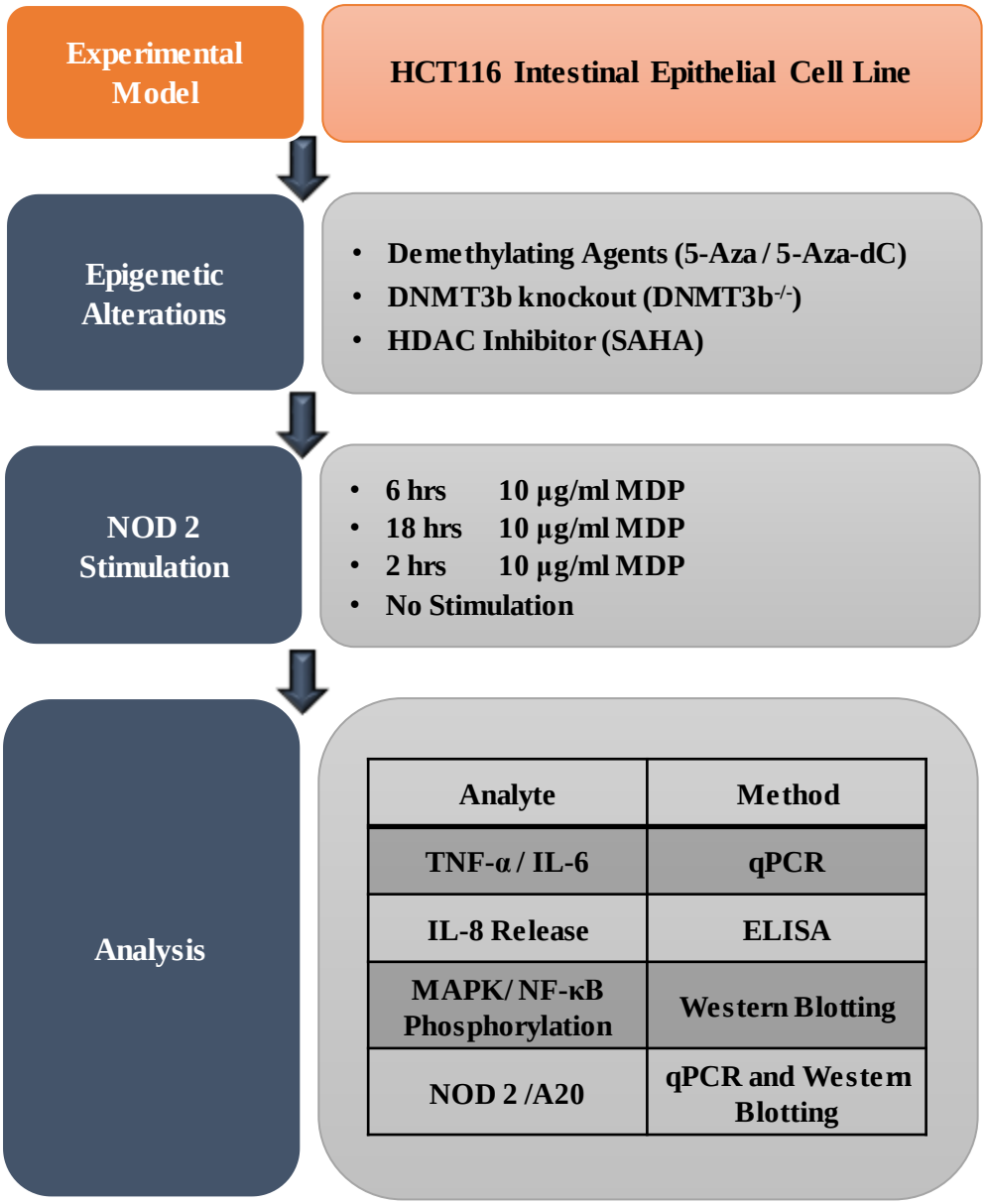

Figure 4.1. Chapter 4 Experimental Design. Outline of epigenetic treatments, NOD 2 stimulation and analysis.

Table 4.1: Chapter 4 Experimental Design Index. Breakdown of treatments, analytes and analysis methods for investigating NOD2 activity, signalling and expression in HCT116 intestinal epithelial cell line.

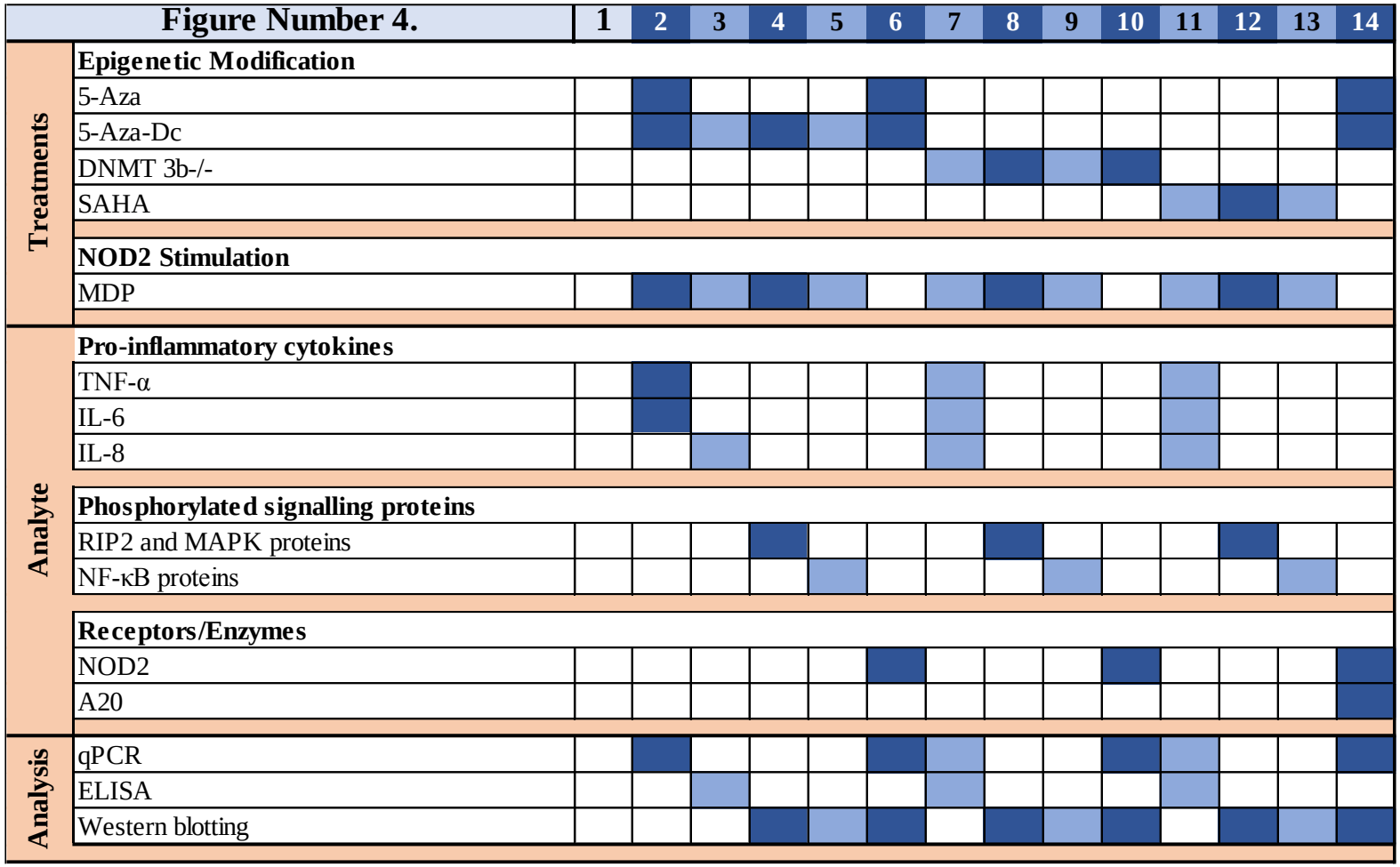

4.4 Results

4.4.1 DNMT1 inhibitor priming increases NOD2-induced pro-inflammatory activity.

The effect of DNA methylation disruption on NOD2-induced pro-inflammatory responses were investigated in HCT116 cells. DNA methylation was interrupted by treating cells with a known demethylating agent; 5 μM 5-Aza or 500 nM 5-Aza-dC, for 72 hours. Following priming with a demethylating agent, cells were stimulated with 10 μg/ml of a NOD2 ligand (MDP) for an additional six or 18 hours. Pro-inflammatory activity was quantified by measuring cytokine (TNF-α and IL-6) mRNA expression, after six hours of MDP, and chemokine (IL-8) release, after 18 hours of MDP. Expression and release were quantified by qPCR and ELISA, respectively.

Stimulation of untreated cells with MDP significantly increased TNF-α expression 18.1-fold ($p < 0.001$). Relative to the untreated control group, priming with 5-Aza exacerbated MDP-induced TNF-α from 18.1-fold to 30.5-fold ($p < 0.001$, relative to untreated + MDP), as depicted in Figure 4.2 A. Similar patterns in IL-6 expression were recorded, but to a lower magnitude. IL-6 expression was marginally increased by MDP alone (1.5-fold $p > 0.05$). Relative to the untreated control group, priming with 5-Aza increased MDP-induced TNF-α from 1.5-fold to 3.4-fold ($p < 0.001$, relative to untreated + MDP), as shown in Figure 4.2 B. Treatment with the more efficient demethylating agent, 5-Aza-dC, had the same effect on TNF-α and IL-6 expression but to a greater magnitude. In this set of experiments, MDP alone was found to increase TNF-α by 17.4-fold ($p < 0.01$) and IL-6 by 2.2-fold ($p > 0.05$).

Relative to the untreated control group, priming with 5-Aza-dC increased MDP-induced TNF-α from 17.4-fold to 260.9-fold ($p < 0.001$, relative to untreated + MDP) and IL-6 from 2.2-fold to 78.8-fold ($p < 0.001$, relative to untreated + MDP), as illustrated in Figure 4.2 C-D.

As stated in the previous chapter, TNF-α and IL-6 protein release from HCT116 cells was undetectable. Therefore, IL-8 release from HCT116 cells was investigated. Time and dose response was investigated to identify an appropriate ligand concentration and stimulation duration (Appendix 3). Basal IL-8 release from HCT116 cells (279.4 ± 10.2 pg/ml) increased approximately 1000-fold following 18 hours of MDP stimulation alone (2585.3 ± 107.1 pg/ml, $p < 0.001$).

Priming with 5-Aza-dC increased MDP-induced IL-8 release from 2585.3 ± 107.1 pg/ml to 3611.3 ± 301.3 pg/ml ($p < 0.001$, relative to untreated + MDP), as shown in Figure 4.3. These data support the pro-inflammatory qPCR findings in Figure 4.2, thereby suggesting that priming with a known demethylating agent enhances responses to NOD2 activation.

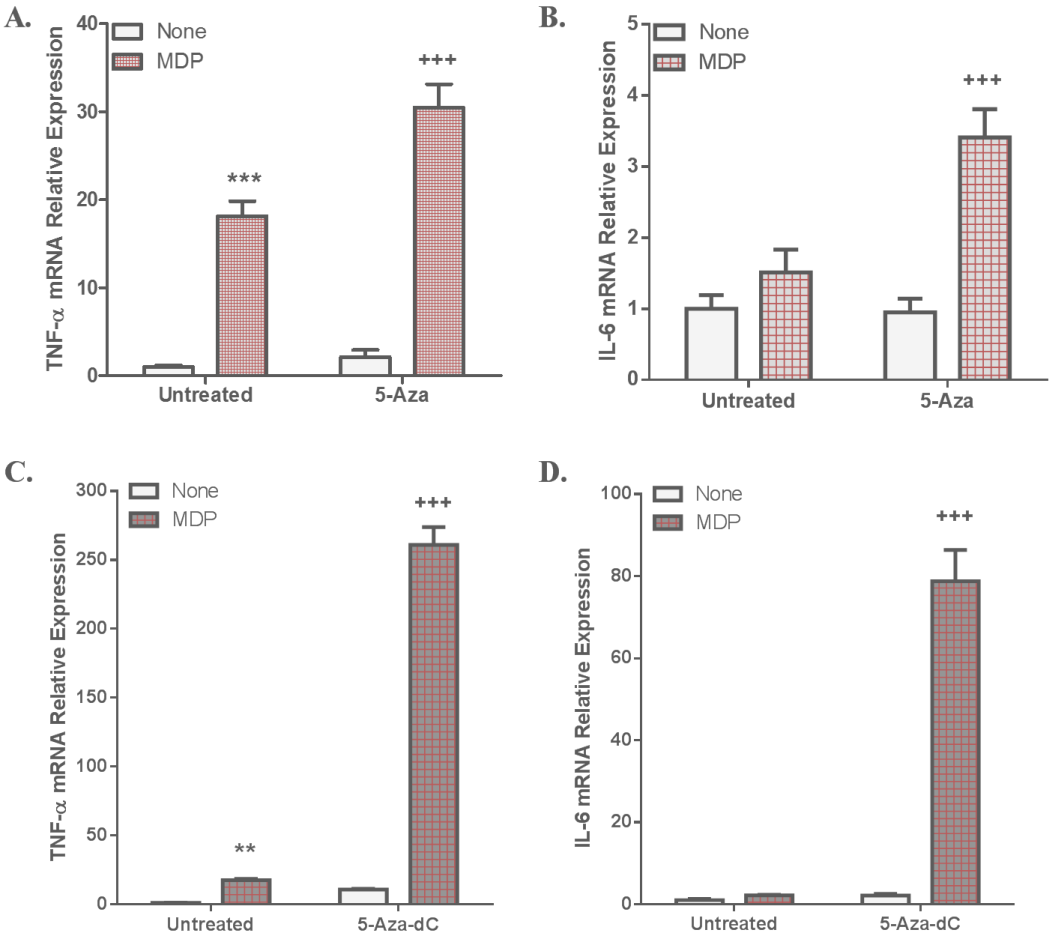

Figure 4.2. NOD2-induced pro-inflammatory cytokine expression in 5-Aza or 5-Aza-dC primed HCT116 cells. A-B) TNF-α and IL-6 mRNA relative expression in HCT116 cells primed with 5 μM 5-Aza for 72 hours and subsequently stimulated with 10 μg/ml MDP for 6 hours. C-D) TNF-α and IL-6 mRNA relative expression in HCT116 cells primed with 500 nM 5-Aza-dC for 72 hours and subsequently stimulated with 10 μg/ml MDP for 6 hours. β-Actin acted as the housekeeping control. "Untreated + None" was set as the control. Data is represented as mean relative expression ± SEM. Statistical analysis was performed using two-way ANOVAs, followed by Bonferroni *post-hoc* test where appropriate. ***** $p < 0.05$ representing **control vs NOD2**, **#** $p < 0.05$ representing **control vs primed**, **+** representing $p < 0.05$ representing **NOD2 vs (primed + NOD2).**

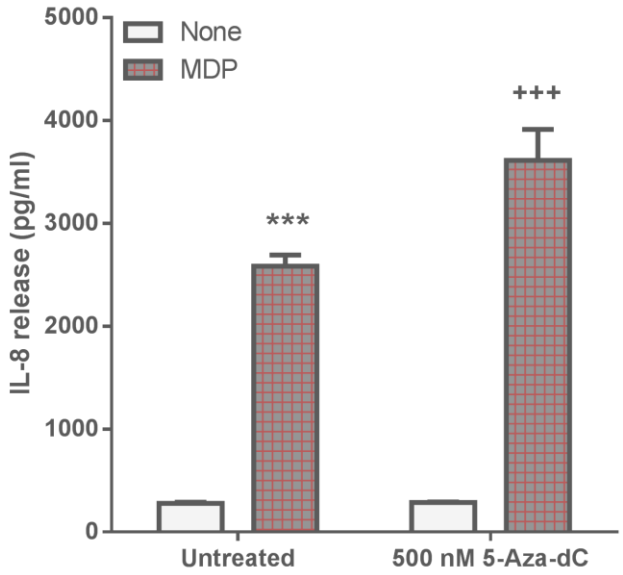

Figure 4.3. NOD2-induced pro-inflammatory IL-8 release from 5-Aza-dC primed HCT116 cells. IL-8 release (pg/ml) from HCT116 cells primed with 500 nM 5-Aza-dC for 72 hours was recorded following stimulation with 10 μg/ml MDP for 18 hours. "Untreated + None" was set as the control. Data is represented as mean absolute concentration ± SEM. Statistical analysis was performed using two-way ANOVAs, followed by Bonferroni *post-hoc* test where appropriate. ***** $p < 0.05$ representing **control vs NOD2**, **#** $p < 0.05$ representing **control vs primed**, **+** $p < 0.05$ representing **NOD2 vs (primed + NOD2).**

4.4.2 DNMT1 inhibitor priming increases NOD2-induced pro-inflammatory RIP2 and MAPK signalling.

Since it was found that treatment with known demethylating agent increased pro-inflammatory activity, the effects of these agents on NOD2-induced signalling was examined next. NOD2 activation initiates a phosphorylation cascade involving RIP2, MAPK and NF-κB proteins. This section focuses on the effects of 5-Aza-dC priming on NOD2-induced phosphorylation of RIP2 and MAPK (ERK2 and p38). Phosphorylation time responses were carried out to select the most appropriate NOD2 stimulation duration (Appendix 5). Based on this investigation, it was decided that cells should be stimulated with 10 μg/ml MDP for two hours. Phosphorylation of the NOD1 adapter protein (RIP2) and MAPK signalling proteins (ERK1/2 and p38) was investigated by western blot analysis. Blots were repeated for three independent experiments, with representative blots shown. Protein expression was quantified by densitometry of phosphorylated, total and housekeeping proteins. Phosphorylated protein expression was normalised relative to their total proteins, and subsequently calculated relative to the untreated control group.

Western blot analysis revealed that MDP stimulation increased phosphorylation of RIP2 (2.2-fold, $p < 0.01$) and ERK2 (2-fold, $p > 0.05$). These responses to MDP were significantly exacerbated by 5-Aza-dC priming. Relative to the untreated control group, priming with 5-Aza-dC exacerbated MDP-induced p-RIP2 from 2.2-fold to 4.2-fold ($p < 0.001$, relative to untreated + MDP), p-ERK2 from 2-fold to 4-fold ($p < 0.01$, relative to untreated + MDP) and p-p38 from 1.1-fold to 1.4-fold ($p < 0.01$, relative to untreated + MDP), as outlined in Figure 4.4. Therefore, priming with a demethylating agent appears to support greater pro-inflammatory signalling following NOD2 activation.

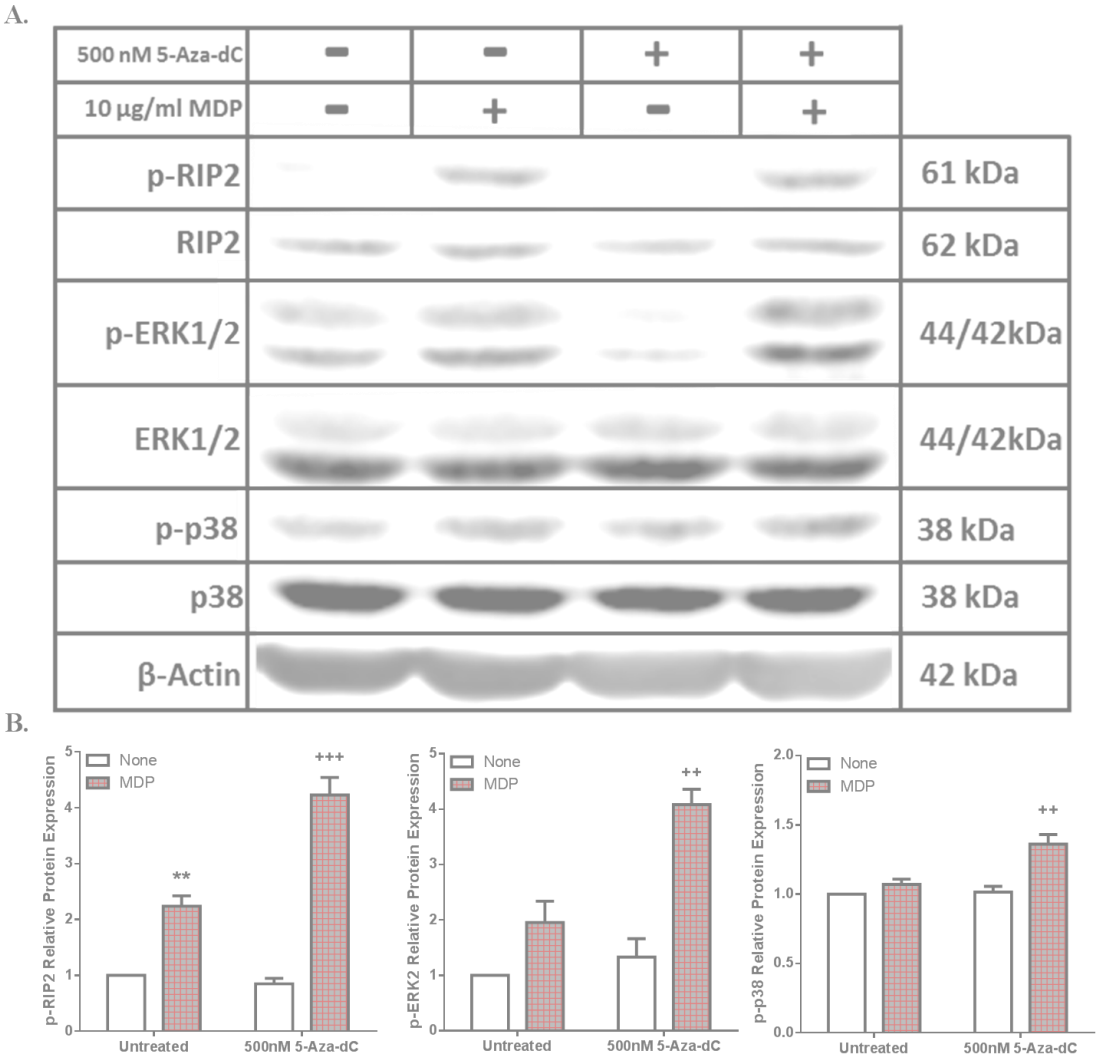

Figure 4.4. NOD2-induced RIP2 and MAPK signalling in 5-Aza-dC primed HCT116 cells. (A) Immunoblots of phosphorylated and total RIP2, ERK1/2 and p38 in 5-Aza-dC primed cells stimulated with 10 µg/ml MDP for two hours. β-Actin acted as the loading control. B) Densitometry of phosphorylated RIP2, ERK1/2 and p38 expression, relative to total protein expression. Untreated + None" was set as the control. Data is represented as mean relative expression ± S.E.M. and analysed using two-way ANOVAs (followed by Bonferroni's *post-hoc* test). ***** $p < 0.05$ representing **control vs NOD2**, **#** $p < 0.05$ representing **control vs priming, +** $p < 0.05$ representing **NOD2 vs (priming + NOD2).**

4.4.3 DNMT1 inhibitor priming increases NOD2-induced pro-inflammatory NF-κB signalling.

To complete the investigation of NOD2-associated pro-inflammatory signalling following priming with a demethylating agent, NF-κB signalling was measured. NOD2 stimulation phosphorylates the NF-κB inhibitor; IkBα, liberating NF-κB from its inhibitory effects. NF-κB is subsequently exposed for phosphorylation / activation. Phosphorylation of the NF-κB subunit; p65, was investigated in this body of work. Phosphorylation of p65 and IκBα was expressed relative to the loading control (β-Actin), since treatment has a direct effect on IκBα total protein.

NOD2 stimulation with 10 μg/ml MDP for two hours increased phosphorylation of p65 (1.9-fold, $p < 0.05$) and p- IkBα (3.5-fold, $p < 0.05$). Relative to the untreated control group, priming with 5-Aza-dC increased MDP-induced p-p65 from 1.9-fold to 3.3-fold ($p < 0.001$, relative to untreated + MDP), as outlined in Figure 4.5, suggesting that the demethylating agent increased NOD2-induced pro-inflammatory NF-κB signalling.

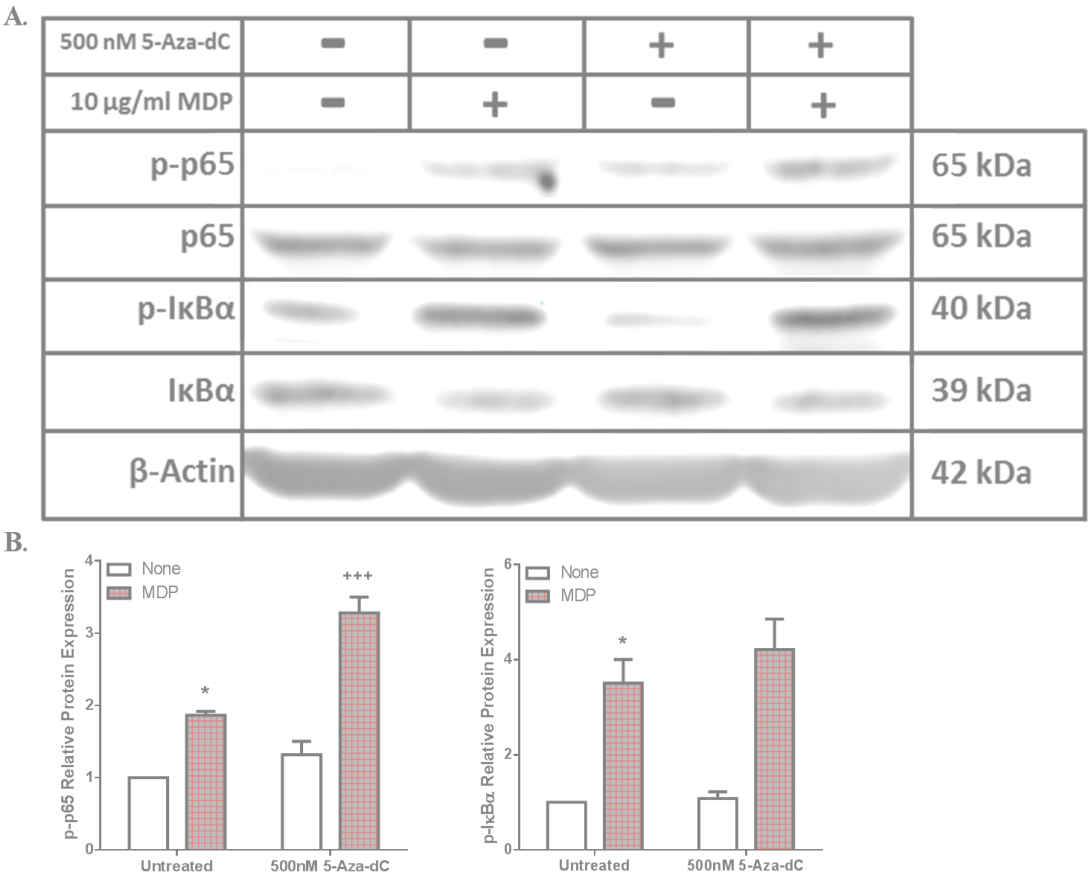

Figure 4.5. MDP-induced NF-κB signalling in 5-Aza-dC primed HCT116 cells. (A) Immunoblots of phosphorylated and total p65 and IκBα in cells primed with 500 nM 5-Aza-dC for 72 hours and subsequently stimulated with 10 µg/ml MDP for two hours. β- Actin acted as the loading control. (B) Densitometry of phosphorylated p65 and IκBα expression, relative to β-Actin expression. Untreated + None" was set as the control. Data is represented as mean relative expression ± S.E.M. and analysed using two-way ANOVAs (followed by Bonferroni's *post-hoc* test). ***** $p < 0.05$ representing **control vs NOD2**, **#** $p < 0.05$ representing **control vs primed**, **+** $p < 0.05$ representing **NOD2 vs (primed + NOD2).**

4.4.4 DNMT1 inhibitor priming increases NOD2 basal expression.

Since priming of cells with a DNMT1 inhibitor increases NOD2-induced pro-inflammatory activity and signalling, the direct effect of these agents on NOD2 expression was investigated by qPCR and western blotting. Treatment of HCT116 cells with 5 μM 5-Aza for 72 hours increased NOD2 protein expression 1.5-fold ($p < 0.05$) (Figure 4.6 C and E). Treatment with the more efficient demethylating agent; 5-Aza-dC (500 nM), for 72 hours, increased NOD2 expression at the mRNA (2.5-fold, $p < 0.001$) and protein (3.3-fold, $p < 0.01$) levels (Figure 4.6 B, D and F). The increased NOD2 expression recorded here, implies that NOD2 expression may be regulated by DNA methylation. This would provide an explanation for the increased pro-inflammatory responses recorded in cells primed with a demethylating agent.

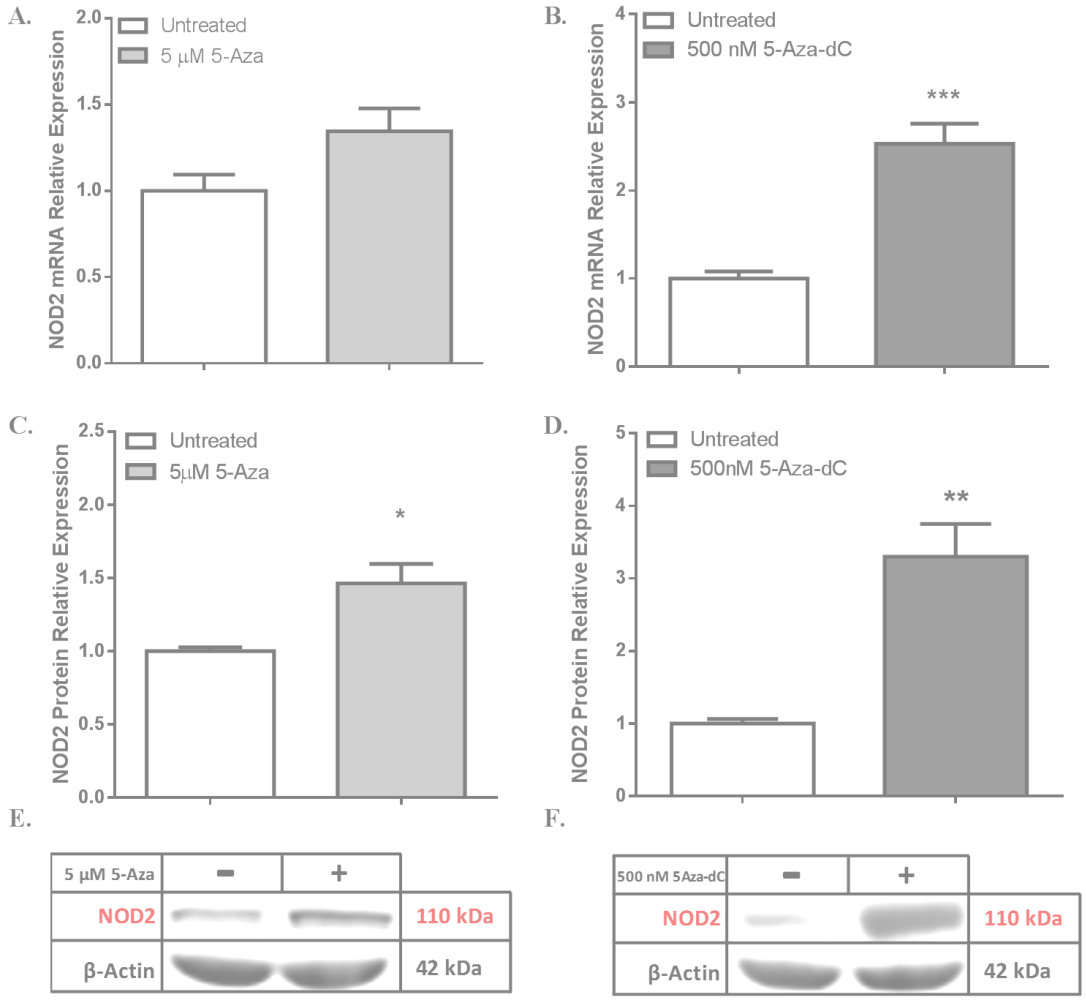

Figure 4.6. NOD2 basal expression following 5-Aza or 5-Aza-dC treatment. (A-B) NOD2 mRNA expression following 5 µM 5-Azacytidine (5-Aza) or 500 nM 5-Aza-2'-deoxycytidine (5-Aza-dC) for 72 hours, relative to β-Actin expression. (C-D) Densitometry of NOD2 protein expression following 5 µM 5-Aza or 500 nM 5-Aza-dC for 72 hours, relative to β-Actin expression. (E-F) Representative immunoblots of NOD2 protein expression following 5 µM 5-Aza or 500 nM 5-Aza-dC for 72 hours, relative to β-Actin expression. Data is represented as mean relative expression ± S.E.M. Statistical analysis was performed using independent t-tests. Significance was recognised at $p < 0.05$, with * representing $p < 0.05$, ** representing $p < 0.01$ and *** representing $p < 0.001$.

4.4.5 NOD2 gene contains CpG islands

Given that NOD2 expression was altered by known demethylating agents, it was proposed that the NOD2 gene could potentially be regulated by DNA methylation. If a gene is regulated by DNA methylation, it must have CpG islands in its sequence. Therefore, bioinformatic analysis was carried out to check for the presence of CpG islands. NOD2 was found to have four CpG islands in its sequence (Table 4.2), thereby further supporting the hypothesis that NOD2 expression is regulated by DNA methylation.

Characteristic	Requirement	Island 1	Island 2	Island 3	Island 4
GC Content	≥ 50%	52.70%	55.47%	81.18%	55.86%
Genomic Length	> 200 b.p.	222b.p.	375b.p.	255b.p.	222b.p.
Observed:Expected	> 0.6	1.67	1.07	0.83	0.70

Table 4.2. CpG Islands identified in the NOD2 gene sequence. CpG rich clusters in gene sequences must pass three main criteria to be classified as a "CpG island"; GC content must be greater than or equal to 50%, the genomic segment must exceed 200 base pair and the ratio of observed CpG dinucleotide content vs expected CpG dinucleotide content must be greater than 0.6. Details of the four CpG islands identified in the NOD2 genome sequence are outlined. Data was generated using the EMBOSS Newcpgreport computer software (EMBL-EBIM Cambridgeshire, UK).

4.4.6 DNMT3b genetic knockout increases NOD2-induced pro-inflammatory activity.

The effect of DNA methylation on NOD2 activity was further investigated using HCT116 cells with DNMT3b, a DNA methylation enzyme, genetically knocked out ($DNMT3b^{-/-}$). Confirmation of this genetic knockout was confirmed in Chapter 3 (Section 3.4.6).

TNF-α and IL-6 expression was quantified in $DNMT3b^{-/-}$ cells, relative to wild-type HCT116 cells, following NOD2 stimulation. This was done to examine if knockout of DNMT3b alters the pro-inflammatory activity triggered by NOD2 stimulation. Stimulation with 10 μg/ml MDP for six hours increased expression of TNF-α (3.6-fold, $p > 0.05$) and IL-6 (5.2-fold, $p > 0.05$). Basal IL-6 expression was significantly higher in $DNMT3b^{-/-}$ cells relative to wild-type cells (19-fold, $p < 0.001$). Relative to the wild-type control group, $DNMT3b^{-/-}$ cells stimulated with MDP exhibited enhanced levels of TNF-α from 3.6-fold to 15.8-fold ($p < 0.001$, relative to wild-type + MDP), and IL-6 from 5.2-fold to 29.2-fold ($p < 0.001$, relative to wild-type + MDP), as shown in Figure 4.7 A-B.

To further investigate NOD2-induced pro-inflammatory activity in $DNMT3b^{-/-}$ cells, IL-8 release was measured. Basal IL-8 release from wild-type HCT116 cells (172 ± 9.7 pg/ml) were increased approximately 6-fold following exposure to MDP (1029 ± 5.2 pg/ml, $p < 0.001$). IL-8 levels dropped to 47.5 ± 1.1 pg/ml in $DNMT3b^{-/-}$ cells ($p < 0.001$). Despite this drop in basal IL-8, these knockout cells showed an exacerbated response to MDP, relative to their wild-type counterparts. MDP stimulated $DNMT3b^{-/-}$ cells released 2803.6 ± 7.5 pg/ml IL-8 ($p < 0.001$, relative to wild-type +MDP), which was almost three times the response recorded in stimulated wild-type cells (Figure 4.7 C). Taken together, these data suggest that NOD2 associated pro-inflammatory activity, represented by increased TNF-α/IL-6 expression and IL-8 release, is augmented when DNMT3b is knocked out. This finding supports the enhanced pro-inflammatory activity recorded earlier in 5-Aza-dC primed cells.

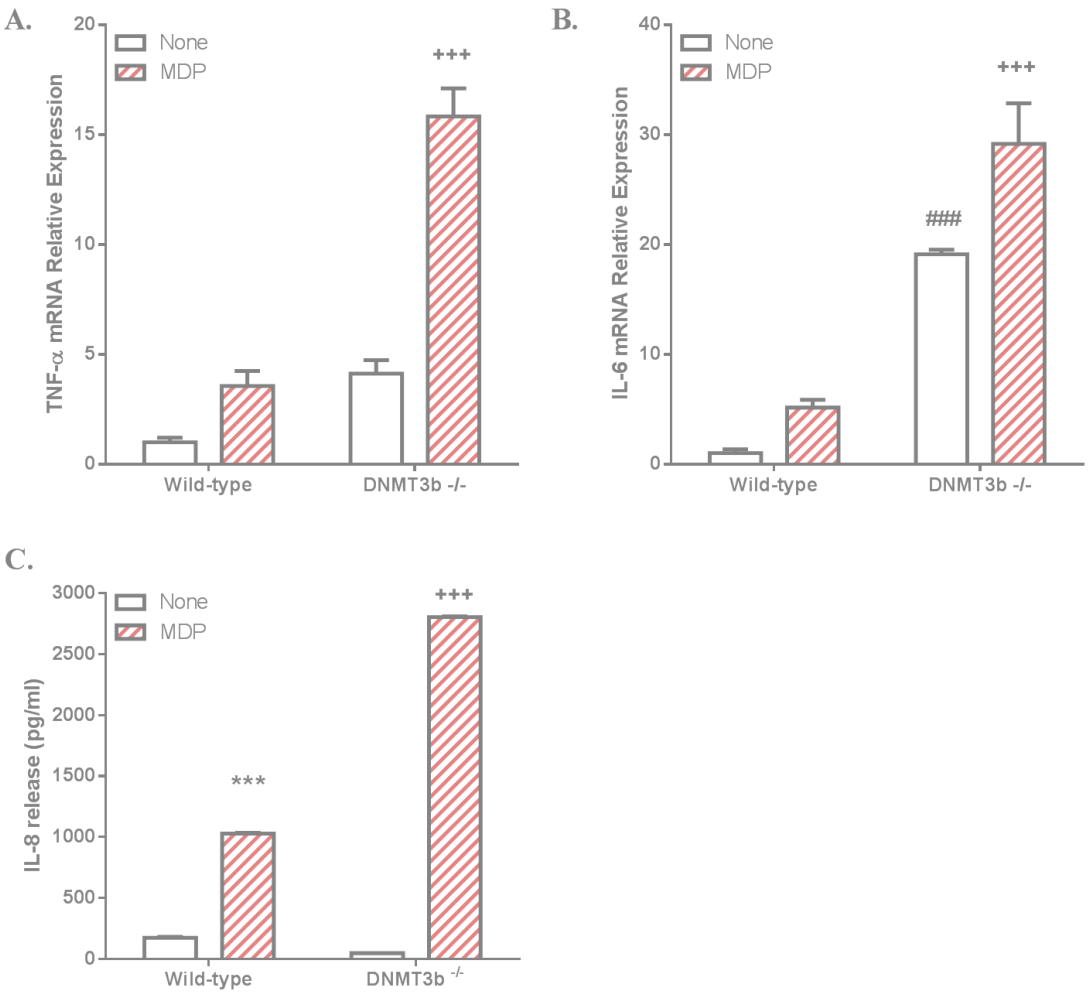

Figure 4.7. NOD2-induced pro-inflammatory cytokine expression and chemokine release in DNMT3b$^{-/-}$ HCT116 cells. A-B) TNF-α and IL-6 mRNA relative expression in DNMT3b$^{-/-}$ cells stimulated with 10 μg/ml MDP for six hours. β-Actin acted as the housekeeping control. "Wild-type + None" was set as the control. Data is represented as mean relative expression ± S.E.M. C) IL-8 release from DNMT3b$^{-/-}$ cells following stimulation with 10 μg/ml MDP for 18 hours. "Wild-type + None" was set as the control. Data is represented as mean absolute ± S.E.M. Statistical analysis was performed using two-way ANOVAs, followed by Bonferroni *post-hoc* test where appropriate. ***** $p < 0.05$ representing **control vs NOD2**, **#** $p < 0.05$ representing **control vs DNMT3b$^{-/-}$**, **+** representing $p < 0.05$ **NOD2 vs (DNMT3b$^{-/-}$ + NOD2).**

4.4.7 DNMT3b genetic knockout increases NOD2-induced pro-inflammatory RIP2 and MAPK signalling.

Since NOD2-induced pro-inflammatory activity was found to be increased in DNMT3b$^{-/-}$ cells, the effect of this knockout on pro-inflammatory RIP2 and MAPK signalling was investigated, relative to their wild-type counterparts. The stimulation duration required to detect phosphorylation was chosen as before, based on the HCT116 preliminary phosphorylation time response analysis (Appendix 5). Cells were stimulated with MDP for two hours. Phosphorylation of the NOD2 adapter protein (RIP2) and MAPK signalling proteins (ERK1/2 and p38) was investigated by western blot analysis. Blots were repeated for three independent experiments, with representative blots shown. Protein expression was quantified by densitometry of phosphorylated, total and housekeeping proteins. Phosphorylated protein expression was normalised relative to their total proteins, and subsequently calculated relative to the untreated control group.

Stimulation of wild-type cells with MDP significantly increased p-RIP2 (2.3-fold, $p < 0.001$), p-ERK2 (4-fold, $p < 0.001$) and p-p38 (1.6-fold, $p < 0.01$). RIP2 and MAPK pro-inflammatory signalling was significantly exacerbated in DNMT3b$^{-/-}$ cells. Relative to the wild-type control group, DNMT3b$^{-/-}$ cells stimulated with MDP exhibited enhanced levels of p-RIP2 from 2.3-fold to 6-fold ($p < 0.001$, relative to wild-type + MDP), p-ERK from 4-fold to 17.3-fold ($p < 0.001$, relative to wild-type + MDP), and p-p38 from 1.6-fold to 2.3-fold ($p < 0.001$, relative to wild-type + MDP), as shown in Figure 4.8. The enhanced RIP2 and MAPK signalling, in the presence of the DNMT3b knockout, suggests that the NOD2 response is potentially being influenced by DNA methylation.

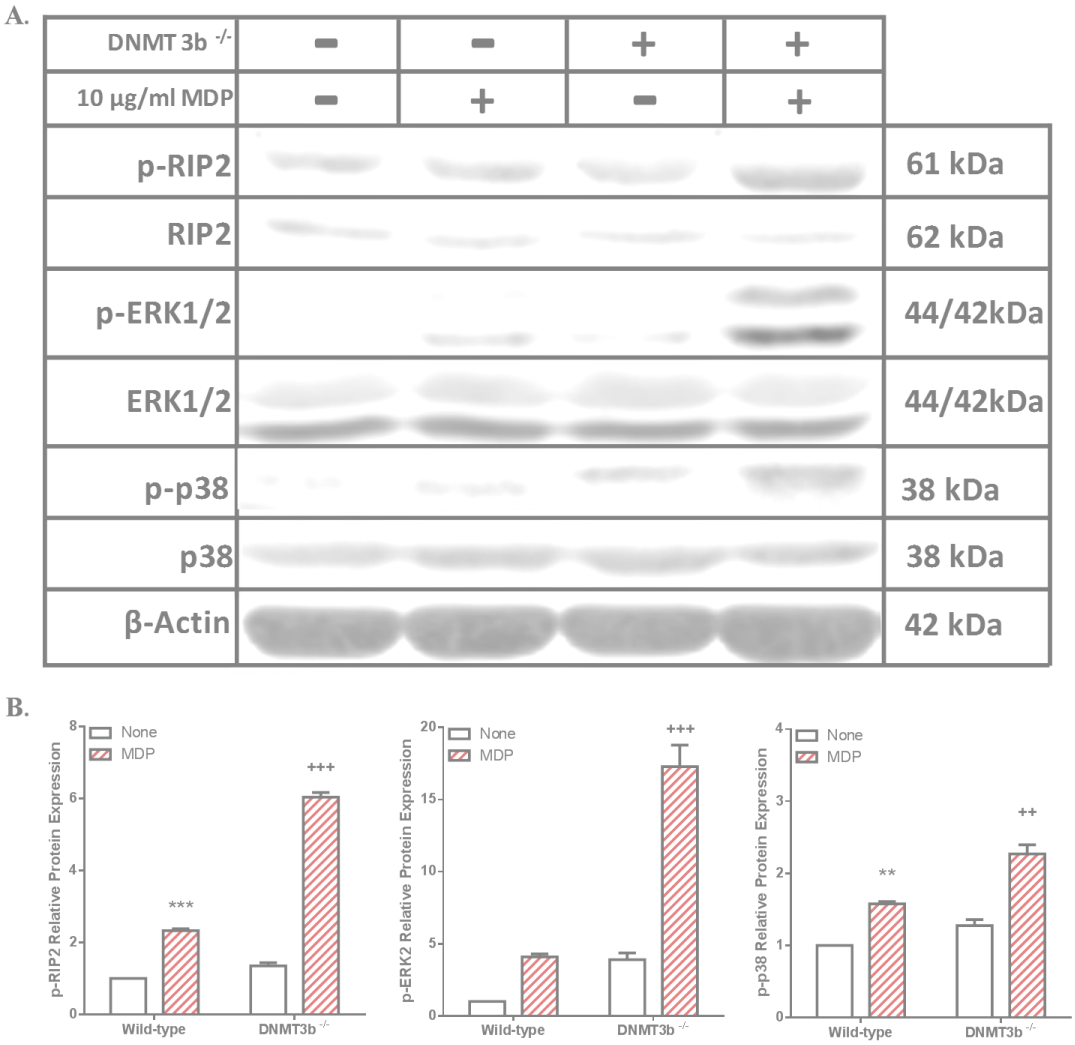

Figure 4.8. NOD2-induced RIP2 and MAPK signalling in DNMT3b-/- HCT116 cells. (A) Immunoblots of phosphorylated and total RIP2, ERK1/2 and p38 in DNMT3b-/- cells stimulated with 10 µg/ml MDP for two hours. β-Actin acted as the loading control. B) Densitometry of phosphorylated RIP2, ERK1/2 and p38 expression, relative to total protein expression. "Wild-type + None" was set as the control. Data is represented as mean relative expression ± S.E.M. and analysed using two-way ANOVAs (followed by Bonferroni's *post-hoc* test). ***** $p < 0.05$ representing **control vs NOD2**, **#** $p < 0.05$ representing **control vs DNMT3b$^{-/-}$, +** $p < 0.05$ representing **NOD2 vs (DNMT3b$^{-/-}$ + NOD2).**

4.4.8 DNMT3b genetic knockout increases NOD2-induced pro-inflammatory NF-κB signalling.

To complete the analysis of NOD2 pro-inflammatory signalling in DNMT3b$^{-/-}$ cells, relative to wild-type HCT116 cells, NF-κB signalling was investigated. To do this, MDP-induced phosphorylation of p65 and IκBα was analysed. Phosphorylation of p65 and IκBα was expressed relative to the loading control (β-Actin), since treatment has a direct effect on IκBα total protein. The same MDP-stimulation duration was chosen as was used for RIP2 and MAPK detection (Appendix 5).

Stimulation of wild-type HCT116 cells with 10 μg/ml MDP for two hours significantly increased p-p65 (4.6-fold, $p < 0.001$) and p-IκBα (2-fold, $p < 0.01$). Basal p-p65 was significantly higher in DNMT3b$^{-/-}$ cells (8.5-fold, $p < 0.001$). Relative to the wild-type control group, DNMT3b$^{-/-}$ cells stimulated with MDP exhibited enhanced levels of p-p65 from 4.6-fold to 9.9-fold ($p < 0.001$, relative to wild-type + MDP) and p-IκBα from 2-fold to 3.3-fold ($p < 0.01$, relative to wild-type + MDP), as outlined in Figure 4.9. This enhanced NF-κB phosphorylation, alongside the increased RIP2 and MAPK activation, together suggest DNMT3b$^{-/-}$ cells are more responsive than wild-type cells to NOD2 stimulation.

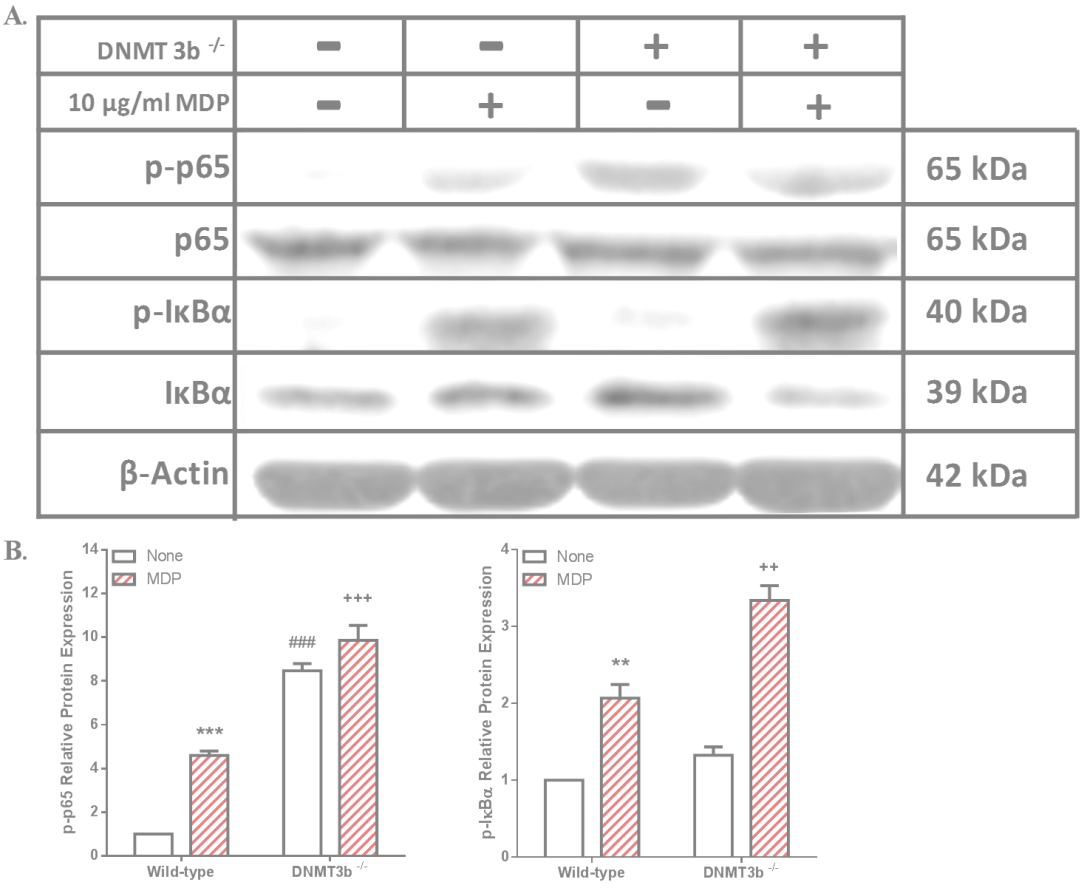

Figure 4.9. MDP-induced NF-κB signalling in DNMT3b-/- primed HCT116 cells. (A) Immunoblots of phosphorylated and total p65 and IκBα in DNMT3b-/- cells stimulated with 10 µg/ml MDP for two hours. β- Actin acted as the loading control. (B) Densitometry of phosphorylated p65 and IκBα expression, relative to β-Actin expression. "Wild-type + None" was set as the control. Data is represented as mean relative expression ± S.E.M. and analysed using two-way ANOVAs (followed by Bonferroni's *post-hoc* test). ***** $p < 0.05$ representing **control vs NOD2**, **#** $p < 0.05$ representing **control vs DNMT3b$^{-/-}$**, **+** $p < 0.05$ representing **NOD2 vs (DNMT3b$^{-/-}$ + NOD2).**

4.4.9 Basal NOD2 expression is higher in DNMT3b$^{-/-}$ HCT116 cells relative to wild-type counterparts.

Since NOD2-induced pro-inflammatory activity and signalling were found to be augmented in DNMT3b$^{-/-}$ cells, NOD2 expression was compared between these knockout and wild-type HCT116 cells to uncover a potential mechanism of action. NOD2 expression was increased at the mRNA (2.3-fold, $p < 0.001$) and protein (1.8-fold, $p < 0.001$) levels (Figure 4.10). This increase in NOD2 expression provides a potential explanation as to why DNMT3b knockout cells are more responsive to NOD2 stimulation.

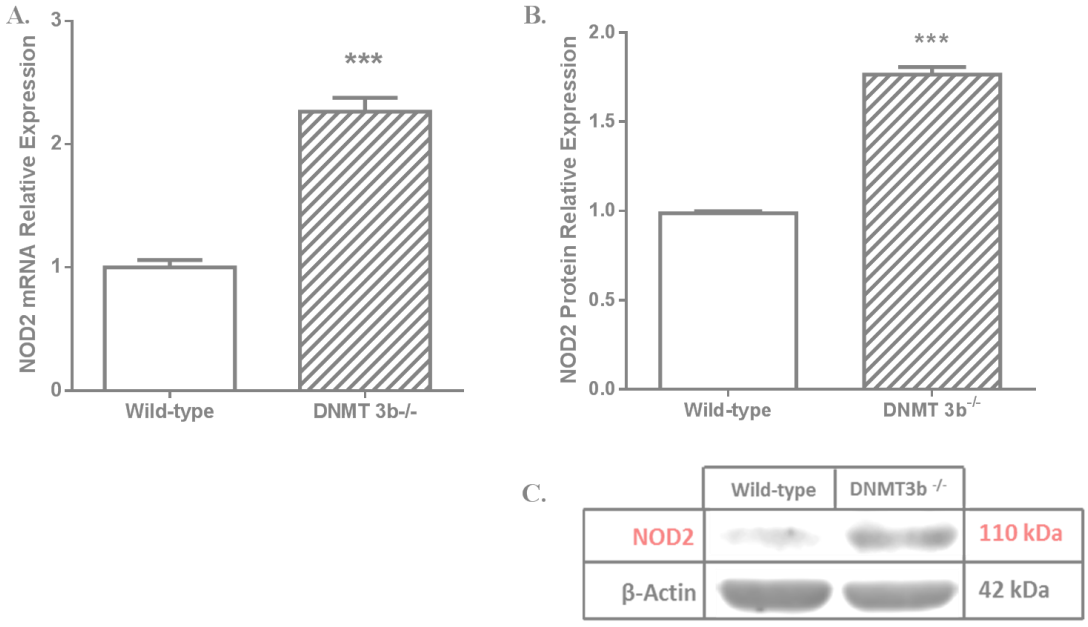

Figure 4.10. NOD2 basal expression in DNMT3b$^{-/-}$ cells. (A) NOD2 mRNA expression in DNMT3b$^{-/-}$ cells, relative to β-Actin expression. (B) Densitometry of NOD2 protein expression in DNMT3b$^{-/-}$ cells, relative to β-Actin expression. (C) Representative immunoblot of NOD2 protein expression in DNMT3b$^{-/-}$ cells. Data is represented as mean relative expression ± S.E.M. Statistical analysis was performed using independent t-tests. Significance was recognised at $p < 0.05$, with * representing $p < 0.05$, ** representing $p < 0.01$ and *** representing $p < 0.001$.

4.4.10 HDAC inhibitor priming reduces NOD2-induced cytokine expression but increases NOD2-induced chemokine release.

The research focus shifts to the effects of another epigenetic modification; histone acetylation, on NOD2-associated activity. HCT116 cells were treated with a well-established histone deacetylase inhibitor (HDACi); suberoylanilide hydroxamic acid (SAHA). HCT116 cells were treated with 10 μM SAHA for 48 hours and subsequently stimulated with 10 μg/ml MDP for either six or 18 hours. The effects of SAHA priming on pro-inflammatory responses to NOD2 stimulation were investigated by quantifying pro-inflammatory cytokine/chemokine expression and release by qPCR and ELISA, respectively. The "Untreated + None" treatment group, was set acted as the control. Pro-inflammatory cytokine expression was calculated relative to this control. Chemokine release was presented as absolute concentrations.

Stimulation of untreated HCT116 cells with MDP for six hours increased expression of pro-inflammatory cytokines; TNF-α (13.4-fold, $p < 0.001$) and IL-6 (4.7-fold, $p < 0.001$). Treatment with SAHA increased basal TNF-α expression (4.9-fold, $p < 0.001$) and IL-6 expression (4.7-fold, $p < 0.001$). Relative to the untreated control, SAHA attenuated NOD2 pro-inflammatory activity, as represented by a reduction in TNF-α from 13.4-fold to 3.5-fold ($p < 0.01$, relative to untreated + MDP) and IL-6 from 4.7-fold to 0.25-fold ($p < 0.01$, relative to untreated + MDP), as shown in Figure 4.11 A-B.

Once again, TNF-α and IL-6 release was below the limits of detection, therefore IL-8 release was investigated. Basal IL-8 release from HCT116 cells (484.6 ± 10.7 pg/ml) was significantly increased following 18 hours of stimulation with 10 μg/ml MDP alone (2560.8 ± 287.8 pg/ml, $p < 0.001$). Basal IL-8 release was enhanced by SAHA priming (1100.7 ± 41.7 pg/ml, $p < 0.01$). Priming with SAHA exacerbated MDP-induced IL-8 release from 2560.8 ± 287.8 pg/ml to 3443.1 ± 78.1 pg/ml ($p < 0.001$, relative to untreated + MDP), as shown in Figure 4.11C. This increase in IL-8 release implies that SAHA-priming enhances responses to NOD2 stimulation, which is contrary to the attenuated TNF-α and IL-6 expression recorded following SAHA treatment. Therefore, the effects of SAHA-priming on NOD2 responses remains unclear.

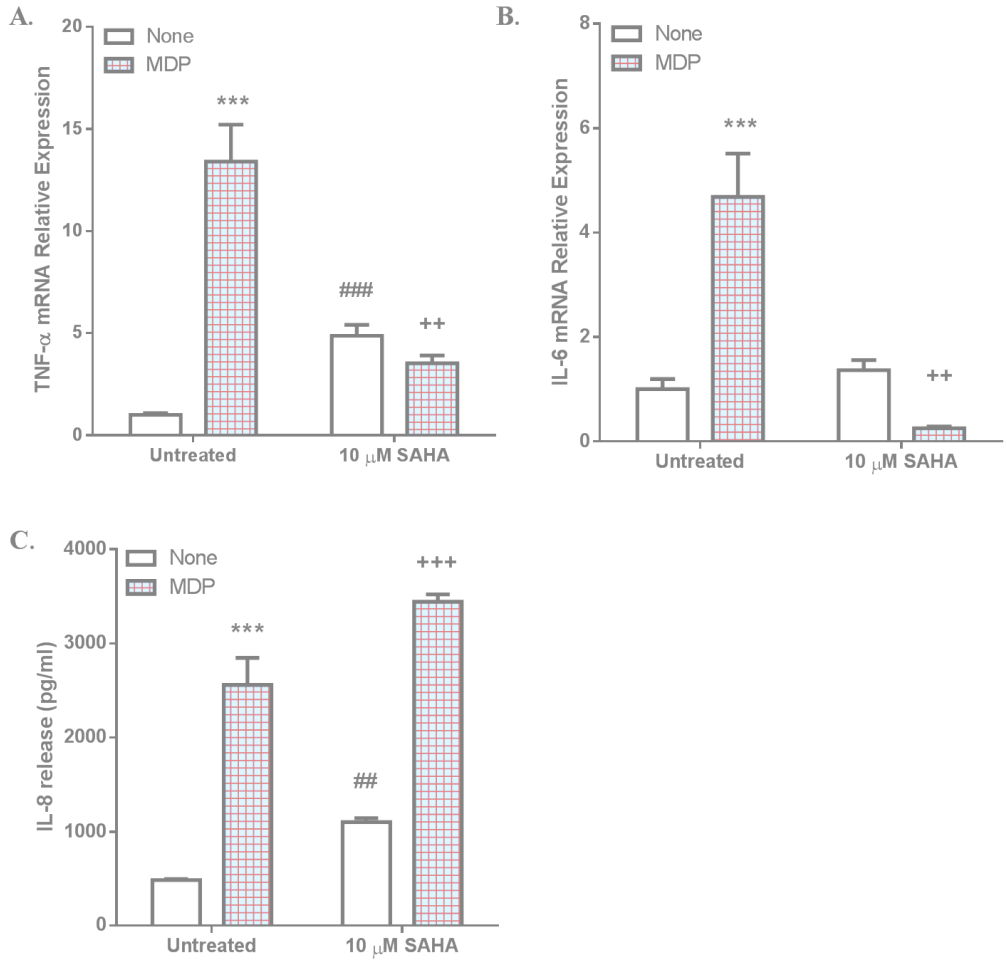

Figure 4.11: NOD2-induced pro-inflammatory activity in SAHA primed HCT116 cells. (A-B) TNF-α and IL-6 mRNA relative expression in HCT116 cells primed with 10 μM SAHA for 48 hours and subsequently simulated with 10 μg/ml MDP for six hours. RPL13A acted as the housekeeping gene. "Untreated + None" was set as the control. Data is represented as mean relative expression ± S.E.M. C) IL-8 release from HCT116 cells primed with 10 μM SAHA for 48 hours and stimulated with 10 μg/ml MDP for 18 hours. "Untreated + None" was set as the control. Data is represented as mean absolute ± S.E.M. Statistical analysis was performed using two-way ANOVAs, followed by Bonferroni *post-hoc* test where appropriate. ***** $p < 0.05$ representing **control vs NOD2**, **#** $p < 0.05$ representing **control vs primed, +** $p < 0.05$ representing **NOD2 vs (primed + NOD2).**

4.4.11 HDAC inhibitor priming increases NOD2-induced RIP2 but reduces MAPK pro-inflammatory signalling in HCT116 cells.

To further investigate the effects of SAHA-priming on NOD2-induced pro-inflammatory responses, RIP2 and MAPK signalling activation was quantified in the absence and presence of SAHA. When carrying out densitometry, phosphorylated proteins were expressed relative to the loading control (β-Tubulin), since SAHA was found to have a direct effect on some total proteins.

HCT116 cells that were stimulated with MDP alone for 2 hours significantly increased RIP2 and MAPK (ERK2 and p38) activation. MDP alone increased p-RIP2 by 1.8-fold ($p < 0.001$), p-ERK by 1.9-fold ($p < 0.05$) and p-p38 by 1.6-fold ($p < 0.05$). Basal RIP2 phosphorylation was enhanced by SAHA treatment (2.3-fold, $p < 0.001$). SAHA also reduced basal ERK2 phosphorylation, but not significantly (0.6-fold, $p > 0.05$). Relative to the untreated control group, priming with SAHA exacerbated MDP-induced p-RIP2 from 1.8-fold to 3.4-fold ($p < 0.001$, relative to untreated + MDP), but attenuated MAPK protein activation (p-ERK2 and p-p38) to wild-type control levels ($p < 0.05$), as outlined in Figure 4.12.

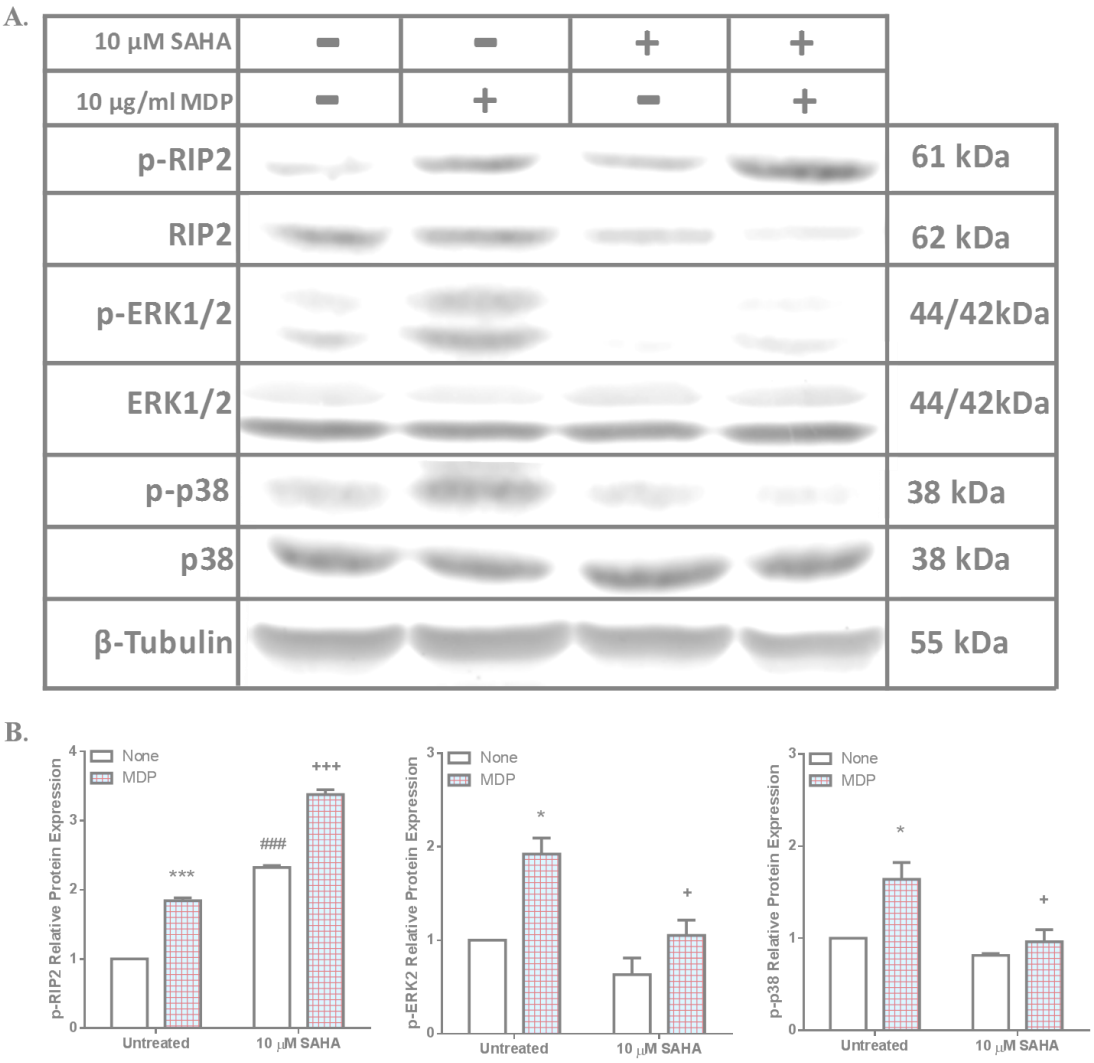

Figure 4.12: MDP-induced RIP2 and MAPK signalling in SAHA-primed HCT116 cells. A) Immunoblots of phosphorylated and total RIP2, p38 and ERK1/2 in cells primed with 10 µM SAHA for 48 hours and subsequently stimulated with MDP (10 µg/ml) for two hours. β-Tubulin acted as the loading control. B) Densitometry of phosphorylated RIP2, p38 and ERK2 expression, relative to β-Tubulin expression. "Untreated + None" was set as the control. Data is represented as mean relative expression ± S.E.M. and analysed using two-way ANOVAs (followed by Bonferroni's *post-hoc* test). ***** $p < 0.05$ representing **control vs NOD1**, **#** $p < 0.05$ representing **control vs primed**, **+** $p < 0.05$ representing **NOD1 vs (primed + NOD1).**

4.4.12 HDAC inhibitor priming reduces NOD2-induced NF-κB pro-inflammatory signalling in HCT116 cells.

To expand on the patterns uncovered in RIP2 and MAPK signalling, SAHAs influence on NF-κB signalling was investigated. Phosphorylation of p65 and IκBα was expressed relative to the loading control (β-Tubulin), since SAHA has a direct effect on total proteins. Stimulation of untreated cells with MDP significantly increased phosphorylation of p65 (2.4-fold, $p < 0.001$) and IκBα (2.9-fold, $p < 0.001$) proteins. SAHA-priming appeared to attenuate NOD2-induced NF-κB signalling. Relative to the untreated control group, priming with SAHA reduced MDP-induced p-p65 from 2.4-fold to 2-fold ($p > 0.05$, relative to untreated + MDP) and p-IκBα from 2.9-fold to 1.7-fold ($p < 0.001$, relative to untreated + MDP). These findings suggest that priming with a HDAC inhibitor reduces NOD2-induced NF-κB signalling.

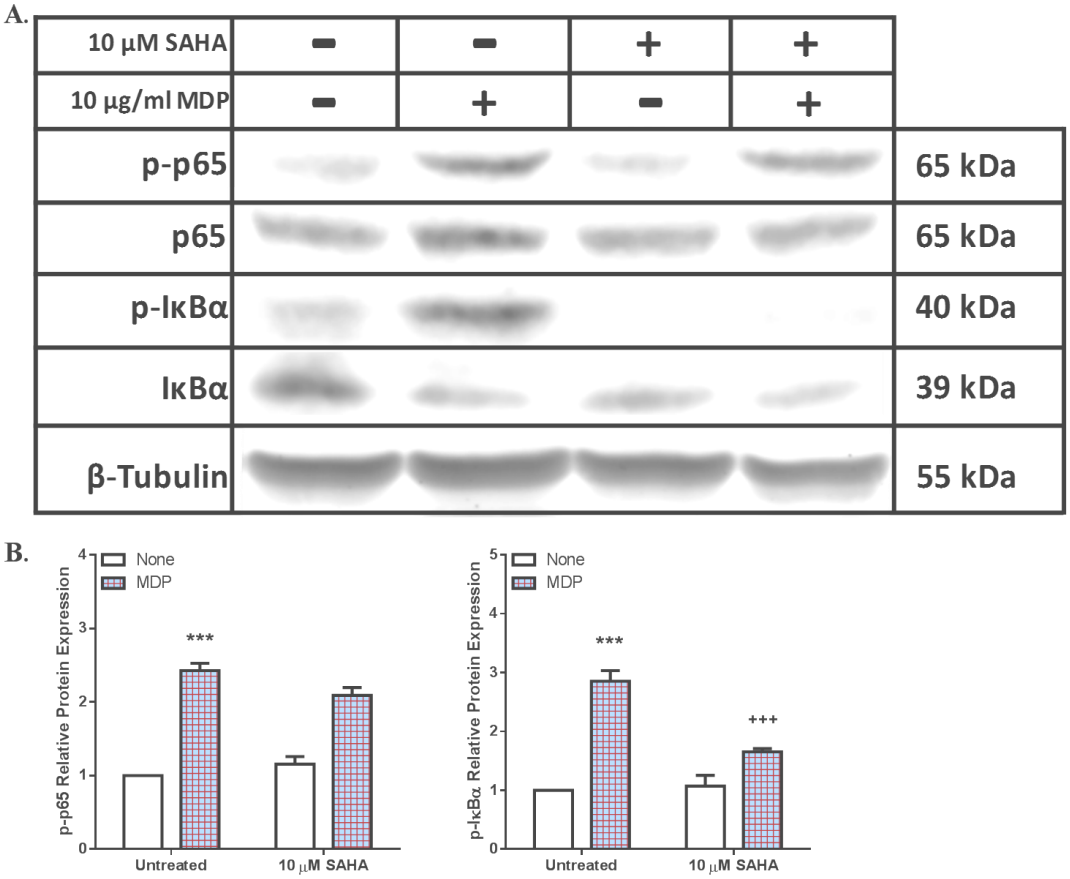

Figure 4.13: MDP-induced NF-κB signalling in SAHA-primed HCT116 cells. (A) Immunoblots of phosphorylated and total p65 and IκBα in cells primed with 10 µM SAHA for 48 hours and subsequently stimulated with 10 µg/ml MDP for two hours. β- Tubulin acted as the loading control. (B) Densitometry of phosphorylated p65 and IκBα expression, relative to β-Tubulin expression. "Untreated + None" was set as the control. Data is represented as mean relative expression ± S.E.M. and analysed using two-way ANOVAs (followed by Bonferroni's *post-hoc* test). ***** $p < 0.05$ representing **control vs NOD2**, **#** $p < 0.05$ representing **control vs primed**, **+** $p < 0.05$ representing **NOD2 vs (primed + NOD2).**

4.4.13 HDAC inhibitor treatment reduces NOD2 receptor expression

Pro-inflammatory activity and signalling, in response to NOD2 stimulation, appears to be decreased in HCT116 cells primed with SAHA. This suggests that the HDAC inhibitor may be reducing NOD2 levels, thereby potentially explaining the reduced responsiveness. NOD2 expression was quantified at the mRNA and protein levels by qPCR and western blotting, respectively. Treatment with 10 μM SAHA for 48 hours appeared to decrease NOD2 mRNA (0.7-fold, $p > 0.05$) and protein (0.6-fold, $p < 0.05$) expression (Figure 4.14 A-C). These decreases could thereby partially account for the reduced response to MDP following SAHA priming.

To further elucidate the negative effects of SAHA on NOD2 responses, expression of a known NOD2 negative regulator; A20, was measured. Treatment with 10 μM SAHA for 48 hours significantly increased A20 protein expression 2.3-fold ($p < 0.05$) (Figure 4.14 D-E). Increased A20 protein, alongside reduced NOD2 expression, could potentially account for the reduced NOD2 activity following SAHA treatment.

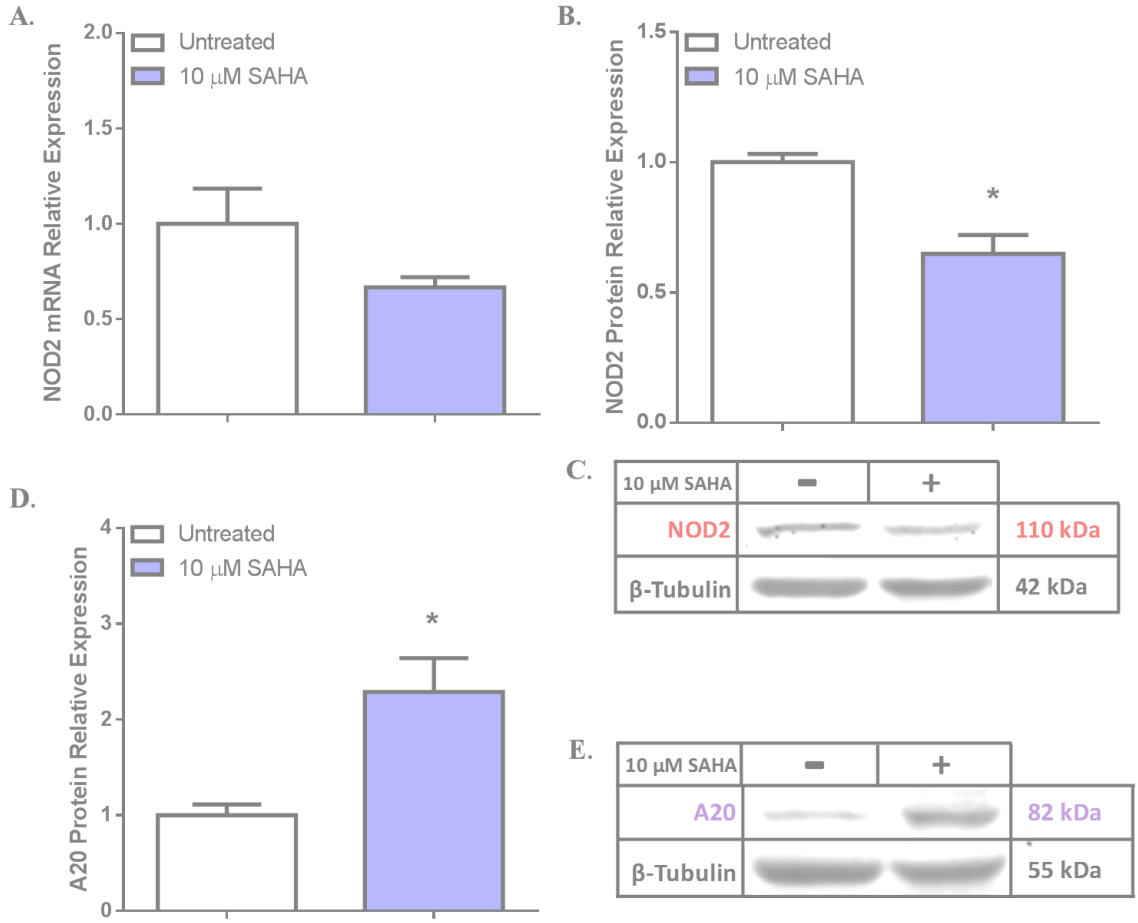

Figure 4.14. NOD2 and A20 basal expression in SAHA treated HCT116 cells. (A) NOD2 mRNA expression in HCT116 cells treated with 10 μM SAHA for 48 hours, relative to RPL13A expression. (B) Densitometry of NOD2 protein expression in SAHA treated cells, relative to β-Tubulin expression. (C) Representative immunoblot of NOD2 protein expression in SAHA treated cells. (D) Densitometry of A20 protein expression in SAHA treated cells, relative to β-Tubulin expression. (C) Representative immunoblot of A20 protein expression in SAHA treated cells. Data is represented as mean relative expression ± S.E.M. Statistical analysis was performed using independent t-tests. Significance was recognised at $p < 0.05$, with * representing $p < 0.05$, ** representing $p < 0.01$ and *** representing $p < 0.001$.

4.5 Discussion of Main Findings

The effects of epigenetic modifications on NOD2 activity, signalling and basal expression in HCT116 cells was under investigation in this chapter. Pharmacological inhibition of DNMT1 or genetic knockout of DNMT3b had a similar effect on NOD2 pro-inflammatory activity as was recorded for NOD1. Priming with a demethylating agent or DNMT3b knockout increased TNF-α/IL-6 expression and IL-8 release in response to NOD2 stimulation. This link between DNA methylation and NOD2 responses was further supported by exacerbated phosphorylation of RIP2/MAPK/NF-κB proteins in 5-Aza-dC primed cells and DNMT3b knockout cells. A direct effect of DNA methylation on NOD2 receptor regulation, in HCT116 cells, was endorsed by an increase in NOD2 expression detected at the mRNA and protein levels, alongside the identification of four CpG islands in the NOD2 gene sequence. The impact of histone acetylation on NOD2 regulation was varied, causing mainly reductions in pro-inflammatory responses. SAHA-priming impeded normal HCT116 pro-inflammatory activity in response to NOD2 stimulation, highlighted through reductions in TNF-α and IL-6 expression relative to untreated cells. Contrary to this reduction in activity, IL-8 release was increased after SAHA priming. This upsurge in IL-8 is most probably unrelated to NOD2 since basal IL-8 levels are increased by SAHA. This HDAC inhibitor has previously been found to induce expression of IL-8 in a NOD2-independent manner, by activating the IKK complex directly, which in turn phosphorylates IkB thereby alleviating NF-κB from its inhibitory effects so it can translocate to the nucleus (Gatla et al., 2017). SAHA also promotes histone H3 hyperacetylation at the IL-8 promoter region, thereby further supporting expression of the underlying gene (Gatla et al., 2017). NOD2 pro-inflammatory MAPK and NF-κB signalling was reduced following SAHA-priming, which supports the attenuated TNF-α/IL-6 expression data. Treatment of HCT116 cells with SAHA reduced NOD2 expression at the mRNA and protein level. The way in which SAHA reduces NOD2 expression and associated responses remains unclear. However, when expression of A20, a negative regulator of NOD2 (Hitotsumatsu et al., 2008, Billmann-Born et al., 2011), was investigated it was found to increase following SAHA treatment. This increase in A20 could potentially contribute to the decrease in NOD2 responses after exposure to the HDAC inhibitor. In conclusion, the current findings suggest for the first time that that DNA methylation directly influences NOD2 activity and expression

in HCT116 cells, as opposed to histone acetylation which appears to diminish NOD2 responses indirectly.

Limitations and Future work.

Identified limitations of the research undertaken and presented in this body of research include the confirmation of; methyl pattern deterioration around NOD genes under demethylating conditions, specificity of demethylating effects, and finally a mechanism underlying the identified effects of SAHA.

Further experimentation could be carried out to address these limitations which apply to NOD2 data in this chapter, as well as NOD1 findings in Chapter 3. Deterioration of DNA methylation patterns surrounding the NOD1/2 genes, following exposure to a demethylating agent or genetic knockout of DNMT3b, could be examined by bisulphite sequencing or melt curve analysis. If diminished NOD1/2 methyl patterns are uncovered under the demethylating conditions it would further support the theory that expression of these receptors is possibly regulated by DNA methylation. This data could potentially confirm/deny whether the increased NOD1/2 expression, and subsequent activity, recorded in this thesis was caused by a direct effect of demethylation on NOD1/2 expression.

Disruption of DNA methylation was found to have significant effects on both NOD1 (Chapter 3) and NOD2 (Chapter 4), however it remains unknown whether such effects are specific to these two receptors or if they apply across all PRRs. Therefore, there would be scope to study expression and response patterns of all other PRRs. If exposure to the demethylating agents or genetic knockout of the DNMT3b enzyme resulted in increased expression and activity of a majority or all other PRRs, it would indicate a highly non-specific effect of demethylation on PRRs. However, if the increases in NOD1/2 expression/activity recorded in this body of work are not found under the same experimental conditions for other PRRs, it could be indicative of a specific regulatory mechanism for NOD1/NOD2 expression and activity.

Finally, additional experimentation could be undertaken to explore the mechanism underlying the apparent indirect effects of SAHA on NOD1/2 expression and activity. Building on the A20 (negative regulator of NOD1/2 receptors) expression data uncovered here, supplementary expression analysis of other identified NOD1/2 regulatory proteins regulators (e.g. TRIM27, Erbin and RNF34) could be performed. A large portion of identified NOD1/2 negative regulators are E3 ubiquitin ligases that

act by targeting the NOD1/2 receptors for proteasomal degradation. Therefore, the effect of SAHA on NOD1/2 regulators could be further examined by treating cells with a proteasome inhibitor, e.g. MG132, before priming cells with SAHA. If NOD1/2 expression and responses to ligand stimulation, in the presence of the proteosomal inhibitor, are no longer significantly lower in SAHA-primed cells than untreated cells it could provide further insight into whether SAHA indirectly alters NOD1/2 via enhanced regulator-guided degradation. Findings from this could therefore provide a potential mechanism for the effects of SAHA on NOD1/2 recorded in this body of research.

Together, this future work could significantly strengthen the data presented here, thereby permitting greater conclusions to potentially be drawn.

Chapter 5 Analysis of NOD1 activity, signalling and expression in the THP-1 monocytic cell line, following epigenetic modification.

5.1 Introduction

To follow on from the findings of Chapter 3 (NOD1 regulation analysis in intestinal epithelial cells), NOD1 became the focus of this research again, but in an alternative experimental model; THP-1 monocytic cell line. This cell line was chosen for analysis since monocytes express NOD1 and play an essential role in the innate immune response (Parihar et al., 2010). NOD1 recognises the dipeptide *γ*-D-glutamyl-mesodiaminopimelic acid (iE-DAP), and to a greater extent the tripeptide; L-Ala-*γ*-D-glutamyl-mesodiaminopimelic acid (TRI-DAP) motif of the peptidoglycan (Girardin et al., 2003). Receptor activation by iE-DAP or TRI-DAP initiates pro-inflammatory responses via RIP2/MAPK/NF-κB signalling. This signalling cascade promotes AP-1 and NF-κB transcription factor activation, thereby promoting expression of pro-inflammatory mediators including; cytokines (e.g. TNF-α and IL-6) and chemokines (e.g. IL-8) (Chen et al., 2009).

The aim of this chapter was to unveil the role played by epigenetic modifications, namely DNA methylation and histone acetylation, in the regulation of NOD1 pro-inflammatory activity and expression. Attempts were made to disrupt DNA methylation patterns and histone acetylation via pharmacological inhibition of DNMT1 (5-Aza or 5-Aza-dC) or HDACs (SAHA), respectively. The differentiation process of monocytes-to-macrophages has been proven to drastically alter the monocyte epigenome (Wallner et al., 2016). Therefore, it was important to examine how this altered epigenome modifies responses to NOD1 stimulation. THP-1 monocytic cells were differentiated using phorbal myristate acetate (PMA).

In this chapter it was hypothesised that NOD1 receptor activity and expression are regulated, in THP-1 monocytic cells, by epigenetic modifications and differentiation.

5.2 Methods

The methods used in this chapter did not differ in any way from those outlined in chapter 2.

5.3 Experimental Design

These experiments were designed to investigate if reduced DNA methylation or enhanced histone acetylation patterns altered NOD1 receptor activity, signalling and expression. THP-1 cells were primed with epigenetic modifying agents that are known to disrupt either DNA methylation (5-Aza/5-Aza-dC) or histone acetylation (SAHA). THP-1 cells were differentiated into macrophage-like cells using PMA.

NOD1 pro-inflammatory activity, signalling and basal expression was investigated in these primed or differentiated cells, relative to untreated cells. NOD1 pro-inflammatory activity was analysed by stimulating the primed cells with a NOD1 ligand for 6/18hours, after which pro-inflammatory cytokine (TNF-α and IL-6) expression and chemokine (IL-8) release were quantified by qPCR and ELISA, respectively. NOD1 pro-inflammatory signalling was investigated by measuring RIP2, MAPK and NF-κB protein phosphorylation after stimulating primed THP-1 cells with NOD1 ligands for 1/3 hours, via western blotting. NOD1 basal expression was quantified in treated vs untreated cells at the mRNA and protein levels by qPCR and western blotting, respectively. All experiments were carried out with at least three independent biological replicates ($n \geq 3$). An overview of the experimental design is presented in Figure 5.1, with a more detailed breakdown outlined in the experimental design index (Table 5.1).

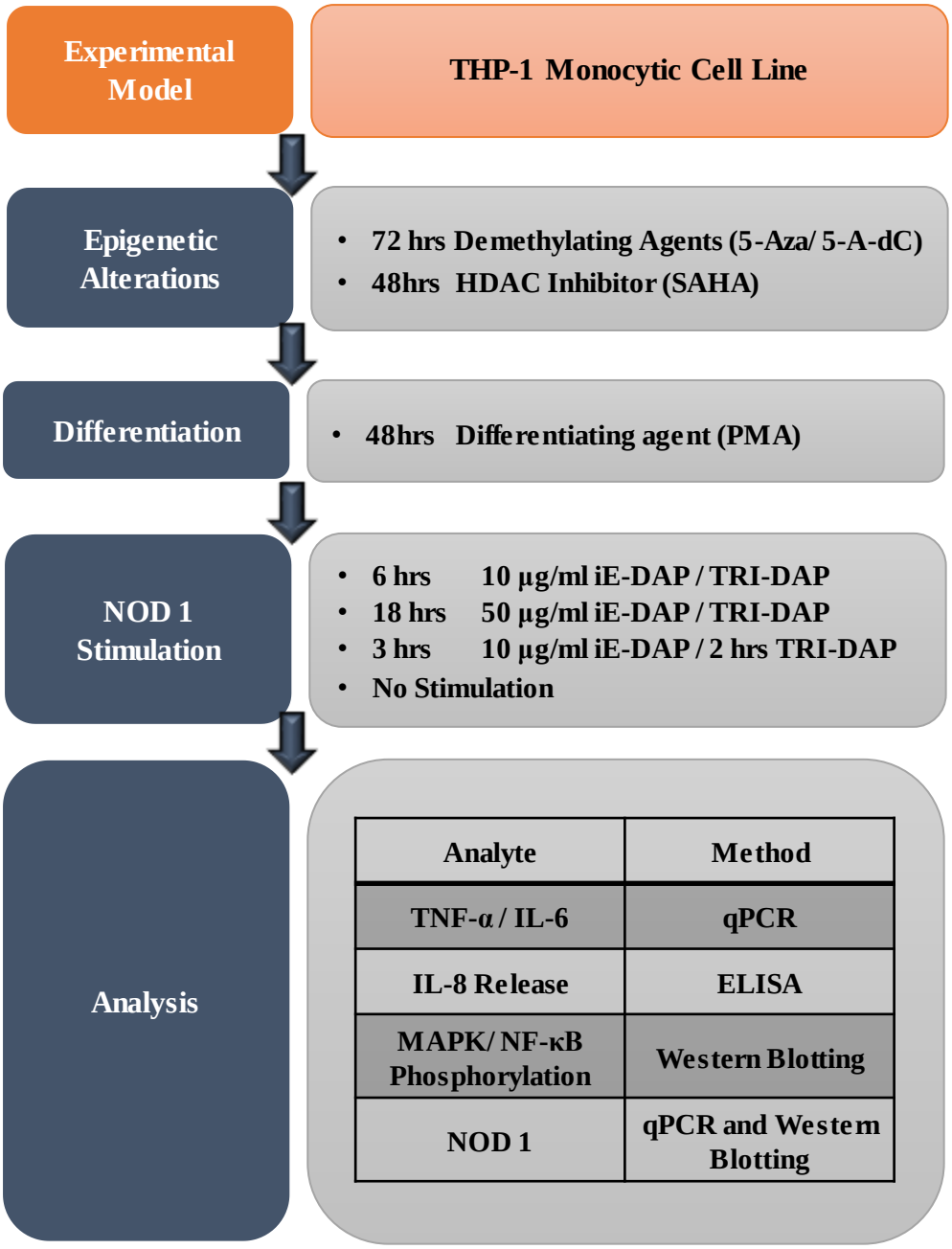

Figure 5.1. Chapter 5 Experimental Design. Outline of epigenetic treatments, NOD 1 stimulation and analysis.

Table 5.1: Chapter 5 Experimental Design Index. Breakdown of treatments, analytes and analysis methods for investigating NOD1 activity, signalling and expression in the THP-1 monocytic cell line.

	Figure Number 5.	1	2	3	4	5	6	7	8	9	10	11	12	13	14	15	16	17	18	19	20	21	22	23
Treatments	**Epigenetic Modification**																							
	5-Aza																							
	5-Aza-Dc																							
	SAHA																							
	PMA																							
	NOD1 Stimulation																							
	iE-DAP																							
	TRI-DAP																							
Analyte	**Pro-inflammatory cytokines**																							
	TNF-α																							
	IL-6																							
	IL-8																							
	Phosphorylated signalling proteins																							
	RIP2 and MAPK proteins																							
	NF-κB proteins																							
	Receptors/Enzymes																							
	NOD1																							
	Markers of Differentiation																							
	Cell Adherence																							
	RSK1																							
	CD16																							
Analysis	qPCR																							
	ELISA																							
	Western blotting																							
	Micropsope Images																							
	Flow cytometry																							

5.4 Results

5.4.1 DNMT1 inhibitor priming increases NOD1-induced pro-inflammatory activity in THP-1 cells.

To determine if disruption of DNA methylation patterns alter how THP-1 monocytic cells respond to NOD1 stimulation, cells were treated with a known demethylating agent prior to NOD1 stimulation. THP-1 cells were treated with a DNA methyltransferase 1 inhibitor, 5 μM 5-Azacytidine (5-Aza) or 500 nM 5-Aza-2'-deoxycytidine (5-Aza-dC), for 72 hours. Following exposure to one of these known demethylating agents, cells were stimulated with a NOD1 ligand. The effect of priming on pro-inflammatory activity was investigated by quantifying cytokine expression, via qPCR analysis, after six hours of stimulation with 10 μg/ml iE-DAP or TRI-DAP. Pro-inflammatory chemokine release was also measured by ELISA following 18 hours of 50 μg/ml iE-DAP or TRI-DAP stimulation. The "Untreated + None" treatment group, acted as the control. Pro-inflammatory cytokine/chemokine expression or release was calculated relative to this control.

NOD1-induced TNF and IL-6 mRNA expression was quantified in the absence or presence of priming. Stimulation with iE-DAP for six hours increased expression of TNF-α (2-fold, $p < 0.01$) and IL-6 (1.9-fold, $p < 0.05$). These responses were not influenced by 5-Aza priming. TRI-DAP induced superior NOD1 pro-inflammatory activity, increasing TNF-α (3.3-fold, $p < 0.001$) and IL-6 (2.8-fold, $p < 0.001$). Relative to the untreated control group, priming with 5-Aza exacerbated TRI-DAP-induced TNF-α from 3.3-fold to 5.3-fold ($p < 0.001$, relative to untreated + TRI-DAP) and IL-6 from 2.8-fold to 4.3-fold ($p < 0.001$, relative to untreated + TRI-DAP), as outlined in Figure 5.2 A-B.

The effects of the more efficient demethylating agent, 5-Aza-dC, were investigated next. Relative to the untreated control group, priming with 5-Aza-dC increased iE-DAP-induced TNF-α from 2-fold to 9-fold ($p < 0.001$, relative to untreated + iE-DAP) and IL-6 from 1.9-fold to 12-fold ($p < 0.001$, relative to untreated + iE-DAP). This demethylating agent also caused a greater impact on responses to TRI-DAP. Relative to the untreated control group, priming with 5-Aza-dC increased TRI-DAP-induced TNF-α from 3.3-fold to 12.4-fold ($p < 0.001$, relative to untreated + TRI-DAP) and IL-6 from 2.8-fold to 29.3-fold ($p < 0.001$, relative to untreated + TRI-DAP), as

outlined in Figure 5.2 C-D. Therefore, it appears that priming with a demethylating agent augments THP-1 pro-inflammatory activity following NOD1 stimulation.

NOD1-induced TNF-α and IL-6 expression patterns were similar in 5-Aza and 5-Aza-dC primed THP-1 cells but were found to a higher magnitude in 5-Aza-dC primed cells. Therefore, from this point only 5-Aza-dC will be used to investigate the effect of DNMT1 inhibitor priming on NOD1 responses in THP-1 cells.

As was found in HCT116 cells, TNF-α and IL-6 release from THP-1 cells was below the limits of detection. Therefore, IL-8 release following NOD1 stimulation of 5-Aza-dC primed cells was quantified by ELISA. Basal IL-8 release (33.7 ± 1.8 pg/ml) was lower than HCT116 cell levels. Time and dose analysis, as outlined in Appendix 4, revealed that THP-1 cells required 50 μg/ml iE-DAP/TRI-DAP stimulation for 18 hours to detect significant changes in IL-8 release. The need for more concentrated NOD1 ligands is potentially due to the lower basal release (33.7 ± 1.8 pg/ml) from THP-1, which was nearly 10-fold lower than what was detected in HCT116 cells. NOD1-stimulation with iE-DAP or TRI-DAP increased IL-8 release to 56 ± 3.4 pg/ml ($p < 0.001$) and 74.7 ± 1.4 pg/ml ($p < 0.001$), respectively. Priming with 5-Aza-dC increased iE-DAP-induced IL-8 release from 56 ± 3.4 pg/ml to 63.1 ± 4.3 pg/ml ($p < 0.05$, relative to untreated + iE-DAP). Priming with 5-Aza-dC increased TRI-DAP-induced IL-8 release from 74.7 ± 1.4 pg/ml to 93 ± 2.8 pg/ml ($p < 0.05$, relative to untreated + iE-DAP), as outlined in Figure 5.3. This IL-8 data matched the TNF-α and IL-6 qPCR findings, suggesting that priming with a DNMT1 inhibitor increases NOD1 pro-inflammatory responses.

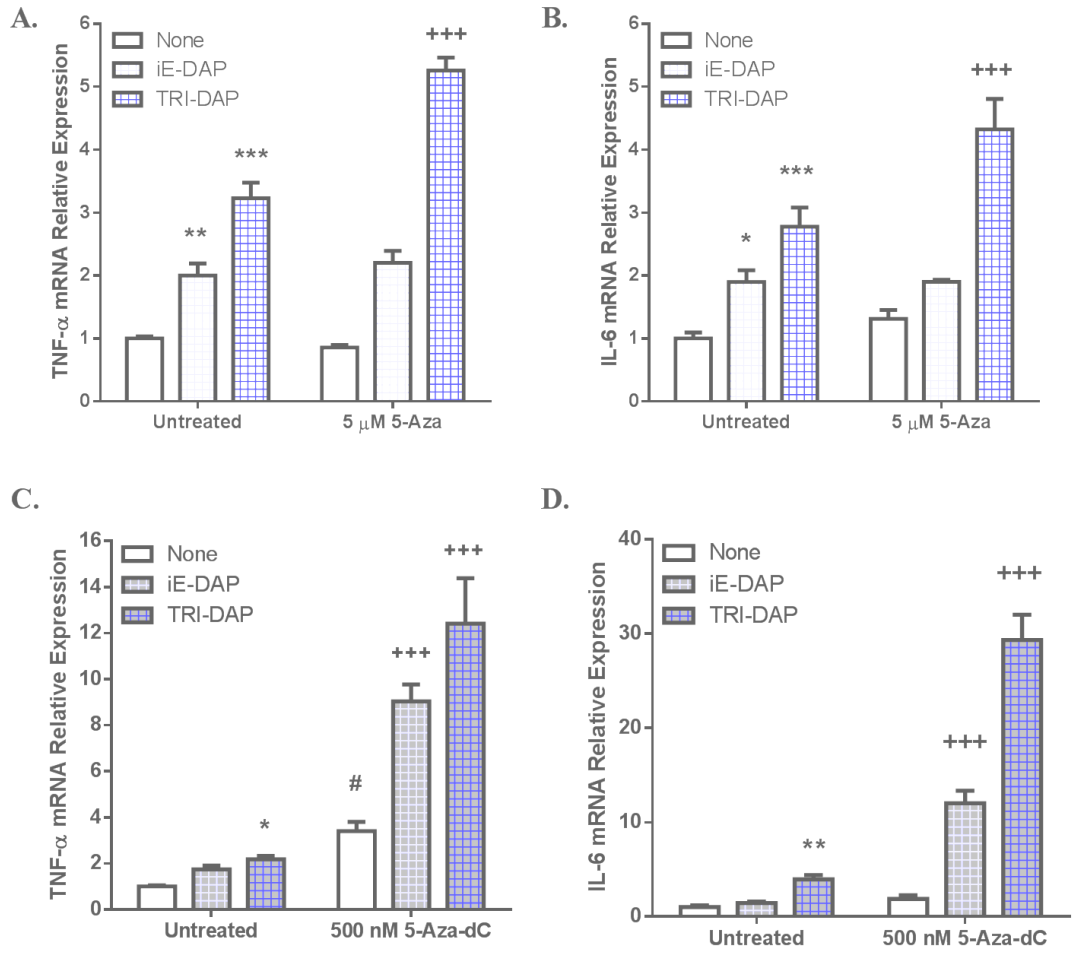

Figure 5.2: NOD1-induced pro-inflammatory cytokine expression in 5-Aza or 5-Aza-dC primed THP-1 cells. A-B) TNF-α and IL-6 mRNA relative expression in THP-1 cells primed with 5 μM 5-Aza for 72 hours and subsequently stimulated with a NOD1 ligand (10 μg/ml iE-DAP/TRI-DAP) for 6 hours. C-D) TNF-α and IL-6 mRNA relative expression in THP-1 cells primed with 500 nM 5-Aza-dC for 72 hours and subsequently stimulated with a NOD1 ligand (10 μg/ml iE-DAP/TRI-DAP) for 6 hours. β-Actin acted as the housekeeping gene. "Untreated + None" was set as the control group. Data is represented as mean relative expression ± S.E.M. Statistical analysis was performed using two-way ANOVAs, followed by Bonferroni *post-hoc* test where appropriate. ***** $p < 0.05$ representing **control vs NOD1**, **#** $p < 0.05$ representing **control vs primed**, **+** $p < 0.05$ representing **NOD1 vs (primed + NOD1).**

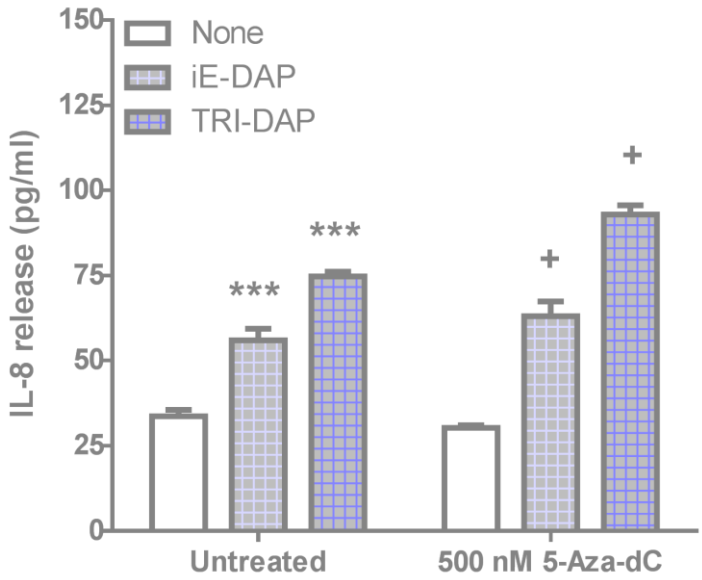

Figure 5.3: NOD1-induced pro-inflammatory IL-8 release from 5-Aza-dC primed THP-1 cells. IL-8 release (pg/ml) from THP-1 cells primed with 500 nM 5-Aza-dC for 72 hours was recorded following NOD1 stimulation with 50 μg/ml iE-DAP/TRI-DAP for 18 hours. "Untreated + None" was set as the control group. Data is represented as absolute concentration ± S.E.M. Statistical analysis was performed using two-way ANOVAs, followed by Bonferroni *post-hoc* test where appropriate. ***** $p < 0.05$ representing **control vs NOD1**, **#** $p < 0.05$ representing **control vs primed**, **+** $p < 0.05$ representing **NOD1 vs (primed + NOD1).**

5.4.2 DNMT1 inhibitor priming increases NOD1-induced pro-inflammatory RIP2 and MAPK signalling in THP-1 cells.

Since priming with a DNMT1 inhibitor was found to enhance pro-inflammatory activity, as represented by increases in TNF-α/IL-6 expression and IL-8 release, the effect of priming on NOD1-induced pro-inflammatory signalling was next examined. Stimulation of the NOD1 receptor triggers the phosphorylation, and thus activation of the RIP2 adapter, MAPK and NF-κB proteins. NOD1-induced phosphorylation of RIP2 and MAPK proteins in 5-Aza-dC primed THP-1 cells was first investigated. Phosphorylation time responses were carried out to select the most appropriate NOD1 stimulation duration (Appendix 6). Based on this investigation, it was decided that cells should be stimulated with iE-DAP for three hours and TRI-DAP for two hours. Phosphorylation of the NOD1 adapter protein (RIP2) and MAPK signalling proteins (ERK2 and p38) was investigated by western blot analysis. Blots were repeated for three independent experiments (n = 3), with representative blots shown. Protein expression was quantified by densitometry of phosphorylated, total and housekeeping proteins. Phosphorylated protein expression was normalised relative to their total proteins, and subsequently calculated relative to the untreated control group.

Stimulation of THP-1 cells with 10 μg/ml iE-DAP significantly increased p- RIP2 (4.1-fold, $p < 0.001$), p-ERK2 (2.6-fold, $p < 0.01$) and p-p38 (1.5-fold, $p < 0.01$). Relative to the untreated control group, priming with 5-Aza-dC increased iE-DAP-induced p-ERK2 from 2.6-fold to 3.8-fold ($p < 0.05$, relative to untreated + iE-DAP) and p-p38 from 1.5-fold to 2.1-fold ($p < 0.001$, relative to untreated + iE-DAP), as depicted in Figure 5.4. Similar patterns were uncovered with TRI-DAP stimulation. Relative to the untreated control group, priming with 5-Aza-dC increased TRI-DAP-induced p-RIP2 from 3.9-fold to 6.8-fold ($p < 0.001$, relative to untreated + TRI-DAP), p-ERK2 from 1.7-fold to 12-fold ($p < 0.001$, relative to untreated + TRI-DAP) and p-p38 from 1.3-fold to 1.9-fold ($p < 0.001$, relative to untreated + TRI-DAP), as outlined in Figure 5.5.

Together, these data highlight that priming of THP-1 cells with a demethylating agent increases their NOD1-induced pro-inflammatory signalling.

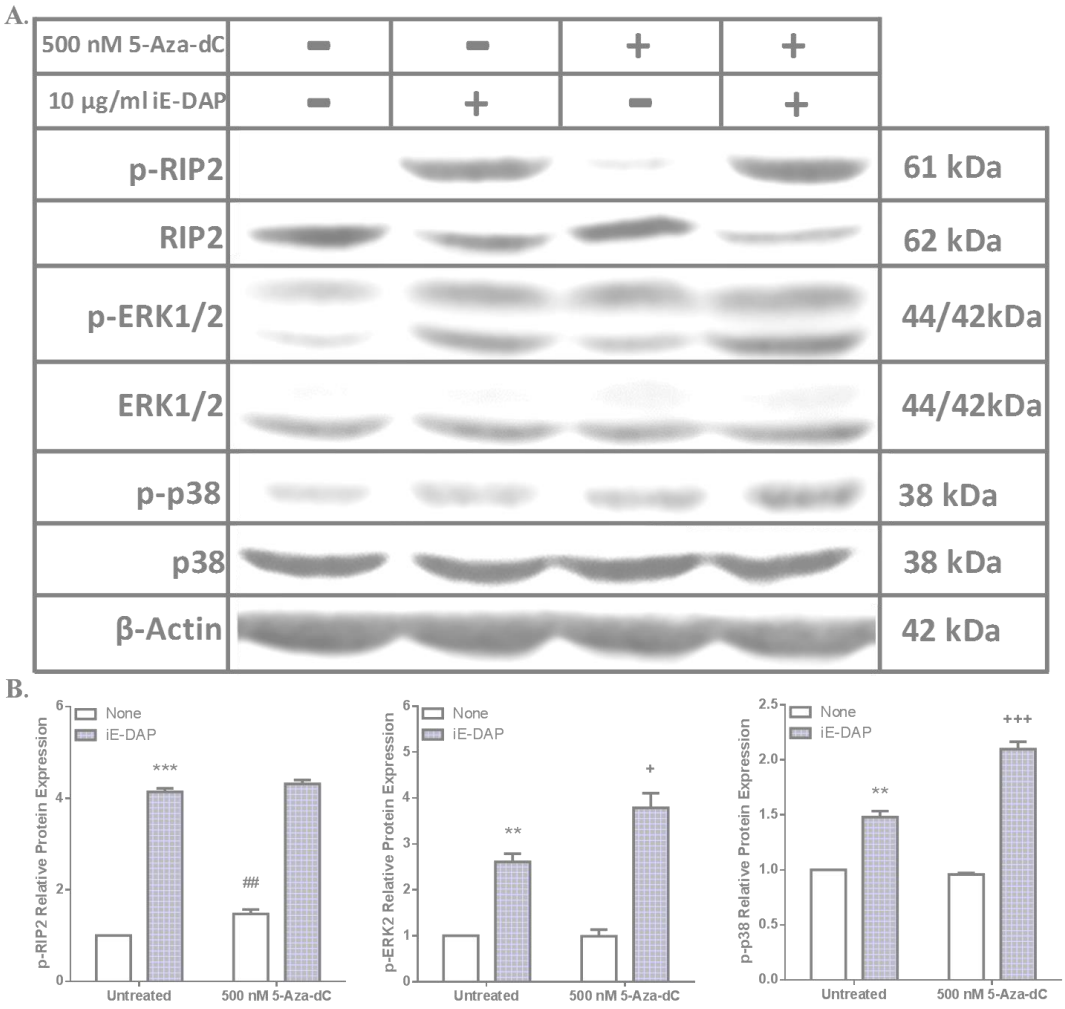

Figure 5.4: IE-DAP-induced RIP2 and MAPK signalling in 5-Aza-dC primed THP-1 cells. (A) Immunoblots of phosphorylated and total RIP2, ERK1/2 and p38 in 5-Aza-dC primed cells stimulated with iE-DAP (10 µg/ml) for three hours. β-Actin acted as the loading control. B) Densitometry of phosphorylated RIP2, ERK1/2 and p38 expression, relative to total protein expression. "Untreated + None" was set as the control group. Data is represented as mean relative expression ± S.E.M and analysed using two-way ANOVAs (followed by Bonferroni's *post-hoc* test). ***** $p < 0.05$ representing **control vs NOD1**, **#** $p < 0.05$ representing **control vs priming, +** $p < 0.05$ representing **NOD1 vs (priming + NOD1).**

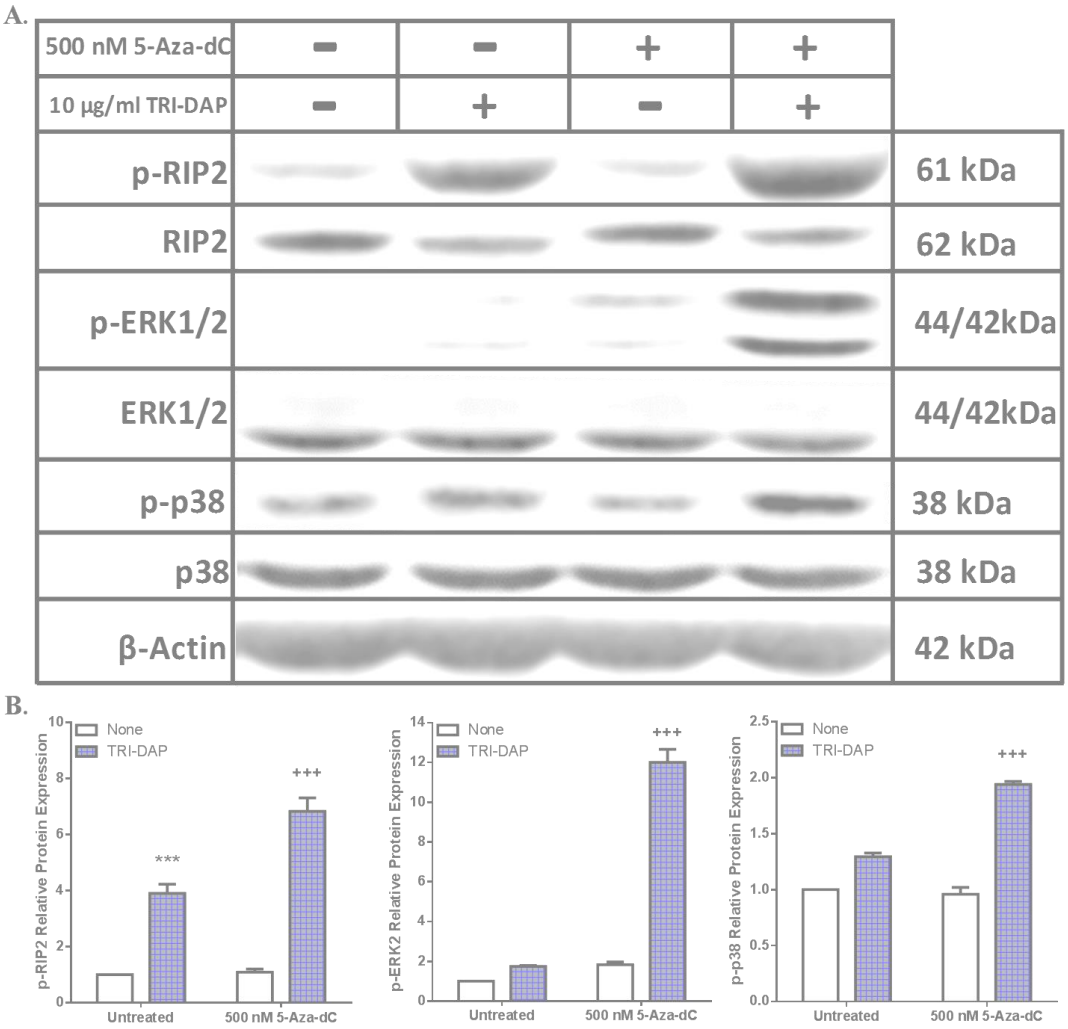

Figure 5.5: TRI-DAP-induced RIP2 and MAPK signalling in 5-Aza-dC primed THP-1 cells. (A) Immunoblots of phosphorylated and total RIP2, ERK1/2 and p38 in 5-Aza-dC primed cells stimulated with TRI-DAP (10 µg/ml) for two hours. β-Actin acted as the loading control. B) Densitometry of phosphorylated RIP2, ERK1/2 and p38 expression, relative to total protein expression. "Untreated + None" was set as the control group. Data is represented as mean relative expression ± S.E.M and analysed using two-way ANOVAs (followed by Bonferroni's *post-hoc* test). ***** $p < 0.05$ representing **control vs NOD1**, **#** $p < 0.05$ representing **control vs priming, +** $p < 0.05$ representing **NOD1 vs (priming + NOD1).**

5.4.3 DNMT1 inhibitor priming increases NOD1-induced pro-inflammatory NF-κB signalling in THP-1 cells.

To complete the investigation of 5-Aza-dC priming on NOD1-induced signalling, its effects on NF-κB signalling were examined next. This involved measuring phosphorylation levels of p65 and IκBα in the absence or presence of priming. The duration of 10 μg/ml iE-DAP/TRI-DAP stimulation required to investigate NF-κB signalling was chosen based on the time response analysis, as outlined in Appendix 6. The same time point chosen matched that used to analyse RIP2 and MAPK signalling; iE-DAP for three hours and TRI-DAP for two hours. Phosphorylation of the p65 and IκBα was investigated by western blot analysis. Blots were repeated for three independent experiments (n = 3), with representative blots shown. Protein expression was quantified by densitometry of phosphorylated, total and housekeeping proteins. Phosphorylated protein expression was normalised relative to the chosen loading control; β-Actin, and subsequently calculated relative to the untreated control group. NOD1 activation by iE-DAP increased p- p65 (2.5-fold, $p < 0.001$) and p-IκBα (2.8-fold, $p < 0.001$). NF-κB signalling, triggered by iE-DAP, was enhanced in 5-Aza-dC-primed THP-1 cells. Relative to the untreated control group, priming with 5-Aza-dC increased iE-DAP-induced p-p65 from 2.5-fold to 3.2-fold ($p < 0.05$, relative to untreated + iE-DAP) and p-IκBα from 2.8-fold to 3.6-fold ($p < 0.01$, relative to untreated + iE-DAP), as outlined in Figure 5.6. TRI-DAP alone increased phosphorylation of p65 (3-fold, $p > 0.05$) and IκBα (4.4-fold, $p < 0.001$). Relative to the untreated control group, priming with 5-Aza-dC increased TRI-DAP-induced p-p65 from 3-fold to 13.2-fold ($p < 0.001$, relative to untreated + TRI-DAP) and p-IκBα from 4.4-fold to 7-fold ($p < 0.001$, relative to untreated + TRI-DAP), as depicted in Figure 5.7. These data match the increases that were detected in RIP2 and MAPK signalling, thereby further suggesting that priming with a demethylating agent increases NOD1 associated pro-inflammatory signalling.

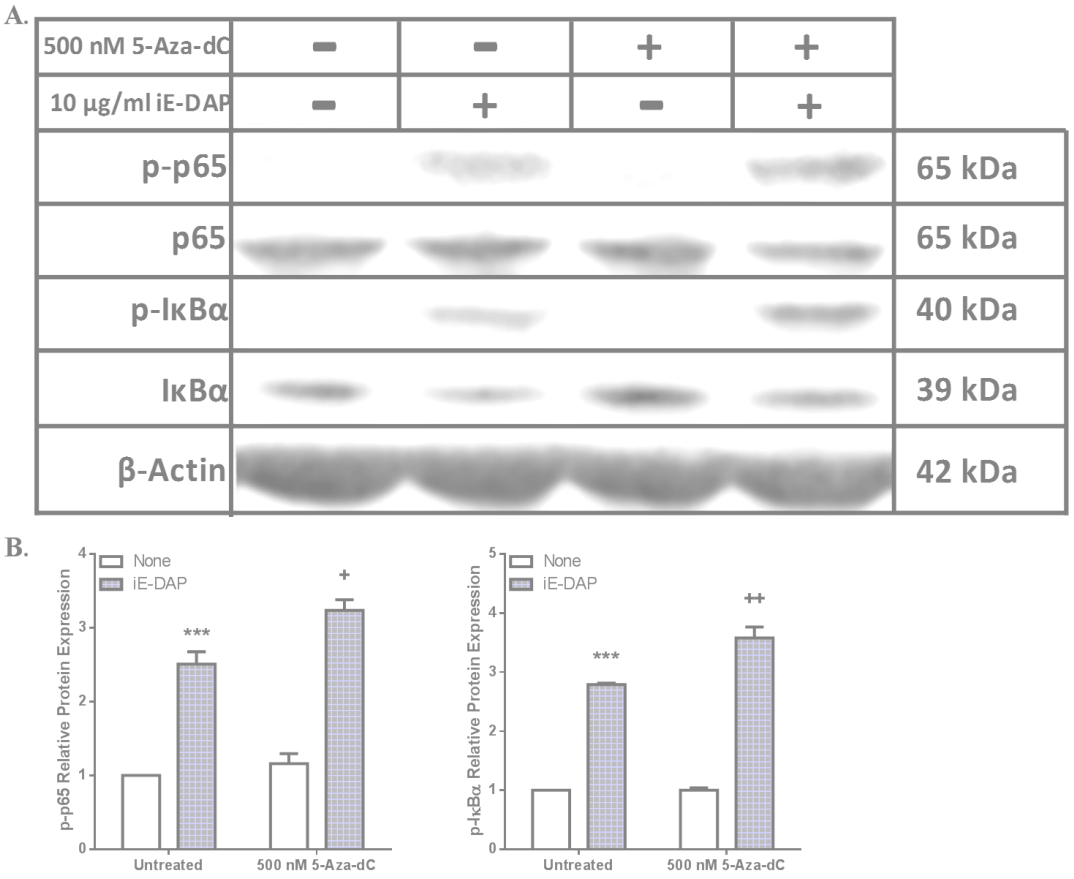

Figure 5.6. IE-DAP-induced NF-κB signalling in 5-Aza-dC primed THP-1 cells. (A) Immunoblots of phosphorylated and total p65 and IκBα in cells primed with 500 nM 5-Aza-dC for 72 hours and subsequently stimulated with IE-DAP (10 µg/ml) for three hours. β- Actin acted as the loading control. (B) Densitometry of phosphorylated p65 and IκBα expression, relative to β-Actin expression. "Untreated + None" was set as the control group. Data is represented as mean relative expression ± S.E.M and analysed using two-way ANOVAs (followed by Bonferroni's *post-hoc* test). ***** $p < 0.05$ representing **control vs NOD1**, **#** $p < 0.05$ representing **control vs primed**, **+** $p < 0.05$ representing **NOD1 vs (primed + NOD1).**

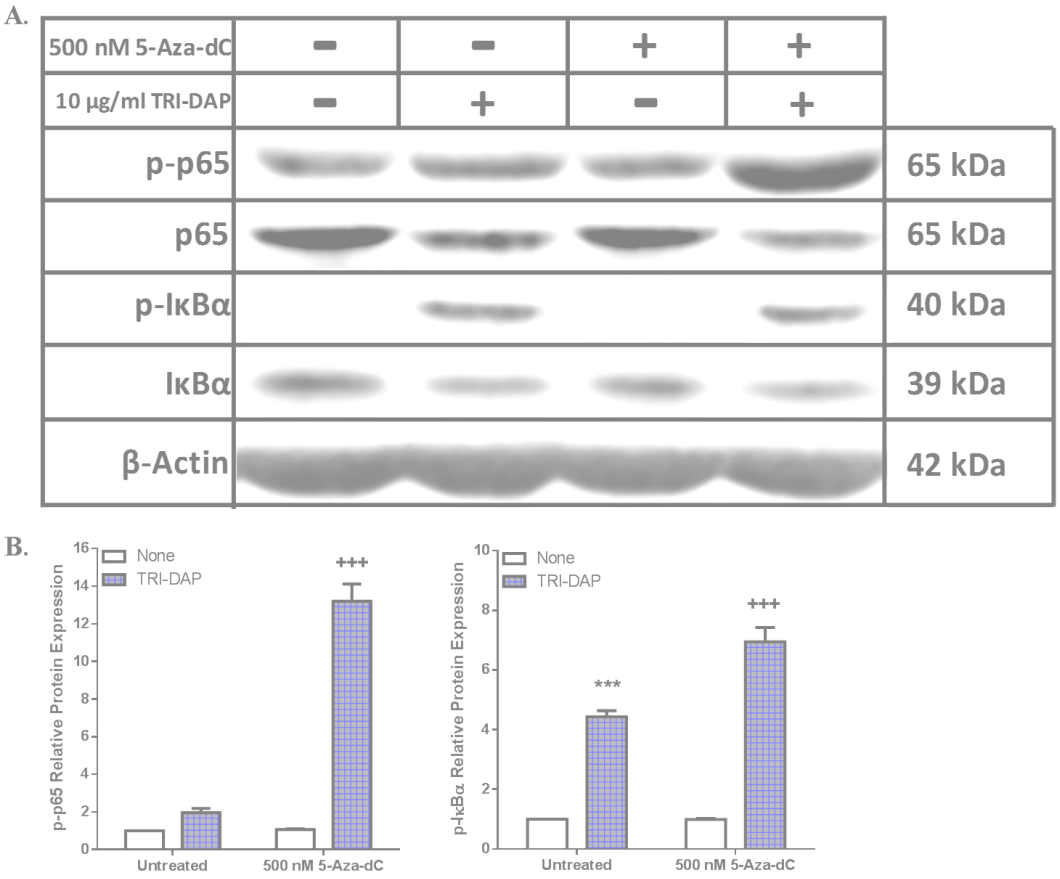

Figure 5.7. TRI-DAP-induced NF-κB signalling in 5-Aza-dC primed THP-1 cells. (A) Immunoblots of phosphorylated and total p65 and IκBα in cells primed with 500 nM 5-Aza-dC for 72 hours and subsequently stimulated with TRI-DAP (10 µg/ml) for two hours. β- Actin acted as the loading control. (B) Densitometry of phosphorylated p65 and IκBα expression, relative to β-Actin expression. "Untreated + None" was set as the control group. Data is represented as mean relative expression ± S.E.M and analysed using two-way ANOVAs (followed by Bonferroni's *post-hoc* test). ***** $p < 0.05$ representing **control vs NOD1**, **#** $p < 0.05$ representing **control vs primed**, **+** $p < 0.05$ representing **NOD1 vs (primed + NOD1).**

5.4.4 DNMT1 inhibitor treatment increases NOD1 expression in THP-1 cells.

Since 5-Aza and 5-Aza-dC priming was found to increase responses to NOD1 ligands, we next asked the question; Are these demethylating agents inducing this response by directly altering NOD1 expression? This was investigated by quantifying NOD1 expression at the mRNA and protein levels via qPCR and western blot analysis. Independent t-test analysis revealed significant increases in NOD1 expression (Figure 5.8). THP-1 cells treated with 5 μM 5-Aza for 72 hours exhibited a significant increase in NOD1 mRNA (1.7-fold, $p < 0.001$) and protein (3-fold, $p < 0.01$) expression (Figure 5.8 A, C and E). Treatment with 500 nM 5-Aza-dC for 72 hours mirrored the effects of 5-Aza, causing a 2.1-fold increase in NOD1 mRNA ($p < 0.001$) and a 3-fold rise in NOD1 protein ($p < 0.001$) expression (Figure 5.8 B, D and F).

This suggests that the demethylating agents are increasing NOD1 expression in THP-1 cells, potentially explaining the augmented pro-inflammatory activity and signalling recorded in our earlier experimentation.

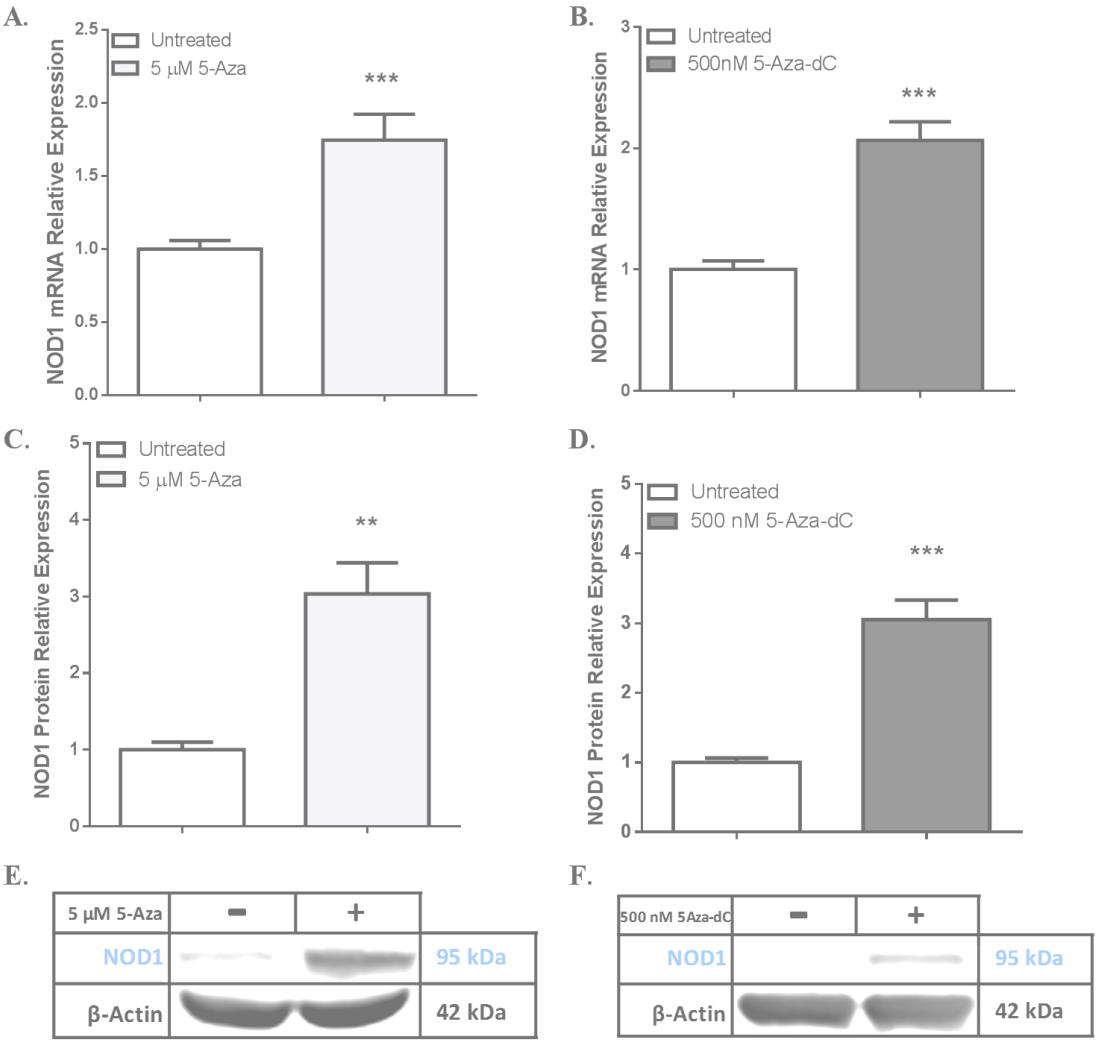

Figure 5.8. NOD1 basal expression in THP-1 cells following 5-Aza or 5-Aza-dC treatment. (A-B) NOD1 mRNA expression following 5 μM 5-Azacytidine (5-Aza) or 500 nM 5-Aza-2'-deoxycytidine (5-Aza-dC) for 72 hours, relative to β-Actin expression. (C-D) Densitometry of NOD1 protein expression following 5 μM 5-Aza or 500 nM 5-Aza-dC for 72 hours, relative to β-Actin expression. (E-F) Representative immunoblots of NOD1 protein expression following 5 μM 5-Aza or 500 nM 5-Aza-dC for 72 hours, relative to β-Actin expression. Data is represented as mean relative expression ± S.E.M. Statistical analysis was performed using independent t-tests. Significance was recognised at $p < 0.05$, with * representing $p < 0.05$, ** representing $p < 0.01$ and *** representing $p < 0.001$.

5.4.5 HDAC inhibitor priming attenuates NOD1-induced pro-inflammatory cytokine expression but enhances chemokine release from THP-1 cells.

The focus of this chapter shifts to the effects of histone acetylation on NOD1 associated responses. The contribution of this epigenetic modification was investigated using a well-established histone deacetylase inhibitor (HDACi); suberoylanilide hydroxamic acid (SAHA). THP-1 cells were treated with 10 μM SAHA for 48 hours and subsequently stimulated with 10 μg/ml NOD1 ligands (iE-DAP/TRI-DAP) for six hours or 50 μg/ml NOD1 ligands (iE-DAP/TRI-DAP) for 18 hours. The effects of SAHA priming on pro-inflammatory responses to NOD1 stimulation were investigated by quantifying pro-inflammatory cytokine/chemokine expression and release by qPCR and ELISA, respectively. The "Untreated + None" treatment group, acted as the control. Pro-inflammatory cytokine expression was calculated relative to this control.

Stimulation of THP-1 cells with iE-DAP for six hours significantly increased TNF-α (2.2-fold, $p < 0.001$) and IL-6 (2.5-fold, $p < 0.05$) mRNA expression. TRI-DAP induced a similar pattern of events, increasing TNF-α (2.8-fold, $p < 0.001$) and IL-6 (4.5-fold, $p < 0.001$). SAHA treatment reduced basal levels of TNF-α (0.6-fold, $p < 0.05$). Relative to the untreated control group, priming with SAHA reduced iE-DAP-induced TNF-α from 2.2-fold to 0.8-fold ($p < 0.001$, relative to untreated + iE-DAP) and IL-6 from 2.5-fold to 1.8-fold ($p > 0.05$, relative to untreated + iE-DAP). Relative to the untreated control group, priming with SAHA reduced TRI-DAP-induced TNF-α from 2.8-fold to 0.6-fold ($p < 0.001$, relative to untreated + TRI-DAP) and IL-6 from 4.5-fold to 2.2-fold ($p < 0.05$, relative to untreated + iE-DAP), as shown in Figure 5.9 A-B.

Since TNF-α and IL-6 release was below the limits of detection, IL-8 release was quantified. Basal IL-8 release from THP-1 cells (15.3 ± 0.6 pg/ml) was significantly increased following 18 hours of stimulation with 50 μg/ml of iE-DAP (44.7 ± 0.4 pg/ml, $p < 0.001$) or TRI-DAP (70 ± 0.6 pg/ml, $p < 0.001$). SAHA treatment was found to increase basal IL-8 release approximately 10-fold (152.7 ± 1.2 pg/ml, $p < 0.001$) relative to the control. Priming with SAHA significantly heightened the IL-8 release after stimulation with iE-DAP to 228.4 ± 1.9 pg/ml ($p < 0.001$, relative to untreated +

iE-DAP) or TRI-DAP to 473.6 ± 8.6 pg/ml ($p < 0.001$, relative to untreated + TRI-DAP), as outlined in Figure 5.9 C.

The mixed effects of SAHA on cytokine expression and chemokine release mean rhat a conclusion cannot be drawn from this experiment as to how SAHA priming alters responses to NOD1 stimulation.

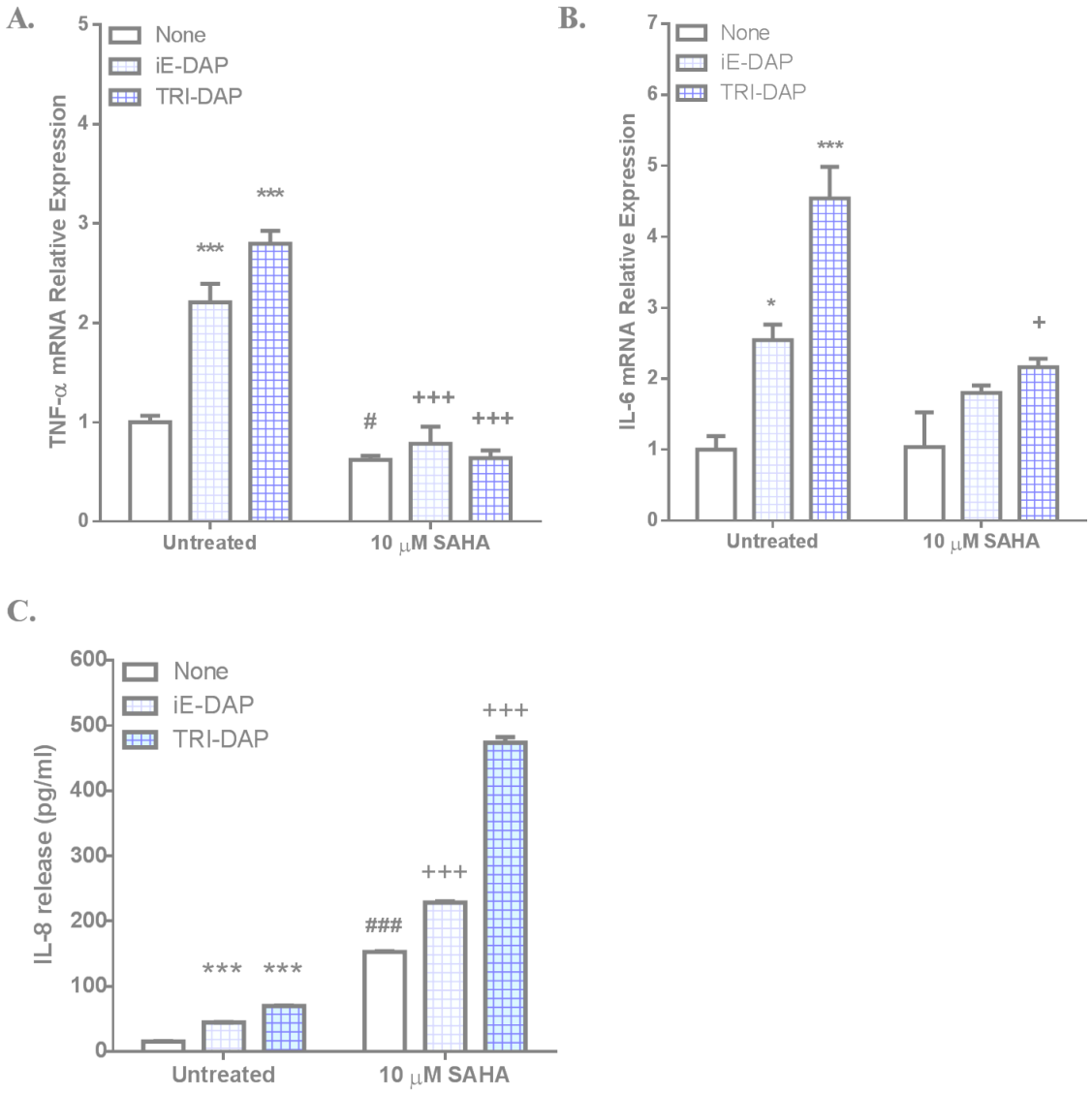

Figure 5.9: NOD1-induced pro-inflammatory activity in SAHA primed THP-1 cells. (A-B) TNF-α and IL-6 mRNA relative expression in THP-1 cells primed with 10 μM SAHA for 48 hours and subsequently simulated with a NOD1 ligand (10 μg/ml iE-DAP/TRI-DAP) for 6 hours. RPL13A acted as the housekeeping control. Data is represented as mean relative expression ± S.E.M. C) IL-8 release from THP-1 cells primed with 10 μM SAHA for 48 hours and stimulated with a NOD1 ligand (50 μg/ml iE-DAP/TRI-DAP) for 18 hours. Data is represented as absolute values ± S.E.M. Statistical analysis was performed using two-way ANOVAs, followed by Bonferroni *post-hoc* test where appropriate. ***** $p < 0.05$ representing **control vs NOD1**, **#** $p < 0.05$ representing **control vs primed**, **+** $p < 0.05$ **NOD1 vs (primed + NOD1).**

5.4.6 HDAC inhibitor priming increases NOD1-induced RIP2 activation but attenuates MAPK signalling in THP-1 cells.

To further investigate the effects of SAHA-priming on NOD1-induced pro-inflammatory responses in THP-1 cells, RIP2 and MAPK signalling activation was quantified in the absence and presence of SAHA. When carrying out densitometry, phosphorylated proteins were expressed relative to the loading control (β-Tubulin), since SAHA appeared to have a direct effect on some total proteins.

Stimulation of THP-1 cells with iE-DAP increased p-RIP2 (1.6-fold, $p > 0.05$), p-ERK2 (2.8-fold, $p < 0.001$) and p-p38 (1.3-fold, $p > 0.05$). SAHA priming increased basal p-RIP2 by 2-fold ($p < 0.05$) but reduced p-p38 by 0.5-fold ($p < 0.001$). Relative to the untreated control group, priming with SAHA increased iE-DAP-induced p-RIP2 from 1.6-fold to 3.7-fold ($p < 0.001$, relative to untreated + iE-DAP) but reduced p-ERK2 from 2.8-fold to 1.2-fold ($p < 0.001$, relative to untreated + iE-DAP) and p-p38 from 1.3-fold to 0.4-fold ($p < 0.001$, relative to untreated + iE-DAP) (Figure 5.10).

NOD1 stimulation with TRI-DAP uncovered a similar pattern of effects, increasing RIP2 and MAPK activation 1.4-fold ($p < 0.05$). Again, SAHA was found to increase basal p-RIP2 (4.4-fold, $p < 0.001$) but slightly reduced levels of p-ERK2 and p-p38 (0.8-fold, $p > 0.05$). Relative to the untreated control group, priming with SAHA increased TRI-DAP-induced p-RIP2 from 1.4-fold to 5.3-fold ($p < 0.001$, relative to untreated + TRI-DAP), but reduced p-ERK2 from 1.4-fold to 0.6-fold ($p < 0.001$, relative to untreated + TRI-DAP) and p-p38 from 1.4-fold back to control levels ($p < 0.05$, relative to untreated + TRI-DAP) (Figure 5.11).

Together, these findings suggest that treatment with a HDAC inhibitor has mixed effects on NOD1 associated pro-inflammatory signalling, increasing RIP2 activation but reducing MAPK activation.

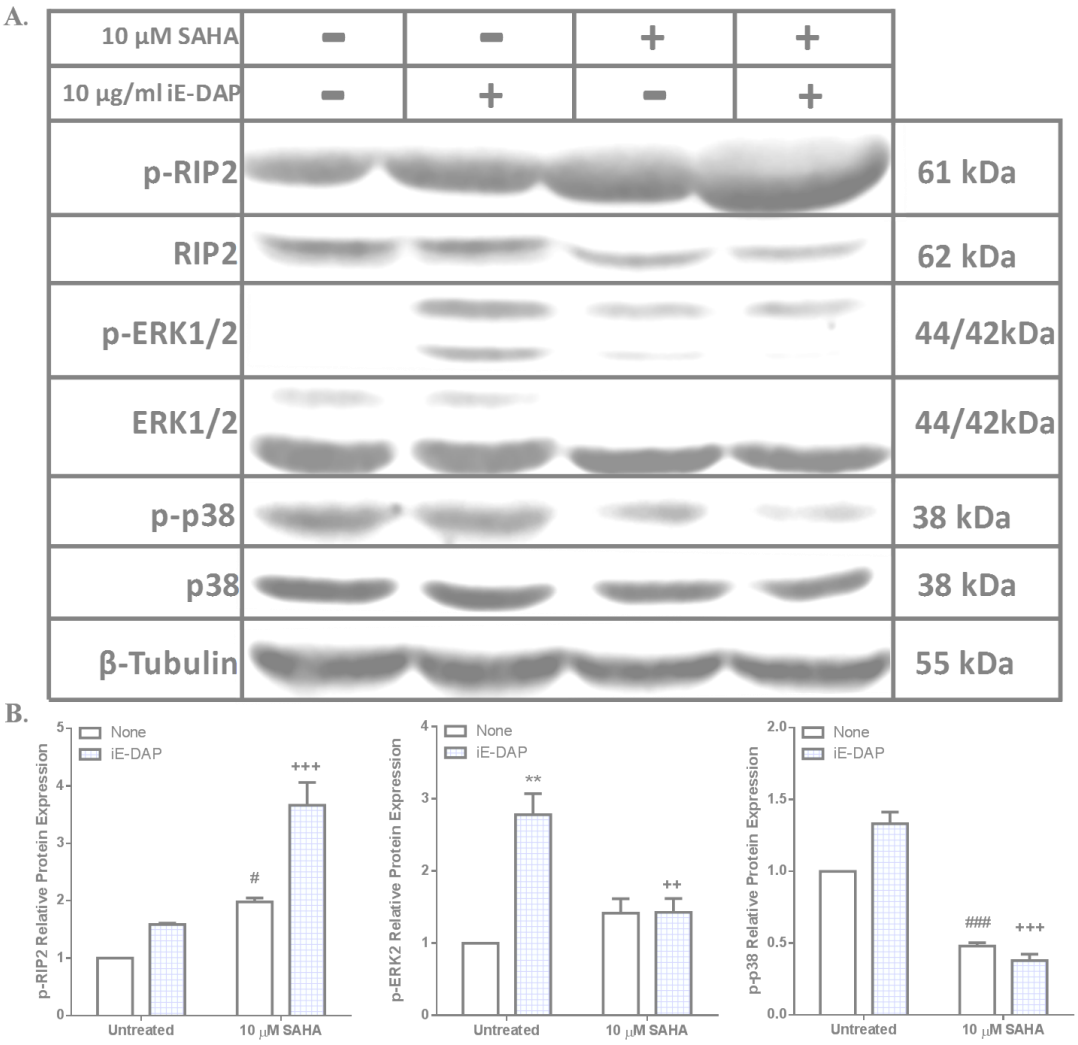

Figure 5.10. IE-DAP-induced RIP 2 and MAPK signalling in SAHA-primed THP-1 cells. A) Immunoblots of phosphorylated and total RIP2, p38 and ERK1/2 in cells primed with 10 µM SAHA for 48 hours and subsequently stimulated with iE-DAP (10 µg/ml) for three hours. β-Tubulin acted as the loading control. B) Densitometry of phosphorylated RIP2, p38 and ERK2 expression, relative to β-Tubulin expression. "Untreated + None" was set as the control group. Data is represented as mean relative expression ± S.E.M and analysed using two-way ANOVAs (followed by Bonferroni's *post-hoc* test). ***** $p < 0.05$ representing **control vs NOD1**, **#** $p < 0.05$ representing **control vs primed**, **+** $p < 0.05$ representing **NOD1 vs (primed + NOD1).**

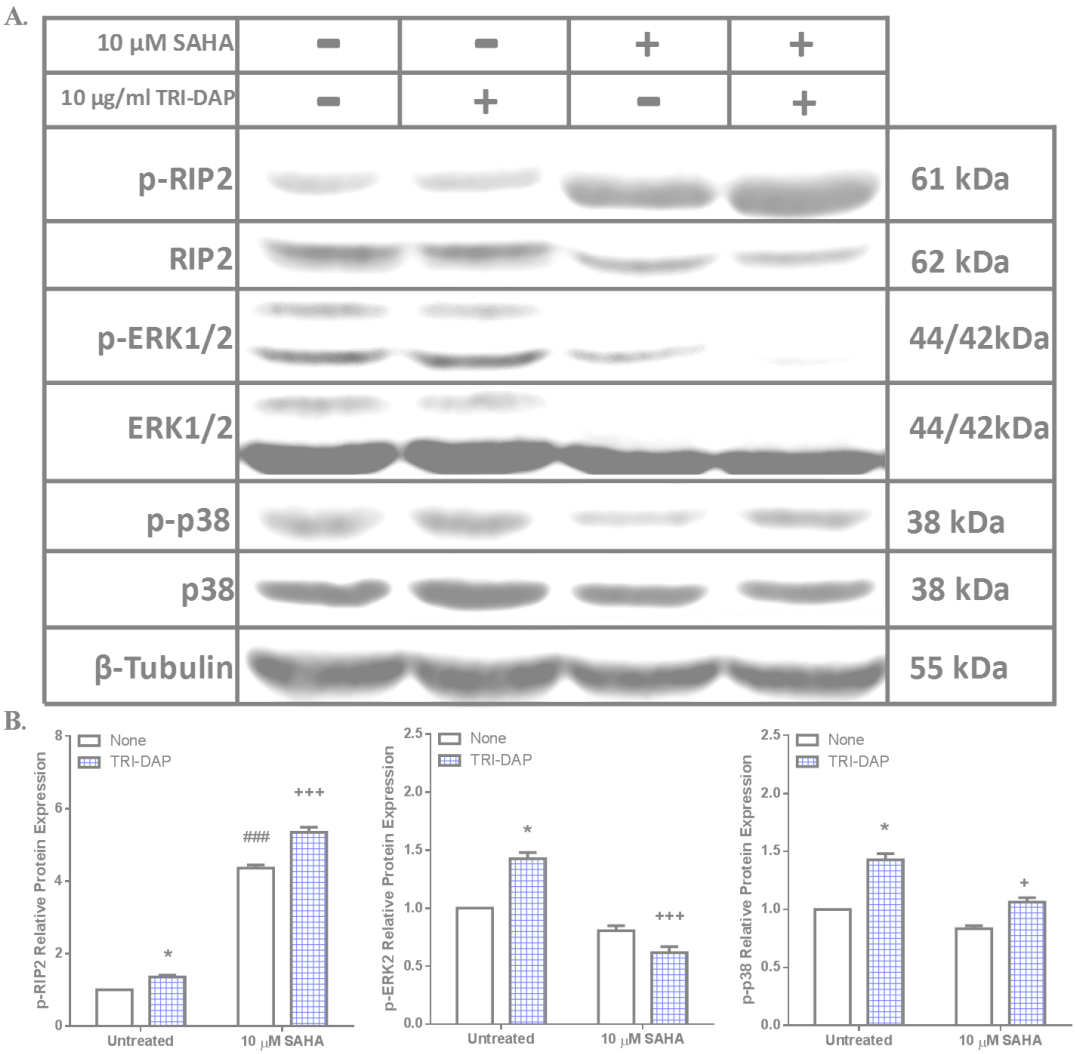

Figure 5.11. TRI-DAP-induced RIP2 and MAPK signalling in SAHA-primed THP-1 cells. A) Immunoblots of phosphorylated and total RIP2, p38 and ERK1/2 in cells primed with 10 µM SAHA for 48 hours and subsequently stimulated with TRI-DAP (10 µg/ml) for two hours. β-Tubulin acted as the loading control. B) Densitometry of phosphorylated RIP2, p38 and ERK2 expression, relative to β-Tubulin expression. "Untreated + None" was set as the control group. Data is represented as mean relative expression ± S.E.M and analysed using two-way ANOVAs (followed by Bonferroni's *post-hoc* test). ***** $p < 0.05$ representing **control vs NOD1**, **#** $p < 0.05$ representing **control vs primed**, **+** $p < 0.05$ representing **NOD1 vs (primed + NOD1).**

5.4.7 HDAC inhibitor priming has varying effects on NF-κB signalling in THP-1 cells.

To complete the investigation of SAHA priming on NOD1 associated pro-inflammatory signalling, phosphorylation of NF-κB proteins (p65 and IκBα) in its absence and presence was investigated next. Phosphorylated p65 and IκBα expression levels were quantified relative to β-Tubulin.

Stimulation of THP-1 cells with iE-DAP alone for three hours increased phosphorylation of p65 (2.4-fold, $p < 0.05$) and IκBα (2.3-fold, $p < 0.001$). Treatment with SAHA increased basal p-p65 levels 3.2-fold ($p < 0.01$) but significantly diminished basal p-IκBα levels (0.3-fold, $p < 0.001$). SAHA-priming was found to have conflicting effects on NOD1-induced pro-inflammatory activity. Relative to the untreated control group, priming with SAHA increased iE-DAP-induced p-p65 from 2.4-fold to 8.4-fold ($p < 0.001$, relative to untreated + iE-DAP), but reduced p-IκBα from 2.3-fold to 0.9-fold ($p < 0.001$, relative to untreated + iE-DAP), as outlined in Figure 5.12.

A similar pattern was uncovered when SAHA-primed cells were stimulated with TRI-DAP, but to a greater magnitude. TRI-DAP stimulation alone induced a significant increase in p-p65 (5.2-fold, $p < 0.001$) and p- IκBα (4.3-fold, $p < 0.001$) expression. As seen in the iE-DAP data, SAHA-priming had differing effects on TRI-DAP-induced p65 and IκBα phosphorylation. Relative to the untreated control group, priming with SAHA increased TRI-DAP-induced p-p65 from 5.2-fold to 15.8-fold ($p < 0.001$, relative to untreated + TRI-DAP), but reduced p-IκBα from 4.3-fold to 2.8-fold ($p < 0.001$, relative to untreated + TRI-DAP), as outlined in Figure 5.13.

Therefore, the effect of SAHA priming on NOD1-associated NF-κB signalling appeared conflicting, which suggests that SAHA is potentially altering NF-κB signalling via a NOD1-independent pathway.

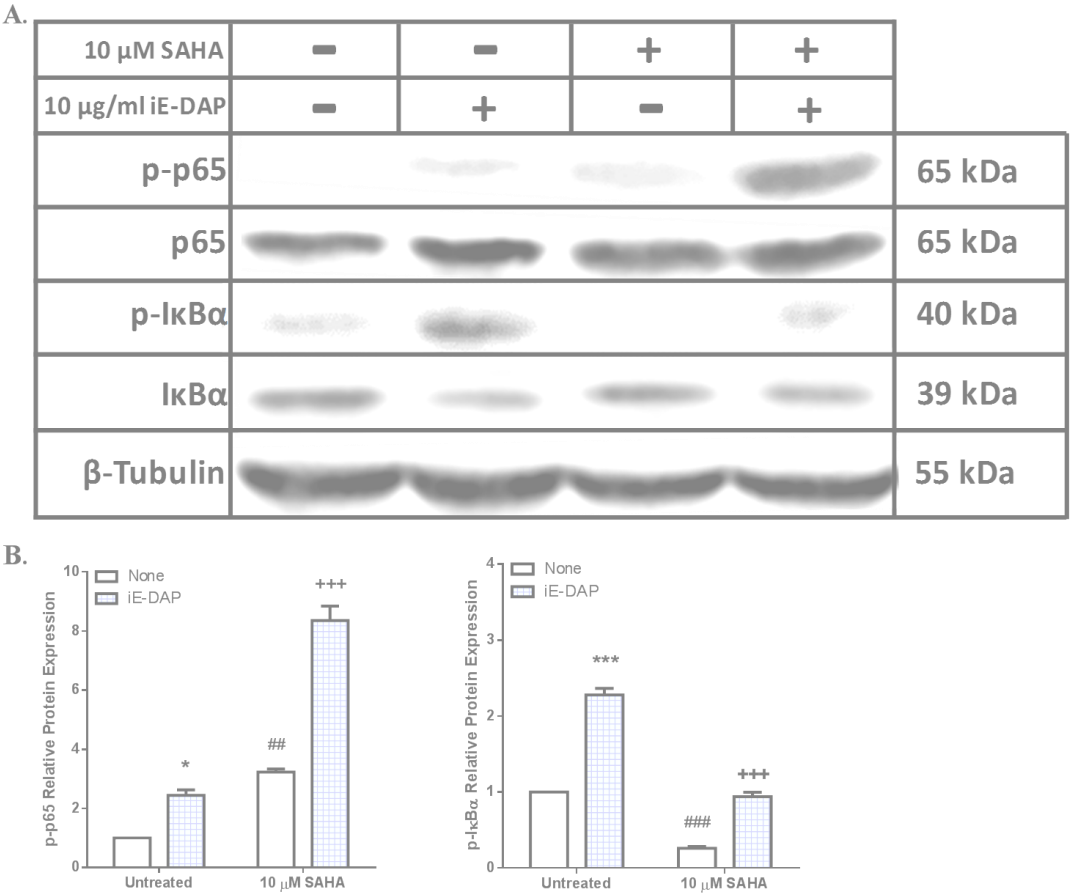

Figure 5.12. IE-DAP-induced NF-κB signalling in SAHA-primed THP-1 cells. (A) Immunoblots of phosphorylated and total p65 and IκBα in cells primed with 10 µM SAHA for 48 hours and subsequently stimulated with iE-DAP (10 µg/ml) for three hours. β- Tubulin acted as the loading control. (B) Densitometry of phosphorylated p65 and IκBα expression, relative to β-Tubulin expression. "Untreated + None" was set as the control group. Data is represented as mean relative expression ± S.E.M and analysed using two-way ANOVAs (followed by Bonferroni's *post-hoc* test). ***** $p < 0.05$ representing **control vs NOD1**, **#** $p < 0.05$ representing **control vs primed**, **+** $p < 0.05$ representing **NOD1 vs (primed + NOD1).**

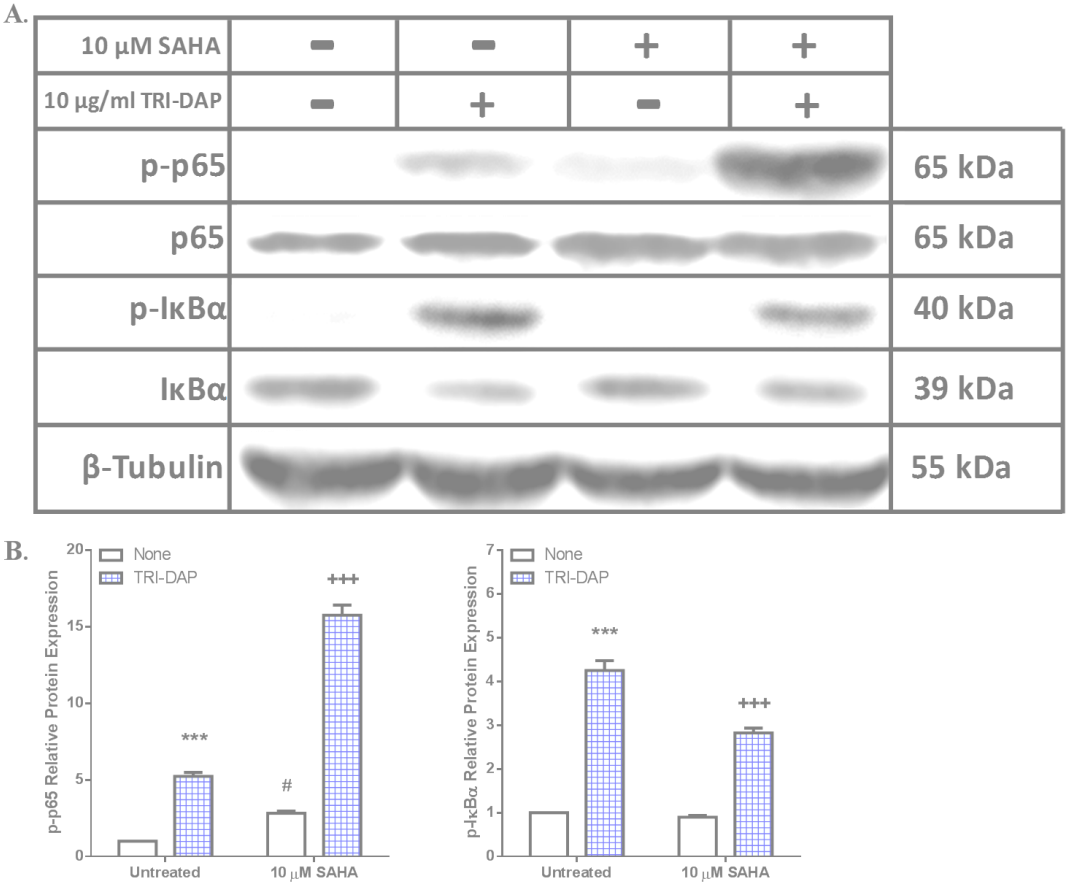

Figure 5.13. TRI-DAP-induced NF-κB signalling in SAHA-primed THP-1 cells. (A) Immunoblots of phosphorylated and total p65 and IκBα in cells primed with 10 µM SAHA for 48 hours and subsequently stimulated with TRI-DAP (10 µg/ml) for two hours. β- Tubulin acted as the loading control. (B) Densitometry of phosphorylated p65 and IκBα expression, relative to β-Tubulin expression. "Untreated + None" was set as the control group. Data is represented as mean relative expression ± S.E.M and analysed using two-way ANOVAs (followed by Bonferroni's *post-hoc* test). ***** $p < 0.05$ representing **control vs NOD1**, **#** $p < 0.05$ representing **control vs primed**, **+** $p < 0.05$ representing **NOD1 vs (primed + NOD1).**

5.4.8 HDAC inhibitor treatment reduces NOD1 mRNA but increases NOD1 protein expression in THP-1 cells.

To explore the underlying mechanism behind the effects of SAHA on NOD1 activity and signalling in THP-1 cells, NOD1 expression was quantified following SAHA treatment. THP-1 cells were treated with 10 μM SAHA for 48 hours, after which NOD1 mRNA and protein expression were quantified by qPCR and western blotting, respectively. NOD1 expression was quantified relative to the chosen housekeeping gene; β-Tubulin. NOD1 mRNA expression significantly declined following SAHA treatment (0.1-fold, $p < 0.001$) (Figure 5.14 A). However, NOD1 protein was found to increase 1.6-fold following SAHA exposure ($p < 0.01$) (Figure 5.14 B-C). Therefore, the effects of SAHA on NOD1 expression remains inconclusive.

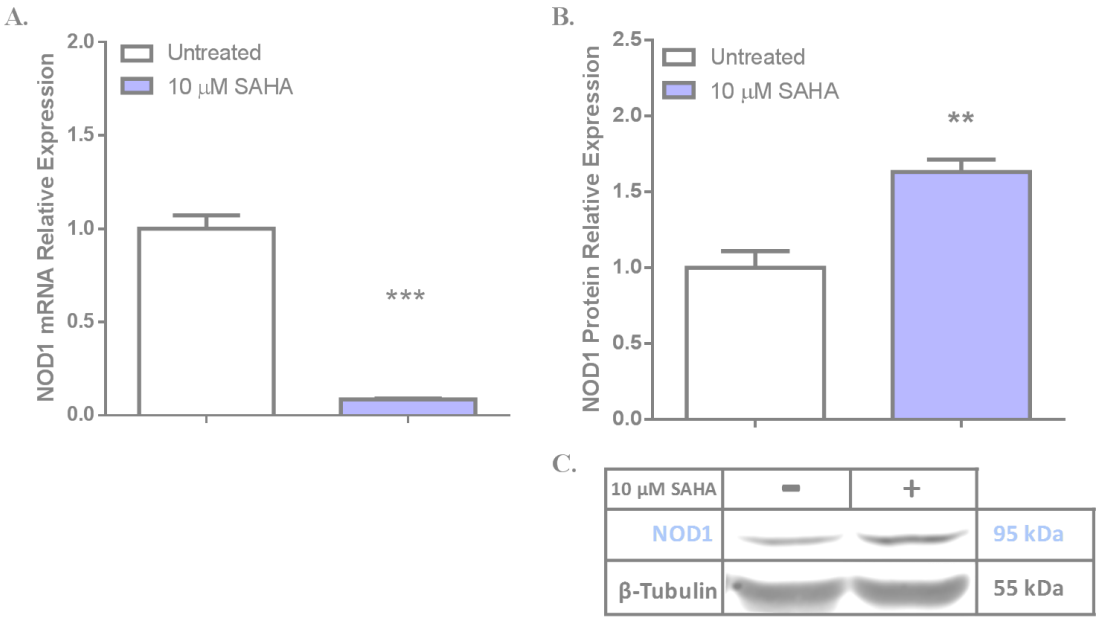

Figure 5.14. NOD1 basal expression in SAHA treated THP-1 cells. (A) NOD1 mRNA expression in THP-1 cells treated with 10 μM SAHA for 48 hours, relative to β-Tubulin expression. (B) Densitometry of NOD1 protein expression in SAHA treated cells, relative to β-Tubulin expression. (C) Representative immunoblot of NOD1 protein expression in SAHA treated cells. Data is represented as mean relative expression ± S.E.M. Statistical analysis was performed using independent t-tests. Significance was recognised at $p < 0.05$, with * representing $p < 0.05$, ** representing $p < 0.01$ and *** representing $p < 0.001$.

5.4.9 Treatment with 10 ng/ml PMA for 48 hours supports the most effective differentiation of THP-1 cells.

THP-1 cells are immature monocytes; therefore, PMA was used to differentiate these cells into mature macrophage-like cells. This was done to explore whether macrophages respond differently to NOD stimulation.

There is no definitive procedure in the literature for PMA-induced monocyte differentiation, therefore time and dose analysis were carried out to establish the most appropriate treatment conditions. THP-1 cells were treated with 0, 1, 10 or 100 ng/ml PMA for either 24, 48 or 72 hours. Following these treatments three main criteria were investigated to analyse differentiation efficiency; cell adherence, RSK1 expression and CD16 cell surface marker expression.

THP-1 cells are suspension cells, however when are differentiated they become adherent. Cells began to exhibit adherence after 24 hours of 10-100 ng/ml PMA, increasing further after 48 hours of treatment, but cells began to die and display a deformed cell structure after 72 hours. The optimum cell adherence was recognised following 10 ng/ml of PMA for 48 hours, as highlighted in Figure 5.15.

Increased RSK1 expression is another indicator of differentiation (Huber et al., 2015). RSK1 protein was analysed in THP-1 cells treated with 0, 1, 10 and100ng/ml PMA for 24, 48 or 72 hours by western blotting. RSK1 densitometry values were normalised relative to the β-Actin loading control. The untreated THP-1 cells (0 ng/ml for 24 hours) was set as the control group. All other normalised values were expressed relative to the control group. Significant increases in RSK1 were detected following treatment with 1 ng/ml PMA for 24 hours (1.6-fold, $p < 0.01$). RSK1 was also significantly increased after 1 ng/ml or 10ng/ml PMA for 48 hours (1.7-fold, $p < 0.01$). RSK1 increased 2-fold after 10 ng/ml PMA for 72 hours (Figure 5.16).

The final criteria explored here to endorse cell differentiation was the expression of the cell surface marker; CD16. When monocytes differentiate, CD16 levels are expected to increase. Therefore, the THP-1 cells were exposed to the same time and dose conditions as were used to investigate for the other two criteria. Samples were analysed for expression of the cell surface marker by flow cytometry. CD16 levels increased significantly after 48 hours of 10 ng/ml PMA (655.9 MFI, $p < 0.01$) and 100 ng/ml (811.4 MFI, $p < 0.001$). Increases were also detected 72 hours after 1 ng/ml

(553.5 MFI, $p < 0.05$), 10 ng/ml (718.9 MFI, $p < 0.001$) and 100 ng/ml (823 MFI, $p < 0.001$) of PMA, as shown in Figure 5.17.

Combining the findings in these three sets of exploratory experiments, it was decided that the optimum PMA culture conditions was 10 ng/ml for 48 hours.

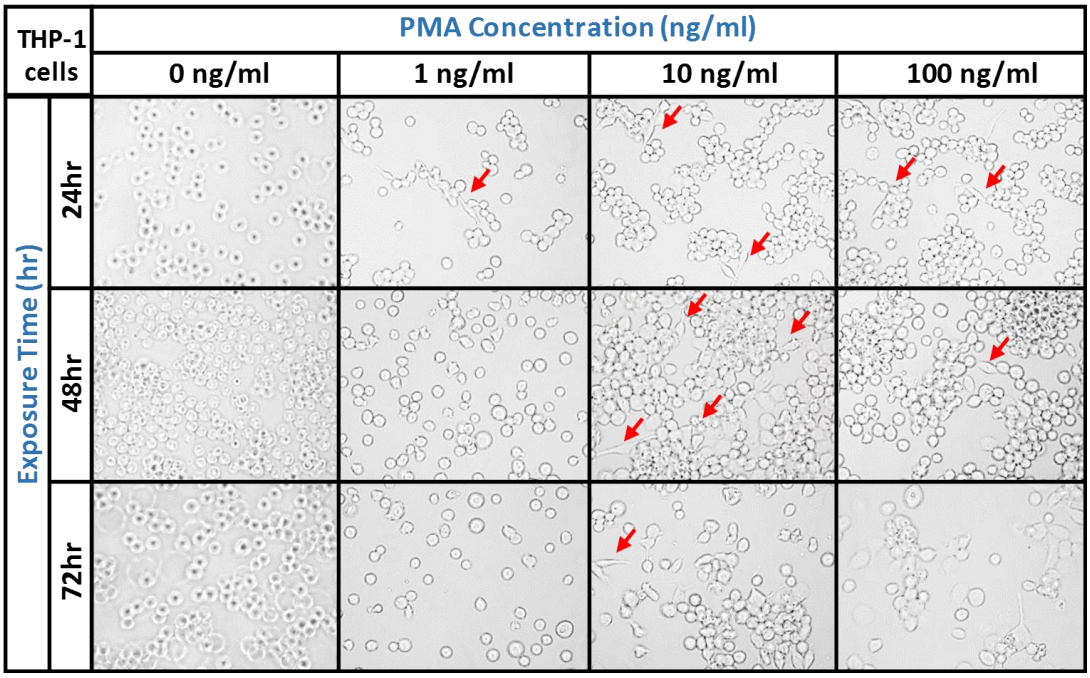

Figure 5.15. Cell adherence following various exposure times to different PMA concentrations. THP-1 cells were exposed to either 0, 1, 10 or 100 ng/ml PMA for either 24, 48 or 72 hours. Cell adherence in response to PMA treatment was investigated and photos were taken. Signs of adherence are indicated by red arrows.

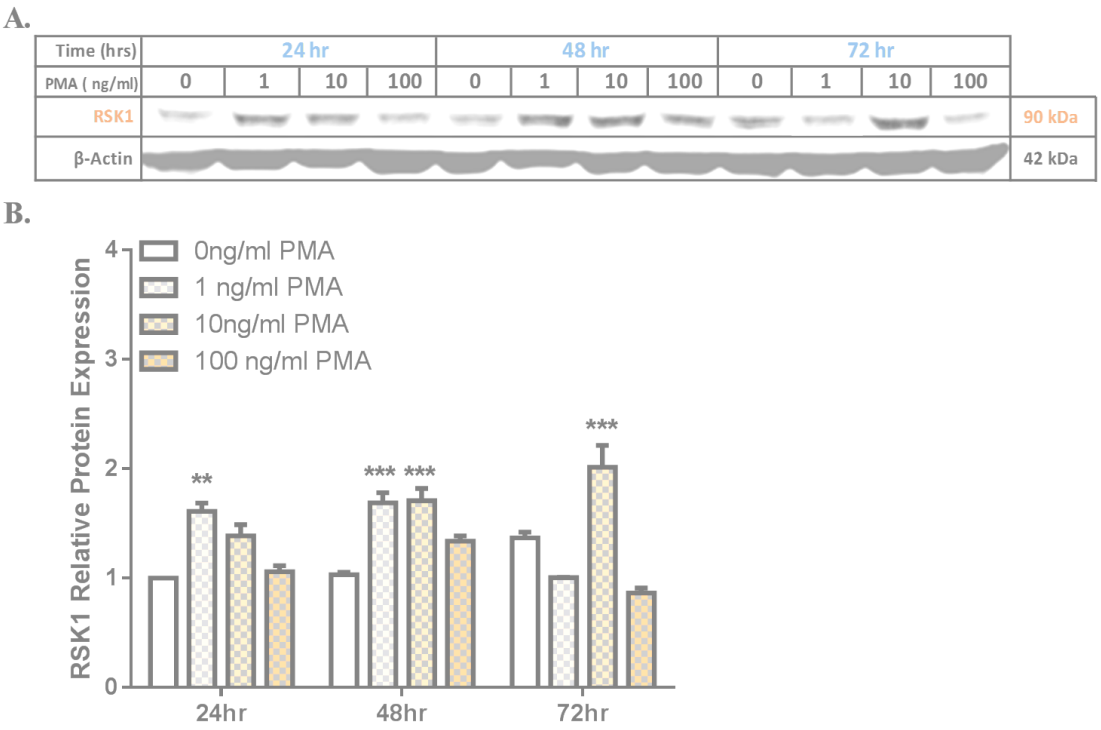

Figure 5.16. RSK1 expression following various exposure times to different PMA concentrations. THP-1 cells were exposed to either 0, 1, 10 or 100 ng/ml PMA for either 24, 48 or 72 hours. (A) Representative immunoblot of RSK1 protein expression in PMA treated cells. (B) Densitometry of RSK1 protein expression in PMA treated cells, relative to β-Actin expression. The untreated THP-1 cells acted as the "control". Data are presented as mean relative expression ± S.E.M. and were analysed using two-way ANOVAs (followed by Bonferroni's *post-hoc* test). * represents significance ($p < 0.05$) relative to the control group.

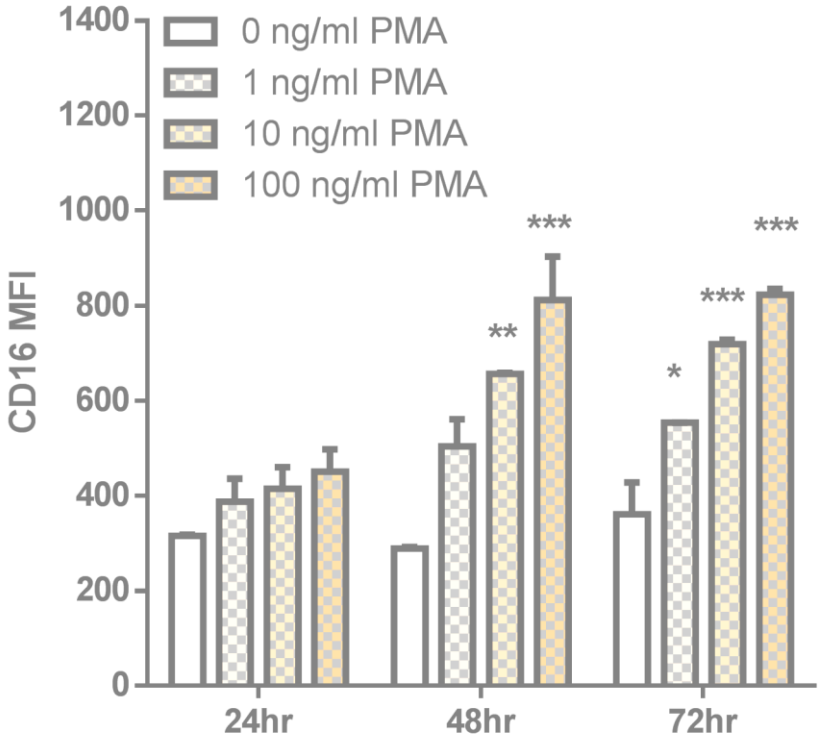

Figure 5.17. Cell surface expression of CD16 following various exposure times to different PMA concentrations. THP-1 cells were exposed to either 0, 1, 10 or 100 ng/ml PMA for either 24, 48 or 72 hours. CD16 marker expression was quantified by flow cytometry. The untreated THP-1 cells acted as the "control". Data are presented as MFI ± S.E.M. and were analysed using two-way ANOVAs (followed by Bonferroni's *post-hoc* test). * represents significance ($p < 0.05$) relative to the control group.

5.4.10 Differentiation of THP-1 cells attenuates NOD1-induced pro-inflammatory activity.

THP-1 cells were differentiated with 10 ng/ml PMA for 48 hours, after which cells were stimulated with 10 μg/ml iE-DAP or TRI-DAP for six or 18 hours. Pro-inflammatory activity was examined by quantifying TNF-α and IL-6 expression by qPCR and IL-8 release by ELISA. Stimulation with iE-DAP for six hours prompted a 4-fold increase in TNF-α ($p < 0.01$) and 2.9-fold increase in IL-6 ($p < 0.001$). PMA induced a significant drop in basal expression of TNF- α (0.7-fold, $p > 0.05$) and IL-6 (0.2-fold, $p < 0.001$). The same pattern was recorded in TRI-DAP stimulated cells, but to a greater magnitude. TRI-DAP increased TNF-α by 10.7-fold ($p < 0.001$) and IL-6 by 6.8-fold ($p < 0.001$). Differentiation of cells with PMA altered these patterns. Relative to the untreated control group, PMA-priming reduced levels of iE-DAP-induced TNF-α from 4-fold to 3.1-fold ($p < 0.01$, relative to untreated + iE-DAP) and IL-6 from 2.9-fold to 1.9-fold ($p < 0.01$, relative to untreated + iE-DAP), as outlined in Figure 5.18 A-B. PMA-driven differentiation also attenuated responses to TRI-DAP stimulation. Relative to the untreated control group, PMA-priming reduced levels of TRI-DAP-induced TNF-α from 10.7-fold to 3.5-fold ($p < 0.01$, relative to untreated + TRI-DAP) and IL-6 from 6.8-fold to 2.3-fold ($p < 0.01$, relative to untreated + TRI-DAP), as outlined in Figure 5.18 A-B.

Since TNF and IL-6 release from THP-1 cells was below the limits of detection, IL-8 release was measured by ELISA to further examine the effect of differentiation on NOD1 activity. Basal IL-8 release from THP-1 cells (17 ± 0.8 pg/ml) was increased by 18 hours of stimulation with 50 μg/ml iE-DAP (44.9 ± 1.7 pg/ml) and TRI-DAP (94 ± 5 pg/ml). Differentiation of THP-1 cells increased basal IL-8 by approximately 70-fold relative to the control (1184.6 ± 28.3 pg/ml, $p < 0.001$). PMA-primed cells that were stimulated with iE-DAP and TRI-DAP had exacerbated pro-inflammatory activity, represented by an increase in IL-8 release to 1263.8 ± 105.4 pg/ml ($p < 0.001$, relative to untreated + iE-DAP) and 1362.74 ± 11.3 pg/ml ($p < 0.001$, relative to untreated + TRI-DAP), respectively (Figure 5.18 C).

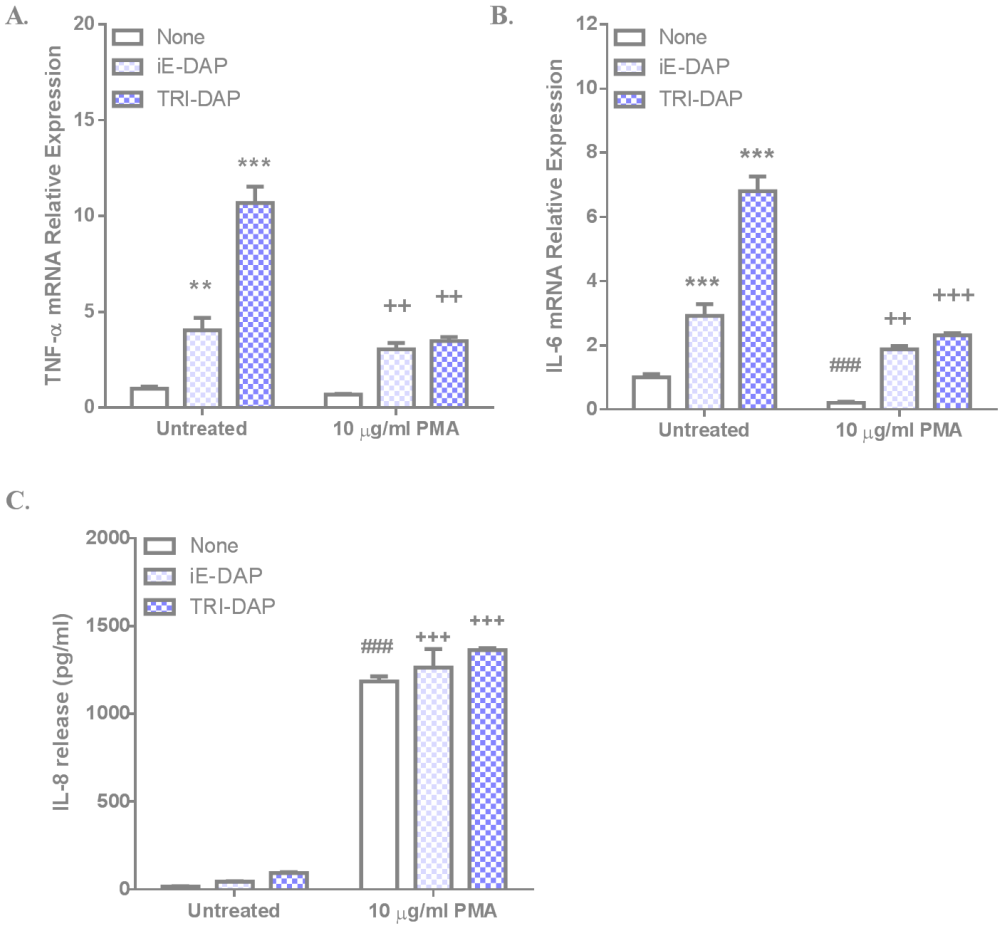

Figure 5.18. NOD1-induced pro-inflammatory activity in differentiated THP-1 cells. (A-B) TNF-α and IL-6 mRNA relative expression in THP-1 cells primed with 10 ng/ml PMA for 48 hours and subsequently simulated with a NOD1 ligand (10 μg/ml iE-DAP/TRI-DAP) for 6 hours. β-Actin acted as the housekeeping gene. "Untreated + None" was set as the control group. Data is represented as mean relative expression ± S.E.M. C) IL-8 release from THP-1 cells primed with 10 ng/ml PMA for 48 hours and stimulated with a NOD1 ligand (50 μg/ml iE-DAP/TRI-DAP) for 18 hours. "Untreated + None" was set as the control group. Data is represented as absolute concentration ± S.E.M. Statistical analysis was performed using two-way ANOVAs, followed by the Bonferroni *post-hoc* test where appropriate. ***** $p < 0.05$ representing **control vs NOD1**, **#** $p < 0.05$ representing **control vs primed**, **+** representing $p < 0.05$ **NOD1 vs (primed + NOD1).**

5.4.11 Differentiation attenuates NOD1-induced RIP2 and MAPK signalling in THP-1 cells.

To further explore the effects of PMA-induced differentiation on THP-1 responses to NOD1 stimulation, RIP2 and MAPK pro-inflammatory signalling were investigated by western blotting. This involved measuring phosphorylation levels of RIP2, ERK2 and p38 in undifferentiated versus differentiated cells. Following treatment with 10 ng/ml PMA for 48 hours, cells were stimulated with 10 μg/ml iE-DAP or TRI-DAP. The duration of iE-DAP/TRI-DAP stimulation required to investigate signalling was chosen based on the THP-1-time response analysis, as outlined in Appendix 6. Based on this analysis the chosen time points for NOD1 stimulation were; three hours with iE-DAP and two hours with TRI-DAP. Blots were repeated for three independent experiments (n = 3), with representative blots shown. Protein expression was quantified by densitometry of phosphorylated, total and housekeeping proteins. Phosphorylated protein expression was normalised relative to the chosen loading control; β-Actin (since PMA altered total protein expression) and subsequently calculated relative to the untreated control group.

Stimulation of untreated cells with iE-DAP significantly increased p- RIP2 (2.7-fold, $p < 0.001$), p-ERK2 (4-fold, $p < 0.001$) and p-p38 (1.3-fold, $p < 0.05$). PMA mediated differentiation of THP-1 cells appeared to decrease basal levels of p-RIP2 (0.3-fold, $p < 0.05$), p-ERK2 (0.8-fold, $p > 0.05$) and p-p38 (0.7-fold, $p < 0.001$). This may explain the attenuated responses of differentiated cells to NOD1 stimulation. Relative to the untreated control group, stimulation of PMA-primed cells with iE-DAP reduced phosphorylation of p-RIP2 from 2.7-fold to 0.5-fold ($p < 0.001$, relative to the untreated + iE-DAP), p-ERK2 from 4-fold to 0.9-fold ($p < 0.001$, relative to untreated + iE-DAP) and p-p38 from 1.3-fold to 0.9-fold ($p < 0.001$, relative to untreated + iE-DAP), as depicted in Figure 5.19.

TRI-DAP studies revealed a similar pattern. Stimulation with TRI-DAP alone increased p- RIP2 (3.2-fold, $p < 0.001$), p-ERK2 (3.3-fold, $p < 0.001$) and p-p38 (1.5-fold, $p < 0.05$). PMA mediated differentiation of THP-1 cells decreased basal levels of p-RIP2 (0.2-fold, $p < 0.05$), p-ERK2 (0.3-fold, $p < 0.05$) and p-p38 (0.8-fold, $p < 0.05$). Relative to the untreated control group, stimulation of PMA-primed cells with TRI-DAP reduced phosphorylation of p-RIP2 from 3.2-fold to 0.3-fold ($p < 0.001$, relative to the untreated + TRI-DAP), p-ERK2 from 3.3-fold to 0.4-fold ($p < 0.001$,

relative to untreated + TRI-DAP) and p-p38 from 1.5-fold to 0.7-fold ($p < 0.001$, relative to untreated + TRI-DAP), as depicted in Figure 5.20.

Collectively, this data suggests that differentiation of THP-1 cells into macrophage-like cells reduces cell response to NOD1 stimulation.

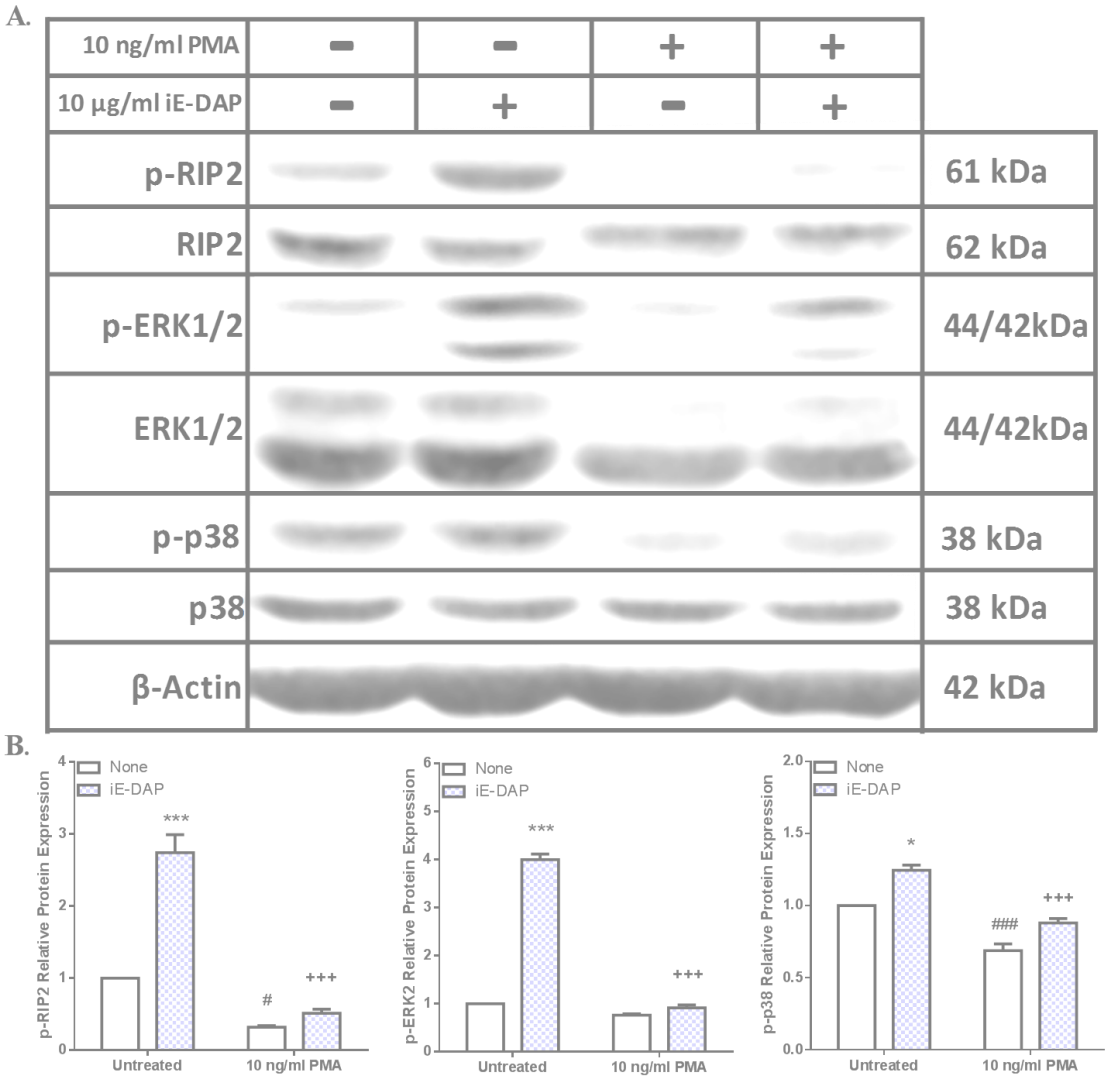

Figure 5.19. IE-DAP-induced RIP2 and MAPK signalling in PMA-primed THP-1 cells. A) Immunoblots of phosphorylated and total RIP2, p38 and ERK1/2 in cells primed with 10 ng/ml PMA for 48 hours and subsequently stimulated with iE-DAP (10 µg/ml) for three hours. β-Actin acted as the loading control. B) Densitometry of phosphorylated RIP2, p38 and ERK2 expression, relative to β-Actin expression. "Untreated + None" was set as the control group. Data is represented as mean relative expression ± S.E.M and analysed using two-way ANOVAs (followed by Bonferroni's *post-hoc* test). ***** $p < 0.05$ representing **control vs NOD1**, **#** $p < 0.05$ representing **control vs primed**, **+** $p < 0.05$ representing **NOD1 vs (primed + NOD1).**

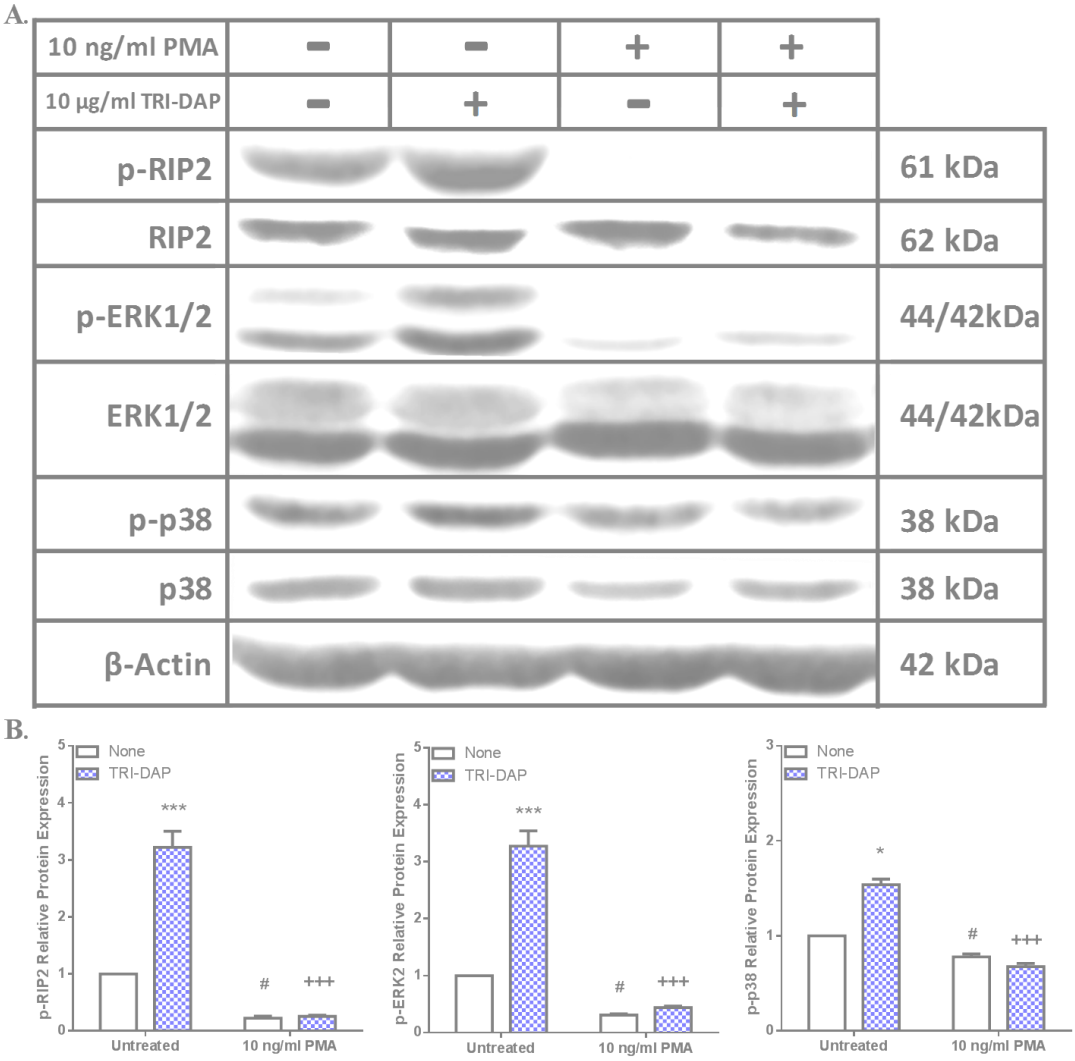

Figure 5.20. TRI-DAP-induced RIP2 and MAPK signalling in PMA-primed THP-1 cells. A) Immunoblots of phosphorylated and total RIP2, p38 and ERK1/2 in cells primed with 10 ng/ml PMA for 48 hours and subsequently stimulated with TRI-DAP (10 µg/ml) for two hours. β-Actin acted as the loading control. B) Densitometry of phosphorylated RIP2, p38 and ERK2 expression, relative to β-Actin expression. "Untreated + None" was set as the control group. Data is represented as mean relative expression ± S.E.M and analysed using two-way ANOVAs (followed by Bonferroni's *post-hoc* test). ***** $p < 0.05$ representing **control vs NOD1**, **#** $p < 0.05$ representing **control vs primed**, **+** $p < 0.05$ representing **NOD1 vs (primed + NOD1).**

5.4.12 Differentiation attenuates NOD1-induced NF-κB signalling in THP-1 cells.

To expand on the patterns uncovered in RIP2 and MAPK signalling, the influence of PMA-driven differentiation on NF-κB signalling was investigated. Phosphorylation of p65 and IκBα was expressed relative to the loading control (β-Actin), since PMA has a direct effect on total proteins. The duration of 10 μg/ml iE-DAP/TRI-DAP stimulation required to investigate NF-κB signalling was chosen based on the time response analysis, as outlined in Appendix 6. The same time point chosen matched that used to analyse RIP2 and MAPK signalling; iE-DAP for three hours and TRI-DAP for two hours. Phosphorylation of the p65 and IκBα was investigated by western blot analysis. Blots were repeated for three independent experiments (n = 3), with representative blots shown. Protein expression was quantified by densitometry of phosphorylated, total and housekeeping proteins. Phosphorylated protein expression was normalised relative to the chosen loading control; β-Actin, and subsequently calculated relative to the untreated control group.

Stimulation of undifferentiated THP-1 cells with iE-DAP increased p-p65 (1.7-fold, $p < 0.01$) and p-IκBα (1.4-fold, $p < 0.05$) proteins. PMA-alone reduced basal p-p65 (0.9-fold, $p > 0.05$) and p- IκBα (0.2-fold, $p < 0.001$). Relative to the untreated control group, PMA-primed cells that were stimulated with iE-DAP exhibited a reduction in p-p65 from 1.7-fold to 1.4-fold ($p > 0.05$, relative to the untreated + iE-DAP) and p-IκBα from 1.4-fold to 0.2-fold ($p < 0.001$, relative to untreated + iE-DAP), as depicted in Figure 5.21.

As was uncovered in iE-DAP studies, TRI-DAP stimulation of untreated THP-1 cells increased p-p65 (6.4-fold, $p < 0.001$) and p-IκBα (5.9-fold, $p < 0.001$). Basal levels of these phosphorylated proteins were diminished following PMA treatment, with both p-p65 and p-IκBα falling 0.7-fold ($p > 0.05$). Relative to the untreated control group, PMA-primed cells that were stimulated with TRI-DAP exhibited a reduction in p-p65 from 6.4-fold to 1.9-fold ($p < 0.001$, relative to the untreated + TRI-DAP) and p- IκBα from 5.9-fold to 1.3-fold ($p < 0.001$, relative to untreated + TRI-DAP), as exhibited in Figure 5.22. Together, these data suggest that when monocytes are differentiated into monocyte-derived macrophages they become less responsive to NOD1 stimuli, as represented by reduced RIP2, MAPK and NF-κB signalling.

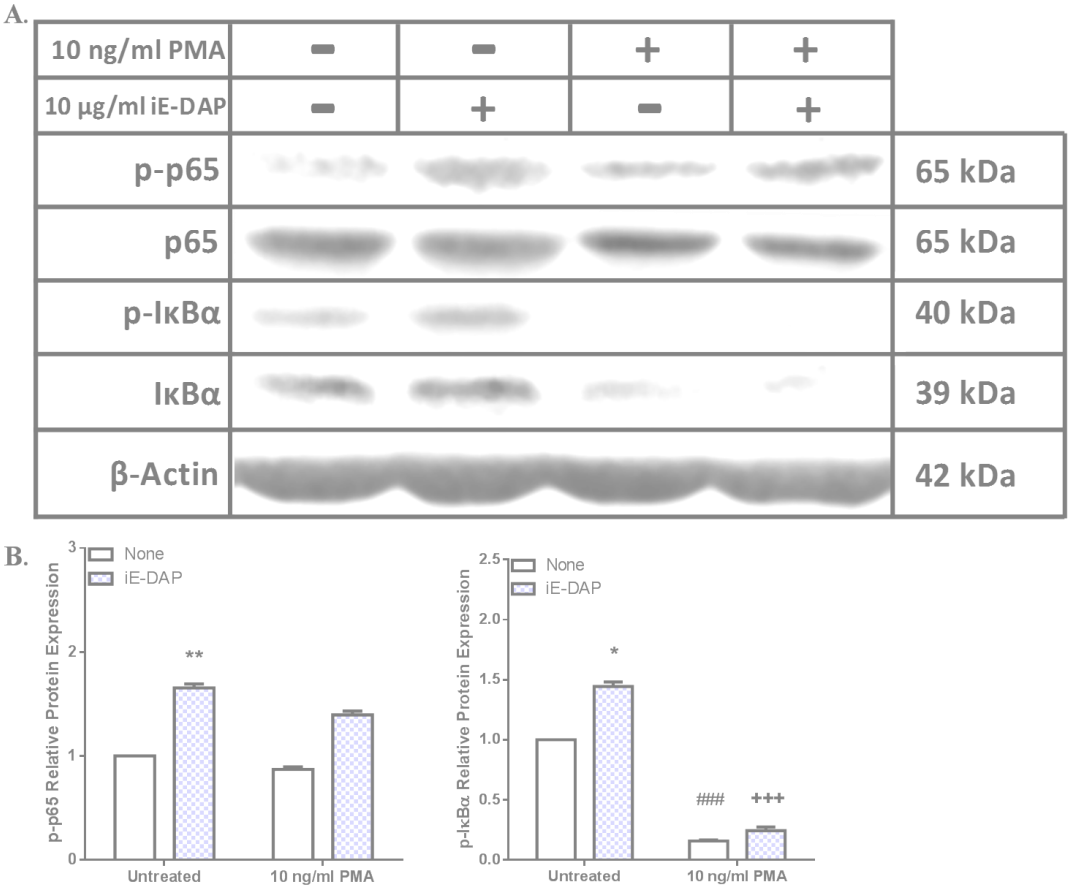

Figure 5.21. IE-DAP-induced NF-κB signalling in PMA-primed THP-1 cells. (A) Immunoblots of phosphorylated and total p65 and IκBα in cells primed with 10 ng/ml PMA for 48 hours and subsequently stimulated with iE-DAP (10 µg/ml) for three hours. β- Actin acted as the loading control. (B) Densitometry of phosphorylated p65 and IκBα expression, relative to β-Actin expression. "Untreated + None" was set as the control group. Data is represented as mean relative expression ± S.E.M and analysed using two-way ANOVAs (followed by Bonferroni's *post-hoc* test). ***** $p < 0.05$ representing **control vs NOD1**, **#** $p < 0.05$ representing **control vs primed**, **+** $p < 0.05$ representing **NOD1 vs (primed + NOD1).**

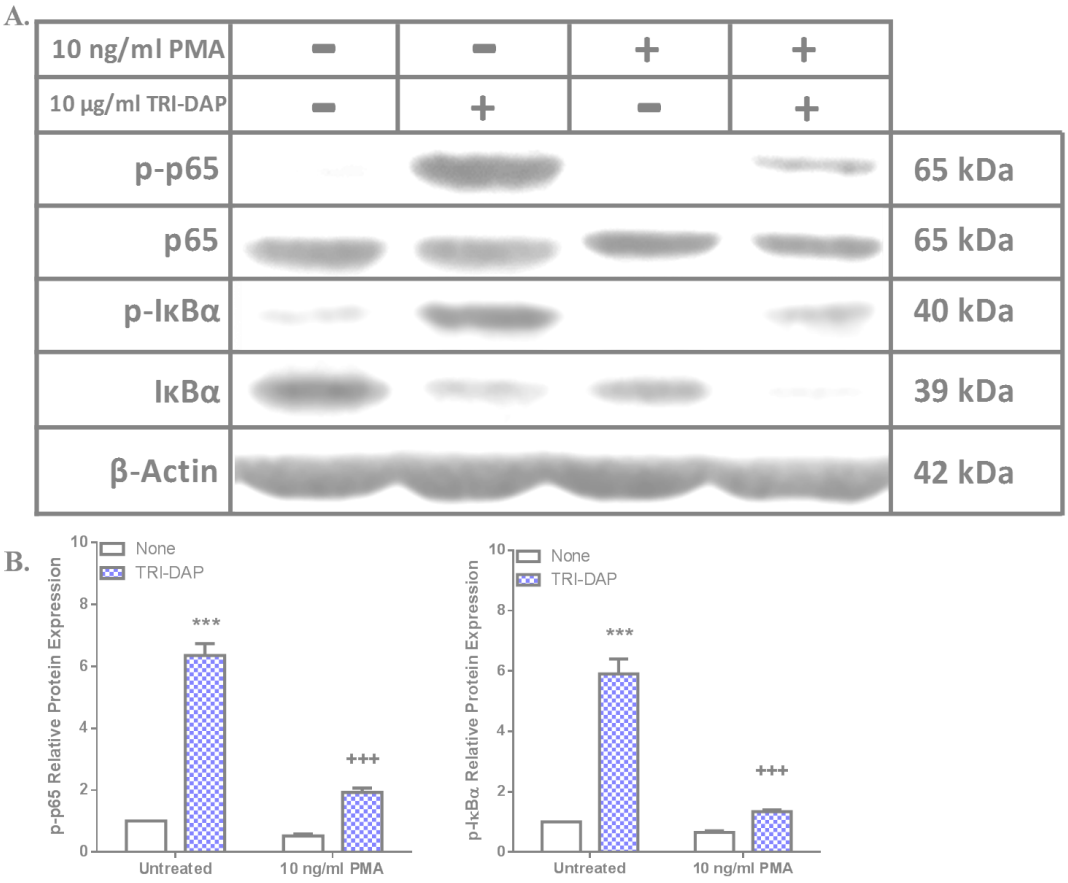

Figure 5.22. TRI-DAP-induced NF-κB signalling in PMA-primed THP-1 cells. (A) Immunoblots of phosphorylated and total p65 and IκBα in cells primed with 10 ng/ml PMA for 48 hours and subsequently stimulated with TRI-DAP (10 µg/ml) for two hours. β- Actin acted as the loading control. (B) Densitometry of phosphorylated p65 and IκBα expression, relative to β-Actin expression. "Untreated + None" was set as the control group. Data is represented as mean relative expression ± S.E.M and analysed using two-way ANOVAs (followed by Bonferroni's *post-hoc* test). ***** $p < 0.05$ representing **control vs NOD1**, **#** $p < 0.05$ representing **control vs primed**, **+** $p < 0.05$ representing **NOD1 vs (primed + NOD1).**

5.4.13 PMA treatment reduces NOD1 expression in THP-1 cells.

To explore the underlying mechanism behind the effects of PMA-driven differentiation on NOD1 activity and signalling in THP-1 cells, NOD1 expression was quantified following PMA treatment. THP-1 cells were treated with 10 ng/ml PMA for 48 hours, after which NOD1 mRNA and protein expression were quantified by qPCR and western blotting, respectively. NOD1 expression was quantified relative to the chosen housekeeping gene; β-Actin. Treatment of THP-1 cells with PMA significantly reduced NOD1 mRNA expression by 0.2-fold ($p < 0.001$) (Figure 5.23 A). This effect was also recorded at the protein level, with PMA inducing a 0.5-fold drop in NOD1 protein expression ($p < 0.001$), as depicted in Figure 5.23 B-C. This data suggests that expression of NOD1 declines when monocytes are differentiated, which could contribute to the reduced pro-inflammatory activity and signalling recorded in PMA-primed cells after NOD1 stimulation.

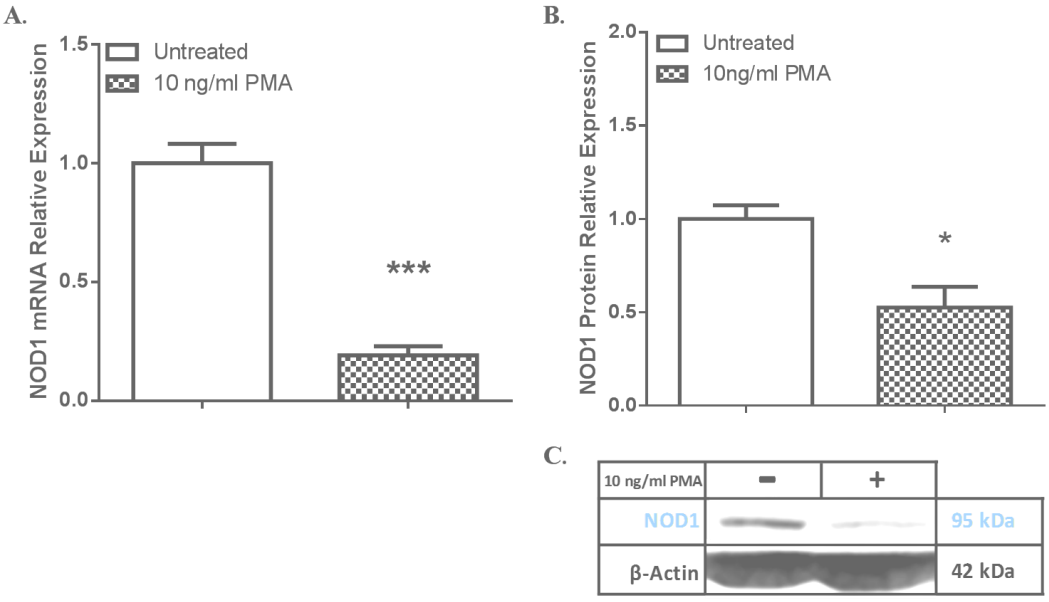

Figure 5.23. NOD1 basal expression in PMA treated THP-1 cells. (A) NOD1 mRNA expression in THP-1 cells treated with 10 ng/ml for 48 hours, relative to β-Actin expression. (B) Densitometry of NOD1 protein expression in PMA treated cells, relative to β-Actin expression. (C) Representative immunoblot of NOD1 protein expression in PMA treated cells. Data is represented as mean relative expression ± S.E.M. Statistical analysis was performed using independent t-tests. Significance was recognised at $p < 0.05$, with * representing $p < 0.05$, ** representing $p < 0.01$ and *** representing $p < 0.001$.

5.5 Discussion of main findings

As was uncovered in Chapter 3, NOD1 pro-inflammatory activity was enhanced in cells primed with a demethylating agent, as exemplified by enhanced TNF-α and IL-6 expression. Release of TNF-α and IL-6 from THP-1 cells however was below the levels of detection. Therefore, pro-inflammatory activity was further investigated by quantifying IL-8 release instead. Priming with 5-Aza-dC was found to augment IL-8 release, thereby strengthening the argument that NOD1 pro-inflammatory activity is increased as a consequence of DNA methylation disruption. NOD1 signalling data complemented this increased activity, with enhanced RIP2/MAPK/NF-kB activation recorded in 5-Aza-dC primed cells. An increase in NOD1 basal expression, at the mRNA and protein levels provided a possible mechanism for this increase in activity and signalling, whereby the demethylating agent increases NOD1 expression directly. This mechanism of regulation is feasible since the NOD1 gene contains two CpG islands in its gene sequence, as was uncovered and discussed in Chapter 3.

The pattern of effects, detailed thus far, of histone acetylation on NOD regulation were observed once again in this chapter. Priming with SAHA caused NOD1 pro-inflammatory activity to wane, as represented by reduced TNF-α and IL-6 mRNA expression. As before, SAHA increased IL-8 release, but this did not imply increased NOD1 activity since SAHA has been shown to increase IL-8 expression via NOD1-independent signalling (Gatla et al., 2017), as earlier discussed. NOD1 associated phosphorylation of MAPKs and IκBα was attenuated in SAHA-primed cells. However, activation of p65 was enhanced by priming. This increase in p-p65 was most likely due to the NOD1-independent signalling induced by SAHA that leads to the increased IL-8 expression. Treatment with the HDAC inhibitor was found to dramatically decrease NOD1 mRNA expression in THP-1 cells, however a conflicting increase in NOD1 protein was recorded. This difference in mRNA and protein is potentially explained by enhanced NOD1 protein stability. As described earlier, literature searches uncovered a SAHA-induced increase in the NOD1 chaperone protein; Hsp70 (Zhao et al., 2006). The augmented stability could thereby be fuelling a false positive for NOD1 expression regulation, and in fact the mRNA data may be more representative of the effects of SAHA on NOD1 expression in THP-1 cells.

Epigenetic modifications are responsible for the major structural and biochemical changes that occur during cell differentiation. Therefore, the effect of PMA-driven monocyte-to-macrophage differentiation, and the associated epigenetic patterns, on NOD1 activity was investigated in the final sections of this chapter. Since epigenetic patterns are known to be altered during this process (Wallner et al., 2016), it provides another avenue for investigation into the effects of epigenetic modifications on NOD1. Monocyte-to-macrophage differentiation resulted in reduced NOD1 pro-inflammatory activity, represented by a decline in NOD1-induced TNF-α and IL-6 expression. Again, similar to SAHA findings, PMA caused an increase in IL-8 release. This differentiation-induced upsurge in IL-8 has been documented previously in the literature (Mahmoud et al., 2014), however the mechanism underlying this increase has not been elucidated. High-throughput screening of the epigenome and genome uncovered differences in expression of almost 5000 out of the 17,515 genes expressed in monocytes and macrophages. Out of this plethora of genes, roughly half were up-regulated, while the others were down-regulated (Wallner et al., 2016). Expression of IL-8 directly, or of an upstream modulator, could be one of the genes altered by PMA differentiation, thereby accounting for the rise in IL-8. Another potential explanation is that IL-8 mRNA stability is significantly increased after differentiation (increasing to more than 15 hours) (Mahmoud et al., 2014). This increase could support enhanced translation and therefore IL-8 release. Taking these findings into consideration, it would appear that the increase in IL-8 release from differentiated cells occurs in a NOD1-independent process, and so its upsurge doesn't imply increased NOD1 activity. NOD1 pro-inflammatory signalling, via RIP2/MAPK/NF-κB proteins, was stunted in differentiated THP-1 cells, thereby supporting the theory that NOD1 response are reduced following differentiation. Reduced NOD1 basal expression in PMA treated THP-1 cells, at the mRNA and protein levels, provided a mechanism for the attenuated NOD1 signalling and activity detected in differentiated cells. Since monocyte-to-macrophage differentiation decreased NOD1 expression and its pro-inflammatory responses, it suggests that one or more of the ~5000 genes, whose expression is altered following differentiation, is a NOD1 positive or negative regulator. In summary of Chapter 5, it was found that NOD1 responses in THP-1 cells are possibly exacerbated directly by DNA methylation, whereas histone acetylation is potentially playing an indirect role in decreasing NOD1 responses and expression. Lastly, differentiation of THP-1 cells, a process associated with enormous epigenetic

rearrangement, caused a decline in NOD1 responses and expression, possibly through up- or down-regulation of NOD1 regulators.

Limitations and Future Work.

The findings presented in this chapter are accompanied by several limitations including; confirmation of enhanced NOD1/2 expression and activation, appropriate indicators of pro-inflammatory activity in SAHA-primed cells, and examination of differentiated THP-1 cell functionality.

As described previously, analysis of methyl patterns surrounding the NOD1 gene sequence should be examined by bisulphite sequencing or melt curve analysis to establish if these patterns were deteriorated under the described demethylating conditions. If methyl patterns are found to be diminished around NOD1/2 promoter regions further experimentation could be undertaken to reveal whether demethylation of the NOD1/2 gene is directly correlated with enhanced transcription. This could be investigated by ChIP analysis, whereby recruitment of transcription machinery to the exposed promoter region could be confirmed/denied thereby providing insight into whether demethylation of the NOD1/2 gene alters its expression.

Additional experimental analysis could be performed to further confirm that NOD1/2 pro-inflammatory activity was enhanced under demethylated conditions. In order for NOD1/2 receptors to relay the pro-inflammatory message it requires a direct interaction with the RIP2 adapter protein. Therefore, co-immunoprecipitation could be carried out to establish whether RIP2 is interacting with the NOD1/2 receptor, thereby providing insight into whether the NOD1/2 receptors are capable of transmitting the pro-inflammatory signal.

Research undertaken in this chapter suggest that pro-inflammatory cytokine/chemokine release may not be the most appropriate indicator of changing pro-inflammatory activity in SAHA-primed cells. Therefore, other indicators of activity could be examined. Anti-microbial peptide release, such as β-defensin, could be measured under the same experimental conditions. Findings from this analysis may provide more insight if SAHA priming is found not to have a direct effect on β-defensin as it did on IL-8 release.

Efficient differentiation of THP-1 cells was supported in this body of research (increased adherence, RSK1 protein and CD16 cell surface marker levels), however these differentiated cells were not tested for their functionality. Phagocytosis assays

could be performed in future experimentation to investigate whether these macrophage-like cells function as macrophages that are capable of ingesting foreign particles (e.g. killed E.coli) labelled with a fluorescent dye.

By addressing these limitations, via the suggested experimentation, it could enhance the quality of the data presented in this research.

Chapter 6 Analysis of NOD2 activity, signalling and expression in the THP-1 monocytic cell line, following epigenetic modification.

6.1 Introduction

As described in Chapter 4, NOD2 is a more general sensor of bacteria, detecting both Gram-positive and -negative bacteria (Moreira and Zamboni, 2012). However, the location of the NOD2 receptor is more selective than NOD1 receptors, with expression only detected in macrophages, monocytes, Paneth intestinal cells and dendritic cells (Inohara et al., 2005). In Chapter 4, results suggested that the epigenome is potentially playing a role in NOD2 regulation. Therefore, focus was switched in this chapter to NOD2 activity, signalling and expression in THP-1 monocytic cells following general epigenetic disruption. THP-1 monocytes were another clear choice for NOD2 investigation, as already mentioned, monocytes are one of the few cell types expressing NOD2 and monocytes are key players in the initiation of the innate immune response (Parihar et al., 2010). NOD2 receptors recognise and bind N-acetylmuramyl-L-Ala-D-isoglutamine, otherwise referred to as muramyl dipeptide (MDP), a conserved motif in all Gram-positive and Gram-negative bacteria (Girardin et al., 2003, Inohara et al., 2003). Activation of this receptor triggers pro-inflammatory signalling via RIP2, MAPK (including ERK1/2 and p38) and NF-κB (including IκBα and p65) signalling. This signalling cascade leads to the activation and translocation of transcription factors (AP-1 and NF-κB), which promote the expression of pro-inflammatory mediators including cytokines (e.g. TNF-α and IL-6) and chemokines (e.g. IL-8) (Chen et al., 2009). Aberrant NOD2 responses have been linked to many chronic inflammatory disorders (Feerick and McKernan, 2017), of which Crohn's disease has been best characterised (Ogura et al., 2001, Hugot et al., 2001). However, the mechanism underlying regulation of NOD2 expression has yet to be elucidated.

The aim of this chapter was to decipher if disruption of epigenetic patterns, including DNA methylation and histone acetylation, could alter THP-1 cell responses to NOD2 stimulation. To investigate if DNA methylation plays a regulatory role in NOD2 pro-inflammatory responses, DNA methylation was pharmacologically disrupted using DNMT1 inhibitors (5-Aza / 5-Aaz-dC). To examine if hyperacetylation alters NOD2 pro-inflammatory responses, cells were treated with a pan-histone deacetylase

inhibitor; suberoylanilide hydroxamic acid (SAHA). The differentiation process of monocytes-to-macrophages has been proven to drastically alter the monocyte epigenome (Wallner et al., 2016). Therefore, it was important to examine how this altered epigenome modifies responses to NOD2 stimulation. THP-1 monocytic cells were differentiated using phorbal myristate acetate (PMA), after which NOD2 activity, signalling and expression.

In this chapter it was hypothesised that NOD2 receptor activity and expression are regulated, in THP-1 monocytic cells, by epigenetic modifications and differentiation.

6.2 Methods

The methods used in this chapter did not differ in any way from those outlined in chapter 2.

6.3 Experimental Design

These experiments were designed to investigate if reduced DNA methylation or enhanced histone acetylation patterns altered NOD2 receptor activity, signalling and expression. THP-1 cells were primed with epigenetic modifying agents that are known to disrupt either DNA methylation (5-Aza/5-Aza-dC) or histone acetylation (SAHA). THP-1 cells were differentiated into macrophage-like cells using PMA.

NOD2 pro-inflammatory activity, signalling and basal expression was investigated in these primed or differentiated cells, relative to untreated cells. NOD2 pro-inflammatory activity was analysed by stimulating the primed cells with a NOD2 ligand for 6/18hours, after which pro-inflammatory cytokine (TNF-α and IL-6) expression and chemokine (IL-8) release were quantified by qPCR and ELISA, respectively. NOD1 pro-inflammatory signalling was investigated by measuring RIP2, MAPK and NF-κB protein phosphorylation after stimulating primed THP-1 cells with a NOD2 ligands for two hours, via western blotting. NOD2 basal expression was quantified in treated vs untreated cells at the mRNA and protein levels by qPCR and western blotting, respectively. All experiments were carried out with at least three independent biological replicates ($n \geq 3$). An overview of the experimental design is presented in Figure 6.1, with a more detailed breakdown outlined in the experimental design index (Table 6.1).

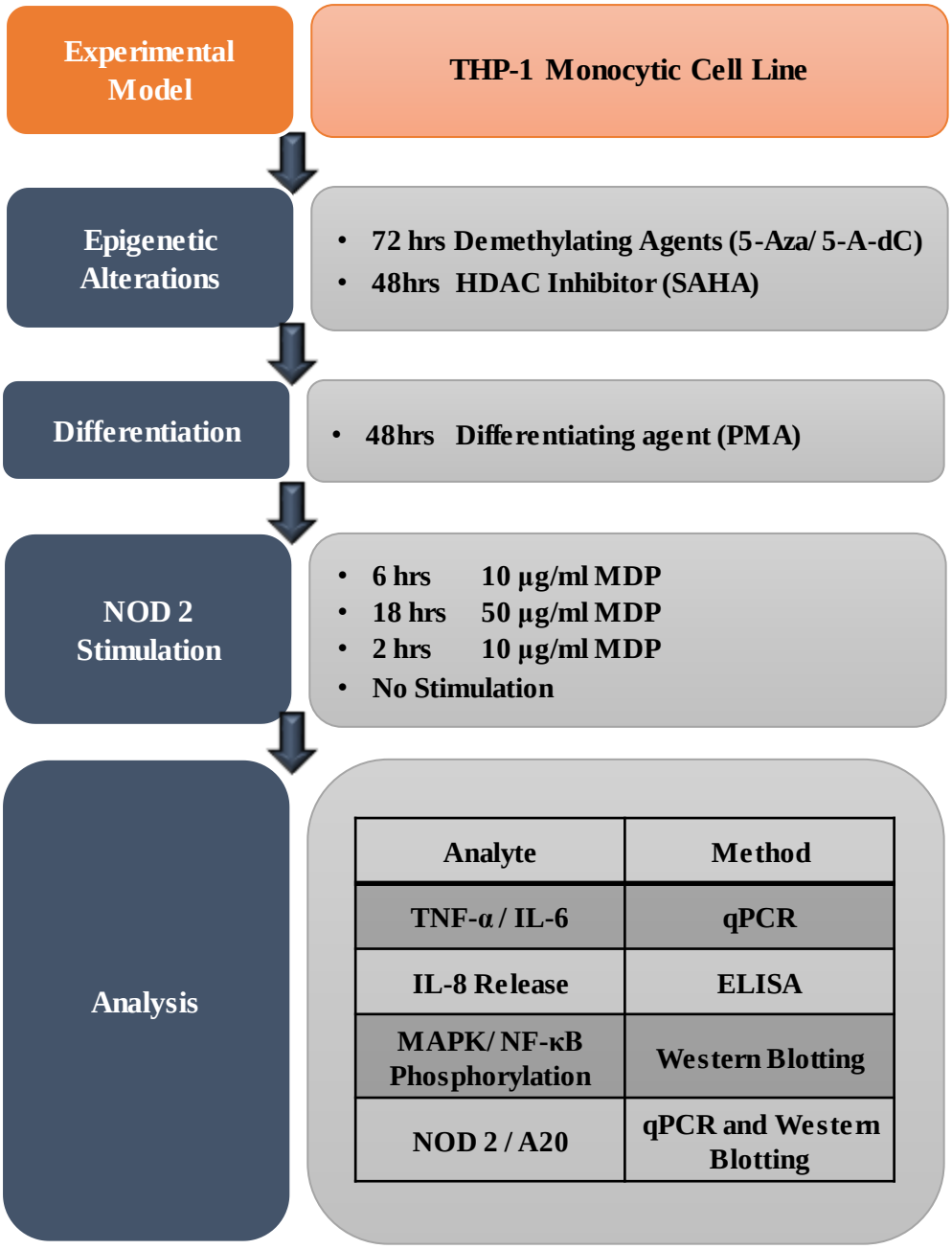

Figure 6.1. Chapter 6 Experimental Design. Outline of epigenetic treatments, NOD 2 stimulation and analysis.

Table 6.1: Chapter 6 Experimental Design Index. Breakdown of treatments, analytes and analysis methods for investigating NOD2 activity, signalling and expression in THP-1 monocytic cell line.

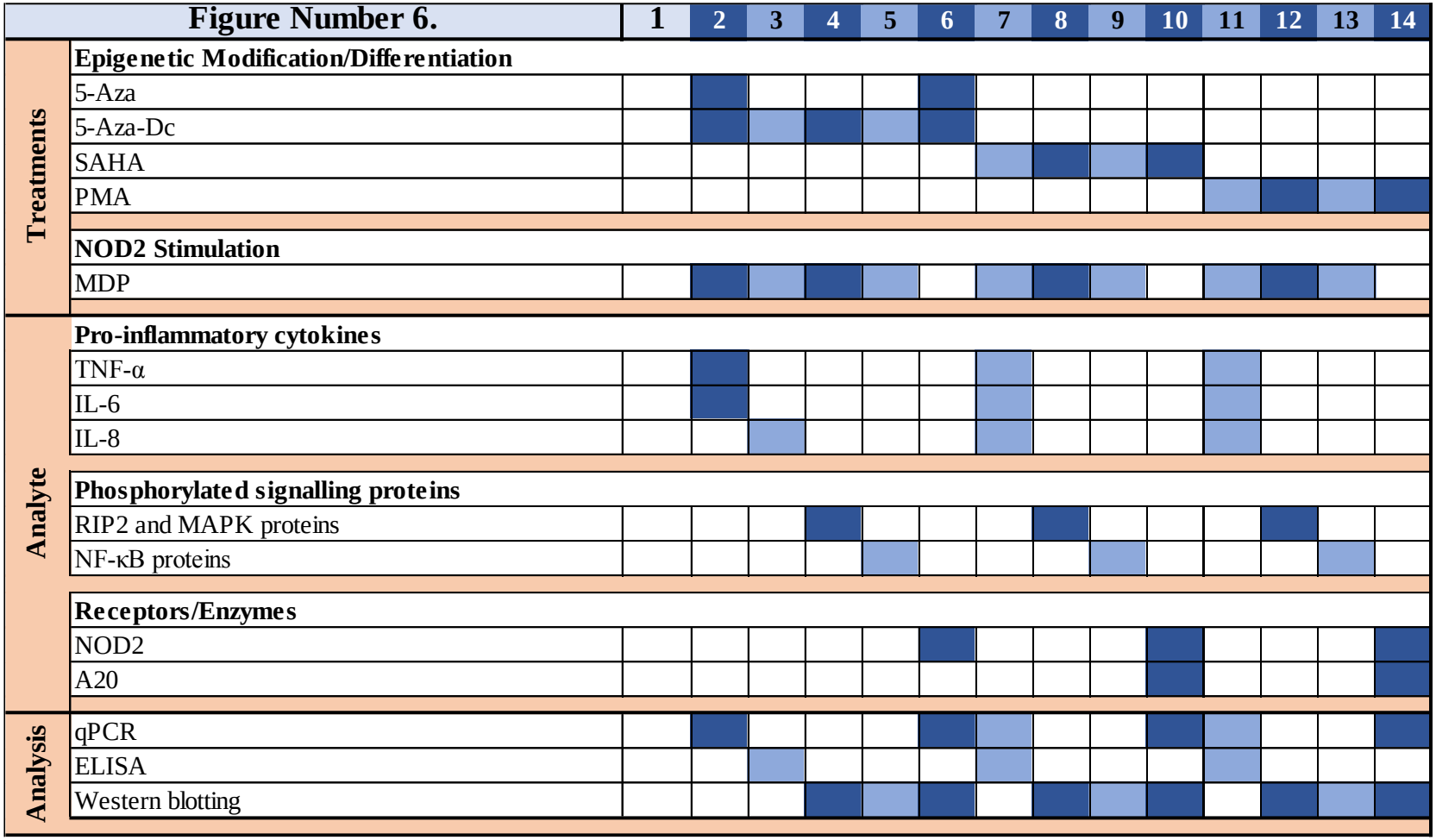

6.4 Results

6.4.1 DNMT1 inhibitor priming increases NOD2-induced pro-inflammatory activity in THP-1 cells.

To investigate if disruption of DNA methylation patterns alters how THP-1 monocytic cells respond to NOD2 stimulation, cells were primed with a known demethylating agent prior to NOD2 stimulation. THP-1 cells were treated with a DNA methyltransferase 1 inhibitor, 5 μM 5-Azacytidine (5-Aza) or 500 nM 5-Aza-2'-deoxycytidine (5-Aza-dC), for 72 hours. Following exposure to one of these known demethylating agents, cells were stimulated with MDP, a NOD2 ligand, for an additional 6 or 18 hours. The effects of DNA methylation disruption on NOD2-induced pro-inflammatory activity were examined by quantifying pro-inflammatory cytokine (TNF-α and IL-6) expression by qPCR and chemokine (IL-8) release by ELISA. The "Untreated + None" treatment group, acted as the control group. Pro-inflammatory cytokine expression was calculated relative to this control.

The effects of 5-Aza treatment on NOD2 pro-inflammatory activity was examined first. TNF-α and IL-6 mRNA expression was increased significantly in THP-1 cells stimulated with MDP by 5.2-fold ($p < 0.001$) and 2.4-fold ($p < 0.01$), respectively. Relative to the untreated control group, 5-Aza-priming increased MDP-induced TNF-α from 5.2-fold to 7.1-fold ($p < 0.001$, relative to untreated + MDP) and IL-6 from 2.4-fold to 10.2-fold ($p < 0.001$, relative to untreated + MDP), as depicted in Figure 6.2 A-B. A similar pattern of events was recorded in 5-Aza-dC-primed THP-1 cells, but to a greater magnitude. Stimulation with MDP alone increased expression of TNF-α (4.4-fold, $p < 0.01$) and IL-6 (7.3-fold, $p < 0.05$). Relative to the untreated control group, priming with 5-Aza-Dc exacerbated MDP-induced TNF-α from 4.4-fold to 13.3-fold ($p < 0.001$, relative to untreated + MDP) and IL-6 from 7.3-fold to 26.2-fold ($p < 0.001$, relative to untreated + MDP), as depicted in Figure 6.2 C-D.

Response patterns of THP-1 cells to 5-Aza were also observed with 5-Aza-dC, but to a higher magnitude. Therefore, the remaining methylation-related experiments presented in this chapter will only investigate effects of 5-Aza-dC priming.

To further investigate effects on NOD2 activity, pro-inflammatory cytokine/chemokine release was analysed by ELISA. TNF-α and IL-6 protein release from THP-1 cells was undetectable. Therefore, focus shifted to IL-8 release from THP-1 cells. Time and dose response was investigated to identify an appropriate ligand concentration and stimulation duration for IL-8 detection (Appendix 4). Analysis revealed that stimulation of THP-1 cells with 50 μg/ml MDP for 18 hours is optimum. Basal IL-8 release from THP-1 cells (33.7 ± 1.8 pg/ml) increased approximately 4-fold to 113.3 ± 2 pg/ml ($p < 0.001$) in response to MDP stimulation. Priming with 5-Aza-Dc slightly increased MDP-induced IL-8 release from 113.3 ± 2 pg/ml to 121.3 ± 7.2 pg/ml ($p > 0.05$, relative to untreated + MDP), as shown in Figure 6.3.

Together the qPCR and ELISA data presented here suggest that priming with a known demethylating agent enhances pro-inflammatory responses to NOD2 stimulation.

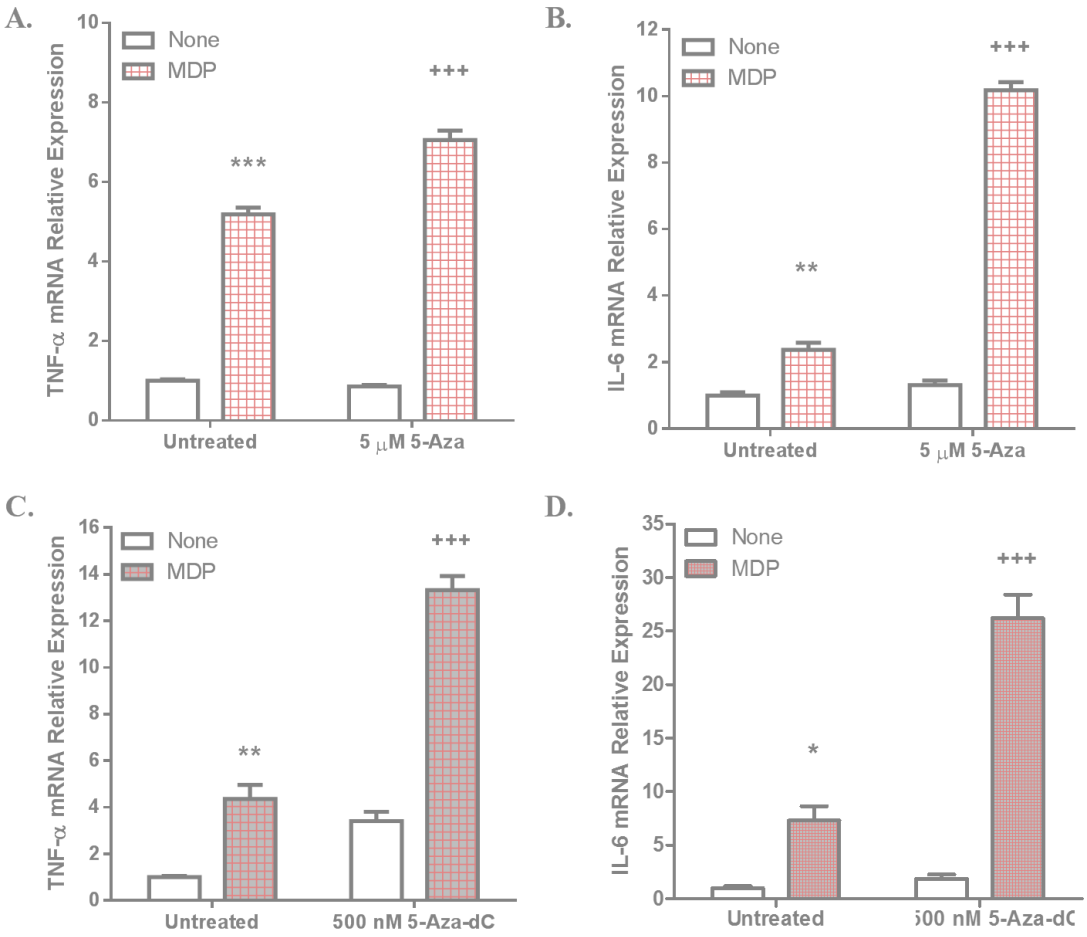

Figure 6.2: NOD2-induced pro-inflammatory cytokine expression in 5-Aza or 5-Aza-dC primed THP-1 cells. A-B) TNF-α and IL-6 mRNA relative expression in THP-1 cells primed with 5 μM 5-Aza for 72 hours and subsequently stimulated with 10 μg/ml MDP for 6 hours. C-D) TNF-α and IL-6 mRNA relative expression in HCT116 cells primed with 500 nM 5-Aza-dC for 72 hours and subsequently stimulated with 10 μg/ml MDP for 6 hours. β-Actin acted as the housekeeping control. "Untreated + None" was set as the control group. Data is represented as mean relative expression ± S.E.M. Statistical analysis was performed using two-way ANOVAs, followed by Bonferroni *post-hoc* test where appropriate. ***** $p < 0.05$ representing **control vs NOD2**, **#** $p < 0.05$ representing **control vs primed**, **+** $p < 0.05$ representing **NOD2 vs (primed + NOD1).**

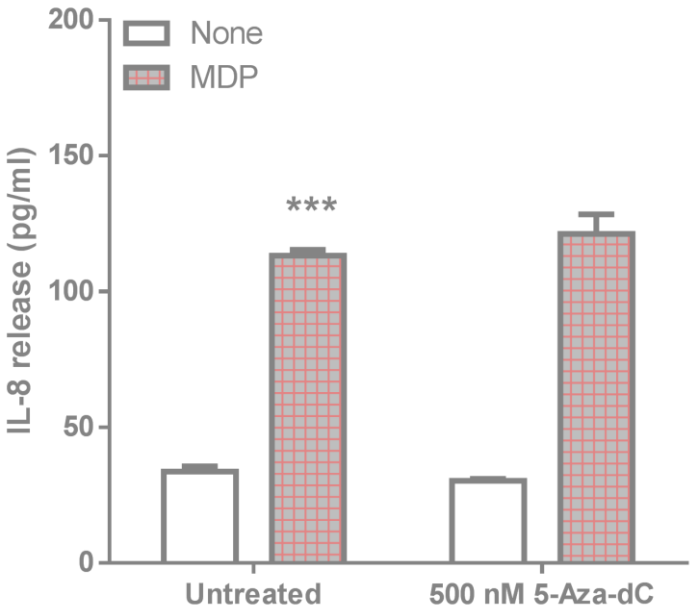

Figure 6.3. NOD2-induced pro-inflammatory IL-8 release from 5-Aza-dC primed THP-1 cells. IL-8 release (pg/ml) from THP-1 cells primed with 500 nM 5-Aza-dC for 72 hours was recorded following stimulation with 50 μg/ml MDP for 18 hours. Data is represented as mean absolute concentration ± S.E.M. Statistical analysis was performed using two-way ANOVAs, followed by Bonferroni *post-hoc* test where appropriate. ***** $p < 0.05$ representing **control vs NOD2**, **#** $p < 0.05$ representing **control vs primed**, **+** $p < 0.05$ representing **NOD2 vs (primed + NOD2).**

6.4.2 DNMT1 inhibitor priming increases NOD2-induced pro-inflammatory RIP2 and MAPK signalling in THP-1 cells.

Since priming with a DNMT1 inhibitor was found to enhance pro-inflammatory activity, as represented by increases in TNF-α/IL-6 expression and IL-8 release, the effect of priming on NOD2-induced pro-inflammatory signalling was next examined. Stimulation of the NOD2 receptor triggers the phosphorylation, and thus activation of the RIP2 adapter, MAPK and NF-κB proteins. NOD2-induced phosphorylation of RIP2 and MAPK proteins in 5-Aza-dC primed THP-1 cells was first investigated. Phosphorylation time responses were carried out to select the most appropriate NOD2 stimulation duration (Appendix 6). Based on this investigation, it was decided that cells should be stimulated with 10 μg/ml MDP for two hours. Phosphorylation of the NOD2 adapter protein (RIP2) and MAPK signalling proteins (ERK2 and p38) was investigated by western blot analysis. Blots were repeated for three independent experiments ($n = 3$), with representative blots shown. Protein expression was quantified by densitometry of phosphorylated, total and housekeeping proteins. Phosphorylated protein expression was normalised relative to their total proteins, and subsequently calculated relative to the untreated control group.

Stimulation of THP-1 cells with MDP alone significantly increased expression of p-RIP2 (3.5-fold, $p < 0.001$), p-ERK2 (2.8-fold, $p < 0.001$) and p-p38 (2.3-fold, $p < 0.001$). Relative to the untreated control group, priming with 5-Aza-Dc exacerbated MDP-induced p-RIP2 from 3.5-fold to 5.6-fold ($p < 0.001$, relative to untreated + MDP), p-ERK2 from 2.8-fold to 2.9-fold ($p > 0.05$, relative to untreated + MDP), and p-p38 from 2.3-fold to 3.3-fold ($p < 0.001$, relative to untreated + MDP), as outlined in Figure 6.4.

These findings suggest that priming with a known demethylating agent increases NOD2 pro-inflammatory signalling in THP-1 cells.

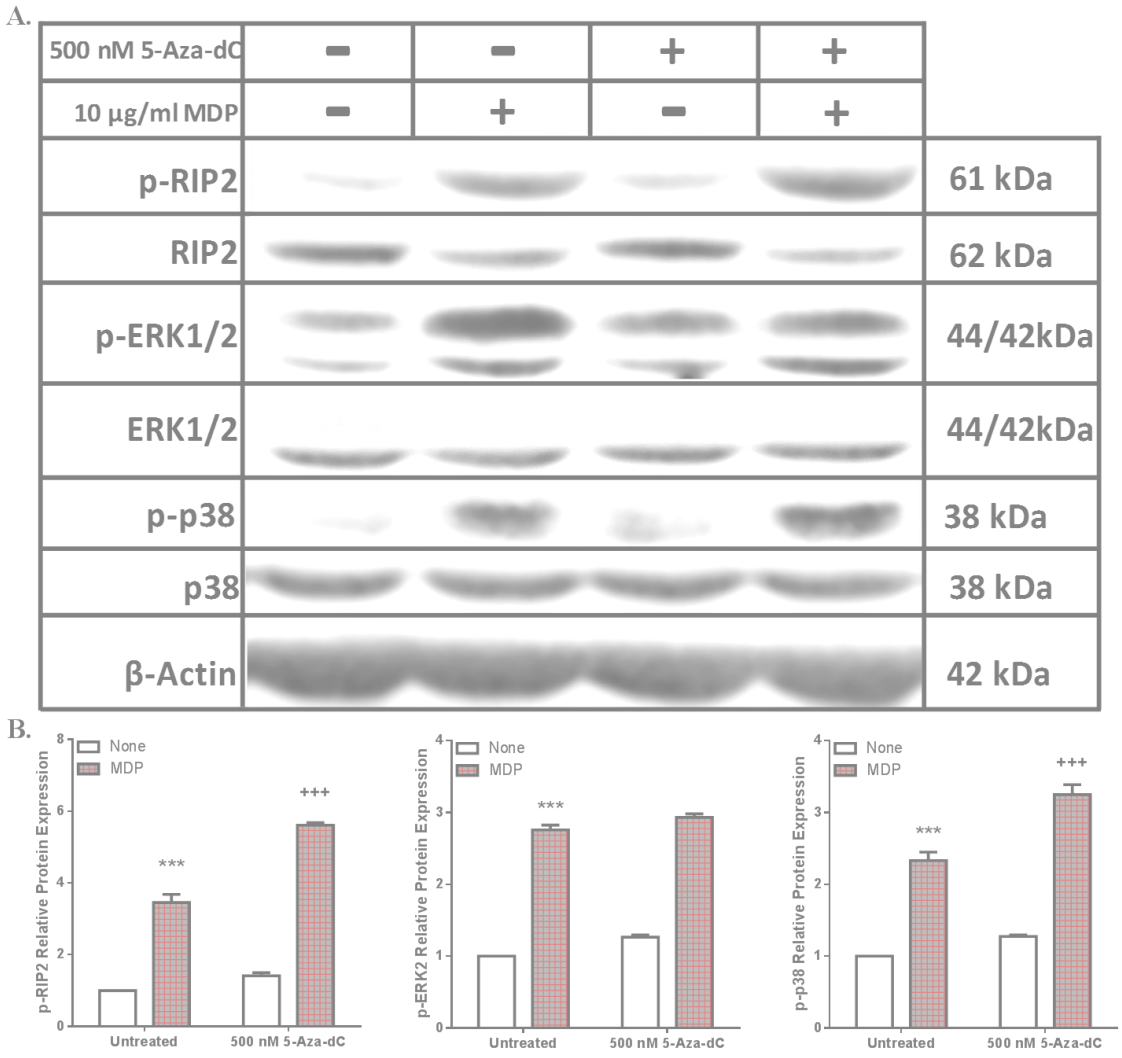

Figure 6.4. MDP-induced RIP2 and MAPK signalling in 5-Aza-dC primed THP-1 cells. (A) Immunoblots of phosphorylated and total RIP2, ERK1/2 and p38 in 5-Aza-dC primed cells stimulated with 10 µg/ml MDP for two hours. β-Actin acted as the loading control. B) Densitometry of phosphorylated RIP2, ERK1/2 and p38 expression, relative to total protein expression. "Untreated + None" was set as the control group. Data is represented as mean relative expression ± S.E.M. and analysed using two-way ANOVAs (followed by Bonferroni's *post-hoc* test). ***** $p < 0.05$ representing **control vs NOD2**, **#** $p < 0.05$ representing **control vs priming, +** $p < 0.05$ representing **NOD2 vs (priming + NOD2).**

6.4.3 DNMT1 inhibitor priming increases NOD2-induced pro-inflammatory NF-κB signalling in THP-1 cells.

To conclude the investigation of 5-Aza-dC priming on NOD2-induced signalling, its effects on NF-κB signalling were examined next. This involved measuring phosphorylation levels of p65 and IκBα in the absence or presence of 5-Aza-dC priming. The duration of 10 μg/ml MDP stimulation required to investigate NF-κB signalling was chosen based on the time response analysis, as outlined in Appendix 6. The same time point chosen matched that used to analyse RIP2 and MAPK signalling; MDP for two hours. Phosphorylation of the p65 and IκBα was investigated by western blot analysis. Blots were repeated for three independent experiments (n = 3), with representative blots shown. Protein expression was quantified by densitometry of phosphorylated, total and housekeeping proteins. Phosphorylated protein expression was normalised relative to the chosen loading control; β-Actin, and subsequently calculated relative to the untreated control group.

Stimulation of THP-1 cells with MDP alone significantly increased phosphorylation of NF-κB proteins; increasing p-p65 by 1.6-fold ($p < 0.05$) and p-IκBα by 2.9-fold ($p < 0.001$). These effects were exacerbated by 5-Aza-dC priming. Relative to the untreated control group, priming with 5-Aza-Dc increased MDP-induced p-p65 from 1.6-fold to 6-fold ($p < 0.001$, relative to untreated + MDP) and p-IκBα from 2.9-fold to 4.6-fold ($p < 0.001$, relative to untreated + MDP), as depicted in Figure 6.5.

The enhanced NF-κB signalling recorded here supports the RIP2 and MAPK data in the previous section. Together, these data suggest that treatment with a demethylating agent enhances NOD2 pro-inflammatory signalling in THP-1 cells.

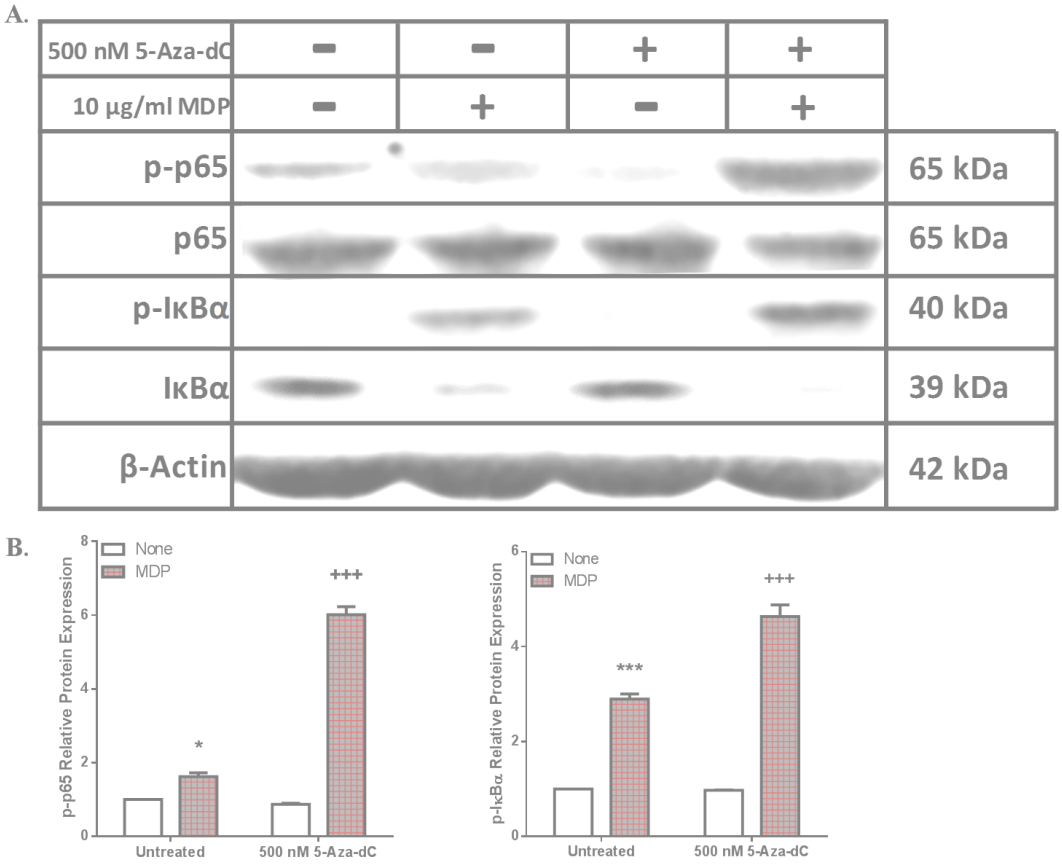

Figure 6.5. MDP-induced NF-κB signalling in 5-Aza-dC primed THP-1 cells. (A) Immunoblots of phosphorylated and total p65 and IκBα in cells primed with 500 nM 5-Aza-dC for 72 hours and subsequently stimulated with 10 µg/ml MDP for two hours. β- Actin acted as the loading control. (B) Densitometry of phosphorylated p65 and IκBα expression, relative to β-Actin expression. "Untreated + None" was set as the control group. Data is represented as mean relative expression ± S.E.M. and analysed using two-way ANOVAs (followed by Bonferroni's *post-hoc* test). ***** $p < 0.05$ representing **control vs NOD2**, **#** $p < 0.05$ representing **control vs primed**, **+** $p < 0.05$ representing **NOD2 vs (primed + NOD2).**

6.4.4 DNMT1 inhibitor treatment increases NOD2 basal expression in THP-1 cells.

Since 5-Aza and 5-Aza-dC priming was found to increase responses to NOD2 receptor activation, we next asked the question; Are these demethylating agents inducing this response by directly altering NOD2 expression? This was investigated by quantifying NOD2 expression at the mRNA and protein levels via qPCR and western blot analysis. Independent t-test analysis revealed significant increases in NOD2 expression (Figure 6.6).

THP-1 cells treated with 5 μM 5-Aza for 72 hours exhibited a significant increase in NOD2 mRNA (2-fold, $p < 0.001$) and protein (3.4-fold, $p < 0.01$) expression (Figure 6.6 A, C and E). Treatment with 500 nM 5-Aza-dC for 72 hours displayed a similar effect on NOD2 expression, but to a greater magnitude. This more efficient demethylating agent significantly increased NOD2 expression at the mRNA (4-fold, $p < 0.001$) and protein (4.2-fold, $p < 0.01$) levels (Figure 6.6 B, D and F)

This implies that the demethylating agents are increasing NOD2 expression in THP-1 cells, potentially explaining the augmented pro-inflammatory activity and signalling recorded in our earlier experimentation.

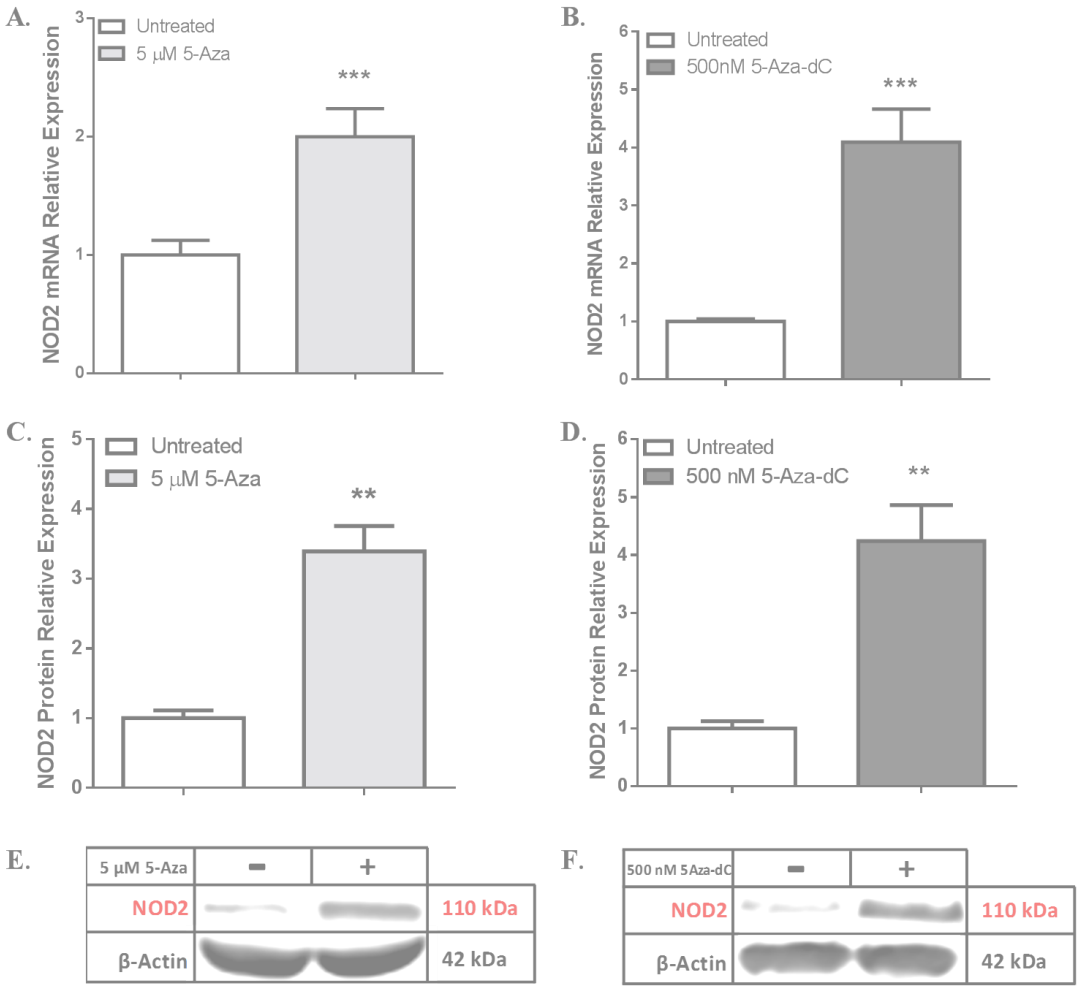

Figure 6.6. NOD2 basal expression in THP-1 cells following 5-Aza or 5-Aza-dC treatment. (A-B) NOD2 mRNA expression following 5 μM 5-Azacytidine (5-Aza) or 500 nM 5-Aza-2'-deoxycytidine (5-Aza-dC) for 72 hours, relative to β-Actin expression. (C-D) Densitometry of NOD2 protein expression following 5 μM 5-Aza or 500 nM 5-Aza-dC for 72 hours, relative to β-Actin expression. (E-F) Representative immunoblots of NOD2 protein expression following 5 μM 5-Aza or 500 nM 5-Aza-dC for 72 hours, relative to β-Actin expression. Data is represented as mean relative expression ± S.E.M. Statistical analysis was performed using independent t-tests. Significance was recognised at $p < 0.05$, with * representing $p < 0.05$, ** representing $p < 0.01$ and *** representing $p < 0.001$.

6.4.5 HDAC inhibitor priming attenuates NOD2-induced pro-inflammatory cytokine expression but enhances chemokine release from THP-1 cells.

The focus of this chapter shifts to the effects of histone acetylation on NOD2 associated responses. The contribution of this epigenetic modification was investigated using a well-established histone deacetylase inhibitor (HDACi); suberoylanilide hydroxamic acid (SAHA). THP-1 cells were treated with 10 μM SAHA for 48 hours and subsequently stimulated with 10 μg/ml MDP for six hours or 50 μg/ml MDP for 18 hours. The effects of SAHA priming on pro-inflammatory responses to NOD2 stimulation were investigated by quantifying TNF-α / IL-6 expression and IL-8 release by qPCR and ELISA, respectively. The "Untreated + None" treatment group, acted as the treatment control. Pro-inflammatory cytokine expression was calculated relative to this control.

The effect of SAHA-priming on NOD2 pro-inflammatory cytokine expression was investigated first. Stimulation of untreated THP-1 cells with 10 μg/ml MDP for six hours increased TNF-α (4.3-fold, $p < 0.001$) and IL-6 (3.2-fold, $p < 0.05$) mRNA expression. Relative to the untreated control group, priming with SAHA attenuated MDP-induced expression of TNF-α from 4.3-fold to 0.6-fold ($p < 0.001$, relative to untreated + MDP) and IL-6 from 3.2-fold to 1.4-fold ($p < 0.05$, relative to untreated + MDP), as depicted in Figure 6.7 A-B.

To examine NOD2 activity further in SAHA-primed cells, attempts were made to quantify TNF-α and IL-6 release in response to stimulation of untreated and primed cells. However, TNF-α and IL-6 release from THP-1 cells was below the limits of detection, therefore IL-8 release was investigated instead. Basal IL-8 release from THP-1 cells (15.3 ± 0.6 pg/ml) was significantly increased following 18 hours of stimulation with 50 μg/ml MDP (75.2 ± 1.7 pg/ml, $p < 0.001$). Treatment of THP-1 cells with SAHA increased basal levels of IL-8 approximately 10-fold, to 152.7 ± 1.2 pg/ml ($p < 0.001$). Priming with SAHA increased MDP-induced IL-8 release approximately 5-fold, from 75.2 ± 1.7 pg/ml to 408.3 ± 1.9 pg/ml ($p < 0.001$, relative to untreated + MDP), as outlined in Figure 6.7C. The qPCR data suggests decreased NOD2 pro-inflammatory responses following treatment with a HDAC inhibitor. The IL-8 release pattern eludes to NOD2-independent effects by the HDAC inhibitor, but this remains unclear.

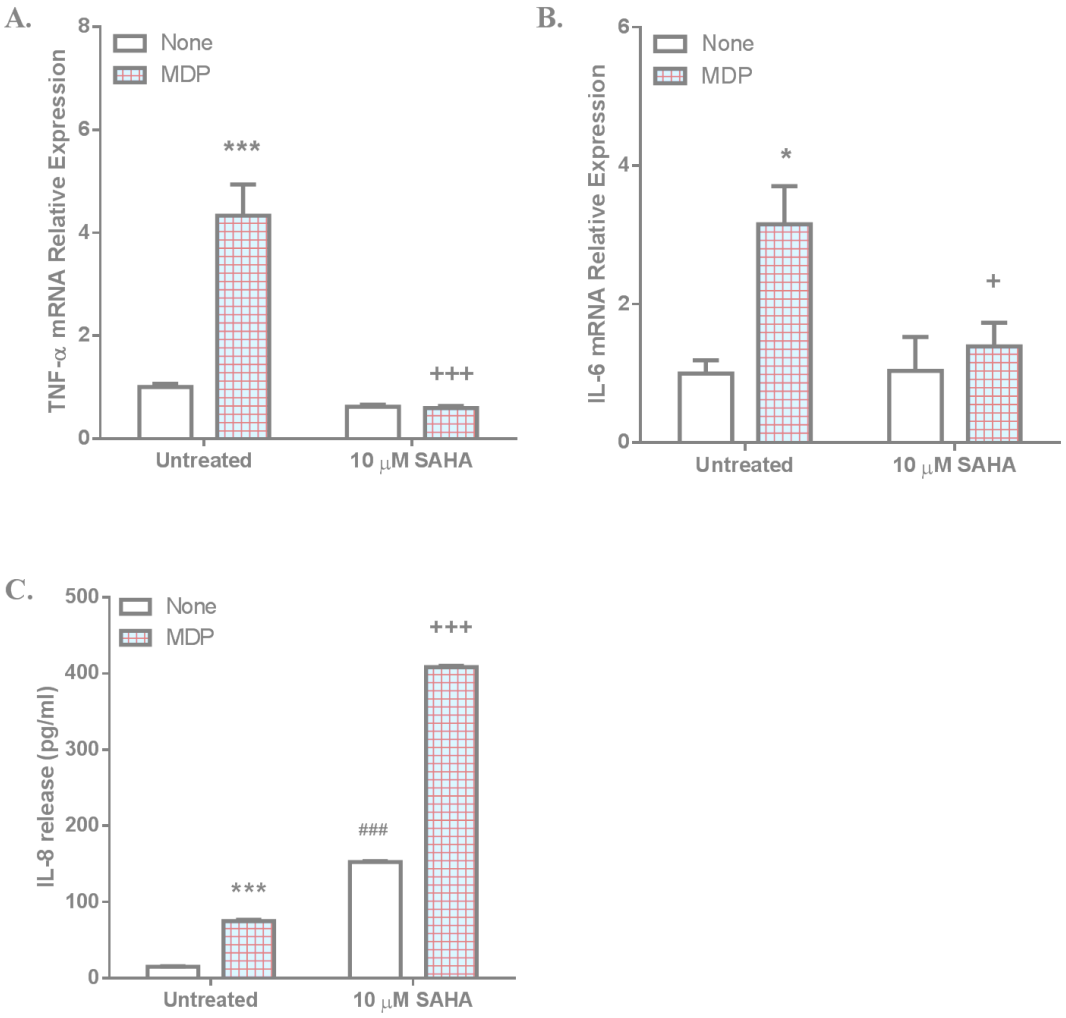

Figure 6.7 NOD2-induced pro-inflammatory activity in SAHA primed THP-1 cells. (A-B) TNF-α and IL-6 mRNA relative expression in THP-1 cells primed with 10 μM SAHA for 48 hours and subsequently simulated with a 10 μg/ml MDP for six hours. RPL13A acted as the housekeeping gene. "Untreated + None" was set as the control group. Data is represented as mean relative expression ± S.E.M. C) IL-8 release from THP-1 cells primed with 10 μM SAHA for 48 hours and stimulated with 50 μg/ml MDP for 18 hours. Data is represented as mean absolute values ± S.E.M. Statistical analysis was performed using two-way ANOVAs, followed by Bonferroni *post-hoc* test where appropriate. ***** $p < 0.05$ representing **control vs NOD2**, **#** $p < 0.05$ representing **control vs primed**, **+** representing $p < 0.05$ **NOD2 vs (primed + NOD2).**

6.4.6 HDAC inhibitor priming increases NOD2-induced RIP2 activation but attenuates MAPK signalling in THP-1 cells.

To further examine the effects of SAHA-priming on NOD2 pro-inflammatory responses in THP-1 cells, RIP2 and MAPK signalling activation was quantified in the absence and presence of SAHA. Phosphorylation time responses were carried out to select the most appropriate NOD2 stimulation duration (Appendix 6). Based on this investigation, it was decided that cells should be stimulated with 10 μg/ml MDP for two hours. Phosphorylation of the NOD2 adapter protein (RIP2) and MAPK signalling proteins (ERK2 and p38) was investigated by western blot analysis. Blots were repeated for three independent experiments (n = 3), with representative blots shown. Protein expression was quantified by densitometry of phosphorylated, total and housekeeping proteins. Phosphorylated protein expression was normalised relative to the loading control (β-Tubulin), since SAHA appeared to have a direct effect on total proteins, and subsequently calculated relative to the untreated control group.

NOD2 stimulation with MDP increased phosphorylation of ERK2 (1.3-fold, $p < 0.05$) and p38 (2.3-fold, $p < 0.001$) in THP-1 cells. SAHA-treatment significantly enhanced basal p-RIP2 (4.3-fold, $p < 0.001$), but attenuated p-ERK2 (0.3-fold, $p < 0.001$) and p-p38 (0.5-fold, $p < 0.001$). Relative to the untreated control group, priming with SAHA increased MDP-induced p-RIP2 from 1.3-fold to 4.3-fold ($p < 0.001$, relative to untreated + MDP) but reduced p-ERK from 1.3-fold to 0.2-fold ($p < 0.001$, relative to untreated + MDP) and p-p38 from 2.3-fold to 0.8-fold ($p < 0.001$, relative to untreated + MDP), as outlined in Figure 6.8.

Together, these findings suggest that treatment with a HDAC inhibitor has mixed effects on NOD1 associated pro-inflammatory signalling, increasing RIP2 activation but reducing MAPK activation.

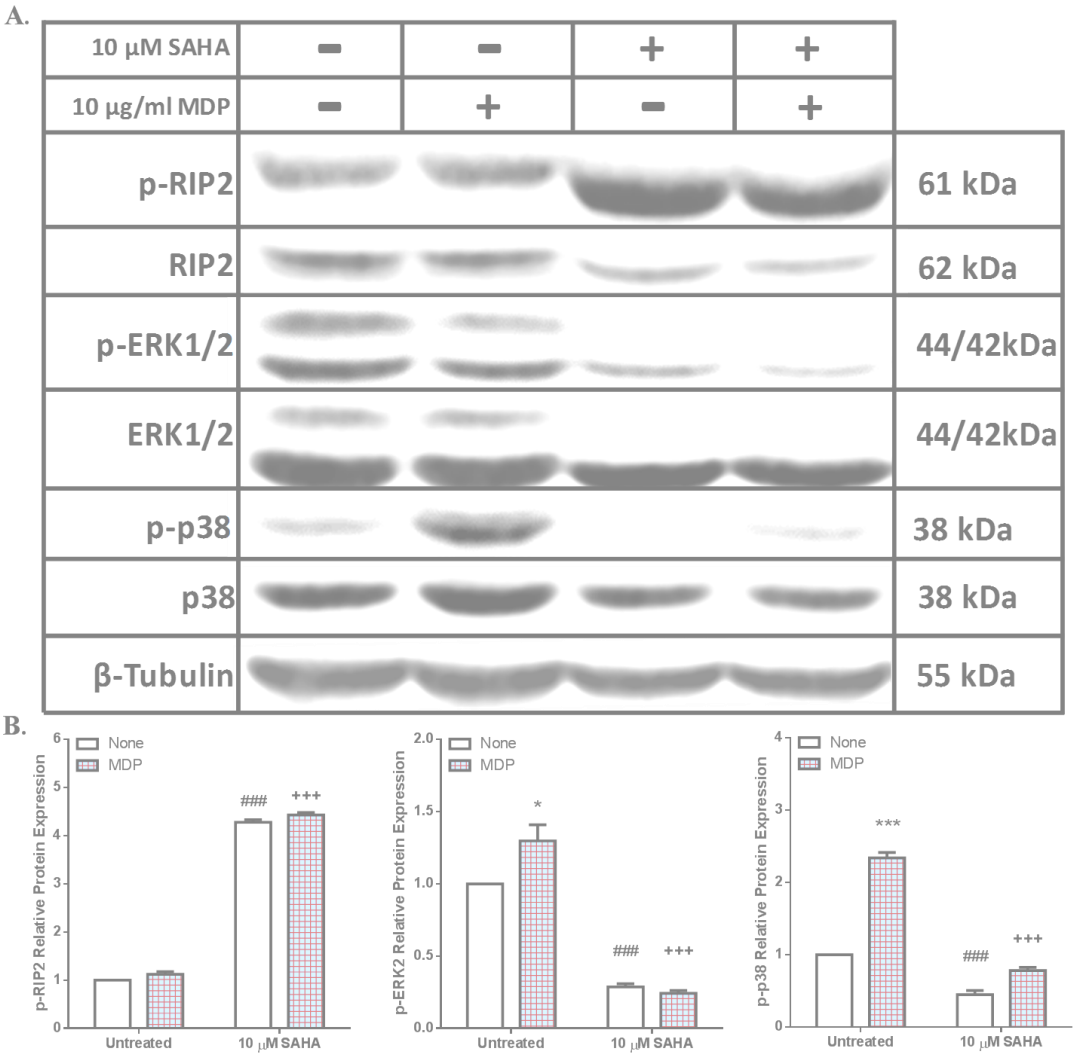

Figure 6.8. MDP-induced RIP2 and MAPK signalling in SAHA-primed THP-1 cells. A) Immunoblots of phosphorylated and total RIP2, p38 and ERK1/2 in cells primed with 10 µM SAHA for 48 hours and subsequently stimulated with MDP (10 µg/ml) for two hours. β-Tubulin acted as the loading control. B) Densitometry of phosphorylated RIP2, p38 and ERK2 expression, relative to β-Tubulin expression. "Untreated + None" was set as the control group. Data is represented as mean relative expression ± S.E.M. and analysed using two-way ANOVAs (followed by Bonferroni's *post-hoc* test). ***** $p < 0.05$ representing **control vs NOD2**, **#** $p < 0.05$ representing **control vs primed**, **+** $p < 0.05$ representing **NOD2 vs (primed + NOD2).**

6.4.7 HDAC inhibitor priming attenuates NOD2-induced NF-κB signalling in THP-1 cells.

To complete the investigation of SAHA priming on NOD2 associated pro-inflammatory signalling, phosphorylation of NF-κB proteins (p65 and IκBα) in its absence and presence was investigated next. The duration of 10 μg/ml MDP stimulation required to investigate NF-κB signalling was chosen based on the time response analysis, as outlined in Appendix 6. The same time point chosen matched that used to analyse RIP2 and MAPK signalling; MDP for two hours. Phosphorylation of the p65 and IκBα was investigated by western blot analysis. Blots were repeated for three independent experiments (n = 3), with representative blots shown. Protein expression was quantified by densitometry of phosphorylated, total and housekeeping proteins. Phosphorylated protein expression was normalised relative to the chosen loading control; β-Tubulin, and subsequently calculated relative to the untreated control group.

Stimulation of THP-1 cells with MDP significantly enhanced NF-κB signalling, represented by increases in p-p65 (4.2-fold, $p < 0.001$) and p-IκBα (3.5-fold, $p < 0.001$). SAHA treatment had differing effects on NF-κB proteins, increasing p-p65 (2-fold, $p < 0.01$) but reducing p-IκBα (0.9-fold, $p > 0.05$). Relative to the untreated control group, priming with SAHA increased MDP-induced p-p65 from 4.2-fold to 5-fold ($p < 0.05$, relative to untreated + MDP) but reduced p- IκBα from 3.5-fold to 1-fold ($p < 0.001$, relative to untreated + MDP), as shown in Figure 6.9.

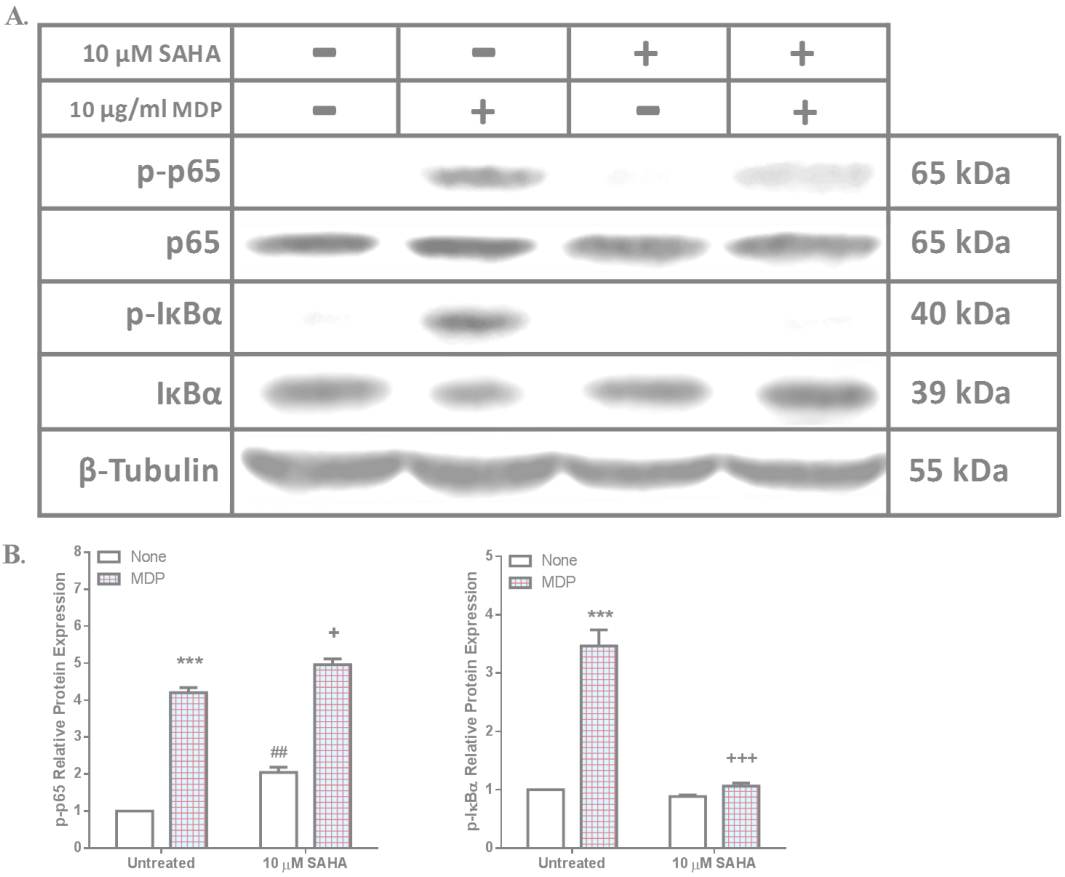

Figure 6.9. MDP-induced NF-κB signalling in SAHA-primed THP-1 cells. (A) Immunoblots of phosphorylated and total p65 and IκBα in cells primed with 10 µM SAHA for 48 hours and subsequently stimulated with 10 µg/ml MDP for two hours. β- Tubulin acted as the loading control. (B) Densitometry of phosphorylated p65 and IκBα expression, relative to β-Tubulin expression. "Untreated + None" was set as the control group. Data is represented as mean relative expression ± S.E.M. and analysed using two-way ANOVAs (followed by Bonferroni's *post-hoc* test). ***** $p < 0.05$ representing **control vs NOD2**, **#** $p < 0.05$ representing **control vs primed**, **+** $p < 0.05$ representing **NOD2 vs (primed + NOD2).**

6.4.8 HDAC inhibitor treatment increases NOD2 protein expression in THP-1 cells.

To explore the underlying mechanism behind the effects of SAHA on NOD2 activity and signalling in THP-1 cells, NOD2 expression was quantified following SAHA treatment. THP-1 cells were treated with 10 μM SAHA for 48 hours, after which NOD2 mRNA and protein expression were quantified by qPCR and western blotting, respectively. NOD2 expression was quantified relative to the chosen housekeeping gene; β-Tubulin. Following treatment with SAHA, NOD2 mRNA expression significantly decreased 0.1-fold ($p < 0.001$) (Figure 6.10 A). However, NOD2 protein expression was increased by SAHA (1.6-fold, $p < 0.01$) (Figure 6.10 B-C). These conflicting results regarding NOD2 expression may be a result of differences in stability. NOD2 expression data was conflicting between mRNA and protein levels. Expression of the NOD2 negative regulator; A20, was also investigated by western blotting. SAHA was found to significantly reduce A20 expression by 0.5-fold ($p < 0.001$), as depicted in Figure 6.10 D-E).

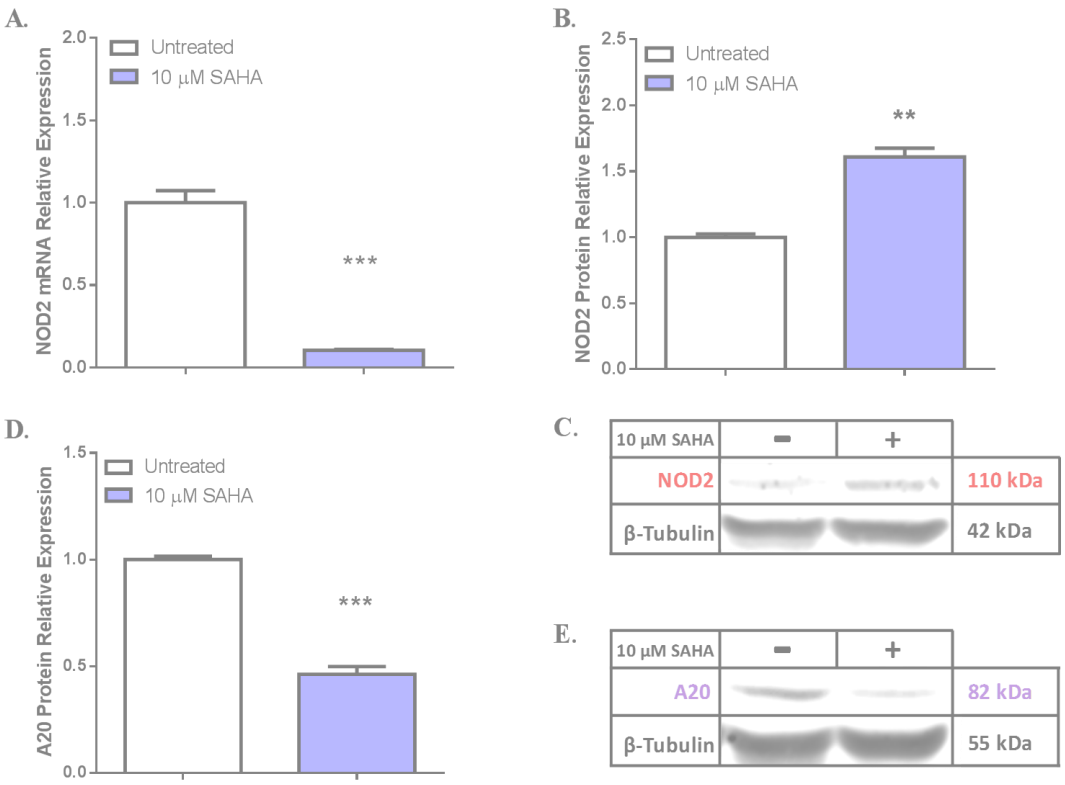

Figure 6.10. NOD2 and A20 basal expression in SAHA treated THP-1 cells. (A) NOD2 mRNA expression in THP-1 cells treated with 10 μM SAHA for 48 hours, relative to β-Tubulin expression. (B) Densitometry of NOD2 protein expression in SAHA treated cells, relative to β-Tubulin expression. (C) Representative immunoblot of NOD2 protein expression in SAHA treated cells. (D) Densitometry of A20 protein expression in SAHA treated cells, relative to β-Tubulin expression. (E) Representative immunoblot of A20 protein expression in SAHA treated cells. Data is represented as mean relative expression ± S.E.M. Statistical analysis was performed using independent t-tests. Significance was recognised at $p < 0.05$, with * representing $p < 0.05$, ** representing $p < 0.01$ and *** representing $p < 0.001$.

6.4.9 Differentiation of THP-1 cells attenuates NOD2-induced pro-inflammatory activity.

THP-1 cells are immature monocytes; therefore, phorbol 12-myristate 13-acetate (PMA) was used to differentiate these cells into mature macrophage-like cells. This was done to explore whether macrophages respond differently to NOD stimulation. PMA time and dose analysis, carried out in Chapter 5 (section 5.4.9), revealed that 10 ng/ml PMA for 48 hours induced optimum differentiation of THP-1 cells.

Stimulation of THP-1 cells with MDP alone increased expression of TNF-α by 20-fold ($p < 0.001$) and IL-6 by 15.2-fold ($p < 0.001$). Relative to the untreated control group, PMA-driven differentiation reduced MDP-induced TNF-α from 20-fold to 2-fold ($p < 0.001$, relative to untreated + MDP) and IL-6 from 15.5-fold to 4.6-fold ($p < 0.001$, relative to untreated + MDP), as shown in Figure 6.11 A-B.

To examine NOD2 activity further in monocyte-derived macrophages, attempts were made to quantify TNF-α and IL-6 release in response to stimulation of untreated and PMA-primed cells. However, TNF-α and IL-6 release from THP-1 cells was below the limits of detection, therefore IL-8 release was investigated instead. Basal IL-8 release from THP-1 cells (17 ± 0.8 pg/ml) increased approximately 5-fold (80.8 ± 2.4 pg/ml, $p < 0.01$) following 18 hours of stimulation with 50 μg/ml MDP. PMA treatment alone significantly increased basal IL-8 levels to 1351.2 ± 31.6 pg/ml ($p < 0.001$). Relative to the untreated control group, PMA-priming increased MDP-induced IL-8 release approximately 17-fold, from 80.8 ± 2.4 pg/ml to 1390.3 ± 70 pg/ml ($p < 0.001$, relative to untreated + MDP) as depicted in Figure 6.11C.

This data suggests that PMA-driven differentiation of THP-1 cells attenuates pro-inflammatory cytokine expression in response to NOD2 stimulation, as represented by reduced TNF-α and IL-6. However, release of IL-8 was increased in differentiated cells, but were not enhanced further by NOD2 stimulation, implying this increase is due to a NOD2-dependent mechanism. Therefore, differentiation of THP-1 cells appears to attenuate NOD2-induced pro-inflammatory activity.

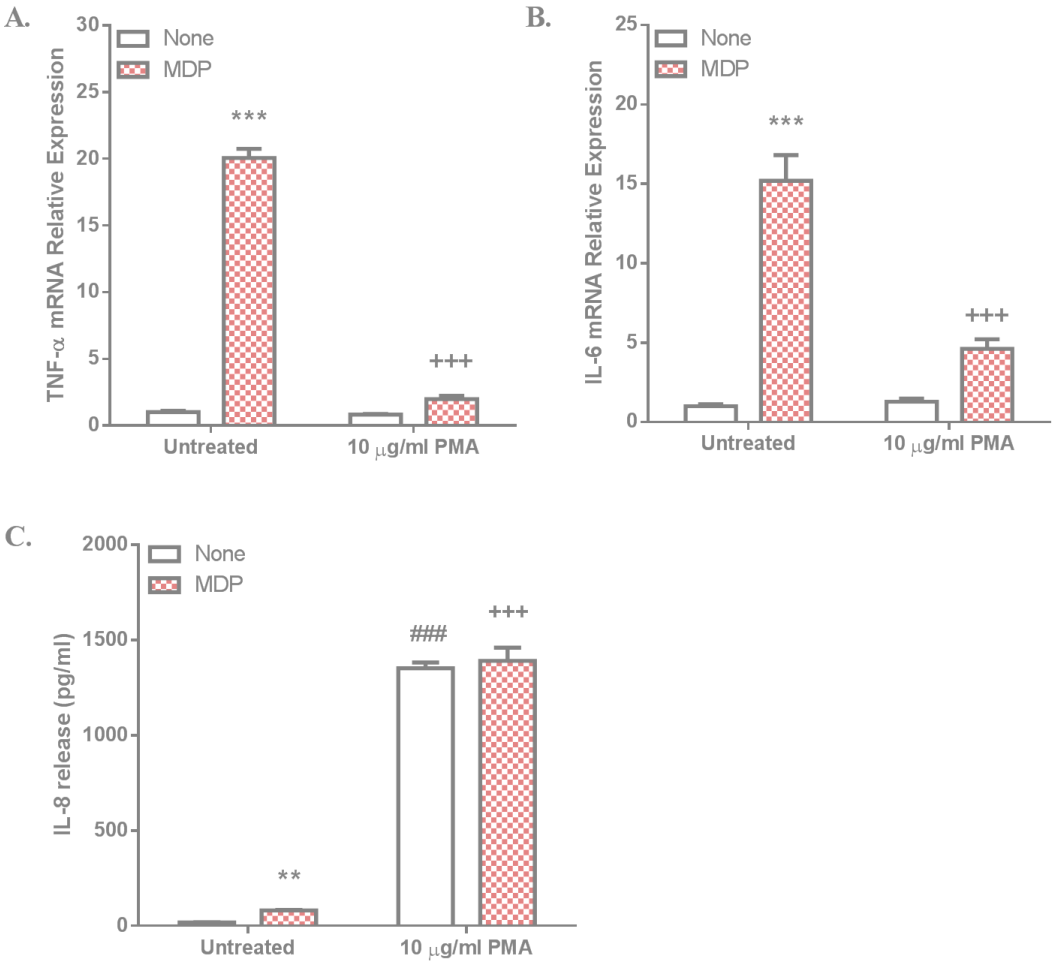

Figure 6.11. NOD2-induced pro-inflammatory activity in differentiated THP-1 cells. (A-B) TNF-α and IL-6 mRNA relative expression in THP-1 cells primed with 10 ng/ml PMA for 48 hours and subsequently simulated with 10 μg/ml MDP for six hours. β-Actin acted as the housekeeping control. "Untreated + None" was set as the control group. Data is represented as mean relative expression ± S.E.M. C) IL-8 release from THP-1 cells primed with 10 ng/ml PMA for 48 hours and stimulated with 50 μg/ml MDP for 18 hours. "Untreated + None" was set as the control group. Data is represented as mean absolute concentration ± S.E.M. Statistical analysis was performed using two-way ANOVAs, followed by Bonferroni *post-hoc* test where appropriate. ***** $p < 0.05$ representing **control vs NOD2**, **#** $p < 0.05$ representing **control vs primed**, **+** $p < 0.05$ representing **NOD2 vs (primed + NOD2).**

6.4.10 Differentiation attenuates NOD2-induced RIP2 and MAPK signalling in THP-1 cells.

To further explore the effects of PMA-induced differentiation on THP-1 responses to NOD2 stimulation, RIP2 and MAPK pro-inflammatory signalling were investigated by western blotting. This involved measuring phosphorylation levels of RIP2, ERK2 and p38 in undifferentiated versus differentiated cells. Following treatment with 10 ng/ml PMA for 48 hours, cells were stimulated with 10 μg/ml MDP. The duration of MDP stimulation required to investigate signalling was chosen based on the THP-1-time response analysis, as outlined in Appendix 6. Based on this analysis the chosen time point for MDP was two hours. Blots were repeated for three independent experiments (n = 3), with representative blots shown. Protein expression was quantified by densitometry of phosphorylated, total and housekeeping proteins. Phosphorylated protein expression was normalised relative to the chosen loading control; β-Actin (since PMA altered total protein expression) and subsequently calculated relative to the untreated control group.

Stimulation of THP-1 cells with MDP increased RIP2 and MAPK signalling, represented by increases in p-RIP2 (2.4-fold, $p < 0.001$), p-ERK2 (1.7-fold, $p < 0.001$) and p-p38 (1.4-fold, $p < 0.001$). PMA-driven differentiation reduced basal levels of these phosphorylated proteins; p-RIP2 (0.2-fold, $p < 0.001$), p-ERK2 (0.5-fold, $p < 0.01$) and p-p38 (0.2-fold, $p < 0.001$). Relative to the untreated control group, PMA-driven differentiation reduced MDP-induced p-RIP2 from 2.4-fold to 0.4-fold ($p < 0.001$, relative to untreated + MDP), p-ERK from 1.7-fold to 0.8-fold ($p < 0.001$, relative to untreated + MDP) and p-p38 from 1.4-fold to 0.4-fold ($p < 0.001$, relative to untreated + MDP), as outlined in Figure 6.12. This data suggests that when monocytes are differentiated into macrophages they become less responsive to NOD2 stimulation, represented by attenuated RIP2 and MAPK signalling.

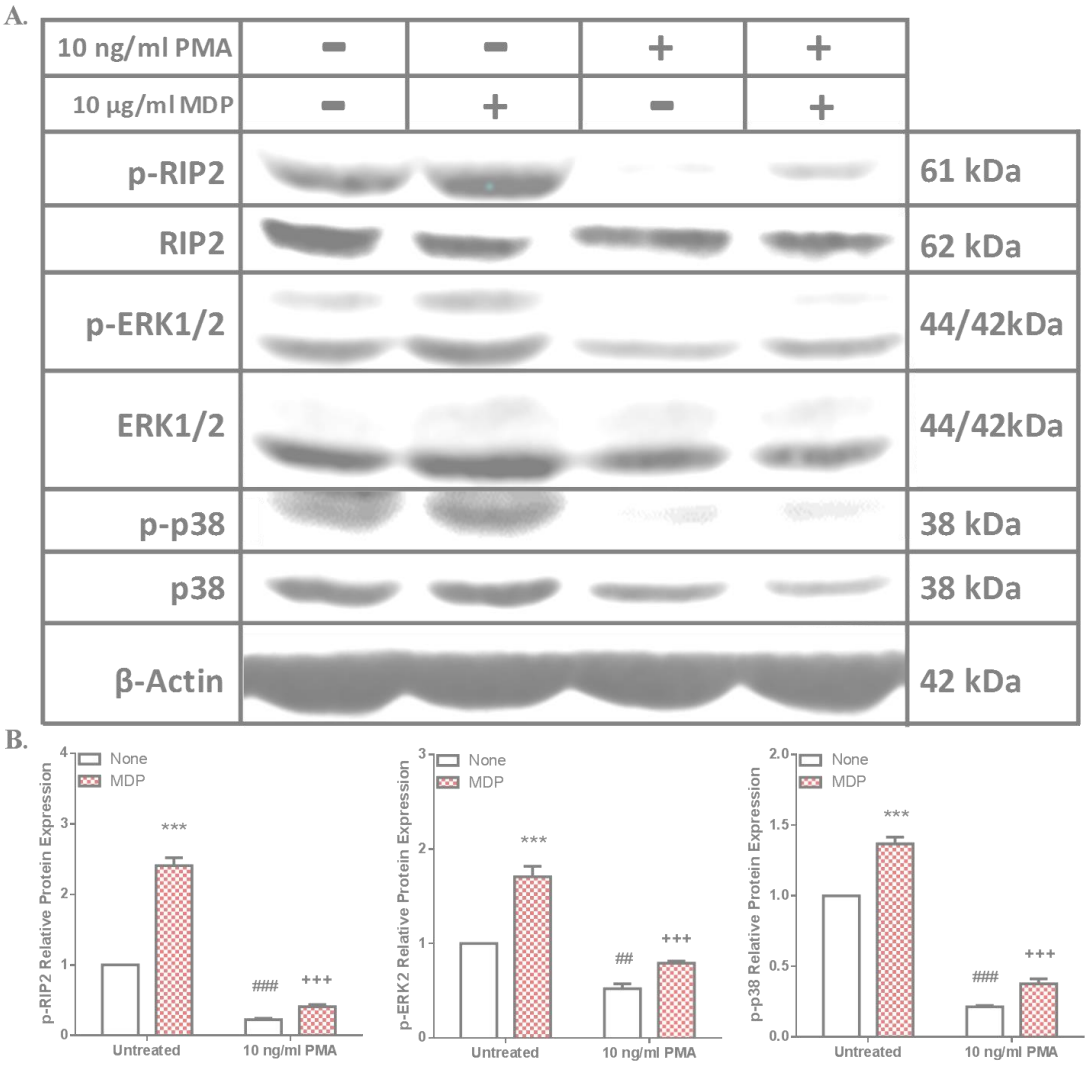

Figure 6.12. MDP-induced RIP2 and MAPK signalling in PMA-primed THP-1 cells. A) Immunoblots of phosphorylated and total RIP2, p38 and ERK1/2 in cells primed with 10 ng/ml for 48 hours and subsequently stimulated with MDP (10 µg/ml) for two hours. β-Actin acted as the loading control. B) Densitometry of phosphorylated RIP2, p38 and ERK2 expression, relative to β-Actin expression. "Untreated + None" was set as the control group. Data is represented as mean relative expression ± S.E.M. and analysed using two-way ANOVAs (followed by Bonferroni's *post-hoc* test). ***** $p < 0.05$ representing **control vs NOD2**, **#** $p < 0.05$ representing **control vs primed**, **+** $p < 0.05$ representing **NOD2 vs (primed + NOD2).**

6.4.11 Differentiation attenuates NOD2-induced NF-κB signalling in THP-1 cells.

To complete the examination of NOD2 signalling in monocyte-derived macrophages relative to their THP-1 counterparts, NF-κB signalling was measured by western blotting. Phosphorylation of p65 and IκBα was expressed relative to the loading control (β-Actin), since PMA has a direct effect on total proteins. The duration of 10 μg/ml MDP stimulation required to investigate NF-κB signalling was chosen based on the time response analysis, as outlined in Appendix 6. The same time point chosen matched that used to analyse RIP2 and MAPK signalling; MDP for two hours. Blots were repeated for three independent experiments, with representative blots shown. Protein expression was quantified by densitometry of phosphorylated, total and housekeeping proteins. Phosphorylated protein expression was normalised relative to the chosen loading control; β-Actin, and subsequently calculated relative to the untreated control group.

Stimulation of THP-1 cells with MDP increased phosphorylation of both p65 and IκBα by 2.7-fold ($p < 0.001$). Differentiation of THP-1 cells with PMA caused a drop in basal p-p65 (0.8-fold, $p > 0.05$) and p-IκBα (0.5-fold, $p < 0.05$). Relative to the untreated control group, PMA-driven differentiation reduced MDP-induced p-p65 from 2.7-fold to 0.6-fold ($p < 0.001$, relative to untreated + MDP), and p-IκBα from 2.7-fold to 0.7-fold ($p < 0.001$, relative to untreated + MDP), as depicted in Figure 6.13.

This reduction in NF-κB signalling, alongside the attenuated RIP2 and MAPK signalling in the previous section, suggest that when monocytes are differentiated into monocyte-derived macrophages they become less responsive to NOD2 stimuli.

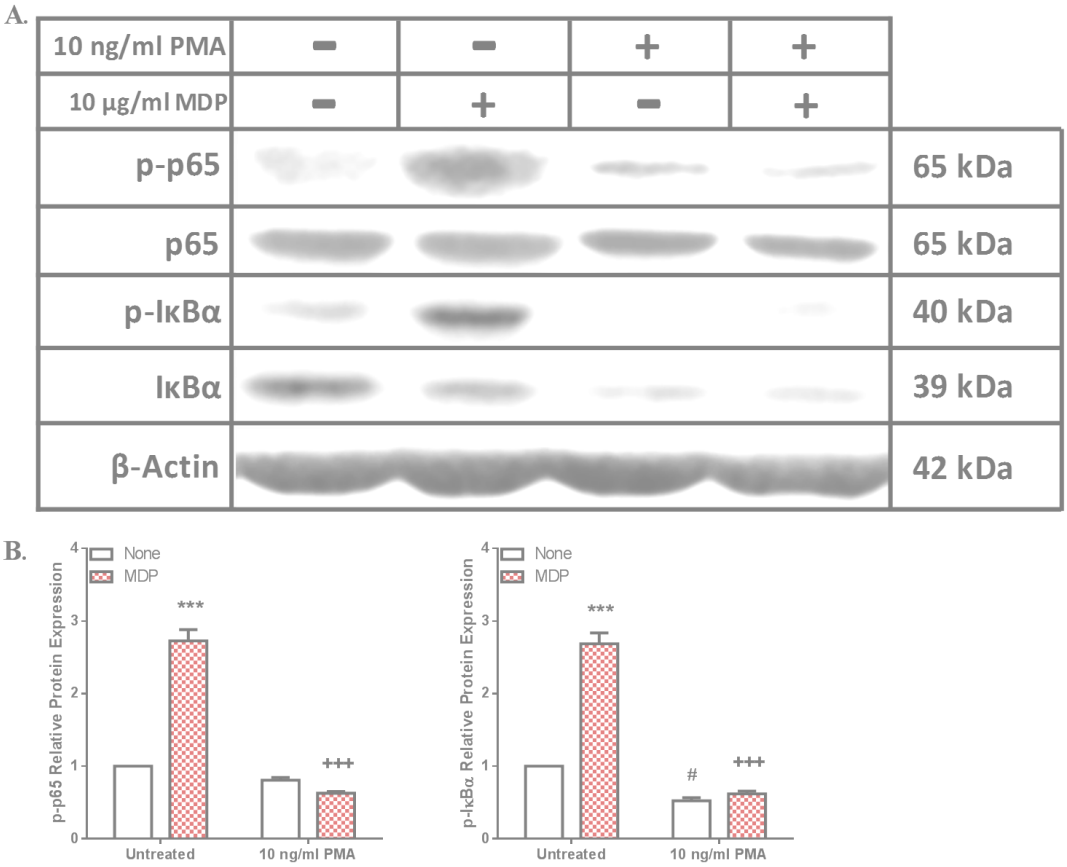

Figure 6.13 MDP-induced NF-κB signalling in PMA-primed THP-1 cells. (A) Immunoblots of phosphorylated and total p65 and IκBα in cells primed with 10 ng/ml PMA for 48 hours and subsequently stimulated with 10 µg/ml MDP for two hours. β-Actin acted as the loading control. (B) Densitometry of phosphorylated p65 and IκBα expression, relative to β-Actin expression. "Untreated + None" was set as the control group. Data is represented as mean relative expression ± S.E.M. and analysed using two-way ANOVAs (followed by Bonferroni's *post-hoc* test). ***** $p < 0.05$ representing **control vs NOD2**, **#** $p < 0.05$ representing **control vs primed**, **+** $p < 0.05$ representing **NOD2 vs (primed + NOD2).**

6.4.12 Differentiation reduces NOD2 expression, but increases A20 expression, in THP-1 cells.

To explore the underlying mechanism behind the reduced NOD2 pro-inflammatory activity and signalling following PMA-driven differentiation of THP-1 cells, NOD2 basal expression was quantified following PMA treatment. THP-1 cells were treated with 10 ng/ml PMA for 48 hours, after which NOD2 mRNA and protein expression were quantified by qPCR and western blotting, respectively. NOD2 expression was quantified relative to the chosen housekeeping gene; β-Actin.

Treatment with PMA significantly lowered NOD2 mRNA expression by 0.3-fold ($p < 0.001$) (Figure 6.14 A). This effect was also detected at the protein level, with PMA treatment reducing NOD2 protein expression 0.7-fold ($p < 0.01$), as shown in Figure 6.14 B-C. This data provides a potential mechanism for how differentiation reduced NOD2 activity and signalling, suggesting that NOD2 expression drops after PMA-driven differentiation. Finally, expression of the NOD2 negative regulator; A20 protein, was quantified by western blot analysis (Figure 6.14 D-E). PMA was found to increase A20 expression by 4.8-fold ($p < 0.001$). This exacerbated A20 in differentiated cells could account for the reduced NOD2 activity and signalling.

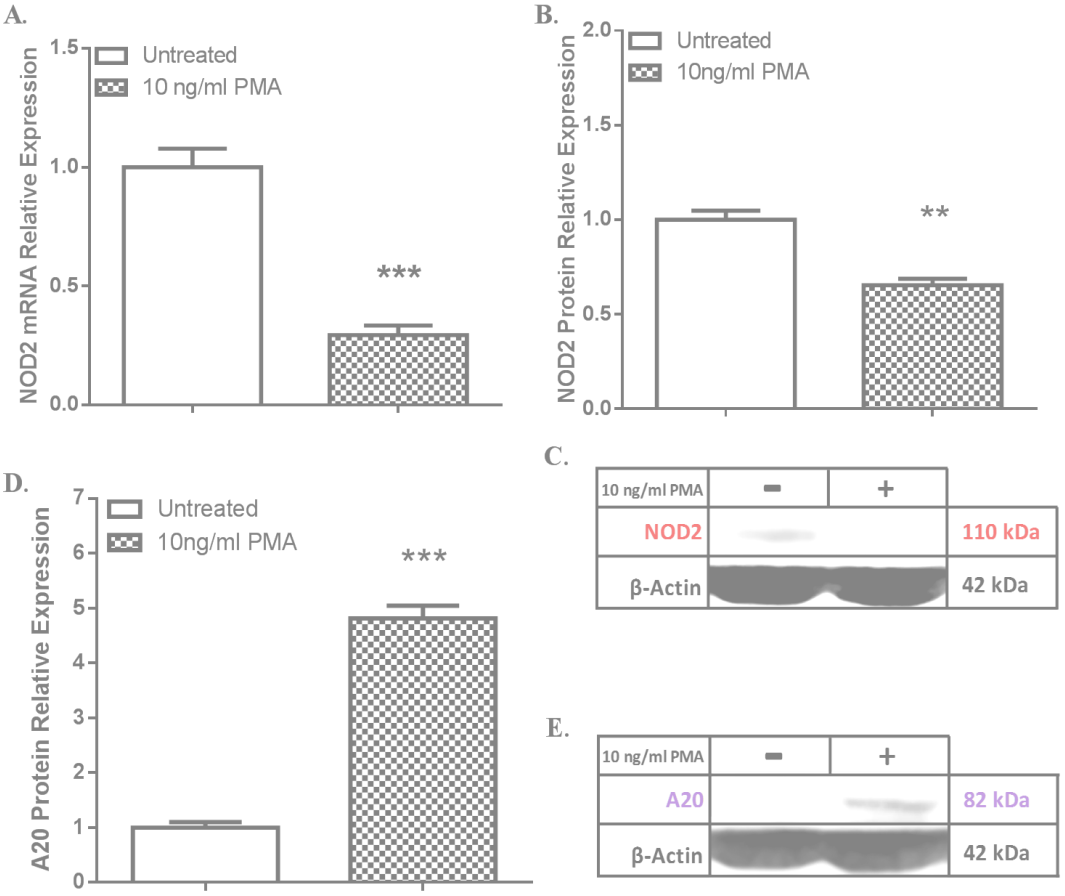

Figure 6.14. NOD2 and A20 basal expression in PMA treated THP-1 cells. (A) NOD2 mRNA expression in THP-1 cells treated with 10 ng/ml for 48 hours, relative to β-Actin expression. (B) Densitometry of NOD2 protein expression in PMA treated cells, relative to β-Actin expression. (C) Representative immunoblot of NOD2 protein expression in PMA treated cells. (D) Densitometry of A20 protein expression in PMA treated cells, relative to β-Actin expression. (E) Representative immunoblot of A20 protein expression in PMA treated cells. Data is represented as mean relative expression ± S.E.M. Statistical analysis was performed using independent t-tests. Significance was recognised at $p < 0.05$, with * representing $p < 0.05$, ** representing $p < 0.01$ and *** representing $p < 0.001$.

6.5 Discussion of main findings

In this chapter, the effects of epigenetic modifications on NOD2 activity, signalling and expression was investigated in THP-1 cells. NOD2 pro-inflammatory activity was enhanced following treatment with demethylating agents, as signified by increased TNF-α / IL-6 expression and IL-8 release. This effect of methylation carried through into signalling patterns, with 5-Aza-dC-priming generally enhancing NOD2 associated RIP2/MAPK/NF-κB signalling. As was uncovered in HCT116 cells, NOD2 expression was increased at the mRNA and protein expression in THP-1 cells after treatment with 5-Aza-dC. Therefore, the enhanced NOD2 responses following disruption of DNA methylation patterns could potentially be explained by direct upregulation of NOD2 receptor expression. Investigation of histone acetylation as a NOD2 regulation mechanism revealed similar patterns to those in previous chapters, whereby NOD2 associated responses were attenuated in HDAC inhibitor primed cells. SAHA-priming reduced NOD2 pro-inflammatory activity in THP-1 cells, as indicated by lower TNF-α and IL-6 expression. Again, basal IL-8 release was increased following SAHA treatment, which is most like due to NOD2-independent signalling triggered by SAHA, as discussed earlier. Activation of NOD2 pro-inflammatory signalling proteins was mainly attenuated in SAHA-primed THP-1 cells, apart from p-p65 and p-RIP2, whose basal expression appeared to be increased directly by SAHA. The enhanced p-p65 was most likely due to NOD2-independent signalling induced by SAHA that leads to the increased IL-8 expression, as before. The mechanism underlying the increase in p-RIP2 remains unclear, however, since SAHA treatment causes significant cell death it may be inducing apoptosis via RIP2 signalling (McCarthy et al., 1998). As expected, from the reduced NOD2 activity and signalling patterns, NOD2 expression was significantly reduced at the mRNA levels following SAHA treatment. This decrease however was not matched at the protein level, where an increase was recorded instead. Again, it is possible that this is a result of increased NOD2 stability inferred by SAHA via increased *hsp70* expression (Zhao et al., 2006).

Finally, differentiation of THP-1 cells was found to attenuate NOD2 associated pro-inflammatory activity, represented by a decline in TNF-α and IL-6 expression following NOD2 stimulation of PMA-primed cells. As was found with NOD1-induced IL-8 release in Chapter 5, NOD2 associated IL-8 was increased following

differentiation of THP-1 cells. Based on findings published in the literature, discussed in Chapter 5, this increase in IL-8 could be a false-positive, since differentiation has been found to increase IL-8 in a NOD2-independent manner and is not further increased by NOD2 activation. Therefore, the IL-8 upsurge doesn't imply increased NOD2 activity. In support of the reduced NOD2 activity following PMA treatment, NOD2 RIP2/MAPK/NF-κB signalling was diminished in differentiated THP-1 cells. Follow-up NOD2 expression studies revealed a reduction at both the mRNA and protein levels. This plunge in expression possibly provides a mechanism for the decreased NOD2 activity and signalling following differentiation. Reduced NOD2 responses may also be a result of increased expression of the NOD2 negative regulator; A20.

Limitations and Future Work.

Reflecting on the findings presented in this body of research additional experimentation could be undertaken to expand on this data. To further investigate whether the increased pro-inflammatory activity recorded in 5-Aza-dC primed cells resulted from enhanced NOD1/2 activation, localisation of the receptors could be examined by immunocytochemistry following stimulation with their respective ligands. NOD1/2 receptors translocate to the plasma membrane upon recognising and binding its ligand (Franchi et al., 2009a). Therefore, if the enhanced pro-inflammatory responses recorded here in 5-Aza-dC primed cells are a result of increased NOD1/2 expression, immunocytochemistry analysis should reveal greater receptor localisation at the plasma membrane in primed cells relative to their un-primed counterparts. Findings from this experimentation could strengthen the argument for demethylation enhancing functional NOD1/2 receptor levels, whereby hypomethylating conditions increase the pool of NOD1/2 receptors available for activation and so is associated with greater pro-inflammatory responses following stimulation.

As was found with NOD1 in Chapter 5, treatment with PMA was associated with decreased NOD2 expression and pro-inflammatory activity. This recorded decrease in NOD1/2 following differentiation could be harnessed to further investigate DNA methylation as a regulatory mechanism for these receptors. This could be done by treating the differentiated cells with 5-Aza-dC and examining whether the diminished NOD1/2 expression and pro-inflammatory responses are restored. If receptor expression and responses in differentiated cells are found to be restored to THP-1 cells

levels it would support NOD1/2 regulation via DNA methylation. However, if receptor expression and responses remain lower in differentiated cells, regardless of 5-Aza-dC priming, it would suggest that another regulatory mechanism may be at play. This additional insight could prove beneficial in drawing more concrete conclusions regarding DNA methylation as a regulatory mechanism for NOD1/2.

Chapter 7 Discussion and Conclusions

Currently, the knowledge regarding NOD-like receptor regulation is in its infancy. Protein regulators of the NOD1/2 receptors have begun to surface, including; A20 (Billmann-Born et al., 2011), RNF34 (Zhang et al., 2014) and Erbin (Kufer et al., 2006). These protein regulators generally exert their regulation by targeting receptor function or stability. However, the regulation of NOD1/2 gene expression has yet to be elucidated.

As outlined in the introduction chapter, NOD1 and NOD2 have been linked to a vast range of chronic inflammatory diseases including, Crohn's disease (Ogura et al., 2003), ulcerative colitis (Verma et al., 2013) and rheumatoid arthritis (Franca et al., 2015). Aberrant NOD1/2 expression has been associated with these diseased states, as reviewed in (Feerick and McKernan, 2017). Although a link has been made between NOD1/2 and disease, none of the current therapies on the market for chronic inflammation act to rectify this dysregulation. This is potentially due to the noticeable knowledge gap regarding how NOD-like receptor gene expression is regulated. This gap needs to be bridged in order to clarify the link between NOD1/2 expression patterns and disease onset. The first step towards this would be to establish the mechanism underlying NOD1/2 expression regulation, which was the main objective of the research undertaken here.

From extensive review of the literature it became more apparent that the epigenome is commonly found to be altered in diseased states (Wilson et al., 2007, Zoghbi and Beaudet, 2016). Hypomethylation of DNA has been directly associated with chronic inflammatory diseases including; Crohn's disease (Nimmo et al., 2012) and rheumatoid arthritis (Karouzakis et al., 2011). In the DNA methylation comparison study, carried out on Crohn's disease patients versus healthy controls, whereby the methylation status of 27,578 CpG sites across the genome were compared, 1117 sites (including the NOD2 gene) of differential methylation were identified in Crohn's patients (Nimmo et al., 2012). Irregular histone acetylation patterns were also identified in inflammatory bowel disease, whereby an *in vivo* study revealed that acetylation of H4 was enhanced in the inflamed mucosa biopsy samples relative to that recorded in the non-inflamed tissue (Tsaprouni et al., 2011). The uncovered

NOD1/2 expression levels and differential epigenetic patterns, linked separately in the literature, led to the postulation that perhaps an altered epigenome could be responsible for the aberrant NOD1/2 expression and subsequent disease development.

Therefore, the current thesis hypothesized that epigenetic modifications alter the pro-inflammatory activity and expression of NOD1 and NOD2 in intestinal epithelial cells and monocytes. The epigenetic modifications selected for investigation included; DNA methylation and histone acetylation. These modifications were chosen, as they are the best characterised contributors to the epigenome (Portela and Esteller, 2010, Zoghbi and Beaudet, 2016), thereby offering a baseline platform on which to build the current research hypothesis.

The current thesis focussed on NOD1 and NOD2 regulation within two cell types and suggested for the first time that both NOD1 and NOD2 receptor responses are directly regulated by DNA methylation while indirectly altered by histone acetylation. This novel conclusion could be drawn from investigation of the pro-inflammatory activity, signalling patterns and receptor expression. Quantification of pro-inflammatory cytokines (TNF-α / IL-6 / IL-8) and signalling proteins (RIP2 / MAPK / NF-κB) revealed increases in cells primed with a demethylating agent (5-Aza/5-Aza-dC). Although pro-inflammatory cytokines expression was readily detectable, cytokine release quantification proved challenging. This phenomenon followed through all studies conducted on both cell types studied in the current thesis. Review of the literature highlighted a lack of data being reported in relation to TNF-α and IL-6 release from HCT116 or THP-1 cells. This absence from published data leads one to postulate that these cytokines may not be stable under these conditions, but this remains unreported. In theory it may be suggested that these cytokines could be degraded by miRNAs (Asirvatham et al., 2009), or potentially bind back onto cytokine receptors potentially on the cell line surface (Panja et al., 1998). But would require further study to fully illuminate the true cause. Quantification of IL-8 chemokine release, chosen based on literature findings (Zhao et al., 2007, Leung et al., 2009), was a successful substitute echoing the patterns of TNF-α and IL-6 mRNA data under hypomethylating conditions. This reinforces the hypothesis that demethylation potentially increases NOD1 and NOD2 pro-inflammatory activity. To strengthen resolve in this hypothesis, the pro-inflammatory activity was investigated further by evaluating trends in DNMT3b$^{-/-}$ HCT116 cells relative to their wild-type counterparts. This secondary path of assessment mirrored the initial findings with some limitations

identified due to off target effects of the genetic knockout. Therefore, the current thesis suggests for the first time that pharmacological inhibition or genetic knockout of DNA methyltransferases enhances NOD1 and NOD2 responses to stimuli. These patterns led to the examination of basal NOD1/NOD2 expression, which was found to increase following DNA methylation disruption. Together, these findings enlighten and suggest that DNA methylation is potentially playing a direct role in NOD1/NOD2 expression regulation in intestinal epithelial cells and monocytes, a previously unreported conclusion. This is a feasible regulation mechanism since bioinformatic analysis revealed the presence of CpG islands in the gene sequence of both NOD1 (two CpG islands) and NOD2 (four CpG islands), which are the sites required to support regulatory DNA methylation. There is also precedent for DNA methylation playing a role in NOD1/NOD2 regulation since previous research has found that treatment with 5-Aza increased the immune response of 63 cell lines (26 breast cancer, 23 ovarian cancer and 14 colorectal cancer cell lines) (Li et al., 2014, Hennessy and McKernan, 2016). This effect of 5-Aza on the immune response could potentially be explained by an up-regulation of NOD1/NOD2 expression and/or responses under the hypomethylating conditions.

Histone acetylation studies offered a parallel assessment of potential NOD1 and NOD2 epigenetic regulation in HCT116 and THP-1 cells via assessment of pro-inflammatory responses and NOD1 expression in cells primed with a hyperacetylating agent (SAHA). Histone acetylation data revealed much more conflicting patterns to those identified with methylation. Treatment with SAHA appeared to have off-target effects in relation to NOD1 and NOD2 in both cell lines. This is supported by SAHA-driven changes in pro-inflammatory and signalling activity patterns, independent of NOD1/NOD2 stimulation. Such NOD1/NOD2 independent effects are potentially observed with the patterns of IL-8 release recorded after SAHA treatment, whereby SAHA alone, without NOD1 / NOD2 stimulation, induced a robust upsurge in IL-8. Review of the literature revealed that SAHA activates the IKK complex directly, inducing NF-κB activation and subsequent IL-8 expression. SAHA also promotes histone H3 hyperacetylation at the IL-8 promoter region, thereby further supporting expression of the underlying gene (Gatla et al., 2017). Conflicting mRNA and protein data for NOD1/NOD2 basal expression after SAHA treatment could be attributed to differences in stability. It has been reported previously that treatment with HDAC inhibitors promote a hyperacetylated state of histone H3 at the promoter and

transcribing regions of the *hsp70* gene, and subsequently increases expression of the gene (Zhao et al., 2006). Hsp70 is a chaperone protein that stabilises NOD1/NOD2 receptor stability, therefore upregulation of this stabilising protein could account for the increased NOD1/NOD2 protein.

Differentiation of the THP-1 cell line into macrophages-like cells was found to generally deplete the NOD1/NOD2 responses and expression that had been observed in undifferentiated THP-1 cells. These findings exhibit similarities to those detected when the role of histone acetylation was under investigation. These attenuated patterns imply that the phorbal-myristate-acetate (PMA), used to differentiate the cells, could, in a similar fashion to the histone deacetylase inhibitor, be having an indirect effect on NOD1/NOD2 activity and expression. It has been reported in the literature that PMA does alter gene expression (Jiang and Fleet, 2012, Jiang et al., 2016). Therefore, it is possible that the differentiation process could be supporting up-regulation of a negative regulator or down-regulation of a positive regulator of the NOD1/NOD2 response. In light of this, expression of the NOD1/NOD2 regulator; A20, was investigated following differentiation. Analysis revealed a significant increase in A20 protein expression following differentiation. This increase was supported by a recent THP-1 based study carried out to establish the role of A20 in monocyte-to-macrophage differentiation. This study uncovered a significant increase in A20 expression during differentiation. They conclude that this upsurge in A20 is required for efficient differentiation and is crucial for cell survival during differentiation of the THP-1 cell line (Osako et al., 2017). These findings, alongside the well-recognised concept that epigenetic modifications contribute to cell differentiation during development (Skinner, 2011), suggest that differentiation is having immense effects on the epigenome and that a portion of the genes affected are potentially attenuating NOD1/NOD2 pro-inflammatory activity and expression.

NOD1 and NOD2 agree in their upregulated pro-inflammatory response patterns, however NOD2 demonstrates a greater response magnitude between untreated and treated groups (in some cases as large as a factor of five compared to NOD1). This trend is a novel uncovering of a potential difference between NOD1 and NOD2 regulation. This direct comparison of NOD1 and NOD2 response under the same demethylating conditions has not been previously reported. One potential rationale for the stronger NOD2 response to demethylation could be attributed to the presence of four CpG islands in the NOD2 gene sequence in contrast to two CpG islands identified

within the NOD1 gene. Perhaps the presence of two extra CpG islands means that the NOD2 gene expression is more tightly regulated by methylation. This correlation has not yet been made, and thus renders further research. If it is indeed the case that NOD2 is more strongly regulated by DNA methylation, as this thesis suggests, it could be due to NOD2 requiring more tight regulation of its responses. NOD2 is a more general sensor of bacteria (Girardin et al., 2003), sensing both Gram-positive and –negative bacteria, and so may require this higher magnitude of regulation to prevent inappropriate inflammatory responses.

Overall, findings from the novel studies presented in this thesis suggest that NOD1 and NOD2 receptor pro-inflammatory activity and expression are indeed regulated at the epigenetic level. The pattern of results presented here, alongside findings already in the literature, allow us to postulate further. The strongest result uncovered, in relation to NOD1/NOD2 expression regulation, is the exacerbated pro-inflammatory activity and expression in cells primed with a demethylating agent, which was consistently documented across all four chapters. This suggests that DNA methylation patterns, at the identified CpG islands, could be regulating NOD1/NOD2 expression and pro-inflammatory responses in a direct manner.

Physicians have few treatment options for chronic inflammatory diseases, with corticosteroid based therapies generally accepted as a go to first option (Katz, 2004, Li et al., 2015, Hellgren et al., 2010, Stelmach et al., 2005). However, many undesirable side-effects and issues with resistance come into play with these therapy options, making them very often an ineffective in treating chronic disease. Several anti-TNF-α drugs also available for inflammation treatment (Stelmach et al., 2005), such as Infliximab (REMICADE®). This genetically engineered antibody binds to and neutralises the human TNF-α with high affinity. This drug is mainly used to treat Crohn's disease patients; however some patients are non-responders or lose their initial response to the drug (Chaparro et al., 2011). Therefore, it appears that there is certainly a need for therapies with greater specificity and efficacy for treatment of chronic inflammatory diseases.

By expanding our knowledge of expression regulation, it could potentially accommodate the development of new therapeutics for treatment of NOD1/NOD2 associated disease. The research presented in this thesis eludes to epigenetic modifications, with more emphasis on DNA methylation, potentially being a key regulatory mechanism for NOD1/NOD2. This is a compelling finding, since adjusting

expression via epigenetic intervention is already a key therapeutic method used in the treatment of certain cancers (Karahoca and Momparler, 2013) including; myelodysplastic syndrome (Christman, 2002, Quintás-Cardama et al., 2010) and Advanced Primary Cutaneous T-Cell Lymphoma (Mann et al., 2007). The epigenetic modifying agents used to conduct this research; 5-Azacytidine (Vidaza®), 5-Aza-deoxycytidine (Decitabine®) and suberoylanilide hydroxamic (Vorinostat®) are the FDA approved pharmacotherapies for the aforementioned cancer types. Vidaza® and Decitabine® act to target and demethylate tumour suppressor genes that have been silenced by hypermethylation, including the *cdkn2b* gene encoding the p15 tumour suppressor protein (Quintás-Cardama et al., 2010, Raj and Mufti, 2006). Vorinostat® acts by triggering hyperacetylation of the cyclin-dependent kinase inhibitor p21, thereby promoting cell cycle arrest (Richon et al., 2000, Mann et al., 2007). The clinical use of these drugs, alongside what is learnt from this thesis, instils optimism for these current therapies to evolve and expand to treat a wider spectrum of ailments including chronic inflammatory diseases.

7.1 Limitations and Future Directions

Although novel findings were uncovered over the course of this thesis, several limitations remain that warrant further experimentation in order to be overcome. All the data presented in this thesis were generated using cancer cell lines, and so there are limitations to the findings. Therefore, it would be advantageous to examine the effects of epigenetic modifications *in vivo*, investigating the effects of Decitabine® (5-Aza-Dc) dosing or DNMT knockout, in mice for example, on NOD1/NOD2 responses and expression. Studies could be expanded further again by acquiring human primary cells, such as monocytes from patients receiving Decitabine® treatment for myelodysplastic syndrome. Genome-wide methylation profiling has been carried out on Decitabine® treated patients in an attempt to gain insight into the localisation and extent of demethylation induced (Yan et al., 2012). Examination of NOD1/NOD2 expression and activity patterns in these cells could provide strong insight into their regulation in the human body.

Pro-inflammatory cytokines/chemokines were quantified throughout this body of research to unveil whether pro-inflammatory activity was altered under hypomethylating, hyperacetylating or differentiating conditions. TNF-α and IL-6 cytokines were chosen to be measured as they are some of the earliest cytokines

released in the innate immune response. These cytokines were detected at the mRNA levels but their release from both cell lines were below the levels of detection, therefore IL-8 release was quantified instead. The qPCR and ELISA data therefore didn't match i.e. different cytokines/chemokines were analysed at the mRNA (TNF/IL-6) and protein (IL-8) levels. Ideally the mechanisms underlying the lack of TNF-α and IL-6 release from cells would have been further investigated and/or IL-8 mRNA expression would have been measured by qPCR to address this mismatch between analytes. However, due to time constraints this was beyond the scope of this thesis. Therefore, future work could involve addressing this qPCR and ELISA data mismatch.

Data presented here demonstrate that treatment with a global demethylating agent or genetic knockout of a DNA methyltransferase enzyme results in increased NOD1/2 activity and expression. However, it has not been proven that these treatments deteriorate the methylation patterns surrounding the NOD1/2 gene sequences. Therefore, investigation of methyl patterns surrounding NOD1 and NOD2 genes is required to confirm the findings of this research. DNA methylation patterns can be examined by bisulphite sequencing (Booth et al., 2013) or melt curve analysis (Smith et al., 2009). The verdict from these studies could confirm/deny whether methyl patterns surrounding NOD1/2 gene sequences are altered in 5-Aza-dC-primed cells or DNMT3b knockout cells. If methylation patterns are found to be deteriorated, it would support DNA methylation as a key NOD1/NOD2 regulator. Methylation patterns surrounding other genes involved in NOD1/2 regulation including negative regulators (e.g. A20, TRIM27 and RNF34) and chaperone proteins (Hsp70 and Hsp90) could be investigated. This could elucidate if global demethylating conditions, created by 5-Aza-dC or genetic knockout of DNMT3b, diminished methyl patterns surrounding these genes. This would address the possibility that altered expression of these genes could be causing or contributing to the increased NOD1/2 expression and associated activity recorded throughout this thesis.

It is generally accepted that demethylation at a gene promoter region is associated with enhanced expression of the downstream gene, however this is not always the case. Therefore, if diminished methyl patterns are identified at the NOD1/2 promoter sequences it would be beneficial to confirm that this hypomethylated state correlates with enhanced transcription. Recruitment of transcription machinery to the exposed

promoter sequence, identified by ChIP analysis, is indicative of transcriptionally active genes.

The hypomethylated state was associated with increased NOD1/2 receptor expression and associated pro-inflammatory activity. Additional experimentation could be carried out to further confirm that the increased NOD1/2 levels were responsible for the enhanced pro-inflammatory activity recorded following stimulation. Experimentation would involve proving that the excess NOD1/2 receptors generated under hypomethylated states are functional i.e. receptors can sense appropriate ligands, undergo conformational changes, translocate to the plasma membrane and initiate pro-inflammatory signalling by binding the RIP2 adapter protein. Immunocytochemistry could be used to establish whether there are more NOD1/2 receptors positioned at the plasma membranes of 5-Aza-dC primed or DNMT3b$^{-/-}$ cells relative to their untreated counterparts. Binding of RIP2 adapter protein to NOD1/2 could be examined by co-immunoprecipitation analysis. Together, this additional data would confirm whether excess NOD1/2 receptors, being produced under hypomethylated conditions, are capable of transmitting signals thereby accounting for the enhanced pro-inflammatory activity recorded in this research.

Although the effects of demethylation on NOD1/2 expression and activity were significant, it has yet to be elucidated whether these effects are specific to NOD1/2 receptors. This should be examined in future work by quantifying other PRR expression and activity under the same priming conditions outlined in this research. Data generated from this experimentation could highlight whether regulation via DNA methylation is a highly non-specific mechanism for all PRRs or is specific to NOD1/2 receptors.

SAHA related research undertaken in this thesis has uncovered novel findings that imply an indirect effect of HDAC inhibition on NOD1/2 expression and activity that warrants further investigation to establish the mechanism underlying these effects. Since NOD1/2 receptor expression and activity are generally diminished in SAHA primed cells it suggests that a protein regulator of NOD1/2 may be upregulated or downregulated under the hyperacetylated conditions. Expression analysis of identified NOD1/2 regulators could be undertaken to establish if SAHA altered their expression. Preliminary studies had begun in this research, where A20 (a negative regulator of NOPD1/2) mRNA expression was found to be increased following SAHA treatment.

This work could be expanded by investigating expression of an array of other regulators e.g. TRIM27, RNF34, PSMA7 and Erbin. Since several NOD1/2 regulators are E3 ubiquitin ligases the role played by these proteins could be further investigated by inhibiting the cells proteasome via treatment with e.g. MG132, prior to SAHA priming. If SAHA priming does not induce the same NOD1/2 expression and activity patterns in cells treated with a proteasome inhibitor, it could strengthen the case for SAHA altering NOD1/2 via regulators.

NOD1/2 expression patterns should complement each other at the mRNA and protein levels, however contradictory NOD1/2 levels were recorded in some SAHA treated cells. This mismatched expression data warrants further investigation. NOD1/2 expression was diminished at the mRNA but enhanced at the protein level, thereby suggesting that SAHA was potentially causing reductions in NOD1/2 expression but possibly enhanced the stability of the proteins via upregulation of a chaperone protein. Expression analysis of NOD1/2 chaperone proteins (Hsp70 or Hsp90) could be carried out to confirm whether enhanced receptor stability was accountable for the increased NOD1/2 protein levels. It would be beneficial to test the activity of these receptors after SAHA, since the diminished downstream pro-inflammatory activity outlined in this research wouldn't be expected if the excess NOD1/2 receptors were indeed functional.

Another limitation of the SAHA related studies is the direct effect of the HDAC inhibitor on IL-8 release. Therefore, unlike with DNA methylation analysis, IL-8 release is not an appropriate model for quantifying differences in SAHA-associated pro-inflammatory activity. Therefore, additional experimentation could be undertaken to identify a more appropriate indicator. Since release of other pro-inflammatory cytokines (TNF-α and IL-6) were found to be below the limits of detection, then perhaps anti-microbial peptide (e.g. β-defensin) release should be investigated next. Data generated from this analysis may provide more insight if SAHA priming is found not to have a direct effect on β-defensin as it did on IL-8 release.

Findings from the THP-1 differentiation studies presented in Chapters 5 and 6 are limited by the lack of functionality confirmation. The differentiated phenotype was confirmed by adherence, RSK1 expression upregulation and enhanced expression of the CD16 cell surface marker. However, it has yet to be elucidated whether these differentiated cells function as macrophages, with the capacity to engulf foreign

particles. This could be tested in future work using a phagocytosis assay, whereby the uptake of fluorescently tagged foreign particles can be monitored and quantified to establish if the differentiated cells function as macrophage cells.

The persistent theme identified throughout the differentiation studies is that NOD1/2 expression and pro-inflammatory activity is significantly diminished under differentiating conditions. This novel finding could be harnessed to further investigate DNA methylation as a regulatory mechanism for NOD1/2. THP-1 cells differentiated with PMA could be subsequently treated with 5-Aza-dC for 72 hours, after which expression analysis could be performed to establish whether the hypomethylating conditions restored NOD1/2 expression and responses in differentiated cells back to THP-1 levels. If 5-Aza-dC was found to have restoring properties it could provide significant support towards the theory proposed in this thesis; that DNA methylation is a potential regulatory mechanism underlying NOD1/2 expression.

Therefore, this body of work has begun the investigation into epigenetic modification-based regulation of NOD1/2 expression and activity. It contains the necessary *in vitro* ground work; whose convincing data patterns justify further investigation. Once the limitations are overcome by future experimentation, the therapeutic potential could be enormous for chronic inflammatory disorders associated with NOD1/2, such as inflammatory bowel disease. As already mentioned, current therapies fall short, treating via symptom relief rather than addressing the underlying cause. If NOD1/2 expression can be altered by targeting and adjusting their surrounding methylation patterns it could provide a breakthrough mechanism for therapy development.

Chapter 8 Bibliography

AKIRA, S., UEMATSU, S. & TAKEUCHI, O. 2006. Pathogen recognition and innate immunity. *Cell,* 124**,** 783-801.

ARSENESCU, R., BRUNO, M. E., ROGIER, E. W., STEFKA, A. T., MCMAHAN, A. E., WRIGHT, T. B., NASSER, M. S., DE VILLIERS, W. J. & KAETZEL, C. S. 2008. Signature biomarkers in Crohn's disease: toward a molecular classification. *Mucosal Immunol,* 1**,** 399-411.

ASIRVATHAM, A. J., MAGNER, W. J. & TOMASI, T. B. 2009. miRNA regulation of cytokine genes. *Cytokine,* 45**,** 58-69.

ATHMAN, R. & PHILPOTT, D. 2004. Innate immunity via Toll-like receptors and Nod proteins. *Curr Opin Microbiol,* 7**,** 25-32.

BAGGIOLINI, M. 1998. Chemokines and leukocyte traffic. *Nature,* 392**,** 565.

BARMADA, M. M., BRANT, S. R., NICOLAE, D. L., ACHKAR, J. P., PANHUYSEN, C. I., BAYLESS, T. M., CHO, J. H. & DUERR, R. H. 2004. A genome scan in 260 inflammatory bowel disease-affected relative pairs. *Inflamm Bowel Dis,* 10**,** 513-20.

BASIL, M. C. & LEVY, B. D. 2016. Specialized pro-resolving mediators: endogenous regulators of infection and inflammation. *Nat Rev Immunol,* 16**,** 51-67.

BASSETT, S. A. & BARNETT, M. P. G. 2014. The role of dietary histone deacetylases (HDACs) inhibitors in health and disease. *Nutrients,* 6**,** 4273-4301.

BAYARSAIHAN, D. 2011. Epigenetic mechanisms in inflammation. *Journal of dental research,* 90**,** 9-17.

BECKER, C. & O'NEILL, L. J. 2007. Inflammasomes in inflammatory disorders: the role of TLRs and their interactions with NLRs. *Seminars in Immunopathology,* 29**,** 239-248.

BEG, A. A., FINCO, T. S., NANTERMET, P. V. & BALDWIN, A. S. 1993. Tumor necrosis factor and interleukin-1 lead to phosphorylation and loss of I kappa B alpha: a mechanism for NF-kappa B activation. *Molecular and Cellular Biology,* 13**,** 3301-3310.

BERCZI, I. & SZENTIVANYI, A. 2003. Cytokines and chemokines. *In:* BERCZI, I. & SZENTIVANYI, A. (eds.) *NeuroImmune Biology.* Elsevier.

BERDASCO, M. & ESTELLER, M. 2013. Genetic syndromes caused by mutations in epigenetic genes. *Human Genetics,* 132**,** 359-383.

BERNI CANANI, R., DI COSTANZO, M. & LEONE, L. 2012. The epigenetic effects of butyrate: potential therapeutic implications for clinical practice. *Clin Epigenetics,* 4**,** 4.

BHALLA, K. N. 2005. Epigenetic and chromatin modifiers as targeted therapy of hematologic malignancies. *J Clin Oncol,* 23**,** 3971-93.

BIANCHI, M. E. 2007. DAMPs, PAMPs and alarmins: all we need to know about danger. *J Leukoc Biol,* 81**,** 1-5.

BIELIG, H., ROMPIKUNTAL, P. K., DONGRE, M., ZUREK, B., LINDMARK, B., RAMSTEDT, M., WAI, S. N. & KUFER, T. A. 2011. NOD-Like Receptor Activation by Outer Membrane Vesicles from Vibrio cholerae Non-O1 Non-O139 Strains Is Modulated by the Quorum-Sensing Regulator HapR. *Infection and Immunity,* 79**,** 1418-1427.

BILLMANN-BORN, S., TILL, A., ARLT, A., LIPINSKI, S., SINA, C., LATIANO, A., ANNESE, V., HASLER, R., KERICK, M., MANKE, T., SEEGERT, D., HANIDU, A., SCHAFER, H., VAN HEEL, D., LI, J., SCHREIBER, S. & ROSENSTIEL, P. 2011. Genome-wide expression profiling identifies an impairment of negative feedback signals in the Crohn's disease-associated NOD2 variant L1007fsinsC. *J Immunol,* 186**,** 4027-38.

BISWAS, A., PETNICKI-OCWIEJA, T. & KOBAYASHI, K. S. 2012. Nod2: a key regulator linking microbiota to intestinal mucosal immunity. *Journal of Molecular Medicine (Berlin, Germany),* 90**,** 15-24.

BLANDER, G. & GUARENTE, L. 2004. The Sir2 family of protein deacetylases. *Annu Rev Biochem,* 73**,** 417-35.

BLAU, E. B. 1985. Familial granulomatous arthritis, iritis, and rash. *J Pediatr,* 107**,** 689-93.

BOGEFORS, J., RYDBERG, C., UDDMAN, R., FRANSSON, M., MÅNSSON, A., BENSON, M., ADNER, M. & CARDELL, L. O. 2010. Nod1, Nod2 and Nalp3 receptors, new potential targets in treatment of allergic rhinitis? *Allergy,* 65**,** 1222-1226.

BOOTH, M. J., OST, T. W. B., BERALDI, D., BELL, N. M., BRANCO, M. R., REIK, W. & BALASUBRAMANIAN, S. 2013. Oxidative bisulfite sequencing of 5-methylcytosine and 5-hydroxymethylcytosine. *Nature Protocols,* 8**,** 1841.

BOURC'HIS, D., XU, G. L., LIN, C. S., BOLLMAN, B. & BESTOR, T. H. 2001. Dnmt3L and the establishment of maternal genomic imprints. *Science,* 294**,** 2536-9.

BOYLE, J. P., MAYLE, S., PARKHOUSE, R. & MONIE, T. P. 2013. Comparative Genomic and Sequence Analysis Provides Insight into the Molecular Functionality of NOD1 and NOD2. *Frontiers in Immunology,* 4**,** 317.

BRADBURY, L. A. & BROWN, M. A. 2007. Genome-wide association study of 14,000 cases of seven common diseases and 3,000 shared controls. *Nature,* 447**,** 661-678.

CANDIDO, E. P., REEVES, R. & DAVIE, J. R. 1978. Sodium butyrate inhibits histone deacetylation in cultured cells. *Cell,* 14**,** 105-13.

CARUSO, R., WARNER, N., INOHARA, N. & NUNEZ, G. 2014. NOD1 and NOD2: signaling, host defense, and inflammatory disease. *Immunity,* 41**,** 898-908.

CHANG, S., MCKINSEY, T. A., ZHANG, C. L., RICHARDSON, J. A., HILL, J. A. & OLSON, E. N. 2004. Histone deacetylases 5 and 9 govern responsiveness of the heart to a subset of stress signals and play redundant roles in heart development. *Mol Cell Biol,* 24**,** 8467-76.

CHANG, S., YOUNG, B. D., LI, S., QI, X., RICHARDSON, J. A. & OLSON, E. N. 2006. Histone deacetylase 7 maintains vascular integrity by repressing matrix metalloproteinase 10. *Cell,* 126**,** 321-34.

CHAPARRO, M., PANES, J., GARCIA, V., MANOSA, M., ESTEVE, M., MERINO, O., ANDREU, M., GUTIERREZ, A., GOMOLLON, F., CABRIADA, J. L., MONTORO, M. A., MENDOZA, J. L., NOS, P. & GISBERT, J. P. 2011. Long-term durability of infliximab treatment in Crohn's disease and efficacy of dose "escalation" in patients losing response. *J Clin Gastroenterol,* 45**,** 113-8.

CHEN, C. M., GONG, Y., ZHANG, M. & CHEN, J. J. 2004. Reciprocal cross-talk between Nod2 and TAK1 signaling pathways. *J Biol Chem,* 279**,** 25876-82.

CHEN, G., SHAW, M. H., KIM, Y. G. & NUNEZ, G. 2009. NOD-like receptors: role in innate immunity and inflammatory disease. *Annu Rev Pathol,* 4**,** 365-98.

CHEN, L., DENG, H., CUI, H., FANG, J., ZUO, Z., DENG, J., LI, Y., WANG, X. & ZHAO, L. 2017. Inflammatory responses and inflammation-associated diseases in organs. *Oncotarget,* 9**,** 7204-7218.

CHOUDHURI, S., CUI, Y. & KLAASSEN, C. D. 2010. Molecular targets of epigenetic regulation and effectors of environmental influences. *Toxicology and applied pharmacology,* 245**,** 378-393.

CHRISTMAN, J. K. 2002. 5-Azacytidine and 5-aza-2′-deoxycytidine as inhibitors of DNA methylation: mechanistic studies and their implications for cancer therapy. *Oncogene,* 21**,** 5483.

CHUANG, D. M., LENG, Y., MARINOVA, Z., KIM, H. J. & CHIU, C. T. 2009. Multiple roles of HDAC inhibition in neurodegenerative conditions. *Trends Neurosci,* 32**,** 591-601.

CLARK, N. M., MARINIS, J. M., COBB, B. A. & ABBOTT, D. W. 2008. MEKK4 sequesters RIP2 to dictate NOD2 signal specificity. *Curr Biol,* 18**,** 1402-8.

DAMARAJU, V. L., MOWLES, D., YAO, S., NG, A., YOUNG, J. D., CASS, C. E. & TONG, Z. 2012. Role of human nucleoside transporters in the uptake and cytotoxicity of azacitidine and decitabine. *Nucleosides Nucleotides Nucleic Acids,* 31**,** 236-55.

DEANS, C. & MAGGERT, K. A. 2015. What do you mean, "epigenetic"? *Genetics,* 199**,** 887-896.

DEATON, A. E. M. & BIRD, A. 2011. CpG islands and the regulation of transcription. *Genes & Development,* 25**,** 1010-1022.

DIDONATO, J. A., HAYAKAWA, M., ROTHWARF, D. M., ZANDI, E. & KARIN, M. 1997. A cytokine-responsive I[kappa]B kinase that activates the transcription factor NF-[kappa]B. *Nature,* 388**,** 548-554.

DUGAN, J., GRIFFITHS, E., SNOW, P., ROSENZWEIG, H., LEE, E., BROWN, B., CARR, D. W., ROSE, C., ROSENBAUM, J. & DAVEY, M. P. 2015. Blau Syndrome–Associated Nod2 Mutation Alters Expression of Full-Length NOD2 and Limits Responses to Muramyl Dipeptide in Knock-in Mice. *The Journal of Immunology,* 194**,** 349-357.

ESTELLER, M. 2007. Epigenetic gene silencing in cancer: the DNA hypermethylome. *Human Molecular Genetics,* 16**,** R50-R59.

FALKENBERG, K. J. & JOHNSTONE, R. W. 2014. Histone deacetylases and their inhibitors in cancer, neurological diseases and immune disorders. *Nat Rev Drug Discov,* 13**,** 673-91.

FEERICK, C. L. & MCKERNAN, D. P. 2017. Understanding the regulation of pattern recognition receptors in inflammatory diseases - a 'Nod' in the right direction. *Immunology,* 150**,** 237-247.

FERREIRA, C. M., VIEIRA, A. T., VINOLO, M. A. R., OLIVEIRA, F. A., CURI, R. & MARTINS, F. D. S. 2014. The Central Role of the Gut Microbiota in Chronic Inflammatory Diseases. *Journal of Immunology Research,* 2014**,** 12.

FILIPPI, M.-D. 2016. Chapter Two - Mechanism of Diapedesis: Importance of the Transcellular Route. *In:* ALT, F. W. (ed.) *Advances in Immunology.* Academic Press.

FIOCCA, R., NECCHI, V., SOMMI, P., RICCI, V., TELFORD, J., COVER, T. L. & SOLCIA, E. 1999. Release of Helicobacter pylori vacuolating cytotoxin by both a specific secretion pathway and budding of outer membrane vesicles. Uptake of released toxin and vesicles by gastric epithelium. *The Journal of Pathology,* 188**,** 220-226.

FRANCA, R., VIEIRA, S. M., TALBOT, J., PERES, R. S., PINTO, L. G., ZAMBONI, D. S., LOUZADA-JUNIOR, P., CUNHA, F. Q. & CUNHA, T. M. 2015. Expression and activity of NOD1 and NOD2/RIPK2 signalling in mononuclear cells from patients with rheumatoid arthritis. *Scand J Rheumatol,* 45**,** 8-12.

FRANCHI, L., PARK, J.-H., SHAW, M. H., MARINA-GARCIA, N., CHEN, G., KIM, Y.-G. & NÚÑEZ, G. 2008. Intracellular NOD-like receptors in innate immunity, infection and disease. *Cellular Microbiology,* 10**,** 1-8.

FRANCHI, L., WARNER, N., VIANI, K. & NUNEZ, G. 2009a. Function of Nod-like receptors in microbial recognition and host defense. *Immunol Rev,* 227**,** 106-28.

FRANCHI, L., WARNER, N., VIANI, K. & NUÑEZ, G. 2009b. Function of Nod-like receptors in microbial recognition and host defense. *Immunological Reviews,* 227**,** 106-128.

FRANK, D. N., ROBERTSON, C. E., HAMM, C. M., KPADEH, Z., ZHANG, T., CHEN, H., ZHU, W., SARTOR, R. B., BOEDEKER, E. C., HARPAZ, N., PACE, N. R. & LI, E. 2011. Disease phenotype and genotype are associated with shifts in intestinal-associated microbiota in inflammatory bowel diseases. *Inflammatory bowel diseases,* 17**,** 179-184.

FRITZ, J. H., GIRARDIN, S. E., FITTING, C., WERTS, C., MENGIN-LECREULX, D., CAROFF, M., CAVAILLON, J.-M., PHILPOTT, D. J. & ADIB-CONQUY, M. 2005. Synergistic stimulation of human monocytes and dendritic cells by Toll-like receptor 4 and NOD1- and NOD2-activating agonists. *European Journal of Immunology,* 35**,** 2459-2470.

FRITZ, J. R. H. & GIRARDIN, S. E. 2005. How Toll-like receptors and Nod-like receptors contribute to innate immunity in mammals. *Journal of Endotoxin Research,* 11**,** 390-394.

FULLERTON, J. N. & GILROY, D. W. 2016. Resolution of inflammation: a new therapeutic frontier. *Nature Reviews Drug Discovery,* 15**,** 551.

GARTEL, A. L. & TYNER, A. L. 1998. The growth-regulatory role of p21 (WAF1/CIP1). *Prog Mol Subcell Biol,* 20**,** 43-71.

GATLA, H. R., ZOU, Y., UDDIN, M. M., SINGHA, B., BU, P., VANCURA, A. & VANCUROVA, I. 2017. Histone Deacetylase (HDAC) Inhibition Induces IkappaB Kinase (IKK)-dependent Interleukin-8/CXCL8 Expression in Ovarian Cancer Cells. *J Biol Chem,* 292**,** 5043-5054.

GIRARDIN, S. E., BONECA, I. G., CARNEIRO, L. A. M., ANTIGNAC, A., JÉHANNO, M., VIALA, J., TEDIN, K., TAHA, M.-K., LABIGNE, A., ZÄTHRINGER, U., COYLE, A. J., DISTEFANO, P. S., BERTIN, J., SANSONETTI, P. J. & PHILPOTT, D. J. 2003a. Nod1 Detects a Unique Muropeptide from Gram-Negative Bacterial Peptidoglycan. *Science,* 300**,** 1584-1587.

GIRARDIN, S. E., BONECA, I. G., VIALA, J., CHAMAILLARD, M., LABIGNE, A., THOMAS, G., PHILPOTT, D. J. & SANSONETTI, P. J. 2003b. Nod2 is a general sensor of peptidoglycan through muramyl dipeptide (MDP) detection. *J Biol Chem,* 278**,** 8869-72.

GIRARDIN, S. E., TOURNEBIZE, R., MAVRIS, M., PAGE, A. L., LI, X., STARK, G. R., BERTIN, J., DISTEFANO, P. S., YANIV, M., SANSONETTI, P. J. & PHILPOTT, D. J. 2001. CARD4/Nod1 mediates NF-kappaB and JNK activation by invasive Shigella flexneri. *EMBO Rep,* 2**,** 736-42.

GIRARDIN, S. E., TRAVASSOS, L. H., HERVÉ, M., BLANOT, D., BONECA, I. G., PHILPOTT, D. J., SANSONETTI, P. J. & MENGIN-LECREULX, D. 2003c. Peptidoglycan Molecular Requirements Allowing Detection by Nod1 and Nod2. *Journal of Biological Chemistry,* 278**,** 41702-41708.

GLOVER, A. B. & LEYLAND-JONES, B. 1987. Biochemistry of azacitidine: a review. *Cancer Treat Rep,* 71**,** 959-64.

GLOZAK, M. A., SENGUPTA, N., ZHANG, X. & SETO, E. 2005. Acetylation and deacetylation of non-histone proteins. *Gene,* 363**,** 15-23.

GRUNDY, S. M., CLEEMAN, J. I., DANIELS, S. R., DONATO, K. A., ECKEL, R. H., FRANKLIN, B. A., GORDON, D. J., KRAUSS, R. M., SAVAGE, P. J., SMITH, S. C., SPERTUS, J. A. & COSTA, F. 2005. Diagnosis

and Management of the Metabolic Syndrome: An American Heart Association/National Heart, Lung, and Blood Institute Scientific Statement. *Circulation,* 112**,** 2735-2752.

GRYDER, B. E., SODJI, Q. H. & OYELERE, A. K. 2012. Targeted cancer therapy: giving histone deacetylase inhibitors all they need to succeed. *Future medicinal chemistry,* 4**,** 505-524.

GUTIERREZ, O., PIPAON, C., INOHARA, N., FONTALBA, A., OGURA, Y., PROSPER, F., NUNEZ, G. & FERNANDEZ-LUNA, J. L. 2002. Induction of Nod2 in myelomonocytic and intestinal epithelial cells via nuclear factor-kappa B activation. *J Biol Chem,* 277**,** 41701-5.

HABERLAND, M., MONTGOMERY, R. L. & OLSON, E. N. 2009. The many roles of histone deacetylases in development and physiology: implications for disease and therapy. *Nature reviews. Genetics,* 10**,** 32-42.

HAHN, J. S. 2005. Regulation of Nod1 by Hsp90 chaperone complex. *FEBS Lett,* 579**,** 4513-9.

HAMZAOUI, K., ABID, H., BERRAIES, A., AMMAR, J. & HAMZAOUI, A. 2012. NOD2 is highly expressed in Behcet disease with pulmonary manifestations. *Journal of Inflammation,* 9**,** 3.

HANSEN, J. D., VOJTECH, L. N. & LAING, K. J. 2011. Sensing disease and danger: A survey of vertebrate PRRs and their origins. *Developmental & Comparative Immunology,* 35**,** 886-897.

HARDISON, S. E. & BROWN, G. D. 2012. C-type lectin receptors orchestrate antifungal immunity. *Nat Immunol,* 13**,** 817-22.

HASEGAWA, M., FUJIMOTO, Y., LUCAS, P. C., NAKANO, H., FUKASE, K., NUNEZ, G. & INOHARA, N. 2008. A critical role of RICK/RIP2 polyubiquitination in Nod-induced NF-kappaB activation. *EMBO J,* 27**,** 373-83.

HE, S. & WANG, X. 2018. RIP kinases as modulators of inflammation and immunity. *Nature Immunology,* 19**,** 912-922.

HE, Y. F., LI, B. Z., LI, Z., LIU, P., WANG, Y., TANG, Q., DING, J., JIA, Y., CHEN, Z., LI, L., SUN, Y., LI, X., DAI, Q., SONG, C. X., ZHANG, K., HE, C. & XU, G. L. 2011. Tet-mediated formation of 5-carboxylcytosine and its excision by TDG in mammalian DNA. *Science,* 333**,** 1303-7.

HELLGREN, K., ILIADOU, A., ROSENQUIST, R., FELTELIUS, N., BACKLIN, C., ENBLAD, G., ASKLING, J. & BAECKLUND, E. 2010. Rheumatoid arthritis, treatment with corticosteroids and risk of malignant lymphomas: results from a case-control study. *Ann Rheum Dis,* 69**,** 654-9.

HENNESSY, C. & MCKERNAN, D. P. 2016. Epigenetics and innate immunity: the 'unTolld' story. *Immunol Cell Biol,* 94**,** 631-9.

HISAMATSU, T., SUZUKI, M. & PODOLSKY, D. K. 2003. Interferon-γ Augments CARD4/NOD1 Gene and Protein Expression through Interferon Regulatory Factor-1 in Intestinal Epithelial Cells. *Journal of Biological Chemistry,* 278**,** 32962-32968.

HITOTSUMATSU, O., AHMAD, R.-C., TAVARES, R., WANG, M., PHILPOTT, D., TURER, E. E., LEE, B. L., SHIFFIN, N., ADVINCULA, R., MALYNN, B. A., WERTS, C. & MA, A. 2008. The Ubiquitin-Editing Enzyme A20 Restricts Nucleotide-Binding Oligomerization Domain Containing 2-Triggered Signals. *Immunity,* 28**,** 381-390.

HOLD, G. L., SMITH, M., GRANGE, C., WATT, E. R., EL-OMAR, E. M. & MUKHOPADHYA, I. 2014. Role of the gut microbiota in inflammatory bowel disease pathogenesis: what have we learnt in the past 10 years? *World J Gastroenterol,* 20**,** 1192-210.

HOVING, J. C., WILSON, G. J. & BROWN, G. D. 2014. Signalling C-type lectin receptors, microbial recognition and immunity. *Cellular microbiology,* 16**,** 185-194.

HSU, L. C., ALI, S. R., MCGILLIVRAY, S., TSENG, P. H., MARIATHASAN, S., HUMKE, E. W., ECKMANN, L., POWELL, J. J., NIZET, V., DIXIT, V. M. & KARIN, M. 2008. A NOD2-NALP1 complex mediates caspase-1-dependent IL-1beta secretion in response to Bacillus anthracis infection and muramyl dipeptide. *Proc Natl Acad Sci U S A,* 105**,** 7803-8.

HU, S., YOU, X., CAO, P., LIU, Z. & CUI, Y. 2013. The expression of NOD1 and NOD2 and the regulation of glucocorticoids on them in allergic rhinitis. *Lin Chung Er Bi Yan Hou Tou Jing Wai Ke Za Zhi,* 27**,** 393-6.

HUBER, R., PANTERODT, T., WELZ, B., CHRISTMANN, M., FRIESENHAGEN, J., WESTPHAL, A., PIETSCH, D. & BRAND, K. 2015. C/EBPbeta-LAP*/LAP Expression Is Mediated by RSK/eIF4B-Dependent Signalling and Boosted by Increased Protein Stability in Models of Monocytic Differentiation. *PLoS One,* 10**,** e0144338.

HUGOT, J.-P., CHAMAILLARD, M., ZOUALI, H., LESAGE, S., CEZARD, J.-P., BELAICHE, J., ALMER, S., TYSK, C., O'MORAIN, C. A., GASSULL, M., BINDER, V., FINKEL, Y., CORTOT, A., MODIGLIANI, R., LAURENT-PUIG, P., GOWER-ROUSSEAU, C., MACRY, J., COLOMBEL, J.-F., SAHBATOU, M. &

THOMAS, G. 2001. Association of NOD2 leucine-rich repeat variants with susceptibility to Crohn's disease. *Nature,* 411**,** 599-603.

HUGOT, J.-P., ZACCARIA, I., CAVANAUGH, J., YANG, H., VERMEIRE, S., LAPPALAINEN, M., SCHREIBER, S., ANNESE, V., JEWELL, D. P., FOWLER, E. V., BRANT, S. R., SILVERBERG, M. S., CHO, J., RIOUX, J. D., SATSANGI, J. & PARKES, M. 2007. Prevalence of CARD15/NOD2 Mutations in Caucasian Healthy People. *Am J Gastroenterol,* 102**,** 1259-1267.

HUMMEL-EISENBEISS, J., HASCHER, A., HALS, P. A., SANDVOLD, M. L., MULLER-TIDOW, C., LYKO, F. & RIUS, M. 2013. The role of human equilibrative nucleoside transporter 1 on the cellular transport of the DNA methyltransferase inhibitors 5-azacytidine and CP-4200 in human leukemia cells. *Mol Pharmacol,* 84**,** 438-50.

INGERSOLL, S. A., AYYADURAI, S., CHARANIA, M. A., LAROUI, H., YAN, Y. & MERLIN, D. 2012. The role and pathophysiological relevance of membrane transporter PepT1 in intestinal inflammation and inflammatory bowel disease. *American Journal of Physiology - Gastrointestinal and Liver Physiology,* 302**,** G484-G492.

INOHARA, N., CHAMAILLARD, M., MCDONALD, C. & NUÑEZ, G. 2005. NOD-LRR proteins: Role in host-microbial interactions and inflammatory disease. *Annual Review of Biochemistry,* 74**,** 355-383.

INOHARA, N., OGURA, Y., CHEN, F. F., MUTO, A. & NUÑEZ, G. 2001. Human Nod1 Confers Responsiveness to Bacterial Lipopolysaccharides. *Journal of Biological Chemistry,* 276**,** 2551-2554.

INOHARA, N., OGURA, Y., FONTALBA, A., GUTIERREZ, O., PONS, F., CRESPO, J., FUKASE, K., INAMURA, S., KUSUMOTO, S., HASHIMOTO, M., FOSTER, S. J., MORAN, A. P., FERNANDEZ-LUNA, J. L. & NUÑEZ, G. 2003. Host recognition of bacterial muramyl dipeptide mediated through NOD2: Implications for Crohn's disease. *Journal of Biological Chemistry,* 278**,** 5509-5512.

IRIZARRY, R. A., LADD-ACOSTA, C., WEN, B., WU, Z., MONTANO, C., ONYANGO, P., CUI, H., GABO, K., RONGIONE, M., WEBSTER, M., JI, H., POTASH, J. B., SABUNCIYAN, S. & FEINBERG, A. P. 2009. The human colon cancer methylome shows similar hypo- and hypermethylation at conserved tissue-specific CpG island shores. *Nat Genet,* 41**,** 178-86.

ISMAIR, M. G., VAVRICKA, S. R., KULLAK-UBLICK, G. A., FRIED, M., MENGIN-LECREULX, D. & GIRARDIN, S. E. 2006. hPepT1 selectively transports muramyl dipeptide but not Nod1-activating muramyl peptides. *Canadian Journal of Physiology and Pharmacology,* 84**,** 1313-1319.

ISSA, J. P. & KANTARJIAN, H. M. 2009. Targeting DNA methylation. *Clin Cancer Res,* 15**,** 3938-46.

ITALIANI, P. & BORASCHI, D. 2014. From Monocytes to M1/M2 Macrophages: Phenotypical vs. Functional Differentiation. *Frontiers in immunology,* 5**,** 514-514.

IYER, J. K. & COGGESHALL, K. M. 2011. Cutting edge: primary innate immune cells respond efficiently to polymeric peptidoglycan, but not to peptidoglycan monomers. *J Immunol,* 186**,** 3841-5.

JABLONKA, E. & LAMB, M. J. 2002. The changing concept of epigenetics. *Ann N Y Acad Sci,* 981**,** 82-96.

JANSSEN, W. J. & HENSON, P. M. 2012. Cellular regulation of the inflammatory response. *Toxicol Pathol,* 40**,** 166-73.

JIA, W., WHITEHEAD, R. N., GRIFFITHS, L., DAWSON, C., BAI, H., WARING, R. H., RAMSDEN, D. B., HUNTER, J. O., CAUCHI, M., BESSANT, C., FOWLER, D. P., WALTON, C., TURNER, C. & COLE, J. A. 2012. Diversity and distribution of sulphate-reducing bacteria in human faeces from healthy subjects and patients with inflammatory bowel disease. *FEMS Immunology & Medical Microbiology,* 65**,** 55-68.

JIANG, H., WONG, C.-Y. A., ABEL, P. W., SCOFIELD, M. A., XIE, Y., WEI, T. & TU, Y. 2016. Phorbol Myristate Acetate Suppresses Breast Cancer Cell Growth via Down-regulation of P-Rex1 Expression. *The FASEB Journal,* 30**,** lb490-lb490.

JIANG, Y. & FLEET, J. C. 2012. Effect of phorbol 12-myristate 13-acetate activated signaling pathways on 1α, 25 dihydroxyvitamin D3 regulated human 25-hydroxyvitamin D3 24-hydroxylase gene expression in differentiated Caco-2 cells. *Journal of cellular biochemistry,* 113**,** 1599-1607.

JONES, P. A. 2012. Functions of DNA methylation: islands, start sites, gene bodies and beyond. *Nat Rev Genet,* 13**,** 484-92.

JONES, P. A. & LIANG, G. 2009. Rethinking how DNA methylation patterns are maintained. *Nat Rev Genet,* 10**,** 805-11.

JONES, P. A. & TAYLOR, S. M. 1980. Cellular differentiation, cytidine analogs and DNA methylation. *Cell,* 20**,** 85-93.

KAMINSKAS, E., FARRELL, A., ABRAHAM, S., BAIRD, A., HSIEH, L.-S., LEE, S.-L., LEIGHTON, J. K., PATEL, H., RAHMAN, A., SRIDHARA, R., WANG, Y.-C. & PAZDUR, R. 2005. Approval Summary: Azacitidine for Treatment of Myelodysplastic Syndrome Subtypes. *Clinical Cancer Research,* 11**,** 3604-3608.

KANNEGANTI, T. D., LAMKANFI, M. & NUNEZ, G. 2007. Intracellular NOD-like receptors in host defense and disease. *Immunity,* 27**,** 549-59.

KANNO, S., NISHIO, H., TANAKA, T., MOTOMURA, Y., MURATA, K., IHARA, K., ONIMARU, M., YAMASAKI, S., KONO, H., SUEISHI, K. & HARA, T. 2015. Activation of an Innate Immune Receptor, Nod1, Accelerates Atherogenesis in Apoe−/− Mice. *The Journal of Immunology,* 194**,** 773-780.

KAPARAKIS, M., TURNBULL, L., CARNEIRO, L., FIRTH, S., COLEMAN, H. A., PARKINGTON, H. C., LE BOURHIS, L., KARRAR, A., VIALA, J., MAK, J., HUTTON, M. L., DAVIES, J. K., CRACK, P. J., HERTZOG, P. J., PHILPOTT, D. J., GIRARDIN, S. E., WHITCHURCH, C. B. & FERRERO, R. L. 2010. Bacterial membrane vesicles deliver peptidoglycan to NOD1 in epithelial cells. *Cellular Microbiology,* 12**,** 372-385.

KARAHOCA, M. & MOMPARLER, R. L. 2013. Pharmacokinetic and pharmacodynamic analysis of 5-aza-2'-deoxycytidine (decitabine) in the design of its dose-schedule for cancer therapy. *Clinical epigenetics,* 5**,** 3-3.

KARATZAS, P. S., GAZOULI, M., SAFIOLEAS, M. & MANTZARIS, G. J. 2014. DNA methylation changes in inflammatory bowel disease. *Annals of gastroenterology,* 27**,** 125-132.

KAROUZAKIS, E., RENGEL, Y., JUNGEL, A., KOLLING, C., GAY, R. E., MICHEL, B. A., TAK, P. P., GAY, S., NEIDHART, M. & OSPELT, C. 2011. DNA methylation regulates the expression of CXCL12 in rheumatoid arthritis synovial fibroblasts. *Genes Immun,* 12**,** 643-652.

KATZ, J. A. 2004. Treatment of inflammatory bowel disease with corticosteroids. *Gastroenterol Clin North Am,* 33**,** 171-89, vii.

KAWAI, T. & AKIRA, S. 2009a. The roles of TLRs, RLRs and NLRs in pathogen recognition. *Int Immunol,* 21**,** 317-37.

KAWAI, T. & AKIRA, S. 2009b. The roles of TLRs, RLRs and NLRs in pathogen recognition ARTICLE. *International Immunology,* 21**,** 317-337.

KAWASAKI, T. & KAWAI, T. 2014. Toll-like receptor signaling pathways. *Frontiers in immunology,* 5**,** 461-461.

KERSSE, K., BERTRAND, M. J. M., LAMKANFI, M. & VANDENABEELE, P. 2011. NOD-like receptors and the innate immune system: Coping with danger, damage and death. *Cytokine & Growth Factor Reviews,* 22**,** 257-276.

KIM, J. G., LEE, S. J. & KAGNOFF, M. F. 2004. Nod1 is an essential signal transducer in intestinal epithelial cells infected with bacteria that avoid recognition by toll-like receptors. *Infect Immun,* 72**,** 1487-95.

KIM, Y.-G., SHAW, M. H., WARNER, N., PARK, J.-H., CHEN, F., OGURA, Y. & NÚÑEZ, G. 2011. Cutting Edge: Crohn's Disease-Associated Nod2 Mutation Limits Production of Proinflammatory Cytokines To Protect the Host from Enterococcus faecalis-Induced Lethality. *The Journal of Immunology,* 187**,** 2849-2852.

KIM, Y. K., SHIN, J.-S. & NAHM, M. H. 2016. NOD-Like Receptors in Infection, Immunity, and Diseases. *Yonsei Med J,* 57**,** 5-14.

KOBAYASHI, K. S., CHAMAILLARD, M., OGURA, Y., HENEGARIU, O., INOHARA, N., NUNEZ, G. & FLAVELL, R. A. 2005. Nod2-dependent regulation of innate and adaptive immunity in the intestinal tract. *Science,* 307**,** 731-4.

KONSOULA, Z. & BARILE, F. A. 2012a. Epigenetic histone acetylation and deacetylation mechanisms in experimental models of neurodegenerative disorders. *J Pharmacol Toxicol Methods,* 66**,** 215-20.

KONSOULA, Z. & BARILE, F. A. 2012b. Epigenetic histone acetylation and deacetylation mechanisms in experimental models of neurodegenerative disorders. *Journal of Pharmacological and Toxicological Methods,* 66**,** 215-220.

KUFER, T. A., KREMMER, E., BANKS, D. J. & PHILPOTT, D. J. 2006. Role for erbin in bacterial activation of Nod2. *Infect Immun,* 74**,** 3115-24.

KUO, H. K., GRIFFITH, J. D. & KREUZER, K. N. 2007. 5-Azacytidine induced methyltransferase-DNA adducts block DNA replication in vivo. *Cancer Res,* 67**,** 8248-54.

LAPPAS, M. 2014. NOD1 expression is increased in the adipose tissue of women with gestational diabetes. *Journal of Endocrinology,* 222**,** 99-112.

LEE, E. G., BOONE, D. L., CHAI, S., LIBBY, S. L., CHIEN, M., LODOLCE, J. P. & MA, A. 2000. Failure to Regulate TNF-Induced NF-κB and Cell Death Responses in A20-Deficient Mice. *Science (New York, N.Y.),* 289**,** 2350-2354.

LEE, J., TATTOLI, I., WOJTAL, K. A., VAVRICKA, S. R., PHILPOTT, D. J. & GIRARDIN, S. E. 2009. pH-dependent internalization of muramyl peptides from early endosomes enables Nod1 and Nod2 signaling. *The Journal of biological chemistry,* 284**,** 23818-23829.

LEE, K. H., BISWAS, A., LIU, Y. J. & KOBAYASHI, K. S. 2012. Proteasomal degradation of Nod2 protein mediates tolerance to bacterial cell wall components. *J Biol Chem,* 287**,** 39800-11.

LEONE, G., D'ALO, F., ZARDO, G., VOSO, M. T. & NERVI, C. 2008. Epigenetic treatment of myelodysplastic syndromes and acute myeloid leukemias. *Curr Med Chem,* 15**,** 1274-87.

LEUNG, C.-H., LAM, W., MA, D.-L., GULLEN, E. A. & CHENG, Y.-C. 2009a. Butyrate mediates nucleotide-binding and oligomerisation domain (NOD) 2-dependent mucosal immune responses against peptidoglycan. *European Journal of Immunology,* 39**,** 3529-3537.

LEUNG, C. H., LAM, W., MA, D. L., GULLEN, E. A. & CHENG, Y. C. 2009b. Butyrate mediates nucleotide-binding and oligomerisation domain (NOD) 2-dependent mucosal immune responses against peptidoglycan. *Eur J Immunol,* 39**,** 3529-37.

LI, H., CHIAPPINELLI, K. B., GUZZETTA, A. A., EASWARAN, H., YEN, R. W., VATAPALLI, R., TOPPER, M. J., LUO, J., CONNOLLY, R. M., AZAD, N. S., STEARNS, V., PARDOLL, D. M., DAVIDSON, N., JONES, P. A., SLAMON, D. J., BAYLIN, S. B., ZAHNOW, C. A. & AHUJA, N. 2014. Immune regulation by low doses of the DNA methyltransferase inhibitor 5-azacitidine in common human epithelial cancers. *Oncotarget,* 5**,** 587-98.

LI, J., WANG, F., ZHANG, H.-J., SHENG, J.-Q., YAN, W.-F., MA, M.-X., FAN, R.-Y., GU, F., LI, C.-F., CHEN, D.-F., ZHENG, P., GU, Y.-P., CAO, Q., YANG, H., QIAN, J.-M., HU, P.-J. & XIA, B. 2015. Corticosteroid therapy in ulcerative colitis: Clinical response and predictors. *World journal of gastroenterology,* 21**,** 3005-3015.

LI, L. H., OLIN, E. J., BUSKIRK, H. H. & REINEKE, L. M. 1970. Cytotoxicity and Mode of Action of 5-Azacytidine on L1210 Leukemia. *Cancer Research,* 30**,** 2760-2769.

LISTA, S., GARACI, F. G., TOSCHI, N. & HAMPEL, H. 2013. Imaging epigenetics in Alzheimer's disease. *Curr Pharm Des,* 19**,** 6393-415.

LISTER, R., PELIZZOLA, M., DOWEN, R. H., HAWKINS, R. D., HON, G., TONTI-FILIPPINI, J., NERY, J. R., LEE, L., YE, Z., NGO, Q. M., EDSALL, L., ANTOSIEWICZ-BOURGET, J., STEWART, R., RUOTTI, V., MILLAR, A. H., THOMSON, J. A., REN, B. & ECKER, J. R. 2009. Human DNA methylomes at base resolution show widespread epigenomic differences. *Nature,* 462**,** 315-22.

LIU, H.-Q., ZHANG, X.-Y., EDFELDT, K., NIJHUIS, M. O., IDBORG, H., BÄCK, M., ROY, J., HEDIN, U., JAKOBSSON, P.-J., LAMAN, J. D., DE KLEIJN, D. P., PASTERKAMP, G., HANSSON, G. K. & YAN, Z.-Q. 2013. NOD2-Mediated Innate Immune Signaling Regulates the Eicosanoids in Atherosclerosis. *Arteriosclerosis, Thrombosis, and Vascular Biology,* 33**,** 2193-2201.

LIU, J., LIU, Y. Y., LIU, J., LI, B. Z., CEN, H., XU, W. D., LENG, R. X., PAN, H. F. & YE, D. Q. 2015. Association between CARD8 rs2043211 polymorphism and inflammatory bowel disease: a meta-analysis. *Immunol Invest,* 44**,** 253-64.

LIVAK, K. J. & SCHMITTGEN, T. D. 2001. Analysis of relative gene expression data using real-time quantitative PCR and the 2(-Delta Delta C(T)) Method. *Methods,* 25**,** 402-8.

LOO, Y.-M. & GALE, M., JR. 2011. Immune signaling by RIG-I-like receptors. *Immunity,* 34**,** 680-692.

LU, J., MCKINSEY, T. A., NICOL, R. L. & OLSON, E. N. 2000a. Signal-dependent activation of the MEF2 transcription factor by dissociation from histone deacetylases. *Proc Natl Acad Sci U S A,* 97**,** 4070-5.

LU, J., MCKINSEY, T. A., ZHANG, C. L. & OLSON, E. N. 2000b. Regulation of skeletal myogenesis by association of the MEF2 transcription factor with class II histone deacetylases. *Mol Cell,* 6**,** 233-44.

LUND, M. E., TO, J., O'BRIEN, B. A. & DONNELLY, S. 2016. The choice of phorbol 12-myristate 13-acetate differentiation protocol influences the response of THP-1 macrophages to a pro-inflammatory stimulus. *Journal of Immunological Methods,* 430**,** 64-70.

LYKO, F. & BROWN, R. 2005a. DNA Methyltransferase Inhibitors and the Development of Epigenetic Cancer Therapies. *Journal of the National Cancer Institute,* 97**,** 1498-1506.

LYKO, F. & BROWN, R. 2005b. DNA methyltransferase inhibitors and the development of epigenetic cancer therapies. *J Natl Cancer Inst,* 97**,** 1498-506.

MAGLINTE, D. D., GOURTSOYIANNIS, N., REX, D., HOWARD, T. J. & KELVIN, F. M. 2003. Classification of small bowel Crohn's subtypes based on multimodality imaging. *Radiol Clin North Am,* 41**,** 285-303.

MAHMOUD, L., AL-ENEZI, F., AL-SAIF, M., WARSY, A., KHABAR, K. S. A. & HITTI, E. G. 2014. Sustained stabilization of Interleukin-8 mRNA in human macrophages. *RNA Biology,* 11**,** 124-133.

MALOY, K. J. & POWRIE, F. 2011. Intestinal homeostasis and its breakdown in inflammatory bowel disease. *Nature,* 474**,** 298-306.

MANICHANH, C., RIGOTTIER-GOIS, L., BONNAUD, E., GLOUX, K., PELLETIER, E., FRANGEUL, L., NALIN, R., JARRIN, C., CHARDON, P., MARTEAU, P., ROCA, J. & DORE, J. 2006. Reduced diversity of faecal microbiota in Crohn's disease revealed by a metagenomic approach. *Gut,* 55**,** 205-211.

MANN, B. S., JOHNSON, J. R., COHEN, M. H., JUSTICE, R. & PAZDUR, R. 2007. FDA Approval Summary: Vorinostat for Treatment of Advanced Primary Cutaneous T-Cell Lymphoma. *The Oncologist,* 12**,** 1247-1252.

MANON, F., FAVIER, A., NUNEZ, G., SIMORRE, J. P. & CUSACK, S. 2007. Solution structure of NOD1 CARD and mutational analysis of its interaction with the CARD of downstream kinase RICK. *J Mol Biol,* 365**,** 160-74.

MARKS, P. A. & BRESLOW, R. 2007. Dimethyl sulfoxide to vorinostat: development of this histone deacetylase inhibitor as an anticancer drug. *Nature Biotechnology,* 25**,** 84.

MARKS, P. A. & DOKMANOVIC, M. 2005. Histone deacetylase inhibitors: discovery and development as anticancer agents. *Expert Opin Investig Drugs,* 14**,** 1497-511.

MARKS, P. A., RIFKIND, R. A., RICHON, V. M., BRESLOW, R., MILLER, T. & KELLY, W. K. 2001. Histone deacetylases and cancer: causes and therapies. *Nature Reviews Cancer,* 1**,** 194.

MARTINON, F. & TSCHOPP, J. 2005. NLRs join TLRs as innate sensors of pathogens. *Trends in Immunology,* 26**,** 447-454.

MAYLE, S., BOYLE, J. P., SEKINE, E., ZUREK, B., KUFER, T. A. & MONIE, T. P. 2014. Engagement of nucleotide-binding oligomerization domain-containing protein 1 (NOD1) by receptor-interacting protein 2 (RIP2) is insufficient for signal transduction. *J Biol Chem,* 289**,** 22900-14.

MCDERMOTT, E., RYAN, E. J., TOSETTO, M., GIBSON, D., BURRAGE, J., KEEGAN, D., BYRNE, K., CROWE, E., SEXTON, G., MALONE, K., HARRIS, R. A., KELLERMAYER, R., MILL, J., CULLEN, G., DOHERTY, G. A., MULCAHY, H. & MURPHY, T. M. 2016. DNA Methylation Profiling in Inflammatory Bowel Disease Provides New Insights into Disease Pathogenesis. *Journal of Crohn's & colitis,* 10**,** 77-86.

MCDONALD, C., CHEN, F. F., OLLENDORFF, V., OGURA, Y., MARCHETTO, S., LÉCINE, P., BORG, J.-P. & NUÑEZ, G. 2005. A Role for Erbin in the Regulation of Nod2-dependent NF-κB Signaling. *Journal of Biological Chemistry,* 280**,** 40301-40309.

MEDZHITOV, R., PRESTON-HURLBURT, P. & JANEWAY, C. A. 1997. A human homologue of the Drosophila Toll protein signals activation of adaptive immunity. *Nature,* 388**,** 394-397.

MICELI-RICHARD, C., LESAGE, S., RYBOJAD, M., PRIEUR, A. M., MANOUVRIER-HANU, S., HAFNER, R., CHAMAILLARD, M., ZOUALI, H., THOMAS, G. & HUGOT, J. P. 2001. CARD15 mutations in Blau syndrome. *Nat Genet,* 29**,** 19-20.

MISKA, E. A., KARLSSON, C., LANGLEY, E., NIELSEN, S. J., PINES, J. & KOUZARIDES, T. 1999. HDAC4 deacetylase associates with and represses the MEF2 transcription factor. *EMBO J,* 18**,** 5099-107.

MOHANAN, V. & GRIMES, C. L. 2014. Hsp70 binds to and stabilizes Nod2, an innate immune receptor involved in Crohn's disease. *Journal of Biological Chemistry*.

MOREIRA, L. O. & ZAMBONI, D. S. 2012. NOD1 and NOD2 Signaling in Infection and Inflammation. *Frontiers in immunology,* 3**,** 328-328.

MUSONE, S. L., TAYLOR, K. E., NITITHAM, J., CHU, C., POON, A., LIAO, W., LAM, E. T., MA, A., KWOK, P. Y. & CRISWELL, L. A. 2011. Sequencing of TNFAIP3 and association of variants with multiple autoimmune diseases. *Genes Immun,* 12**,** 176-82.

NIMMO, E. R., PRENDERGAST, J. G., ALDHOUS, M. C., KENNEDY, N. A., HENDERSON, P., DRUMMOND, H. E., RAMSAHOYE, B. H., WILSON, D. C., SEMPLE, C. A. & SATSANGI, J. 2012. Genome-wide methylation profiling in Crohn's disease identifies altered epigenetic regulation of key host defense mechanisms including the Th17 pathway. *Inflammatory Bowel Diseases,* 18**,** 889-899.

NISHIO, H., KANNO, S., ONOYAMA, S., IKEDA, K., TANAKA, T., KUSUHARA, K., FUJIMOTO, Y., FUKASE, K., SUEISHI, K. & HARA, T. 2011. Nod1 Ligands Induce Site-Specific Vascular Inflammation. *Arteriosclerosis, Thrombosis, and Vascular Biology,* 31**,** 1093-1099.

OGURA, Y., BONEN, D. K., INOHARA, N., NICOLAE, D. L., CHEN, F. F., RAMOS, R., BRITTON, H., MORAN, T., KARALIUSKAS, R., DUERR, R. H., ACHKAR, J.-P., BRANT, S. R., BAYLESS, T. M., KIRSCHNER, B. S., HANAUER, S. B., NUNEZ, G. & CHO, J. H. 2001a. A frameshift mutation in NOD2 associated with susceptibility to Crohn's disease. *Nature,* 411**,** 603-606.

OGURA, Y., INOHARA, N., BENITO, A., CHEN, F. F., YAMAOKA, S. & NÚÑEZ, G. 2001b. Nod2, a Nod1/Apaf-1 Family Member That Is Restricted to Monocytes and Activates NF-κB. *Journal of Biological Chemistry,* 276**,** 4812-4818.

OGURA, Y., LALA, S., XIN, W., SMITH, E., DOWDS, T. A., CHEN, F. F., ZIMMERMANN, E., TRETIAKOVA, M., CHO, J. H., HART, J., GREENSON, J. K., KESHAV, S. & NUNEZ, G. 2003. Expression of NOD2 in Paneth cells: a possible link to Crohn's ileitis. *Gut,* 52**,** 1591-7.

OPITZ, B., PUSCHEL, A., BEERMANN, W., HOCKE, A. C., FORSTER, S., SCHMECK, B., VAN LAAK, V., CHAKRABORTY, T., SUTTORP, N. & HIPPENSTIEL, S. 2006. Listeria monocytogenes activated p38 MAPK and induced IL-8 secretion in a nucleotide-binding oligomerization domain 1-dependent manner in endothelial cells. *J Immunol,* 176**,** 484-90.

OPPENHEIM, J. J. & YANG, D. 2005. Alarmins: chemotactic activators of immune responses. *Current Opinion in Immunology,* 17**,** 359-365.

OSAKO, M., ITSUMI, M., YAMAGUCHI, H., TAKEUCHI, H. & YAMAOKA, S. 2017. A20 restores phorbol ester-induced differentiation of THP-1 cells in the absence of nuclear factor-κB activation. *Journal of Cellular Biochemistry,* 119**,** 1475-1487.

OSPELT, C., BRENTANO, F., JUNGEL, A., RENGEL, Y., KOLLING, C., MICHEL, B. A., GAY, R. E. & GAY, S. 2009. Expression, regulation, and signaling of the pattern-recognition receptor nucleotide-binding oligomerization domain 2 in rheumatoid arthritis synovial fibroblasts. *Arthritis Rheum,* 60**,** 355-63.

OTT, S. J., MUSFELDT, M., WENDEROTH, D. F., HAMPE, J., BRANT, O., FÖLSCH, U. R., TIMMIS, K. N. & SCHREIBER, S. 2004. Reduction in diversity of the colonic mucosa associated bacterial microflora in patients with active inflammatory bowel disease. *Gut,* 53**,** 685-693.

PANJA, A., GOLDBERG, S., ECKMANN, L., KRISHEN, P. & MAYER, L. 1998. The Regulation and Functional Consequence of Proinflammatory Cytokine Binding on Human Intestinal Epithelial Cells. *The Journal of Immunology,* 161**,** 3675-3684.

PARAMEL, G. V., FOLKERSEN, L., STRAWBRIDGE, R. J., ELMABSOUT, A. A., SARNDAHL, E., LUNDMAN, P., JANSSON, J. H., HANSSON, G. K., SIRSJO, A. & FRANSEN, K. 2013. CARD8 gene encoding a protein of innate immunity is expressed in human atherosclerosis and associated with markers of inflammation. *Clin Sci (Lond),* 125**,** 401-7.

PARIHAR, A., EUBANK, T. D. & DOSEFF, A. I. 2010. Monocytes and macrophages regulate immunity through dynamic networks of survival and cell death. *Journal of innate immunity,* 2**,** 204-215.

PARK, J. H., KIM, Y. G., MCDONALD, C., KANNEGANTI, T. D., HASEGAWA, M., BODY-MALAPEL, M., INOHARA, N. & NUNEZ, G. 2007. RICK/RIP2 mediates innate immune responses induced through Nod1 and Nod2 but not TLRs. *J Immunol,* 178**,** 2380-6.

PEART, M. J., SMYTH, G. K., VAN LAAR, R. K., BOWTELL, D. D., RICHON, V. M., MARKS, P. A., HOLLOWAY, A. J. & JOHNSTONE, R. W. 2005. Identification and functional significance of genes regulated by structurally different histone deacetylase inhibitors. *Proceedings of the National Academy of Sciences of the United States of America,* 102**,** 3697-3702.

PORTELA, A. & ESTELLER, M. 2010. Epigenetic modifications and human disease. *Nat Biotechnol,* 28**,** 1057-68.

PORTELA, A. & ESTELLER, M. 2011. Epigenetic modifications and human disease. *Nat Biotechnol,* 28**,** 1057-68.

PROBST, A. V., DUNLEAVY, E. & ALMOUZNI, G. 2009. Epigenetic inheritance during the cell cycle. *Nat Rev Mol Cell Biol,* 10**,** 192-206.

QUINTÁS-CARDAMA, A., SANTOS, F. P. S. & GARCIA-MANERO, G. 2010. Therapy with azanucleosides for myelodysplastic syndromes. *Nature Reviews Clinical Oncology,* 7**,** 433.

RAJ, K. & MUFTI, G. J. 2006. Azacytidine (Vidaza(R)) in the treatment of myelodysplastic syndromes. *Therapeutics and clinical risk management,* 2**,** 377-388.

RAMANAN, D., TANG, M. S., BOWCUTT, R., LOKE, P. & CADWELL, K. 2014. Bacterial sensor Nod2 prevents inflammation of the small intestine by restricting the expansion of the commensal Bacteroides vulgatus. *Immunity,* 41**,** 311-24.

REHMAN, A., SINA, C., GAVRILOVA, O., HASLER, R., OTT, S., BAINES, J. F., SCHREIBER, S. & ROSENSTIEL, P. 2011. Nod2 is essential for temporal development of intestinal microbial communities. *Gut,* 60**,** 1354-62.

RHEE, I., BACHMAN, K. E., PARK, B. H., JAIR, K. W., YEN, R. W., SCHUEBEL, K. E., CUI, H., FEINBERG, A. P., LENGAUER, C., KINZLER, K. W., BAYLIN, S. B. & VOGELSTEIN, B. 2002. DNMT1 and DNMT3b cooperate to silence genes in human cancer cells. *Nature,* 416**,** 552-6.

RICHMOND, A. L., KABI, A., HOMER, C. R., MARINA-GARCIA, N., NICKERSON, K. P., NESVIZHSKII, A. I., SREEKUMAR, A., CHINNAIYAN, A. M., NUNEZ, G. & MCDONALD, C. 2012. The nucleotide synthesis enzyme CAD inhibits NOD2 antibacterial function in human intestinal epithelial cells. *Gastroenterology,* 142**,** 1483-92 e6.

RICHON, V. M., SANDHOFF, T. W., RIFKIND, R. A. & MARKS, P. A. 2000. Histone deacetylase inhibitor selectively induces p21WAF1 expression and gene-associated histone acetylation. *Proceedings of the National Academy of Sciences of the United States of America,* 97**,** 10014-10019.

RIGGS, M. G., WHITTAKER, R. G., NEUMANN, J. R. & INGRAM, V. M. 1977. n-Butyrate causes histone modification in HeLa and Friend erythroleukaemia cells. *Nature,* 268**,** 462-4.

RIUS, M., STRESEMANN, C., KELLER, D., BROM, M., SCHIRRMACHER, E., KEPPLER, D. & LYKO, F. 2009a. Human concentrative nucleoside transporter 1-mediated uptake of 5-azacytidine enhances DNA demethylation. *Mol Cancer Ther,* 8**,** 225-31.

RIUS, M., STRESEMANN, C., KELLER, D., BROM, M., SCHIRRMACHER, E., KEPPLER, D. & LYKO, F. 2009b. Human concentrative nucleoside transporter 1-mediated uptake of 5-azacytidine enhances DNA demethylation. *Molecular Cancer Therapeutics,* 8**,** 225-231.

ROSENSTIEL, P., FANTINI, M., BRAUTIGAM, K., KUHBACHER, T., WAETZIG, G. H., SEEGERT, D. & SCHREIBER, S. 2003. TNF-alpha and IFN-gamma regulate the expression of the NOD2 (CARD15) gene in human intestinal epithelial cells. *Gastroenterology,* 124**,** 1001-9.

ROSS, R. 1999. Atherosclerosis--an inflammatory disease. *N Engl J Med,* 340**,** 115-26.

RUSSELL, R. K., NIMMO, E. R. & SATSANGI, J. 2004. Molecular genetics of Crohn's disease. *Current Opinion in Genetics & Development,* 14**,** 264-270.

RUTHENBURG, A. J., LI, H., PATEL, D. J. & ALLIS, C. D. 2007. Multivalent engagement of chromatin modifications by linked binding modules. *Nat Rev Mol Cell Biol,* 8**,** 983-94.

SASAWATARI, S., OKAMURA, T., KASUMI, E., TANAKA-FURUYAMA, K., YANOBU-TAKANASHI, R., SHIRASAWA, S., KATO, N. & TOYAMA-SORIMACHI, N. 2011. The solute carrier family 15A4 regulates TLR9 and NOD1 functions in the innate immune system and promotes colitis in mice. *Gastroenterology,* 140**,** 1513-25.

SAXONOV, S., BERG, P. & BRUTLAG, D. L. 2006. A genome-wide analysis of CpG dinucleotides in the human genome distinguishes two distinct classes of promoters. *Proc Natl Acad Sci U S A,* 103**,** 1412-7.

SCHAFFLER, H., DEMIRCIOGLU, D. D., KUHNER, D., MENZ, S., BENDER, A., AUTENRIETH, I. B., BODAMMER, P., LAMPRECHT, G., GOTZ, F. & FRICK, J. S. 2014. NOD2 stimulation by Staphylococcus aureus-derived peptidoglycan is boosted by Toll-like receptor 2 costimulation with lipoproteins in dendritic cells. *Infect Immun,* 82**,** 4681-8.

SCHEPPACH, W., SOMMER, H., KIRCHNER, T., PAGANELLI, G. M., BARTRAM, P., CHRISTL, S., RICHTER, F., DUSEL, G. & KASPER, H. 1992. Effect of butyrate enemas on the colonic mucosa in distal ulcerative colitis. *Gastroenterology,* 103**,** 51-6.

SEKSIK, P., RIGOTTIER-GOIS, L., GRAMET, G., SUTREN, M., POCHART, P., MARTEAU, P., JIAN, R. & DORÉ, J. 2003. Alterations of the dominant faecal bacterial groups in patients with Crohn's disease of the colon. *Gut,* 52**,** 237-242.

SHAHBAZIAN, M. D. & GRUNSTEIN, M. 2007. Functions of site-specific histone acetylation and deacetylation. *Annu Rev Biochem,* 76**,** 75-100.

SHAW, M. H., REIMER, T., KIM, Y.-G. & NUÑEZ, G. 2008. NOD-like receptors (NLRs): bona fide intracellular microbial sensors. *Current Opinion in Immunology,* 20**,** 377-382.

SILHAVY, T. J., KAHNE, D. & WALKER, S. 2010. The bacterial cell envelope. *Cold Spring Harbor perspectives in biology,* 2**,** a000414-a000414.

SIMMS, L. A., DOECKE, J. D., WALSH, M. D., HUANG, N., FOWLER, E. V. & RADFORD-SMITH, G. L. 2008. Reduced alpha-defensin expression is associated with inflammation and not NOD2 mutation status in ileal Crohn's disease. *Gut,* 57**,** 903-10.

SKINNER, M. K. 2011. Role of epigenetics in developmental biology and transgenerational inheritance. *Birth defects research. Part C, Embryo today : reviews,* 93**,** 51-55.

SMITH, E., JONES, M. E. & DREW, P. A. 2009. Quantitation of DNA methylation by melt curve analysis. *BMC cancer,* 9**,** 123-123.

SPARROW, D. B., MISKA, E. A., LANGLEY, E., REYNAUD-DEONAUTH, S., KOTECHA, S., TOWERS, N., SPOHR, G., KOUZARIDES, T. & MOHUN, T. J. 1999. MEF-2 function is modified by a novel co-repressor, MITR. *EMBO J,* 18**,** 5085-98.

STELIOU, K., BOOSALIS, M. S., PERRINE, S. P., SANGERMAN, J. & FALLER, D. V. 2012. Butyrate histone deacetylase inhibitors. *BioResearch open access,* 1**,** 192-198.

STELMACH, R., NUNES, M. D. P. T., RIBEIRO, M. & CUKIER, A. 2005. Effect of Treating Allergic Rhinitis With Corticosteroids in Patients With Mild-to-Moderate Persistent Asthma. *CHEST,* 128**,** 3140-3147.

TAHILIANI, M., KOH, K. P., SHEN, Y., PASTOR, W. A., BANDUKWALA, H., BRUDNO, Y., AGARWAL, S., IYER, L. M., LIU, D. R., ARAVIND, L. & RAO, A. 2009. Conversion of 5-methylcytosine to 5-hydroxymethylcytosine in mammalian DNA by MLL partner TET1. *Science,* 324**,** 930-5.

TAKADA, H., YOKOYAMA, S. & YANG, S. 2002. Enhancement of endotoxin activity by muramyldipeptide. *J Endotoxin Res,* 8**,** 337-42.

TALKINGTON, D. F. 2013. Real-time PCR in Food Science: Current Technology and Applications. *Emerging Infectious Diseases,* 19**,** 1352-1353.

TARAKHOVSKY, A. 2010. Tools and landscapes of epigenetics. *Nature Immunology,* 11**,** 565.

TERAO, Y., NISHIDA, J., HORIUCHI, S., RONG, F., UEOKA, Y., MATSUDA, T., KATO, H., FURUGEN, Y., YOSHIDA, K., KATO, K. & WAKE, N. 2001. Sodium butyrate induces growth arrest and senescence-like phenotypes in gynecologic cancer cells. *Int J Cancer,* 94**,** 257-67.

THOMPSON, M. R., KAMINSKI, J. J., KURT-JONES, E. A. & FITZGERALD, K. A. 2011. Pattern recognition receptors and the innate immune response to viral infection. *Viruses,* 3**,** 920-940.

TIGNO-ARANJUEZ, J. T., ASARA, J. M. & ABBOTT, D. W. 2010. Inhibition of RIP2's tyrosine kinase activity limits NOD2-driven cytokine responses. *Genes Dev,* 24**,** 2666-77.

TING, J. P., LOVERING, R. C., ALNEMRI, E. S., BERTIN, J., BOSS, J. M., DAVIS, B. K., FLAVELL, R. A., GIRARDIN, S. E., GODZIK, A., HARTON, J. A., HOFFMAN, H. M., HUGOT, J. P., INOHARA, N., MACKENZIE, A., MALTAIS, L. J., NUNEZ, G., OGURA, Y., OTTEN, L. A., PHILPOTT, D., REED, J. C., REITH, W., SCHREIBER, S., STEIMLE, V. & WARD, P. A. 2008. The NLR gene family: a standard nomenclature. *Immunity,* 28**,** 285-7.

TRAUB, S., KUBASCH, N., MORATH, S., KRESSE, M., HARTUNG, T., SCHMIDT, R. R. & HERMANN, C. 2004. Structural requirements of synthetic muropeptides to synergize with lipopolysaccharide in cytokine induction. *J Biol Chem,* 279**,** 8694-700.

TROMP, G., KUIVANIEMI, H., RAPHAEL, S., ALA-KOKKO, L., CHRISTIANO, A., CONSIDINE, E., DHULIPALA, R., HYLAND, J., JOKINEN, A., KIVIRIKKO, S., KORN, R., MADHATHERI, S., MCCARRON, S., PULKKINEN, L., PUNNETT, H., SHIMOYA, K., SPOTILA, L., TATE, A. & WILLIAMS, C. J. 1996. Genetic linkage of familial granulomatous inflammatory arthritis, skin rash, and uveitis to chromosome 16. *Am J Hum Genet,* 59**,** 1097-107.

TSAPROUNI, L. G., ITO, K., POWELL, J. J., ADCOCK, I. M. & PUNCHARD, N. 2011. Differential patterns of histone acetylation in inflammatory bowel diseases. *Journal of inflammation (London, England),* 8**,** 1-1.

TURNER, M. D., NEDJAI, B., HURST, T. & PENNINGTON, D. J. 2014. Cytokines and chemokines: At the crossroads of cell signalling and inflammatory disease. *Biochim Biophys Acta,* 1843**,** 2563-2582.

UNGERSTEDT, J. S., SOWA, Y., XU, W. S., SHAO, Y., DOKMANOVIC, M., PEREZ, G., NGO, L., HOLMGREN, A., JIANG, X. & MARKS, P. A. 2005. Role of thioredoxin in the response of normal and transformed cells to histone deacetylase inhibitors. *Proc Natl Acad Sci U S A,* 102**,** 673-8.

VANDENABEELE, P. & BERTRAND, M. J. 2012. The role of the IAP E3 ubiquitin ligases in regulating pattern-recognition receptor signalling. *Nat Rev Immunol,* 12**,** 833-44.

VAVRICKA, S. R., MUSCH, M. W., CHANG, J. E., NAKAGAWA, Y., PHANVIJHITSIRI, K., WAYPA, T. S., MERLIN, D., SCHNEEWIND, O. & CHANG, E. B. 2004. hPepT1 transports muramyl dipeptide, activating NF-κB and stimulating IL-8 secretion in human colonic Caco2/bbe cells. *Gastroenterology,* 127**,** 1401-1409.

VEGA, R. B., HARRISON, B. C., MEADOWS, E., ROBERTS, C. R., PAPST, P. J., OLSON, E. N. & MCKINSEY, T. A. 2004a. Protein kinases C and D mediate agonist-dependent cardiac hypertrophy through nuclear export of histone deacetylase 5. *Mol Cell Biol,* 24**,** 8374-85.

VEGA, R. B., MATSUDA, K., OH, J., BARBOSA, A. C., YANG, X., MEADOWS, E., MCANALLY, J., POMAJZL, C., SHELTON, J. M., RICHARDSON, J. A., KARSENTY, G. & OLSON, E. N. 2004b. Histone deacetylase 4 controls chondrocyte hypertrophy during skeletogenesis. *Cell,* 119**,** 555-66.

VEREECKE, L., SZE, M., MC GUIRE, C., ROGIERS, B., CHU, Y., SCHMIDT-SUPPRIAN, M., PASPARAKIS, M., BEYAERT, R. & VAN LOO, G. 2010. Enterocyte-specific A20 deficiency sensitizes to tumor necrosis factor-induced toxicity and experimental colitis. *J Exp Med,* 207**,** 1513-23.

VERMA, R., VERMA, N. & PAUL, J. 2013. Expression of inflammatory genes in the colon of ulcerative colitis patients varies with activity both at the mRNA and protein level. *Eur Cytokine Netw,* 24**,** 130-8.

VIALA, J., CHAPUT, C., BONECA, I. G., CARDONA, A., GIRARDIN, S. E., MORAN, A. P., ATHMAN, R., MEMET, S., HUERRE, M. R., COYLE, A. J., DISTEFANO, P. S., SANSONETTI, P. J., LABIGNE, A., BERTIN, J., PHILPOTT, D. J. & FERRERO, R. L. 2004. Nod1 responds to peptidoglycan delivered by the Helicobacter pylori cag pathogenicity island. *Nat Immunol,* 5**,** 1166-74.

VON KAMPEN, O., LIPINSKI, S., TILL, A., MARTIN, S. J., NIETFELD, W., LEHRACH, H., SCHREIBER, S. & ROSENSTIEL, P. 2010. Caspase recruitment domain-containing protein 8 (CARD8) negatively regulates NOD2-mediated signaling. *J Biol Chem,* 285**,** 19921-6.

WALLNER, S., SCHRÖDER, C., LEITÃO, E., BERULAVA, T., HAAK, C., BEIßER, D., RAHMANN, S., RICHTER, A. S., MANKE, T., BÖNISCH, U., ARRIGONI, L., FRÖHLER, S., KLIRONOMOS, F., CHEN, W., RAJEWSKY, N., MÜLLER, F., EBERT, P., LENGAUER, T., BARANN, M., ROSENSTIEL, P., GASPARONI, G., NORDSTRÖM, K., WALTER, J., BRORS, B., ZIPPRICH, G., FELDER, B., KLEIN-HITPASS, L., ATTENBERGER, C., SCHMITZ, G. & HORSTHEMKE, B. 2016. Epigenetic dynamics of monocyte-to-macrophage differentiation. *Epigenetics & chromatin,* 9**,** 33-33.

WATANABE, T., ASANO, N., KITANI, A., FUSS, I. J., CHIBA, T. & STROBER, W. 2011. Activation of type I IFN signaling by NOD1 mediates mucosal host defense against Helicobacter pylori infection. *Gut Microbes,* 2**,** 61-5.

WATANABE, T., KITANI, A., MURRAY, P. J. & STROBER, W. 2004. NOD2 is a negative regulator of Toll-like receptor 2-mediated T helper type 1 responses. *Nature immunology,* 5**,** 800-808.

WEHKAMP, J., HARDER, J., WEICHENTHAL, M., SCHWAB, M., SCHÄFFELER, E., SCHLEE, M., HERRLINGER, K. R., STALLMACH, A., NOACK, F., FRITZ, P., SCHRÖDER, J. M., BEVINS, C. L., FELLERMANN, K. & STANGE, E. F. 2004. NOD2 (CARD15) mutations in Crohn's disease are associated with diminished mucosal α-defensin expression. *Gut,* 53**,** 1658-1664.

WEHKAMP, J., SALZMAN, N. H., PORTER, E., NUDING, S., WEICHENTHAL, M., PETRAS, R. E., SHEN, B., SCHAEFFELER, E., SCHWAB, M., LINZMEIER, R., FEATHERS, R. W., CHU, H., LIMA, H., FELLERMANN, K., GANZ, T., STANGE, E. F. & BEVINS, C. L. 2005. Reduced Paneth cell α-defensins in ileal Crohn's disease. *Proceedings of the National Academy of Sciences of the United States of America,* 102**,** 18129-18134.

WILLIAMS, K., CHRISTENSEN, J. & HELIN, K. 2012. DNA methylation: TET proteins—guardians of CpG islands? *EMBO Reports,* 13**,** 28-35.

WILSON, A. S., POWER, B. E. & MOLLOY, P. L. 2007. DNA hypomethylation and human diseases. *Biochimica et Biophysica Acta (BBA) - Reviews on Cancer,* 1775**,** 138-162.

WOLFKAMP, S. C., VERSEYDEN, C., VOGELS, E. W., MEISNER, S., BOONSTRA, K., PETERS, C. P., STOKKERS, P. C. & TE VELDE, A. A. 2014. ATG16L1 and NOD2 polymorphisms enhance phagocytosis in monocytes of Crohn's disease patients. *World J Gastroenterol,* 20**,** 2664-72.

WU, P., GENG, S., WENG, J., DENG, C., LU, Z., LUO, C. & DU, X. 2015. The hENT1 and DCK genes underlie the decitabine response in patients with myelodysplastic syndrome. *Leukemia Research,* 39**,** 216-220.

XU, W. S., PARMIGIANI, R. B. & MARKS, P. A. 2007. Histone deacetylase inhibitors: molecular mechanisms of action. *Oncogene,* 26**,** 5541.

XU, W. S., PEREZ, G., NGO, L., GUI, C. Y. & MARKS, P. A. 2005. Induction of polyploidy by histone deacetylase inhibitor: a pathway for antitumor effects. *Cancer Res,* 65**,** 7832-9.

YAMAOKA, S., COURTOIS, G., BESSIA, C., WHITESIDE, S. T., WEIL, R., AGOU, F., KIRK, H. E., KAY, R. J. & ISRAËL, A. 1998. Complementation Cloning of NEMO, a Component of the IκB Kinase Complex Essential for NF-κB Activation. *Cell,* 93**,** 1231-1240.

YAN, P., FRANKHOUSER, D., MURPHY, M., TAM, H.-H., RODRIGUEZ, B., CURFMAN, J., TRIMARCHI, M., GEYER, S., WU, Y.-Z., WHITMAN, S. P., METZELER, K., WALKER, A., KLISOVIC, R., JACOB, S., GREVER, M. R., BYRD, J. C., BLOOMFIELD, C. D., GARZON, R., BLUM, W., CALIGIURI, M. A., BUNDSCHUH, R. & MARCUCCI, G. 2012. Genome-wide methylation profiling in decitabine-treated patients with acute myeloid leukemia. *Blood,* 120**,** 2466-2474.

YANG, L., TANG, Z., ZHANG, H., KOU, W., LU, Z., LI, X., LI, Q. & MIAO, Z. 2013. PSMA7 Directly Interacts with NOD1 and Regulates its Function. *Cellular Physiology and Biochemistry,* 31**,** 952-959.

YANG, X., LAY, F., HAN, H. & JONES, P. A. 2010. Targeting DNA methylation for epigenetic therapy. *Trends in Pharmacological Sciences,* 31**,** 536-546.

YOKOTA, K., MIYAZAKI, T., HEMMATAZAD, H., GAY, R. E., KOLLING, C., FEARON, U., SUZUKI, H., MIMURA, T., GAY, S. & OSPELT, C. 2012. The pattern-recognition receptor nucleotide-binding oligomerization domain--containing protein 1 promotes production of inflammatory mediators in rheumatoid arthritis synovial fibroblasts. *Arthritis Rheum,* 64**,** 1329-37.

YU, N.-K., BAEK, S. H. & KAANG, B.-K. 2011. DNA methylation-mediated control of learning and memory. *Molecular brain,* 4**,** 5-5.

ZHANG, C. L., MCKINSEY, T. A., CHANG, S., ANTOS, C. L., HILL, J. A. & OLSON, E. N. 2002. Class II histone deacetylases act as signal-responsive repressors of cardiac hypertrophy. *Cell,* 110**,** 479-88.

ZHANG, J., VISSER, F., KING, K. M., BALDWIN, S. A., YOUNG, J. D. & CASS, C. E. 2007. The role of nucleoside transporters in cancer chemotherapy with nucleoside drugs. *Cancer Metastasis Rev,* 26**,** 85-110.

ZHANG, R., ZHAO, J., SONG, Y., WANG, X., WANG, L., XU, J., SONG, C. & LIU, F. 2014. The E3 ligase RNF34 is a novel negative regulator of the NOD1 pathway. *Cell Physiol Biochem,* 33**,** 1954-62.

ZHANG, Y., KWON, S., YAMAGUCHI, T., CUBIZOLLES, F., ROUSSEAUX, S., KNEISSEL, M., CAO, C., LI, N., CHENG, H. L., CHUA, K., LOMBARD, D., MIZERACKI, A., MATTHIAS, G., ALT, F. W., KHOCHBIN, S. & MATTHIAS, P. 2008. Mice lacking histone deacetylase 6 have hyperacetylated tubulin but are viable and develop normally. *Mol Cell Biol,* 28**,** 1688-701.

ZHAO, L., HU, P., ZHOU, Y., PUROHIT, J. & HWANG, D. 2011. NOD1 activation induces proinflammatory gene expression and insulin resistance in 3T3-L1 adipocytes. *Am J Physiol Endocrinol Metab,* 301**,** E587-98.

ZHAO, L., KWON, M. J., HUANG, S., LEE, J. Y., FUKASE, K., INOHARA, N. & HWANG, D. H. 2007. Differential modulation of Nods signaling pathways by fatty acids in human colonic epithelial HCT116 cells. *J Biol Chem,* 282**,** 11618-28.

ZHAO, Y. M., CHEN, X., SUN, H., YUAN, Z. G., REN, G. L., LI, X. X., LU, J. & HUANG, B. Q. 2006. Effects of histone deacetylase inhibitors on transcriptional regulation of the hsp70 gene in Drosophila. *Cell Research,* 16**,** 566.

ZHENG, Y., SHANG, F., AN, L., ZHAO, H. & LIU, X. 2018. NOD2-RIP2 contributes to the inflammatory responses of mice in vivo to Streptococcus pneumoniae. *Neurosci Lett,* 671**,** 43-49.

ZHONG, Y., KINIO, A. & SALEH, M. 2013. Functions of NOD-Like Receptors in Human Diseases. *Frontiers in immunology,* 4**,** 333-333.

ZHOU, Y.-J., LIU, C., LI, C.-L., SONG, Y.-L., TANG, Y.-S., ZHOU, H., LI, A., LI, Y., WENG, Y. & ZHENG, F.-P. 2015. Increased NOD1, but not NOD2, activity in subcutaneous adipose tissue from patients with metabolic syndrome. *Obesity,* 23**,** 1394-1400.

ZOGHBI, H. Y. & BEAUDET, A. L. 2016. Epigenetics and Human Disease. *Cold Spring Harbor Perspectives in Biology,* 8.

ZUREK, B., PROELL, M., WAGNER, R. N., SCHWARZENBACHER, R. & KUFER, T. A. 2012a. Mutational analysis of human NOD1 and NOD2 NACHT domains reveals different modes of activation. *Innate Immun,* 18**,** 100-11.

ZUREK, B., SCHOULTZ, I., NEERINCX, A., NAPOLITANO, L. M., BIRKNER, K., BENNEK, E., SELLGE, G., LERM, M., MERONI, G., SODERHOLM, J. D. & KUFER, T. A. 2012b. TRIM27 negatively regulates NOD2 by ubiquitination and proteasomal degradation. *PLoS One,* 7**,** e41255.

Appendix 1 . Survival Data in HCT116 Cells

MTT assay analysis was used to establish the effect of epigenetic altering drugs (DNMT1 inhibitors and HDAC inhibitors) and NOD ligands, used in this body of research, on HCT116 viability. This was done to decipher the optimum treatment conditions with these agents to prevent excessive cell death. Viability was recorded at varying concentrations and time points.

DNMT1 inhibitors investigated included 5-Azacytidine (5-Aza) and 5-Aza-2'-deoxycytidine (5-Aza-dC). Cells were treated with 0 μM, 0.5 μM, 1 μM, 5 μM, 10 μM and 50 μM of 5-Aza for 24, 48 or 72 hours (Figure A1.1 A) or 0 nM, 100 nM, 500 nM, 1 μM, 5 μM and 50 μM of 5-Aza-dC for 24, 48 or 72 hours (Figure A1.1 B). Percentage cell viability was calculated relative to the untreated cells at 24 hours. Two-way ANOVA statistical analysis was carried out, alongside Bonferroni *post hoc* analysis, to investigate changes in cell viability. None of the 5-Aza treatments had a significant effect on cell viability ($p > 0.05$). However, viability was significantly reduced 48 hours after 1 μM (75 ± 3.1%, $p < 0.01$), 5 μM (73 ± 4.3%, $p < 0.001$) and 50 μM (61.8 ± 1.1 %, $p < 0.001$) 5-Aza-dC. Treatment with 50 μM 5-Aza-dC for 72 hours also reduced cell viability (61.8 ± 3.8%, $p < 0.001$) (Figure A1.1 B).

HDAC inhibitors investigated included suberoylanilide hydroxamic acid (SAHA) and trichostatin A (TSA). Cell were treated with 0 μM, 1 μM, 10 μM and 100 μM SAHA or TSA or 24, 48 or 72 hours (Figure A1.2 A-B). Percentage cell viability was calculated relative to the untreated cells at 24 hours. Two-way ANOVA statistical analysis was carried out, alongside Bonferroni *post hoc* analysis, to investigate changes in cell viability. Both HDAC inhibitors were found to be cytotoxic in a time- and dose-dependent manner. SAHA reduced viability at all time points and at all concentrations investigated (Figure A1.2 A). At 24 hours, SAHA reduced viability at 1 μM (86.7 ± 1.5%, $p < 0.001$), 10 μM (83.6 ± 1.6%, $p < 0.001$) and 100 μM (76.6 ± 1.4 %, $p < 0.001$). At 48 hours, SAHA reduced viability at 1 μM (54.2 ± 2.5%, $p < 0.001$), 10 μM (51.2 ± 1%, $p < 0.001$) and 100 μM (44.1 ± 0.8 %, $p < 0.001$). At 72 hours, SAHA reduced viability at 1 μM (38.7 ± 1%, $p < 0.001$), 10 μM (26.6 ± 0.5%, $p < 0.001$) and 100 μM (19.9 ± 1.6 %, $p < 0.001$). TSA reduced viability at all time points and at all concentrations investigated (Figure A1.2 B). At 24 hours, TSA reduced viability at 1 μM (95.1 ± 0.6%, $p < 0.01$), 10 μM (89.1 ± 0.6%, $p < 0.001$) and

100 μM (62.2 ± 1 %, $p < 0.001$). At 48 hours, TSA reduced viability at 1 μM (47.9 ± 0.5%, $p < 0.001$), 10 μM (47.3 ± 1.3%, $p < 0.001$) and 100 μM (28.3 ± 0.9 %, $p < 0.001$). At 72 hours, TSA reduced viability at 1 μM (54.1 ± 1.9%, $p < 0.001$), 10 μM (17.7 ± 1.8%, $p < 0.001$) and 100 μM (5.2 ± 1.2 %, $p < 0.001$).

NOD ligands investigated included; NOD1 ligands (iE-DAP and TRI-DAP) and a NOD2 ligand (MDP). Cells were treated with 0 ng/ml, 1 ng/ml, 10 ng/ml and 100 ng/ml of iE-DAP, TRI-DAP or MDP for 1, 3, 6 and 24 hours (Figure A1.3 A-C). Percentage cell viability was calculated relative to the 1hr untreated cells. Two-way ANOVA statistical analysis was carried out, alongside Bonferroni *post hoc* analysis, to investigate changes in cell viability. None of the NOD ligand treatments had a significant effect on cell viability ($p > 0.05$).

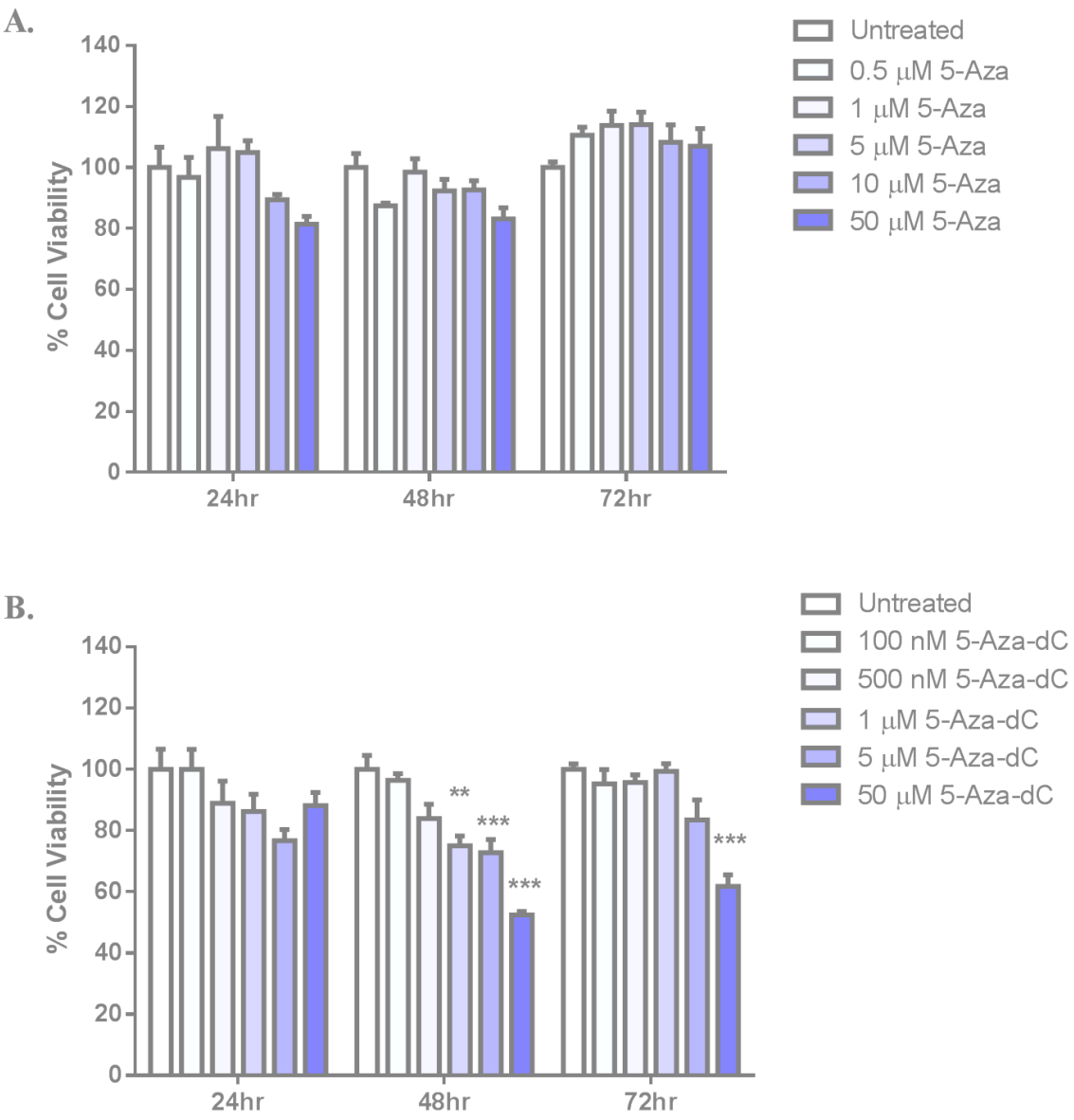

Figure A1.1. Cell viability of HCT116 cells following DNMT1 inhibitor treatment at various times and doses. A) HCT116 cells were treated with increasing doses of 5-Azacytidine (0-50μM 5-Aza) for 24, 48 or 72 hours. B) HCT116 cells were treated with increasing doses of 5-Aza-deoxycytidine (0-50μM 5-Aza-dC) for 24, 48 or 72 hours. Percentage cell viability was calculated relative to the 24 hr untreated cells (control). Data is represented as % cell viability ± SEM. Statistical analysis was performed using Two-way ANOVAs, followed by Bonferroni *post-hoc* test where appropriate. Significance was recognised at $p < 0.05$, with * representing $p < 0.05$, ** representing $p < 0.01$ and *** representing $p < 0.001$ **(control vs DNMT1 inhibitor).**

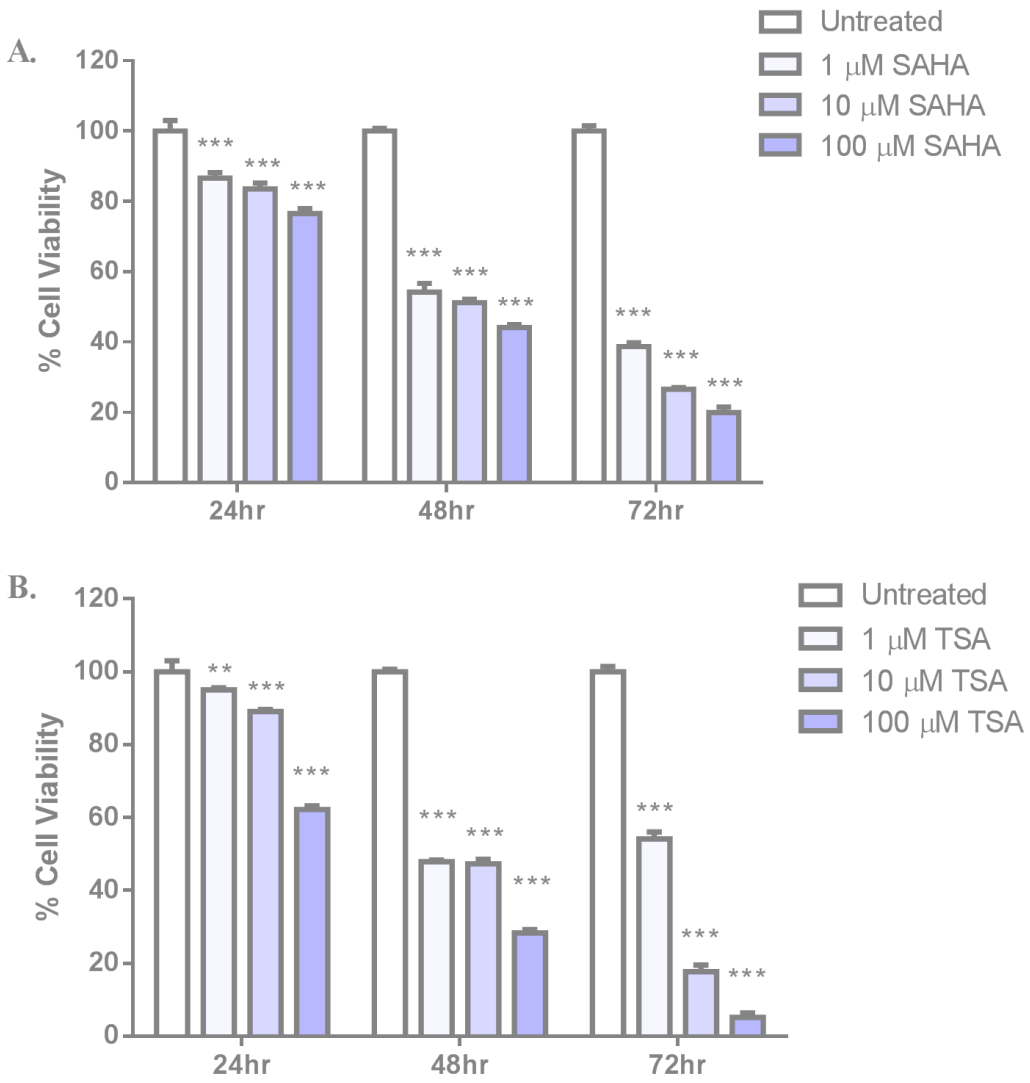

Figure A1.2. Cell viability of HCT116 cells following HDAC inhibitor treatment at various times and doses. A) HCT116 cells were treated with increasing doses of suberoylanilide hydroxamic acid (0-100 μM SAHA) for 24, 48 or 72 hours. B) HCT116 cells were treated with increasing doses of trichostatin A (0-100 μM TSA) for 24, 48 or 72 hours. Percentage cell viability was calculated relative to the 24 hr untreated cells (control). Data is represented as % cell viability ± SEM. Statistical analysis was performed using Two-way ANOVAs, followed by Bonferroni *post-hoc* test where appropriate. Significance was recognised at $p < 0.05$, with * representing $p < 0.05$, ** representing $p < 0.01$ and *** representing $p < 0.001$ **(control vs HDAC inhibitor).**

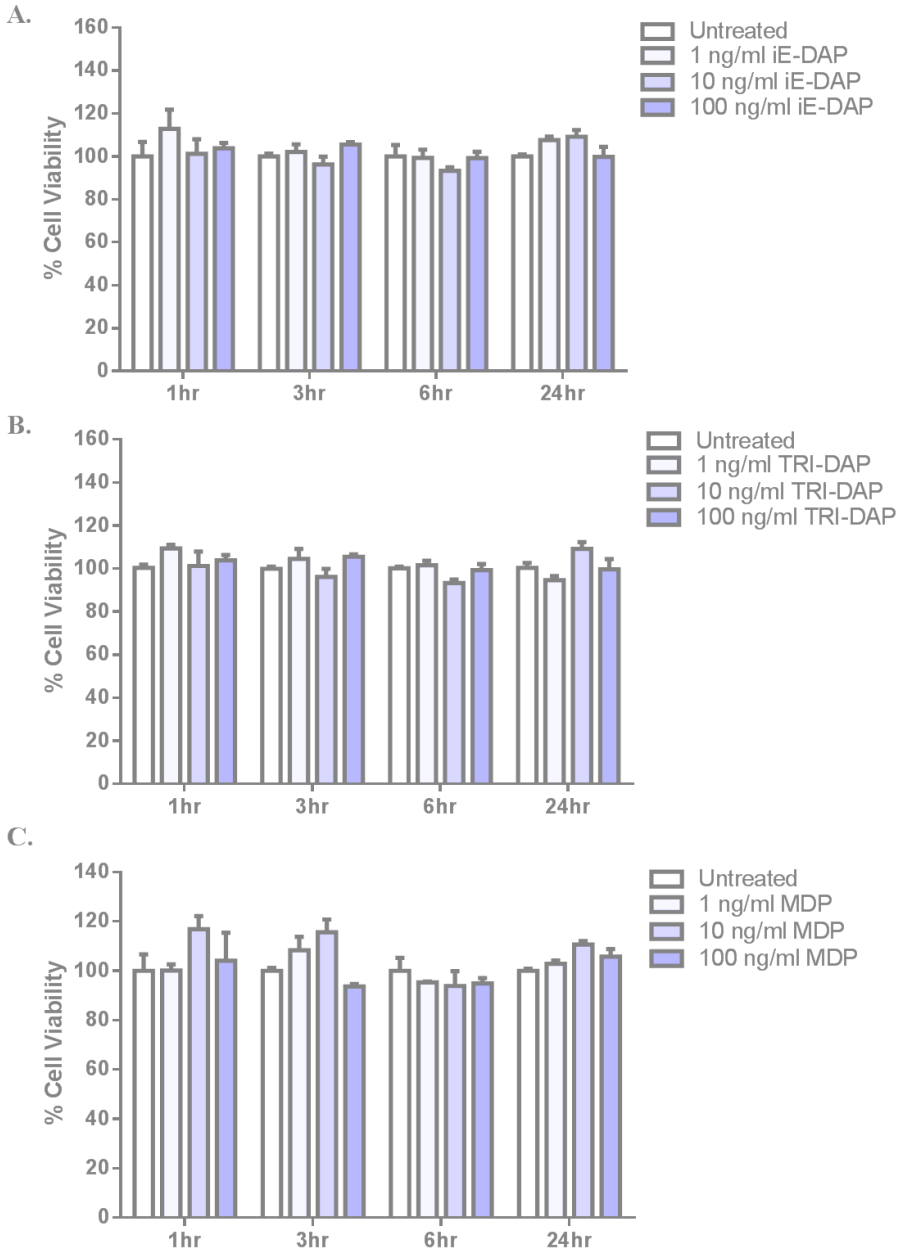

Figure A1.3. Cell viability of HCT116 cells following NOD ligand treatment at various times and doses. A-B) HCT116 cells were treated with increasing doses of NOD1 ligand (0-100 ng/ml iE-DAP/TRI-DAP) for 1, 3, 6 or 24 hours. C) HCT116 cells were treated with increasing doses of NOD2 ligand (0-100 ng/ml MDP) for 1, 3, 6 or 24 hours. Percentage cell viability was calculated relative to the 1 hr untreated cells (control). Data is represented as % cell viability ± SEM. Statistical analysis was performed using Two-way ANOVAs, followed by Bonferroni *post-hoc* test where appropriate. Significance was recognised at $p < 0.05$, with * representing $p < 0.05$, ** representing $p < 0.01$ and *** representing $p < 0.001$ **(control vs NOD ligand).**

Appendix 2 . Survival Data in THP-1 Cells

MTT assay analysis was used to establish the effect of epigenetic altering drugs (DNMT1 inhibitors and HDAC inhibitors) and NOD ligands, used in this body of research, on THP-1viability. This was done to decipher the optimum treatment conditions with these agents to prevent excessive cell death. Viability was recorded at varying concentrations and time points.

DNMT1 inhibitors investigated included 5-Azacytidine (5-Aza) and 5-Aza-2'-deoxycytidine (5-Aza-dC). Cells were treated with 0 μM, 0.5 μM, 1 μM, 5 μM, 10 μM and 50 μM of 5-Aza for 24, 48 or 72 hours (Figure A2.1 A) or 0 nM, 100 nM, 500 nM, 1 μM, 5 μM and 50 μM of 5-Aza-dC for 24, 48 or 72 hours (Figure A2.1 B). Percentage cell viability was calculated relative to the untreated cells at 24 hours. Two-way ANOVA statistical analysis was carried out, alongside Bonferroni *post hoc* analysis, to investigate changes in cell viability. None of the 5-Aza treatments had a significant effect on cell viability ($p > 0.05$). However, 5-Aza-dC reduced viability at specific times/doses (Figure A2.1 B). At 24 hours, 5-Aza-dC reduced viability at 500 nM (69.9 ± 3.1%, $p < 0.01$), 1 μM (74.2 ± 6.8%, $p < 0.05$), 5 μM (75 ± 4.9%, $p < 0.05$) and 50 μM (64.1 ± 10.8 %, $p < 0.001$). At 72 hours, 5-Aza-dC reduced viability at 1 μM (71.3 ± 3%, $p < 0.01$), 5 μM (73 ± 3.3%, $p < 0.05$) and 50 μM (74.3 ± 4.6 %, $p < 0.05$).

HDAC inhibitors investigated included suberoylanilide hydroxamic acid (SAHA) and trichostatin A (TSA). Cell were treated with 0 μM, 1 μM, 10 μM and 100 μM SAHA or TSA or 24, 48 or 72 hours (Figure A2.2 A-B). Percentage cell viability was calculated relative to the untreated cells at 24 hours. Two-way ANOVA statistical analysis was carried out, alongside Bonferroni *post hoc* analysis, to investigate changes in cell viability. Both HDAC inhibitors were found to be cytotoxic in a time- and dose-dependent manner. SAHA reduced viability at specific time points and concentrations investigated (Figure A2.2 A). At 48 hours, SAHA reduced viability at 10 μM (87 ± 6.9%, $p < 0.001$) and 100 μM (82 ± 2.7%, $p < 0.001$). At 72 hours, SAHA reduced viability at 1 μM (42 ± 1.9%, $p < 0.001$), 10 μM (39.2 ± 4%, $p < 0.001$) and 100 μM (24.6 ± 2 %, $p < 0.001$). TSA reduced viability at specific time points and concentrations investigated (Figure A2.2 B). At 48 hours, TSA reduced viability at 100 μM (41.8 ± 6.3 %, $p < 0.001$). At 72 hours, TSA reduced viability at 1 μM (49.9

± 7.8%, $p < 0.001$), 10 μM (16.2 ± 1.5%, $p < 0.001$) and 100 μM (7.2 ± 1.3 %, $p < 0.001$).

NOD ligands investigated included; NOD1 ligands (iE-DAP and TRI-DAP) and a NOD2 ligand (MDP). Cells were treated with 0 ng/ml, 1 ng/ml, 10 ng/ml and 100 ng/ml of iE-DAP, TRI-DAP or MDP for 1, 3, 6 and 24 hours (Figure A2.3 A-C). Percentage cell viability was calculated relative to the 1hr untreated cells. Two-way ANOVA statistical analysis was carried out, alongside Bonferroni *post hoc* analysis, to investigate changes in cell viability. None of the NOD ligand treatments had a significant effect on cell viability ($p > 0.05$).

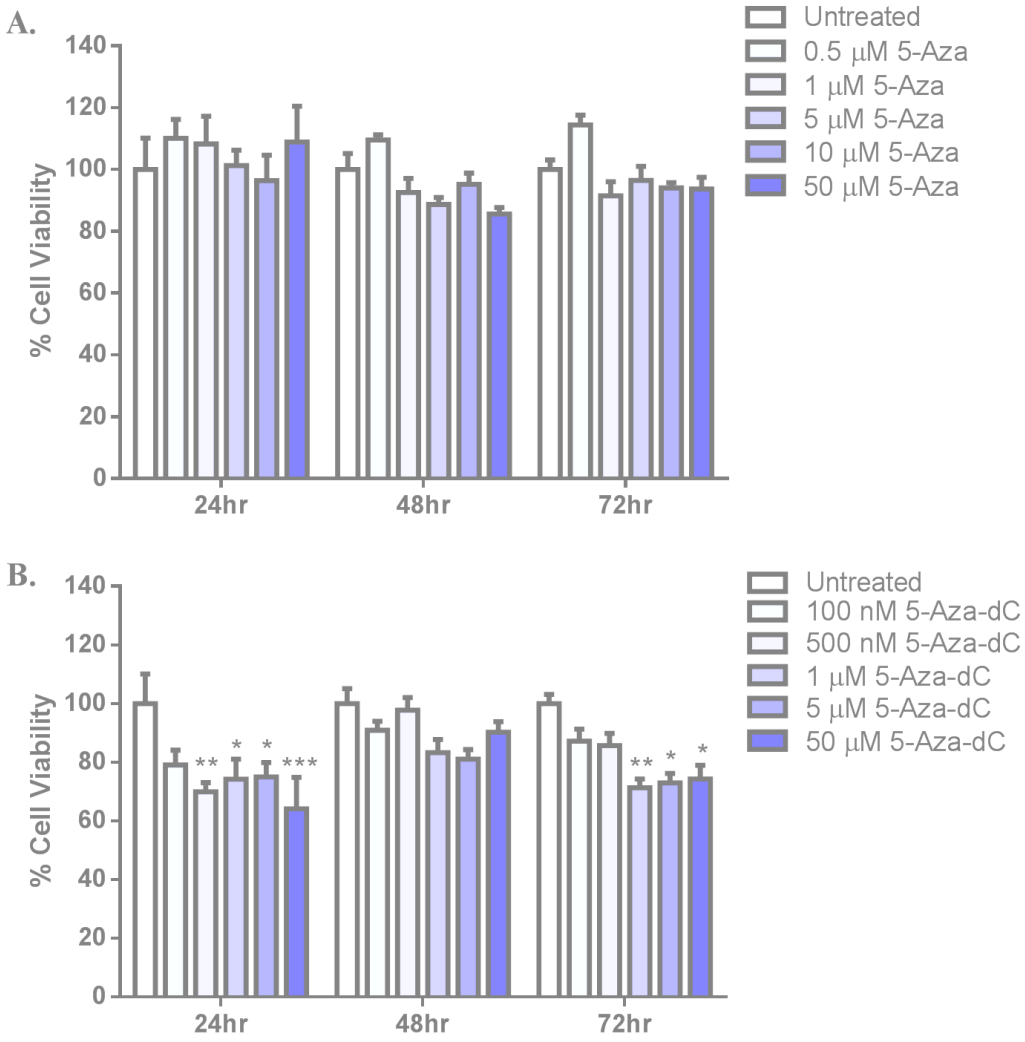

Figure A2.1. Cell viability of THP-1 cells following DNMT1 inhibitor treatment at various times and doses. A) THP-1 cells were treated with increasing doses of 5-Azacytidine (0-50μM 5-Aza) for 24, 48 or 72 hours. B) THP-1 cells were treated with increasing doses of 5-Aza-deoxycytidine (0-50μM 5-Aza-dC) for 24, 48 or 72 hours. Percentage cell viability was calculated relative to the 24 hr untreated cells (control). Data is represented as % cell viability ± SEM. Statistical analysis was performed using Two-way ANOVAs, followed by Bonferroni *post-hoc* test where appropriate. Significance was recognised at $p < 0.05$, with * representing $p < 0.05$, ** representing $p < 0.01$ and *** representing $p < 0.001$ **(control vs DNMT1 inhibitor).**

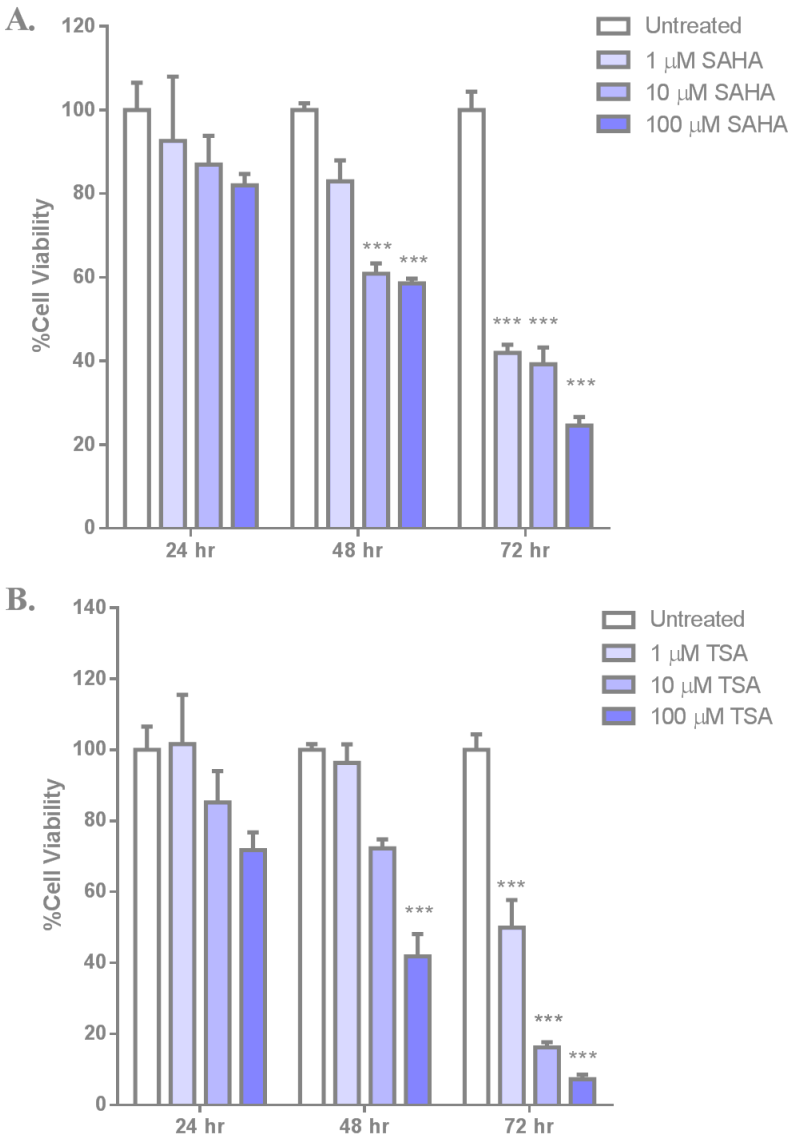

Figure A2.2. Cell viability of THP-1 cells following HDAC inhibitor treatment at various times and doses. A) THP-1 cells were treated with increasing doses of suberoylanilide hydroxamic acid (0-100 μM SAHA) for 24, 48 or 72 hours. B) THP-1 cells were treated with increasing doses of trichostatin A (0-100 μM TSA) for 24, 48 or 72 hours. Percentage cell viability was calculated relative to the 24 hr untreated cells (control). Data is represented as % cell viability ± SEM. Statistical analysis was performed using Two-way ANOVAs, followed by Bonferroni *post-hoc* test where appropriate. Significance was recognised at $p < 0.05$, with * representing $p < 0.05$, ** representing $p < 0.01$ and *** representing $p < 0.001$ **(control vs HDAC inhibitor).**

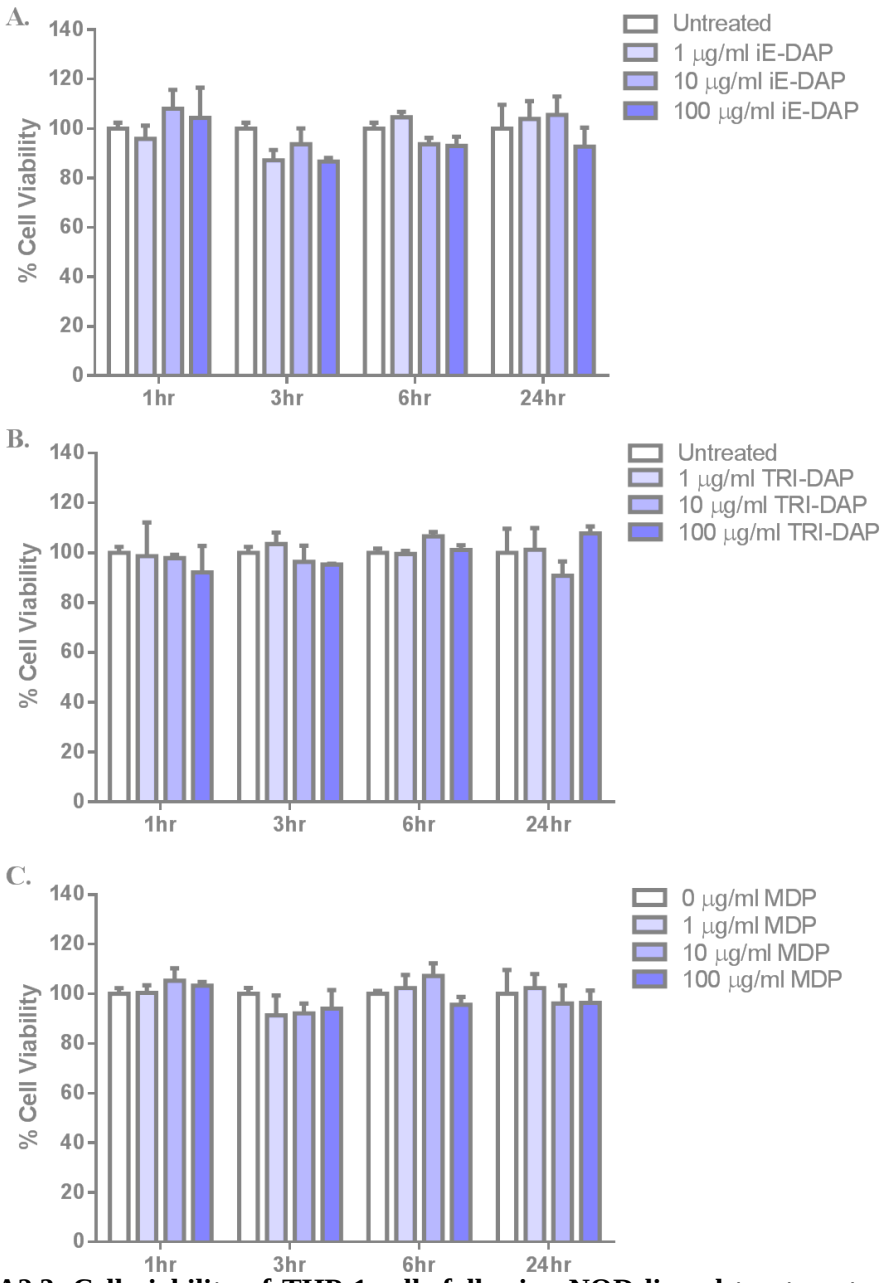

Figure A2.3. Cell viability of THP-1 cells following NOD ligand treatment at various times and doses. A-B) THP-1 cells were treated with increasing doses of NOD1 ligand (0-100 ng/ml iE-DAP/TRI-DAP) for 1, 3, 6 or 24 hours. C) THP-1 cells were treated with increasing doses of NOD2 ligand (0-100 ng/ml MDP) for 1, 3, 6 or 24 hours. Percentage cell viability was calculated relative to the 1 hr untreated cells (control). Data is represented as % cell viability ± SEM. Statistical analysis was performed using Two-way ANOVAs, followed by Bonferroni *post-hoc* test where appropriate. Significance was recognised at $p < 0.05$, with * representing $p < 0.05$, ** representing $p < 0.01$ and *** representing $p < 0.001$ **(control vs NOD ligand).**

Appendix 3 . IL-8 Time and Dose Release from HCT116 cells in response to NOD receptor activation

Release of IL-8 from HCT116 cells can be quantified by ELISA analysis to measure NOD1 and NOD2 pro-inflammatory activity in response to ligand stimulation. Time and dose response analysis was carried out to establish optimum NOD1/NOD2 stimulation times to accommodate efficient IL-8 detection.

HCT116 cells were stimulated with a NOD1 ligand (iE-DAP or TRI-DAP) or NOD2 ligand (MDP) at several concentrations (10 / 20 / 50 μg/ml) over a range of time points (6 / 18 / 24 hours). IL-8 release in response to NOD1/2 stimulation increased in a time and dose response. Significant increases in IL-8 was recorded at majority of concentrations and time points. From this time and dose response data, it was chosen that the HCT116 cells would be stimulated with 10 μg/ml iE-DAP or TRI-DAP or MDP for 18 hours.

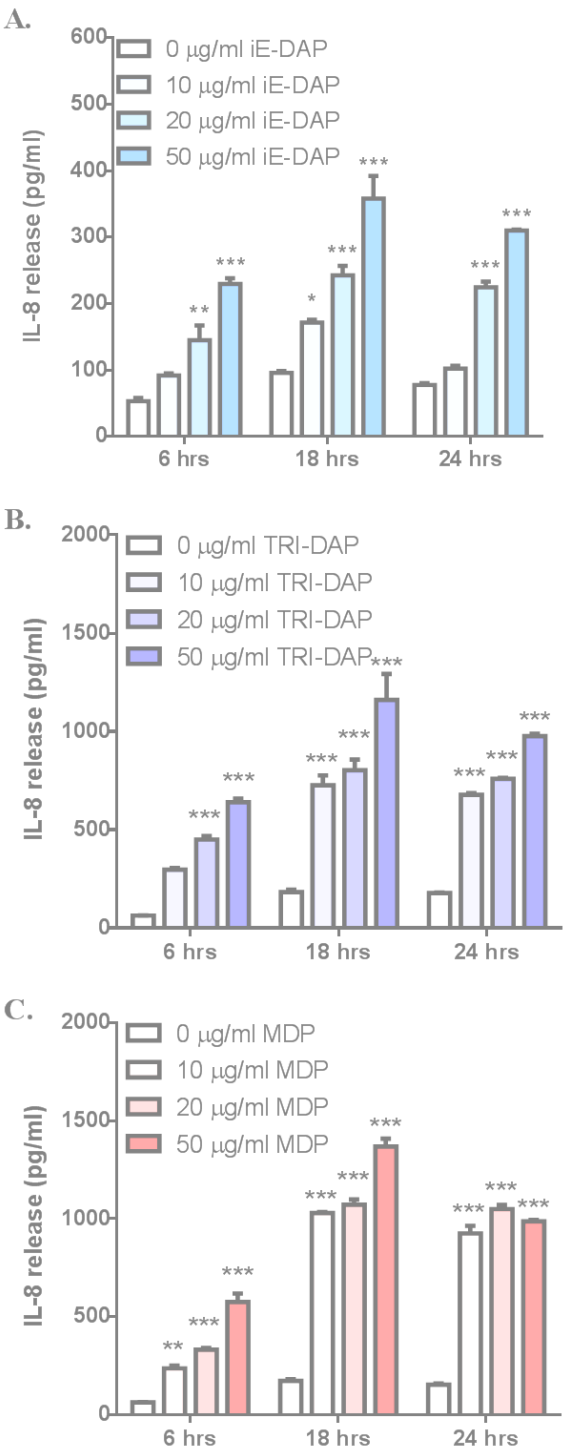

Figure A3.1. IL-8 time and dose release from HCT116 cells. IL-8 release from HCT116 cells stimulated for 6 / 18 / 24 hours with 10 / 20 / 50 µg/ml of A) iE-DAP or B) TRI-DAP or C) MDP. Data is presented as mean absolute concentrations ± S.E.M. Statistical analysis was performed using two-way ANOVAs, followed by Dunnetts *post-hoc* test where appropriate. Significance was recognised at $p < 0.05$, with * representing $p < 0.05$, ** representing $p < 0.01$ and *** representing $p < 0.001$ **(control vs NOD ligand).**

Appendix 4 . IL-8 Time and Dose Release from THP-1 cells in response to NOD receptor activation

Release of IL-8 from THP-1 cells can be quantified by ELISA analysis to measure NOD1 and NOD2 pro-inflammatory activity in response to ligand stimulation. Time and dose response analysis was carried out to establish optimum NOD1/NOD2 stimulation times to accommodate efficient IL-8 detection.

THP-1 cells were stimulated with a NOD1 ligand (iE-DAP or TRI-DAP) or NOD2 ligand (MDP) at several concentrations (10 / 20 / 50 μg/ml) over a range of time points (6 / 18 / 24 hours). IL-8 release from THP-1 cells was lower than from HCT116 cells. IL-8 release in response to NOD1/2 stimulation increased in a time and dose response. Significant increases in IL-8 was recorded at majority of concentrations and time points. From this time and dose response data, it was chosen that the THP-1 cells would be stimulated with 50 μg/ml iE-DAP or TRI-DAP or MDP for 18 hours.

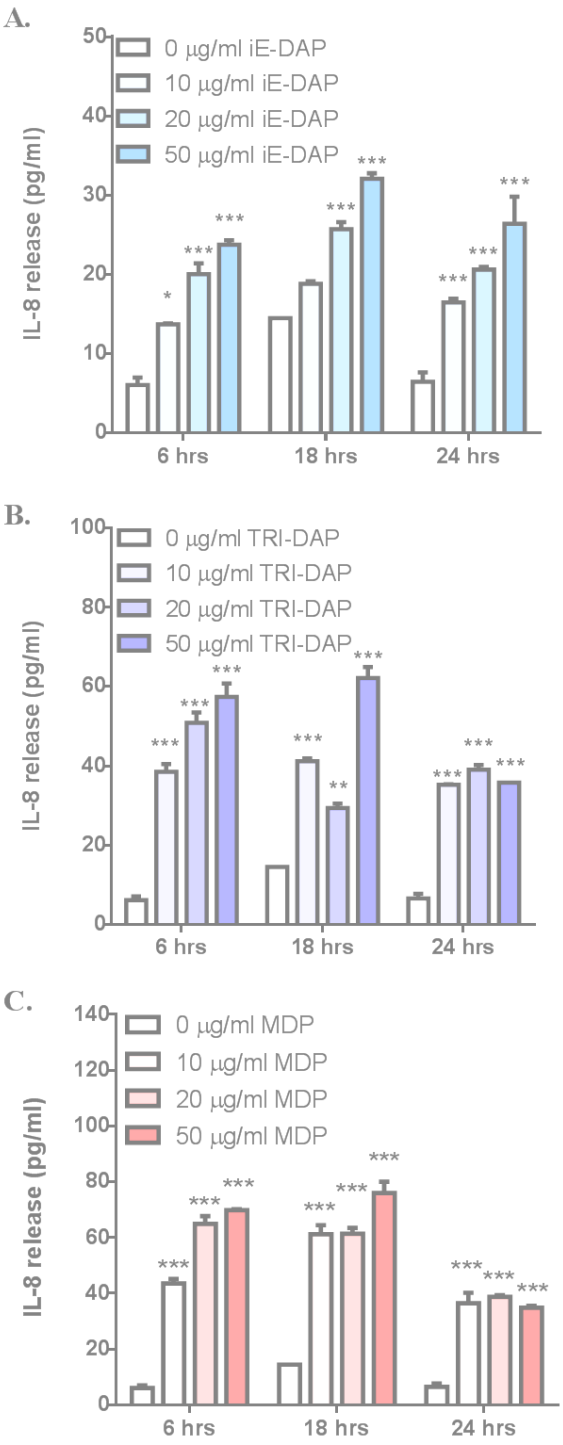

Figure A4.1. IL-8 time and dose release from THP-1 cells. IL-8 release from THP-1 cells stimulated for 6 / 18 / 24 hours with 10 / 20 / 50 µg/ml of A) iE-DAP or B) TRI-DAP or C) MDP. Data is presented as mean absolute concentrations ± S.E.M. Statistical analysis was performed using two-way ANOVAs, followed by Dunnetts *post-hoc* test where appropriate. Significance was recognised at $p < 0.05$, with * representing $p < 0.05$, ** representing $p < 0.01$ and *** representing $p < 0.001$ **(control vs NOD ligand).**

Appendix 5 . MAPK / NF-κB Phosphorylation Time Response in HCT116 cells.

Phosphorylation of MAPK and NF-κB signalling proteins can be quantified by western blot analysis to establish NOD1 and NOD2 responses to ligand stimulation. MAPK proteins (p38 and ERK) and NF-κB proteins (p65 and IκBα) are unstable in their phosphorylated state, therefore time response analysis was carried out to establish optimum NOD1/NOD2 stimulation times to accommodate their detection. HCT116 cells were stimulated with 10 μg/ml of a NOD1 ligand (iE-DAP or TRI-DAP) or NOD2 ligand (MDP) over a range of time points; 0, 5, 15, 30, 60, 90, 120, 180 and 360 minutes. Peak phosphorylation was identified from these blots, allowing an appropriate NOD1/2 stimulation time to be chosen. Phosphorylation of MAPK and NF-κB proteins generally peaked at 180 minutes following iE-DAP stimulation (Figure A5.1), 60 minutes following TRI-DAP (Figure A5.2) and 120 minutes following MDP (Figure A5.3).

Therefore, these stimulation times (3 hrs iE-DAP, 1 hr TRI-DAP and 2 hrs MDP) were used when investigating NOD1/NOD2 associated MAPK and NF-κB signalling in Chapter 3 and Chapter 4 of this research.

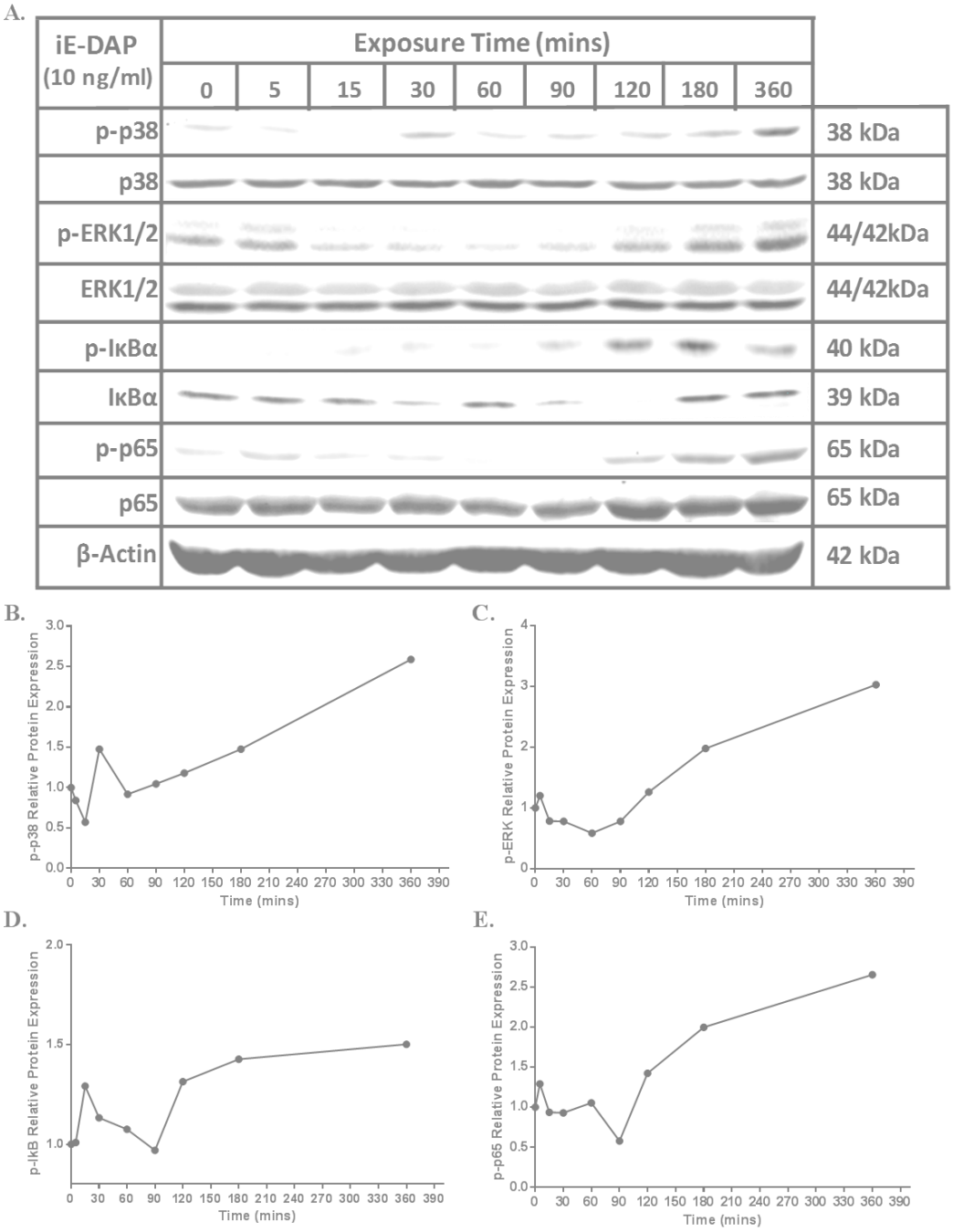

Figure A5.1. Phosphorylation time and dose response data for HCT116 cells stimulated with iE-DAP. A) Immunoblots of phosphorylated and total p38, ERK, IκBα and p65 in HCT116 cells stimulated with 10 μg/ml iE-DAP for 0, 5, 15, 30, 60, 90, 120, 180, 360 minutes. β- Actin acted as the loading control. (B-E) Densitometry of phosphorylated, relative to β-Actin expression.

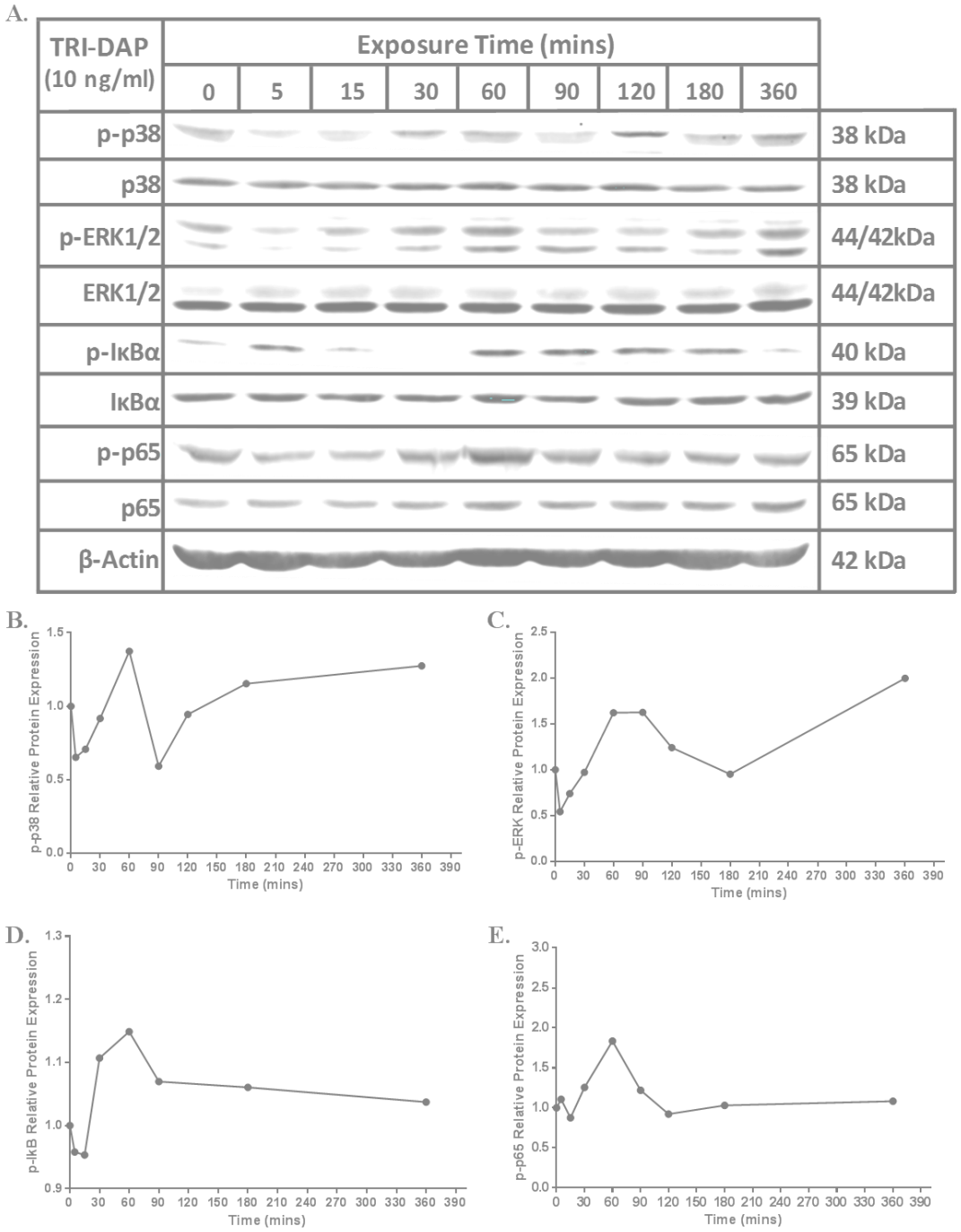

Figure A5.2. Phosphorylation time and dose response data for HCT116 cells stimulated with TRI-DAP. A) Immunoblots of phosphorylated and total p38, ERK, IκBα and p65 in HCT116 cells stimulated with 10 μg/ml TRI-DAP for 0, 5, 15, 30, 60, 90, 120, 180, 360 minutes. β- Actin acted as the loading control. (B-E) Densitometry of phosphorylated proteins, relative to β-Actin expression.

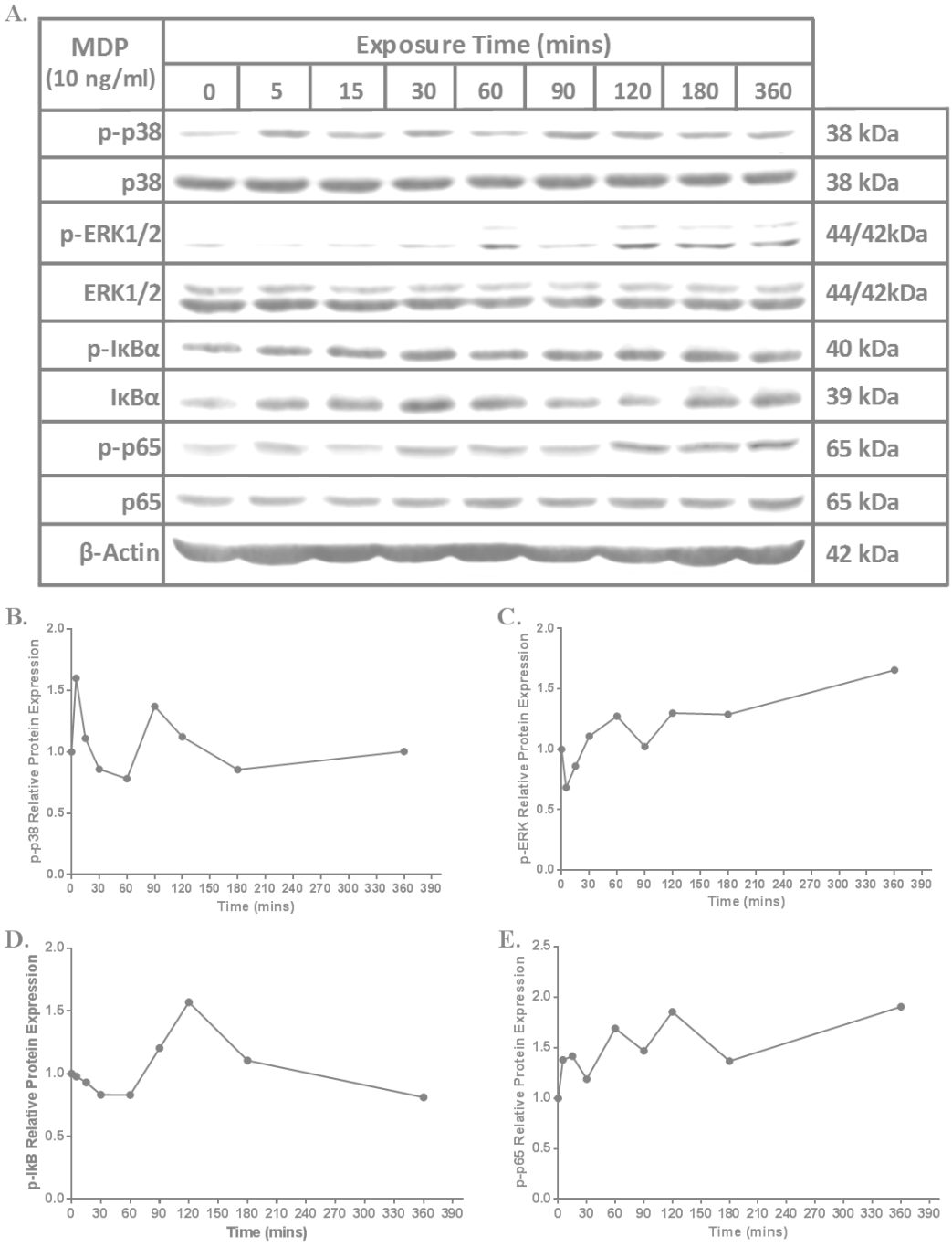

Figure A5.3. Phosphorylation time and dose response data for HCT116 cells stimulated with MDP. A) Immunoblots of phosphorylated and total p38, ERK, IκBα and p65 in HCT116 cells stimulated with 10 μg/ml MDP for 0, 5, 15, 30, 60, 90, 120, 180, 360 minutes. β- Actin acted as the loading control. (B-E) Densitometry of phosphorylated proteins, relative to β-Actin expression.

Appendix 6 . MAPK / NF-κB Phosphorylation Time Response in THP-1 cells.

Phosphorylation of MAPK and NF-κB signalling proteins can be quantified by western blot analysis to establish NOD1 and NOD2 responses to ligand stimulation. MAPK proteins (p38 and ERK) and NF-κB proteins (p65 and IκBα) are unstable in their phosphorylated state, therefore time response analysis was carried out to establish optimum NOD1/NOD2 stimulation times to accommodate their detection. THP-1 cells were stimulated with 10 μg/ml of a NOD1 ligand (iE-DAP or TRI-DAP) or NOD2 ligand (MDP) over a range of time points; 0, 5, 15, 30, 60, 90, 120, 180 and 360 minutes. Peak phosphorylation was identified from these blots, allowing an appropriate NOD1/2 stimulation time to be chosen. Phosphorylation of MAPK and NF-κB proteins generally peaked at 180 minutes following iE-DAP stimulation (Figure A6.1), 120 minutes following TRI-DAP (Figure A6.2) and 120 minutes following MDP (Figure A6.3).

Therefore, these stimulation times (3 hrs iE-DAP, 2 hr TRI-DAP and 2 hrs MDP) were used when investigating NOD1/NOD2 associated MAPK and NF-κB signalling in Chapter 5 and Chapter 6 of this research.

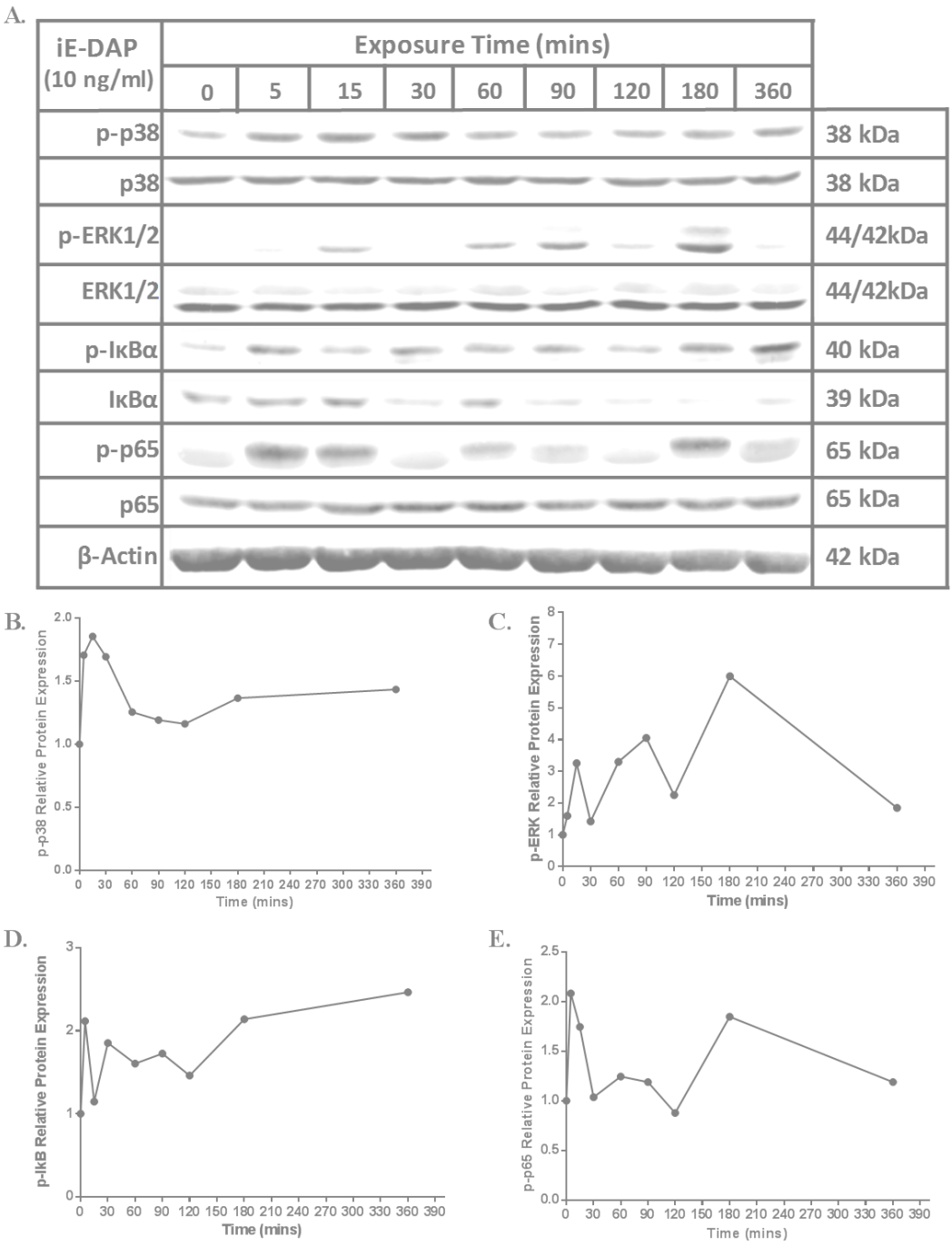

Figure A6.1. Phosphorylation time and dose response data for THP-1 cells stimulated with iE-DAP. A) Immunoblots of phosphorylated and total p38, ERK, IκBα and p65 in THP-1 cells stimulated with 10 μg/ml iE-DAP for 0, 5, 15, 30, 60, 90, 120, 180, 360 minutes. β-Actin acted as the loading control. (B-E) Densitometry of phosphorylated, relative to β-Actin expression.

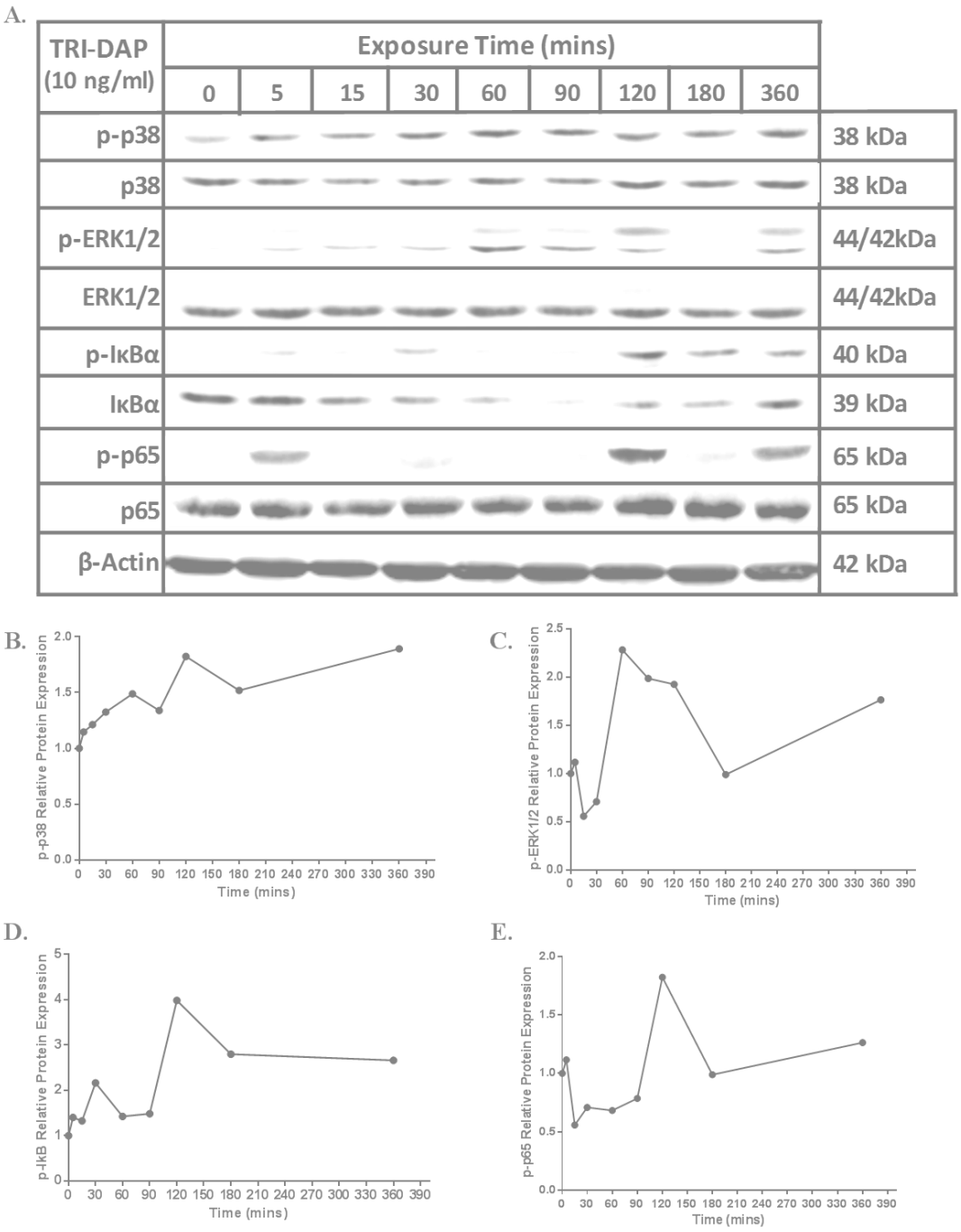

Figure A6.2. Phosphorylation time and dose response data for THP-1 cells stimulated with TRI-DAP. A) Immunoblots of phosphorylated and total p38, ERK, IκBα and p65 in THP-1 cells stimulated with 10 μg/ml TRI-DAP for 0, 5, 15, 30, 60, 90, 120, 180, 360 minutes. β- Actin acted as the loading control. (B-E) Densitometry of phosphorylated proteins, relative to β-Actin expression.

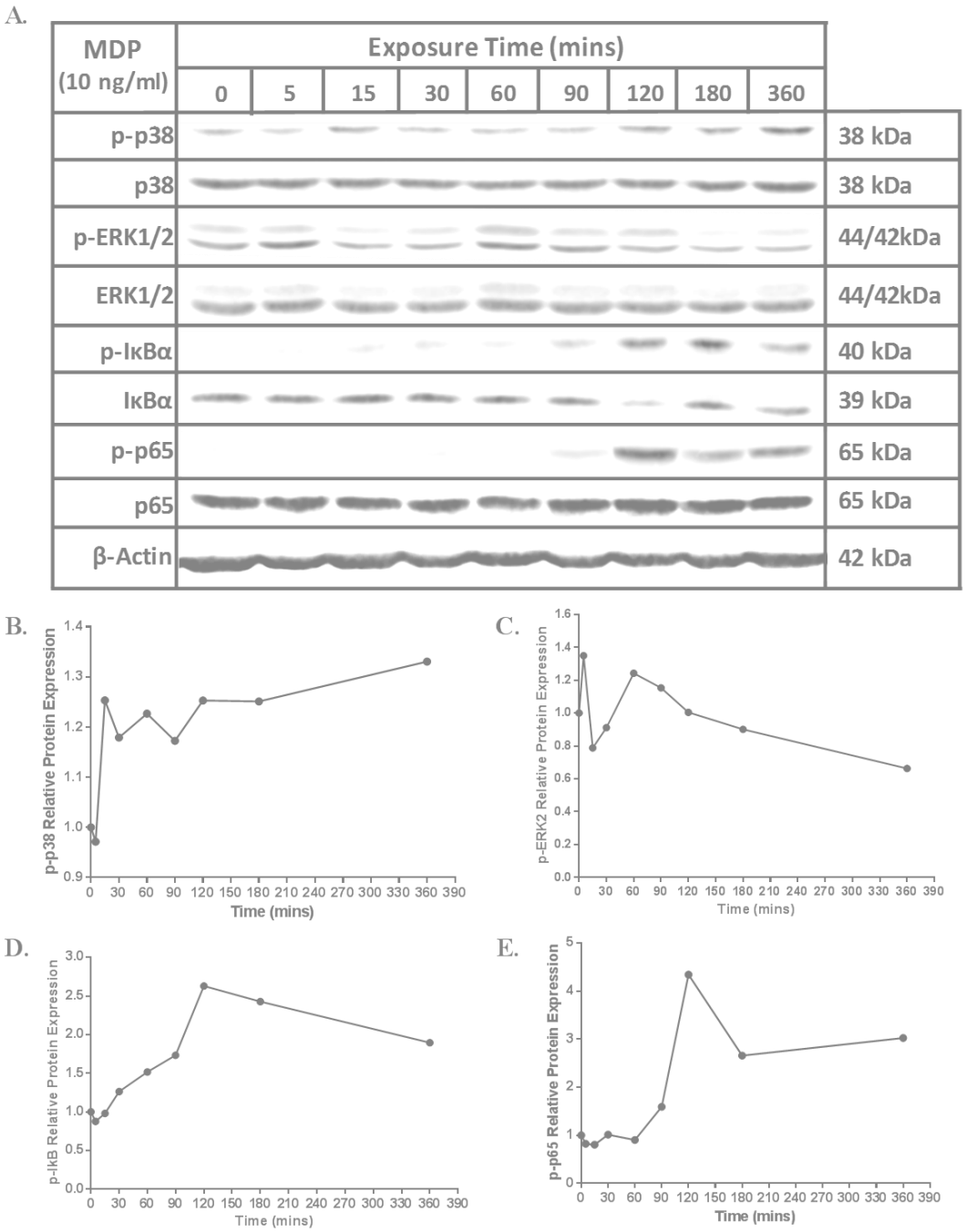

Figure A6.3. Phosphorylation time and dose response data for THP-1 cells stimulated with MDP. A) Immunoblots of phosphorylated and total p38, ERK, IκBα and p65 in THP-1 cells stimulated with 10 μg/ml MDP for 0, 5, 15, 30, 60, 90, 120, 180, 360 minutes. β- Actin acted as the loading control. (B-E) Densitometry of phosphorylated proteins, relative to β-Actin expression.

Appendix 7 . Housekeeping Gene Validation for qPCR Analysis

Analysis was carried out to check if housekeeping genes were appropriate for normalising gene expression in the presence of epigenetic modifying, cell differentiating and NOD stimulating agents. For a gene to be recognised as an appropriate housekeeping gene, it should not be directly altered by the treatment under investigation. β-Actin is one of the most commonly used housekeeping gene, and so was the first gene to be examined. Ct values were examined to check if β-Actin expression was altered by the various treatments used throughout the course of this research; 5-Aza, 5-Aza-dC, NOD1/NOD2 ligands, SAHA and PMA, in both HCT116 cells (Figure A7.1 A-B) and THP-1 cells (Figure A7.1 C-D). β-Actin was found to remain unchanged by 5-Aza, 5-Aza-Dc, NOD1/NOD2 ligands and PMA in both HCT116 cells and THP-1 cells. However, SAHA appeared to reduce β-Actin expression, represented by increases in Ct values, in both HCT116 cells (Figure A7.1 A) and THP-1 cells (Figure A7.1 C). Review of the literature suggested that ribosomal RPL13A could be appropriate. Therefore, expression of this gene was investigated after SAHA, and was found to remain unchanged by the treatment, represented by unchanged Ct values, in both HCT116 cells (Figure A7.1 B) and THP-1 cells (Figure A7.1 D). Therefore, β-Actin was used as the housekeeping gene for qPCR analysis for all treatments, expect SAHA. Instead RPL13A was used as the housekeeping gene following SAHA treatments.

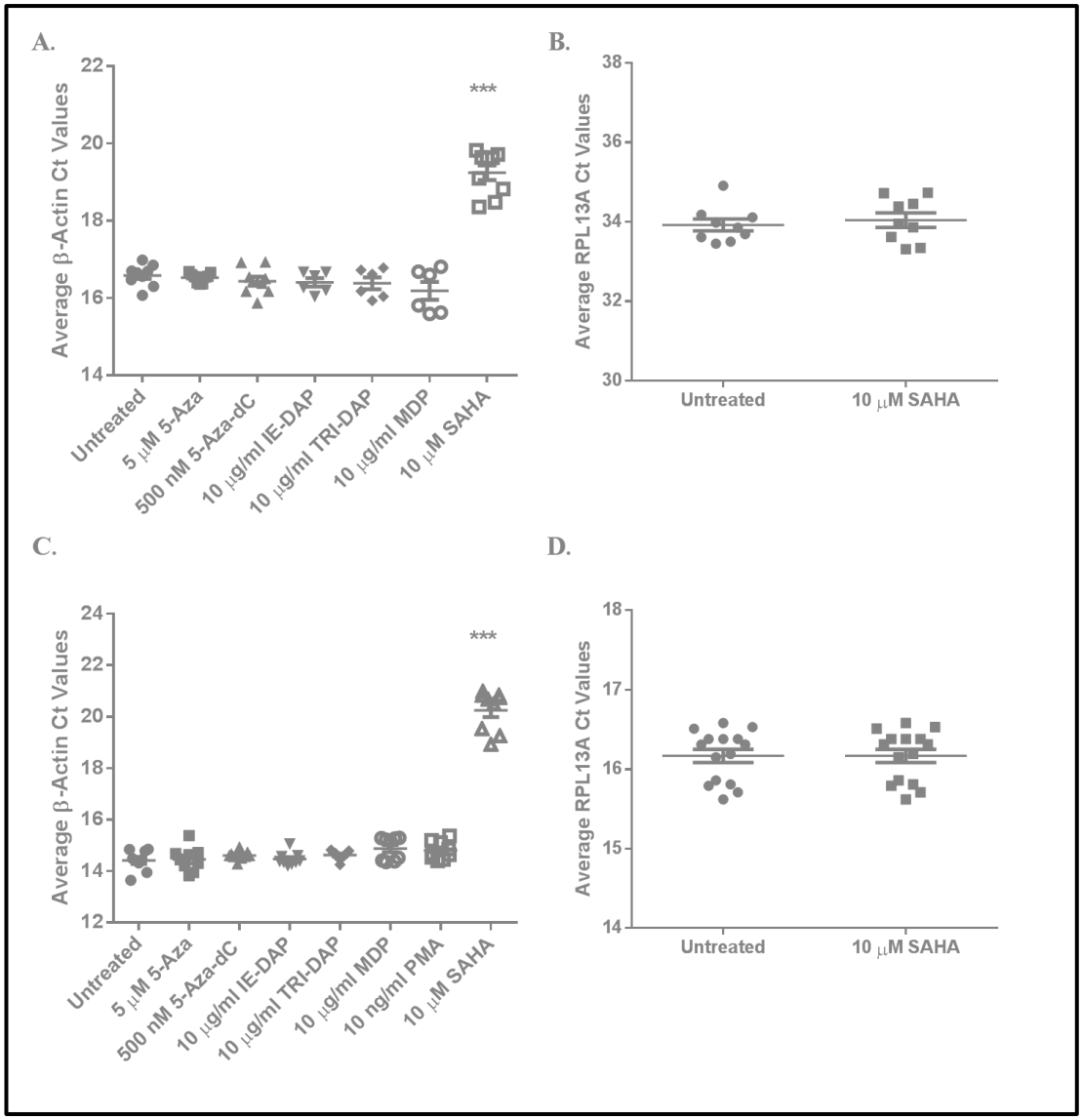

Figure A7.1. HCT116 and THP-1 housekeeping gene validation for qPCR analysis. A) β-Actin Ct values after treatment of HCT116 cells with 5-Aza, 5-Aza-dC, NOD ligands or SAHA. B) RPL13A Ct values after treatment of HCT116 cells with SAHA. C) β-Actin Ct values after treatment of THP-1 cells with 5-Aza, 5-Aza-dC, NOD ligands, PMA or SAHA. D) RPL13A Ct values after treatment of THP-1 cells with SAHA. Statistical analysis was performed using independent t-tests or one-way ANOVAs, followed by Dunnetts *post-hoc* test where appropriate. Significance was recognised at $p < 0.05$, with * representing $p < 0.05$, ** representing $p < 0.01$ and *** representing $p < 0.001$, relative to the untreated control.

Appendix 8 . Loading Control Validation for Western Blot Analysis

Analysis was carried out to check if loading proteins were appropriate for normalising protein expression in the presence of epigenetic modifying, cell differentiating and NOD stimulating agents. For a protein to be recognised as an appropriate loading control, it should not be directly altered by the treatment under investigation. β-Actin is one of the most commonly used loading control, and so was the first gene to be examined. Densitometry revealed no change in HCT116 β-Actin after 5-Aza, 5-Aza-dC, NOD1/2 ligands or DNMT3b-/-, and so β-Actin was considered an appropriate loading control for these treatments (Figure A8.1 A-C). However, SAHA was found to significantly reduce β-Actin protein levels (Figure A8.1 A &D), therefore β-Tubulin was investigated as an alternative. β-Tubulin remained unaltered by SAHA, and so was chosen as the alternative loading control for all SAHA treatments of HCT116 cells (Figure A8.1 E-F).

Densitometry revealed no change in THP-1 β-Actin after 5-Aza, 5-Aza-dC, NOD1/2 ligands or PMA, and so β-Actin was considered an appropriate loading control for these treatments (Figure A8.2 A-D). However, SAHA was found to significantly reduce β-Actin protein levels (Figure A8.2 A&E), therefore β-Tubulin was investigated as an alternative. β-Tubulin remained unaltered by SAHA, and so was chosen as the alternative loading control for all SAHA treatments of THP-1 cells (Figure A8.2 F-G).

Finally, since β-Actin is very abundant in both HCT116 and THP-1 cells, it was important to ensure that differences between loading concentrations could still be distinguished. Therefore, a protein gradient was tested to further validate β-Actin (Figure A8.3 A-D). Differences can be detected between protein increments (0, 10, 20, 30, 40, 50, 60 μg/ml). This further validates β-Actin as an appropriate housekeeping gene, since 30 μg/ml protein was loaded per well in all western blots in the current thesis.

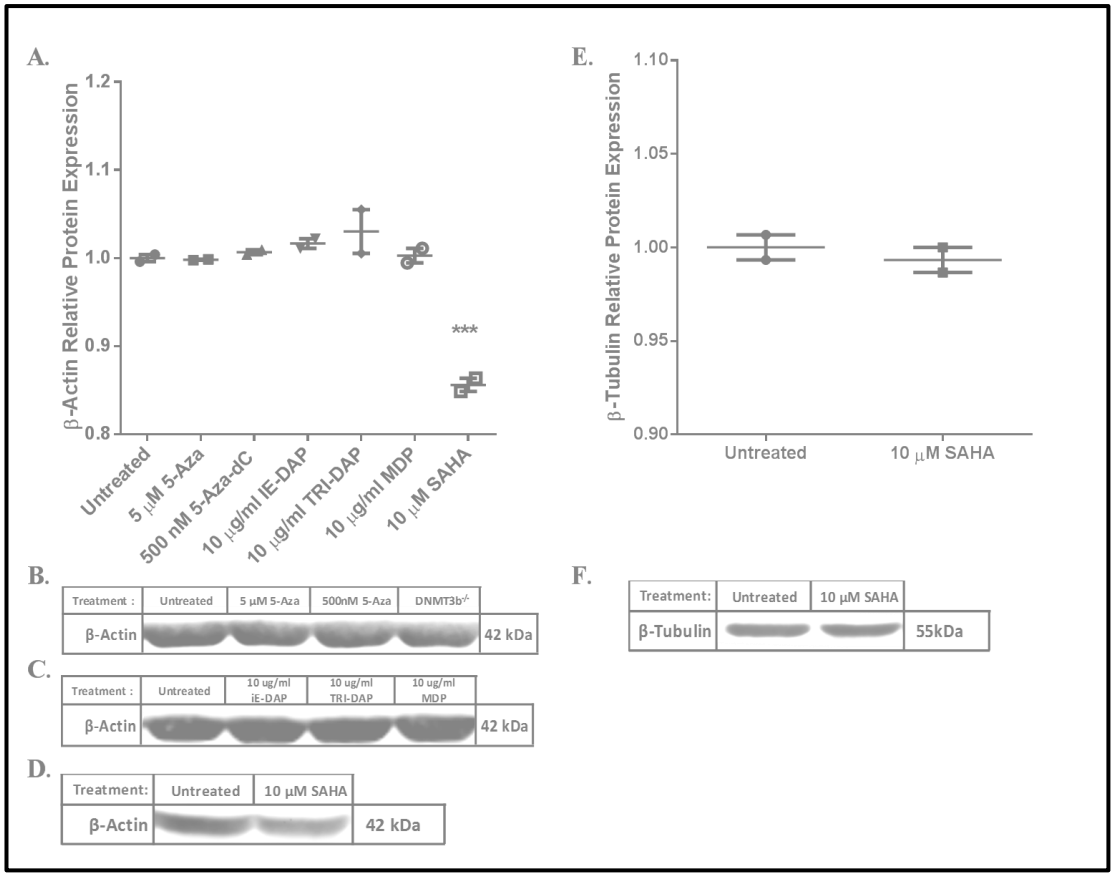

Figure A8.1. HCT116 loading control validation for western blot analysis. A) β-Actin Ct values after treatment of HCT116 cells with 5-Aza, 5-Aza-dC, NOD ligands or SAHA. B) Immunoblot of β-Actin after 5-Aza, 5-Aza-dC or DNMT3b-/-. C) Immunoblot of β-Actin after NOD1/2 ligands. D) Immunoblot of β-Actin after SAHA. E) β-Tubulin Ct values after treatment with SAHA. F) Immunoblot of β-Tubulin after SAHA. Statistical analysis was performed using independent t-tests or one-way ANOVAs, followed by Dunnetts *post-hoc* test where appropriate. Significance was recognised at $p < 0.05$, with * representing $p < 0.05$, ** representing $p < 0.01$ and *** representing $p < 0.001$, relative to the untreated control.

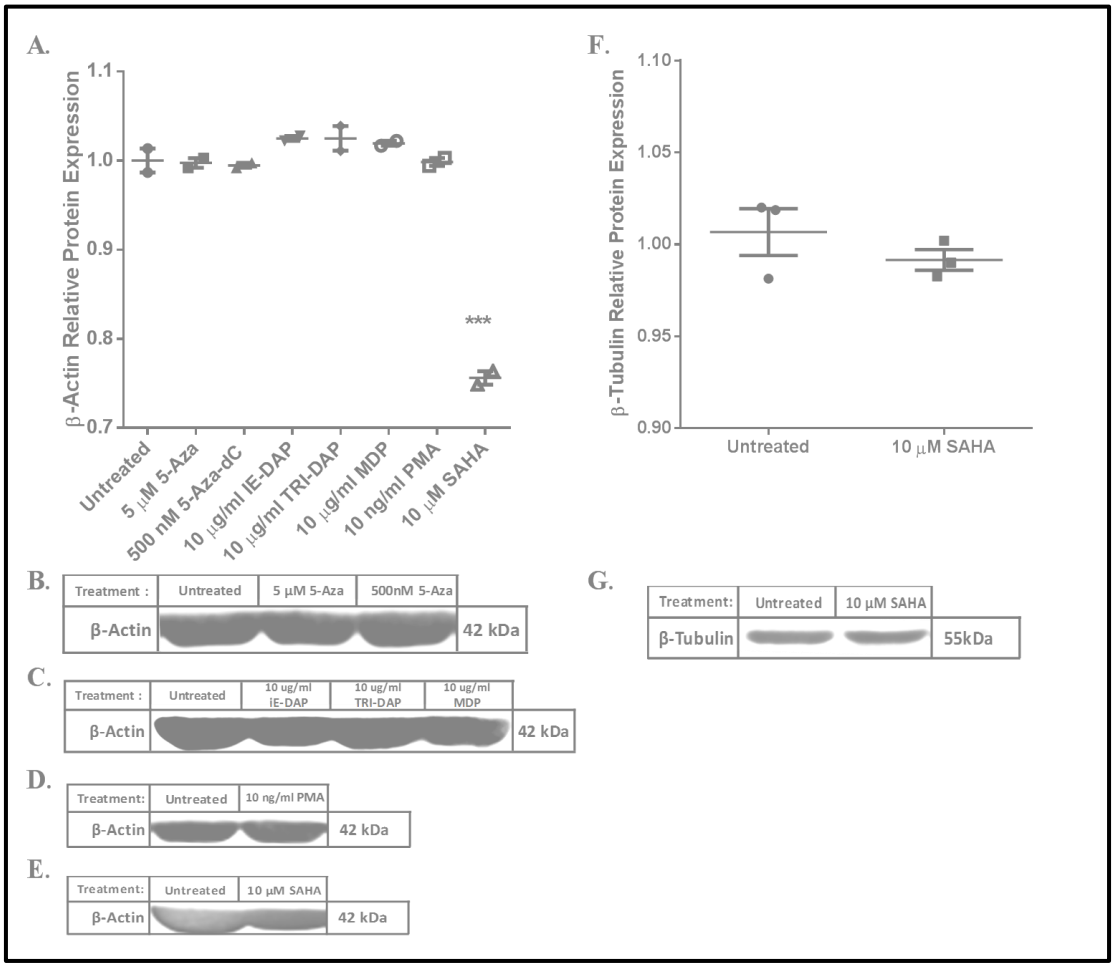

Figure A8.2. THP-1 loading control validation for western blot analysis. A) β-Actin Ct values after treatment of THP-1 cells with 5-Aza, 5-Aza-dC, NOD ligands, PMA or SAHA. B) Immunoblot of β-Actin after 5-Aza, 5-Aza-Dc. C) Immunoblot of β-Actin after NOD1/2 ligands. D) Immunoblot of β-Actin after PMA. E) Immunoblot of β-Actin after SAHA. F) β-Tubulin Ct values after treatment with SAHA. G) Immunoblot of β-Tubulin after SAHA. Statistical analysis was performed using independent t-tests or one-way ANOVAs, followed by Dunnetts *post-hoc* test where appropriate. Significance was recognised at $p < 0.05$, with * representing $p < 0.05$, ** representing $p < 0.01$ and *** representing $p < 0.001$, relative to the untreated control.

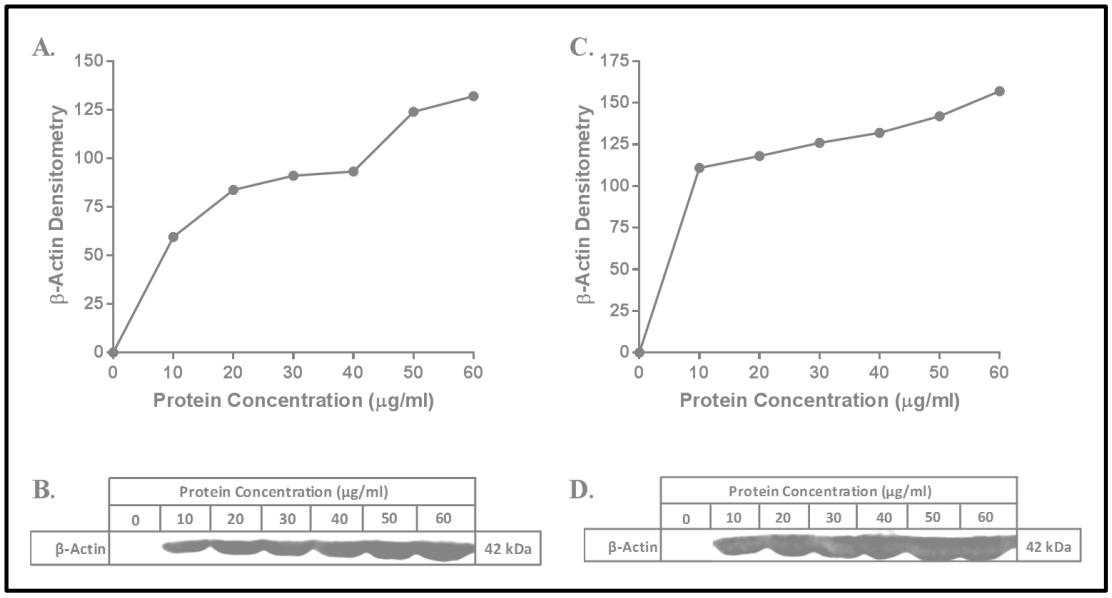

Figure A8.3. HCT116 and THP-1 loading control protein gradient for western blot analysis. A) β-Actin densitometry at 10, 20, 30, 40, 50 and 60 μg/ml HCT116 protein. B) Immunoblot of HCT116 β-Actin protein gradient. C) β-Actin densitometry at 10, 20, 30, 40, 50 and 60 μg/ml THP-1 protein. D) Immunoblot of THP-1 β-Actin protein gradient.